EVOLUTION OF THE NORTHEAST ZONE BRECCIA BODY, MOUNT POLLEY MINE, BRITISH COLUMBIA

by

MEGHAN LEA JACKSON
BSc, New Mexico Institute of Mining and Technology, 2002

A THESIS SUBMITTED IN PARTIAL FULFILLMENT OF THE DEGREE OF

MASTER OF SCIENCE

in

THE FACULTY OF GRADUATE STUDIES
(Geological Science)

THE UNIVERSITY OF BRITISH COLUMBIA
(Vancouver)

October 2008

ABSTRACT

The Mount Polley deposit in north-central British Columbia is a Cu-Au porphyry system related to alkaline magmatism. The deposit is composed of numerous discrete zones of Cu-Au mineralization related to bodies of hydrothermal breccia, including the Northeast zone which hosted a pre-mining proven and probable reserve of approximately 11 Mt of ore averaging 0.88% Cu and 0.28 g/t Au. The polylithic breccia body at the Northeast zone is irregular in shape and intruded by multiple generations of post-mineral dykes. Post-mineral faults cut the breccia, making the original breccia geometry unclear. 11,000 meters of core logging along two vertical sections perpendicular to the long axis of the orebody show that a significant percentage (locally >50%) of the breccia is composed of K-feldspar-phyric monzonite porphyry clasts. Many of these have globular shapes, implying that this material was ductile at the time of brecciation. Cu-sulfides are most abundant in and immediately above zones containing the greatest concentration of K-feldspar-phyric monzonite porphyry clasts. This relationship suggests that the fluids responsible for both mineralization and brecciation originated during this phase of intrusion. Most of the Cu-Au-bearing sulfide minerals form hydrothermal chemical infill in the breccia. Where fine-grained clastic material is abundant or where movement of clasts was minimal, sulfides are generally less abundant or absent. The entire breccia body of the Northeast Zone at Mount Polley appears to be the result of a single brecciation event. Variation in breccia character within the body is attributable to variations in fluid flux, pre-existing rock character, and fluidization processes. Furthermore, the permeability structure established during the brecciation event exerted the fundamental control over ore distribution within the breccia body.

TABLE OF CONTENTS

LIST OF TABLES

LIST OF FIGURES

CHAPTER 1

CHAPTER 2

CHAPTER 3

CHAPTER 4

CHAPTER 5

CHAPTER 6

ACKNOWLEDGEMENTS

This work forms part of a larger Mineral Deposits Research Unit-Centre for Ore Deposit Exploration Studies (University of British Columbia/University of Tasmania) research project investigating shallow- and deep-level alkalic mineral deposits, in collaboration with the Geological Survey of Canada. Funding and field support was provided by Amarc Resources Ltd., Anglogold-Ashanti, Barrick Gold Corp., Imperial Metals Corp., Lysander Minerals Corp., Newcrest Mining Ltd., Newmont Mining Corp., Novagold Resources Inc., Teck Cominco Ltd., NSERC-CRD and Geoscience BC. Logistical and field support from Terrane Minerals Corp., Eastfield Resources Ltd. and Lihir Gold Mine is also acknowledged. This work draws heavily from the observations and analyses of the Imperial Metals geologists working at Mount Polley. Lee Ferriera, Chris Taylor, Leif Bjornson, and particularly Chris Rees and Jacqueline Blackwell were enormously helpful. Pat McAndless and Steve Robertson provided support at every stage of the project. Jim Logan, Dave Bailey, and Adam Bath lent their perspective on Mt. Polley based on their experience in a number of roles. The input of Claire Chamberlain, Kirstie Simpson, Dave Cooke, Andrew Davies, Greg Dipple, and Ben Kennedy strongly shaped the conclusions drawn here. My fellow students in the alkalic research group, MDRU, and the Earth and Ocean Sciences department were invaluable: Evan Crawford, Janina Micko, Amber Henry, Malissa Washburn, Paul Jago, Kevin Byrne, and Heidi Pass. Special thanks are also due to Natasha Gainer and Jen McPherson for logistical and emotional support.

DEDICATION

This thesis is dedicated to the night people and to the siren tribe;

the fact that they don't understand what we're doing,

means we're doing it well.

Chapter 1 -Significance of the Mount Polley deposit

Introduction

Porphyry Cu-Au mineralization is the product of physical and chemical interactions between intrusions, country rock, and fluids (Guilbert and Clark, 1980). Hydrothermal, magmatic, and tectonic breccias are common features of these systems (Sillitoe, 1985). Breccia formation in magmatic-hydrothermal systems reflects not just the chemistry of the fluids responsible, but also the timing and the energetics of the system (McPhie et al., 1993). Detailed description of breccia characteristics can lead to enhanced understanding of not only the chemical but the physical evolution of fluids within a hydrothermal system (McPhie et al., 1993). Breccias are data-rich geological features resulting from complex and often spatially and temporally overlapping processes. In mineralizing systems, breccias can enhance, inhibit or destroy the deposition of economic minerals (Burnham, 1979; Burnham, 1985; Sillitoe, 1985; Bushnell, 1988; Zweng and Clark, 1995; Serrano et al., 1996). Describing the features, internal organization, and ultimately the genesis of breccia features can be a powerful tool in understanding a hydrothermal system. The hydrothermal system that produced mineralization at Mount Polley is particularly important because Mount Polley represents an example of a little-examined class of porphyry deposits related to alkaline, rather than calc-alkaline, rocks (Sillitoe, 2002; Holliday and Cooke, 2007).

The Mount Polley Cu-Au porphyry

The Mount Polley Cu-Au mine in central British Columbia (figure 1.1) exploits an orebody consisting of at least five discrete porphyry Cu-Au-Ag ore zones (figure 1.2)

associated with magmatic-hydrothermal breccias (Barr et al., 1976; Lang et al., 1995b; Logan and Mihalynuk, 2005). These breccias are coeval with monzonitic intrusions emplaced into the alkalic volcanic rocks of the Quesnel terrane (Hodgson et al., 1976; Fraser, 1994a and b; Fraser et al., 1995; Rees et al., 2005, 2006; Logan and Mihalynuk, 2005; Logan et al., 2007). The Northeast ore zone, on which this study is focused, provides evidence of the direct connection between the intrusion, brecciation, and mineralization processes.

The Northeast Zone is important because it represents a small yet high grade ore zone (Deyell, 2005; Deyell and Tosdal, 2005; Jackson et al., 2007; Pass et al., 2007; Imperial Metals Corporation, 2007). The processes which resulted in the Northeast Zone mineralization may provide clues to mechanisms which concentrate and focus fluid flow in other alkalic porphyry systems. Recognizing focused fluid flow guides exploration keyed to finding economic mineralization. Due to their atypical alteration expression as compared to calc-alkalic systems, finding the zone of most focused fluid flow in alkalic hydrothermal systems is not straightforward; additional guides to exploration in prospective zones of alkalic magmatism would add value to both academic and economic comprehension of these systems.

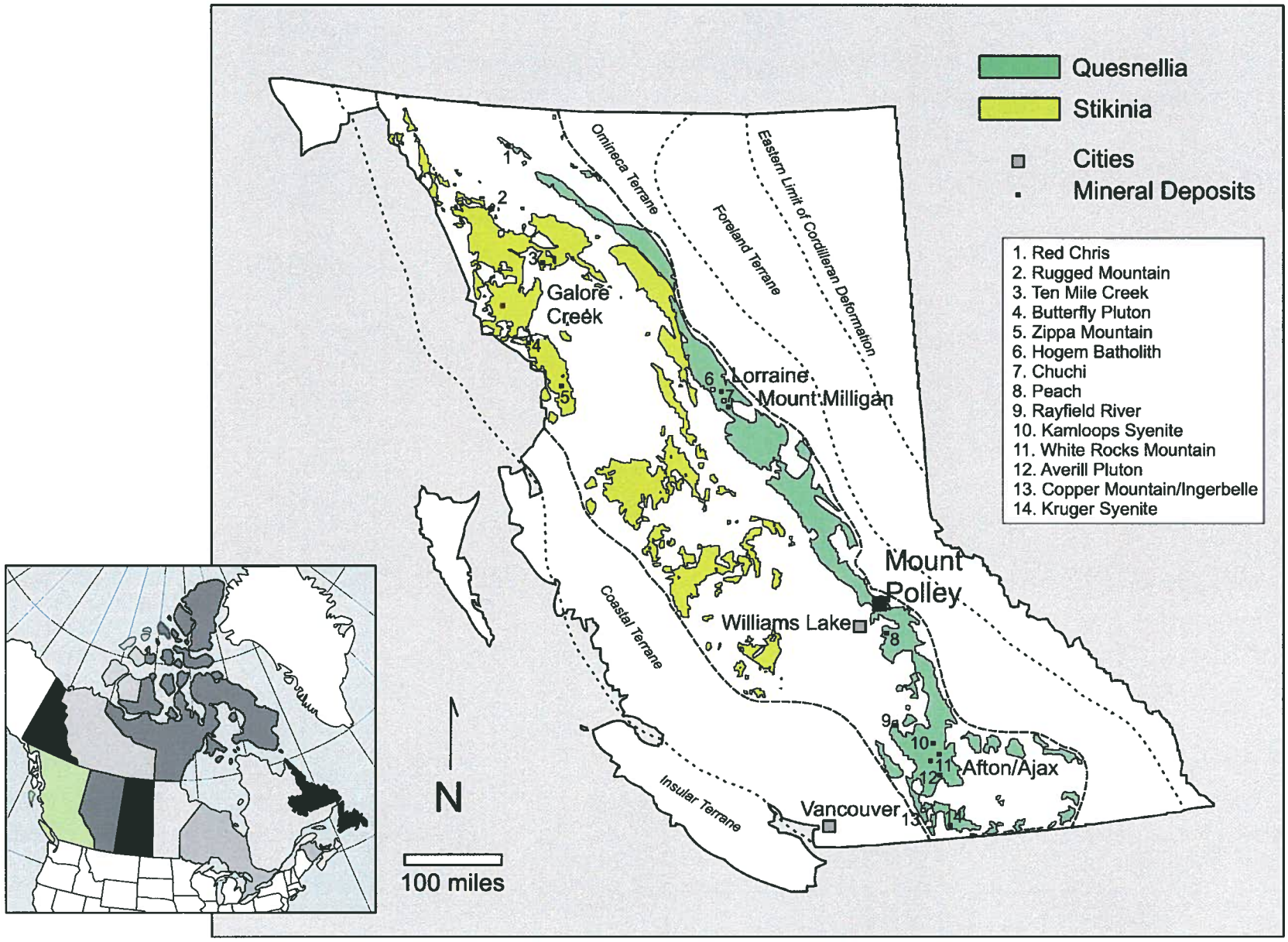
Quesnellia
Stikinia
Cities
Mineral Deposits
1. Red Chris
2. Rugged Mountain
3. Ten Mile Creek
4. Butterfly Pluton
5. Zippa Mountain
6. Hogem Batholith
7. Chuchi
8. Peach
9. Rayfield River
10. Kamloops Syenite
11. White Rocks Mountain
12. Averill Pluton
13. Copper Mountain/Ingerbelle
14. Kruger Syenite
Omineca Terrane
Foreland Terrane
Eastern Limit of Cordilleran Deformation
Coastal Terrane
Insular Terrane
Galore Creek
Lorraine
Mount Milligan
Mount Polley
Williams Lake
Afton/Ajax
Vancouver
N
100 miles

Figure 1.1- The location of Mount Polley and other alkalic porphyry deposits and alkalic intrusive centers in the Quesnel and Stikine terranes. Inset shows the location of British Columbia (green). Redrafted from www.mapplace.bc.ca.

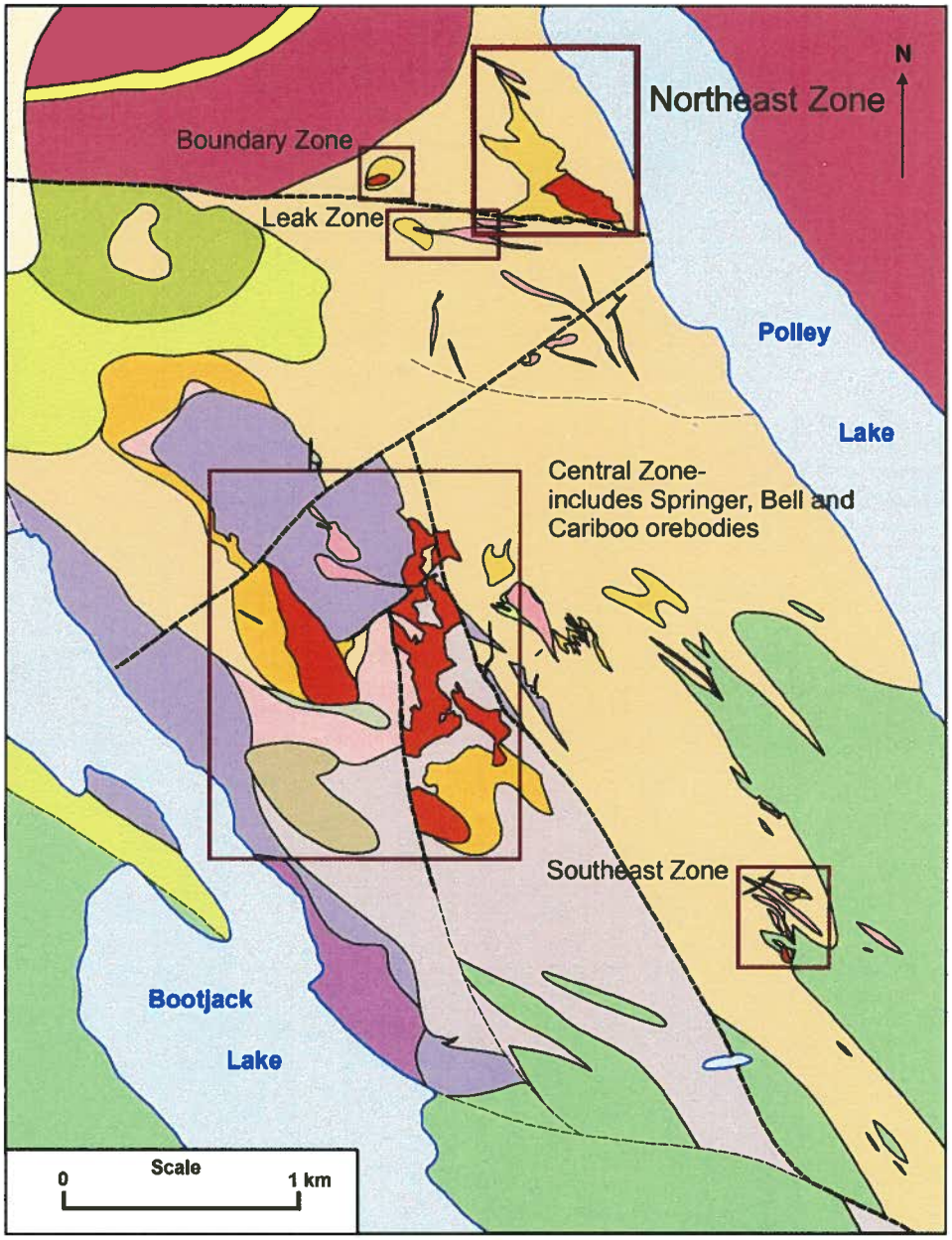

- Quaternary: Till, glaciofluvial, glaciolacustrine deposits.
- Quartz latite (Early Jurassic, 197 Ma)
- Breccia, conglomerate. Polymictic, intrusive-clast rich, matrix-supported.
- Augite-porphyry and mafic dikes.
- Polymictic fragmental hydrothermal breccia, minor jigsaw-fit breccia and igneous breccia.
- Hydrothermal breccia in Core Zone of Mount Polley Complex. Red indicates Cu-Au min.
- Potassium feldspar-(plagioclase-)phyric monzonite.
- Plagioclase feldspar porphyry (monzodiorite).
- Non-bedded, matrix-rich fragmental breccia of monzonitic material.
- Monzodioritic porphyry fragmental breccia, clast-supported.
- Monzodiorite and monzonite, undivided.
- Igneous (and hydrothermal) breccia in mixed monzodiorite, diorite.
- Uneven-textured diorite to monzodiorite.
- Even-textured equigranular augite(-biotite) diorite to monzodiorite.
- Pyroxenite.
- Basaltic to andesitic intrusive and extrusive rocks.

Figure 1.2- Geologic map of the Mount Polley Property, with ore zones delineated by red rectangles. Mineralized zones within breccia bodies are shown in red. Map courtesy of Chris Rees, Imperial Metals.

The primary goal of this study is to clarify the connection between magmatism, brecciation, and mineralization. This study includes examination of 10,340 meters of core, 142 thin sections, and 58 major and trace element chemical analyses. Two cross-sections perpendicular to the apparent long axis of the breccia body were constructed, concentrating on the description and internal architecture of the breccia, and on the pre-, syn-, and post-breccia intrusive rocks. Spatial and temporal relationships between mineralization, intrusion, brecciation and alteration are described.

The first and second chapters of the thesis address the general characteristics and regional geology of the Mount Polley area, and summarizes previous studies undertaken in the area. The third chapter addresses the igneous rocks and magmatic evolution of the Northeast Zone at Mount Polley. The features and internal organization of the breccia body, making the connection between the magmatic and the hydrothermal systems, are described in the fourth chapter of the thesis. This chapter also includes evidence contributing to describing the energetics of the breccia system. The fifth chapter of the thesis describes the alteration zonation observed within and around the breccia body, and presents data contributing to deciphering the chemical evolution of the fluids responsible for brecciation and mineralization. The sixth chapter presents the conclusions of the thesis, and advances a hypothesis explaining the observed features.

The significance of alkaline hydrothermal systems

The majority of porphyry and epithermal copper and gold deposits currently known are associated with rocks of medium to high-K calc-alkalic composition (Sillitoe, 2002, Holliday and Cooke, 2007). A minority of volcanoplutonic hydrothermal deposits, the alkalic porphyry and epithermal deposits, are spatially and temporally associated with

arc-related volcanic and intrusive rocks of alkalic composition (Lang et al., 1995, Jensen and Barton, 2000, Sillitoe, 2002, Holliday and Cooke, 2007). Due to their comparative rarity, alkalic porphyries have not received the same attention that led to the systematic description of the calc-alkalic deposit class (Holliday and Cooke, 2007).

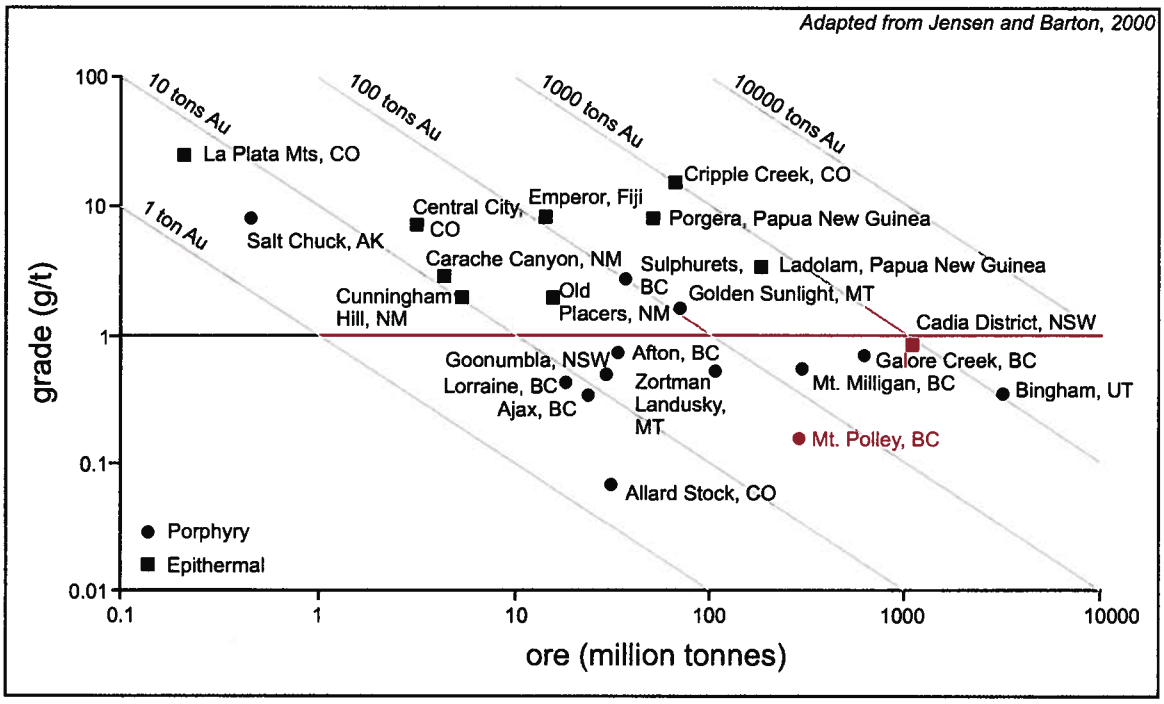

Figure 1.3- Major alkalic related Au deposits of the world. The red line divides porphyry from epithermal systems. From Jensen and Barton, 2000

Although less common than their calc-alkalic cousins, alkalic Cu-Au deposits are of economic significance (Lang et al., 1995, Jensen and Barton, 2000). They include some of the world's highest grade and largest porphyry-related gold resources (figure 1.3 and Table 1.1), as well as some of the largest gold accumulations in epithermal settings (Jensen and Barton, 2000). Though alkalic porphyry Cu-Au deposits occur in relatively few districts, they are still attractive exploration targets due to their high grades, high Au:Cu ratios, and potential for valuable co-product commodities, including platinum group elementss (Eliopoulos and Economou-Eliopoulos, 1985; Thompson et al., 2002).

Table 1.1- Characteristics of some alkalic-related mineral deposits.

DEPOSIT	TYPE	TONNAGE	CU (%)	AU (G/T)	AU (T)	MO (%)	REFERENCES
British Columbia							
Afton/Ajax	Porphyry	241.7 Mt	0.345	0.18	--	--	Abacus Mining Corp, 2008
Similco	Porphyry	129 Mt	0.393	0.155	--	--	MINFILE, 1996
Mount Polley	Porphyry	130 Mt					Imperial Metals, 2007
Mouse Mountain	Porphyry	Undefined	--	--	--	--	Jonnes et al., 2007
Mount Milligan	Porphyry	205.9 Mt	0.25	0.6	--	--	Jago et al., 2007
Lorraine	Porphyry	32 Mt	0.66	0.25			Eastfield Group, 1998
Red Chris	Porphyry	276 Mt	0.349	0.266	--	--	Imperial Metals, 2007
Galore Creek	Porphyry	786 Mt	0.52	0.29	--	--	NovaGold, 2008
Schaft Creek	Porphyry						
Lachlan Fold Belt							
Ridgeway	Porphyry	54 Mt	0.77	2.5	132.6		Wilson et al., 2007
Cadia (district)	Porphyry	767 Mt	--	--	586		Wilson et al., 2007
Cowal	Porphyry/epithermal						
Goonumbla	Porphyry	30 Mt	0.91	0.5	--		Heithersay and Walshe,
Endeavour	Porphyry	63.6 Mt	1.1	0.5	--		1995
Great Plains Margin							
La Plata/Allard stock	Porphyry/epithermal	32 Mt	0.4	0.07	>13		Kelly and Luddington, 2002
Central City	L.S. Epithermal	3.2 Mt	--	7.2	>33		Jensen and Barton, 2000
Boulder County	L.S. Epithermal				30		Jensen and Barton, 2000
Cripple Creek	L.S. Epithermal	>211 Mt	--	>1	683		Kelly and Luddington, 2002
Rosita Hills	L.S. Epithermal		--	--	3		Jensen and Barton, 2000
Elizabethtown-Baldy	L.S. Epithermal		--	--	15		Kelly and Luddington, 2002
Cerrillos	Epithermal		--	--	0.1		Kelly and Luddington, 2002
Old Placers district	Epithermal/skarn		--	--	>51		Kelly and Luddington, 2002
New Placers	Skarn/epithermal		--	--	3.6		Kelly and Luddington, 2002
Jicarilla	Epithermal/skarn		--	--	0.5		Kelly and Luddington, 2002
White Oaks	Epithermal		--	--	5.1		Kelly and Luddington, 2002
Nogal-Bonito	Poprhyry		--	--	>9.7		Kelly and Luddington, 2002
Orogrande	Porphyry		--	--	0.5		Kelly and Luddington, 2002
Organ Mountains	Porphyry		--	--	0.4		Kelly and Luddington, 2002
Villa Ahumada	Porphyry		--	--			
Golden Sunlight		4.7 Mt	--	1.6			
Zortman-Landusky			--				Jensen and Barton, 2000
Republic			--				
Papua New Guinea							
Mount Kare	Porphyry	51.5	0.23	--	--	--	
Porgera	Epithermal	51 Mt	--	7			Richards and Ledlie, 2003
Lihir/Ladolam	Poprhyry/Epithermal	258 Mt	--	2.83			Lihir Gold Limited, 2007
China/Southeast Asia							
Phu-phu	Porphyry						
Yulong	Porphyry		--	7.3	40		Zhou et al, 2002
Yao'an	Porphyry						
Serbomacedonian Massif							Eliopoulos and Economou-
Skouries	Porphyry	206 Mt	0.54	0.8			Eliopoulos, 1985
Fiji							
Tauva	Epithermal		--				
Emperor	Epithermal	14.7 Mt	--	8.1	--		
Others							Jensen and Barton, 2000
Malmbjerg	Porphyry	>150 Mt	--	--	--	0.23	
Almaden (Hg)	Epithermal		--	--	--	--	Brooks et al, 2004
Palabora	Carbonatite	850 Mt	0.5	--	--	--	
Bingham	Porphyry	>1000 Mt	0.56	0.35	--	0.035	Groves and Veilreicher,
Mountain Pass (REE)	Carbonatite	34 Mt	--	--	--	--	2001

Alkalic deposits are imperfectly represented by models based on calc-alkalic porphyry deposits (Jensen and Barton, 2000). Part of the difficulty in describing and

interpreting the common features of alkalic porphyries lies in the rocks themselves. Alkaline rocks are believed to compose only 1/1000th of the igneous rocks in the earth's crust, yet they are described using 17% of igneous nomenclature (Sørenson, 1974). The rarity and complexity of the alkalic rocks results in a poor understanding of the chemical, physical, hydrothermal, and tectonic properties and affiliations of these rocks (Lueck and Russell, 1994, Lang et al., 1995). Instead, models based on porphyry systems in calc-alkalic rocks have driven models of alkalic deposits (Sillitoe, 2002). Increased awareness of the economic importance of the alkalic class of porphyry and epithermal deposits emphasizes the need to produce more representative models of these anomalous, but economically attractive mineralizing systems (Holliday and Cooke, 2007).

Alkalic porphyry systems are typically high-grade porphyry-style deposits associated with small volume pipe-like intrusions that have surface expressions of only a few hundred square meters (Lueck and Russell, 1994, Lang et al., 1995, Lickfold et al., 2007; Holliday and Cooke, 2007). Characteristics of some orebodies associated with alkaline rocks are summarized in Table 1.2. Especially in the silica-undersaturated systems of British Columbia (Figure 1.1), alkalic porphyries are associated with complex composite intrusions, some including both alkaline and calc-alkaline rocks (Lueck and Russell, 1994, Lang et al., 1995). Despite the fact that alkalic melts are generally higher in CO_2, SO_4, and halogens than their calc-alkaline equivalents, areas of mineralization in alkaline rocks typically feature restricted alteration haloes as well (Bailey and Hampton, 1990, Sillitoe, 2002). This small footprint makes them difficult exploration targets, so practical guides and accurate deposit models are required to assist exploration (Holliday and Cooke, 2007).

Table 1.2- Characteristics of alkalic porphyry systems

CHARACTERISTICS OF ALKALIC PORPHYRY SYSTEMS		
Feature	**Deposits**	**Sources**
Igneous features		
Complex, small volume, pipe-like intrusions	Mount Polley, Skouries, Cadia	Logan et al., 2007, Eliopoulos and Economou-Eliopoulos, 1995, Lickfold et al, 2007, Jensen and Barton, 2000
Shoshonitic chemistry	B.C. systems, Skouries, Lachlan Foldbelt systems	Lang et al., 1995, Eliopoulos and Economou-Eliopoulos, 1995, Lickfold et al, 2007, Jensen and Barton, 2000, Holliday et al., 2002
Petrogenetically associated volcanic rock	Cadia, Mount Polley, Galore Creek	Logan and Bath, 2005, Lickfold et al, 2007
Mineralization associated with the most evolved intrusive phase	Cadia, Mount Polley	Logan and Bath, 2005, Lickfold et al., 2007
Silica-saturated intrusions	Cadia, Mount Milligan	Lang et al., 1995, Lickfold et al., 2007
Silica-undersaturated intrusions	Mount Polley, Galore Creek	Lang et al., 1995, Logan and Bath, 2005
Alteration features		
Argillic assemblages restricted to late structure penetrating the orebody	Mount Polley, Cadia	Lickfold et al., 2007, Logan et al., 2007, Logan and Bath, 2005
K-silicate constructive alteration associated with ore	Mount Polley, Galore Creek, Cadia	Lickfold et al., 2007, Logan et al., 2007, Logan and Bath, 2006
Large volumes of K-metasomatism surrounding the orebody	Galore Creek, Cadia	Lickfold et al., 2007, Logan et al., 2007
"Reddening"; hematite dusting of feldspars	Mount Polley, Afton-Ajax, Cadia	Lickfold et al., 2007, Logan et al., 2007
Tectonic associations		
Complex island arcs with alkaline and calc-alkaline magmatism	BC porphyries, Lachlan foldbelt poprhyries	Lang et al., 1995, Logan and Bath, 2006, Logan and Mihalynuk, 2005
Other associated mineralization		
Low-sulfidation alkalic epithermal	La Plata, Cadia	Jensen and Barton, 1995, Lickfold et al., 2007
Skarn (developed in carbonate and reactive volcanic rocks	Mount Polley, Galore Creek	Rees et al., 2006, Logan et al., 2007

Unlike calc-alkalic porphyry systems, the alkalic systems do not usually have associated advanced argillic alteration assemblages, and no connection to high sulfidation epithermal deposits has been demonstrated (Lang et al., 1995, Jensen and Barton, 2000, Sillitoe, 2002, Holliday and Cooke, 2007). These features are attributed to the high neutralization capacities of the alkaline host rocks, which reduce the lateral mobility of acidic fluids (Jensen and Barton, 2000, Sillitoe, 2002). Phyllic alteration in alkalic porphyry systems is typically restricted to late fault and vein zones that penetrate the waning hydrothermal system. The subtle nature of the peripheral hypogene alteration assemblages (variants on potassic, calc-potassic, sodic, calc-sodic and propylitic alteration) makes identifying the focus for fluid flow difficult further than a few hundred meters away from the mineralized center. Research has suggested that a systematic vertical and lateral zonation in sulfur isotopic composition surrounds some mineralized porphyry complexes (Deyell, 2005; Wilson et al., 2003), and mineralogical changes have also been noted (Sketchley et al., 1995; Lang et al., 1995b; Wolfe et al., 1996; Wilson et al., 2003; Gifkins et al., 2005).

Certain alteration assemblages in alkalic systems are distinct from those found in calc-alkalic systems. In the porphyry environment (e.g. Lang et al., 1995; Wilson et al., 2003), these include a Cu-Au-Ag and Mo-Au associations, and distinctive alteration assemblages characterized by high-temperature Na- (albite) and Ca-bearing (diopside, actinolite, and/or garnet) minerals (Jensen and Barton, 2000, Holliday and Cooke, 2007 and references therein).

Alkalic porphyry-related mineral deposits as a class have been examined by a number of researchers. Sillitoe (2002) discussed a variety of characteristics and localities distinguishing alkalic from calc-alkaline porphyry deposits worldwide. On more restricted scales, Cooke et al. (2006) examined the alkalic porphyry related mineralization of the Lachlan fold belt in great detail, Kelly and Ludington (2002) and MacLemore (2002) synthesized research undertaken on the Great Plains margin alkalic-related epithermal and porphyry deposits, and the characteristics of deposits in the Quesnel and Stikine terranes of British Columbia were summarized by Lang et al. (1995). Other alkalic-related mineral deposits that have been covered in great detail on a deposit scale include Porgera (Ronacher et al., 2004, Ronacher et al., 2002, and references therein), Skouries (Frei, 1997, and Eliopoulos and Economou-Eliopoulos, 1995), Lihir (Gemell et al, 2004, Carman, 1994 and 2003 and Mueller et al., 2002) and Cadia-Ridgeway (Wilson et al., 2003, Wilson et al., 2007 Lickfold et al., 2007 and references therein).

The Mount Polley system

Describing the mineralization at Mount Polley requires some adaptation of common terminology. Although a number of economic ore zones exist on and around the Mount Polley property, none of the ore zones, independent of the others, would represent minable reserves. Thus, each mineralized zone does not constitute an ore body. Similarly, the group of ore zones does not meet the legal description of a mining district. Thus, the Mount Polley "orebody" consists of multiple deposits, referred to here as ore zones and distinguished more on the basis of engineering (planned pits) than geological discontinuity. The cluster of ore zones is referred to as the Mount Polley deposit or

orebody. The term Mount Polley district is not used, as this formal legal designation has not been adopted for Mount Polley or the presently unexploited present in the surrounding area.

In British Columbia, individual alkalic deposits represent a range of depths and temperature of formation, from the "magmatic" environment of Lorraine (Nixon and Peatfield, 2003) through the "typical" porphyry environment of Mt. Milligan and the Cariboo-Bell zone of Mount Polley (Enns et al., 1995; Fraser et al., 1995; Sketchley et al., 1995) to the potentially shallower breccia environment at the top of the systems potentially represented by the Northeast zone of Mount Polley.

The widespread presence of hydrothermal breccia in the ore zones of Mount Polley distinguish this alkalic system from many of the other alkalic porphyry systems in British Columbia. Hydrothermal breccias are reported to be common at Galore Creek (Enns et al., 1995), where they in part host Cu-Au ore but they can also lack any significant Cu and Au values (Lang et al., 1995). Of the many deposits around the Iron Mask batholith, only the DM and Crescent deposits are hosted in significant hydrothermal breccia (Lang et al., 1995). Hydrothermal breccias are present but reportedly insignificant at Copper Mountain or Mount Milligan (Lang et al., 1995; Sketchley et al., 1995). Although the tonnage of the various deposits varies considerably; grade correlates with the presence of significant breccia at Mount Polley and Galore Creek, with the highest grades occurring in breccia bodies (see Table 1 in Lang et al., 1995).

Hydrothermal breccia forms where the ambient fluid pressure exceeds the lithostatic load of the overlying rock column coupled with the tensile strength of the

surrounding rock (Burnham, 1985 and 1997). Thus, breccias should be more common in shallow upper crustal environments. As such, it is tempting to suggest that Mount Polley represents one of the shallower alkalic porphyry deposits in BC. As an analogy, Zweng and Clark (1995) used fluid inclusions from the breccia-hosted >800 Mt Toquepala porphyry Cu-Mo system in southern Perú to suggest that it formed at much shallower depths than the nearby vein-dominated >1,200 Mt Cuajone porphyry Cu-Mo deposit. Unfortunately, the lack of appropriate minerals in most alkalic porphyry systems in British Columbia from which depth of formation can be determined, coupled with limited geologic constraints on the scale of post-mineral erosion and deformation of the Triassic and Early Jurassic deposits, has to date precluded establishing any independent constraints on their depth of formation (Lang et al., 1995).

The Mount Polley orebody is hosted within one of many alkalic intrusions emplaced into volcanic rocks of the Quesnel terrane (Figure 1.4) (Lang et al, 1995). These intrusions range in composition from orbicular psuedoleucite syenite to diorite (Bath and Logan, 2006). Mineralization associated with these intrusions is generally breccia and vein-hosted chalcopyrite with lesser bornite and associated gold, commonly with K-feldspar-magnetite alteration assemblages (Panteleyev et al., 1996). The intrusive complex is a north to northwest-trending body composed primarily of equigranular to porphyritic diorite, monzodiorite, and monzonite intruded by syenite dikes. U-Pb and $^{40}Ar/^{39}Ar$ geochronology from several of the intrusive phases in the complex give ages between 201 and 205 Ma, indicating a Late Triassic age (Bailey and Archibald, 1990; Mortensen *et al.*, 1995; Logan et al., 2007).

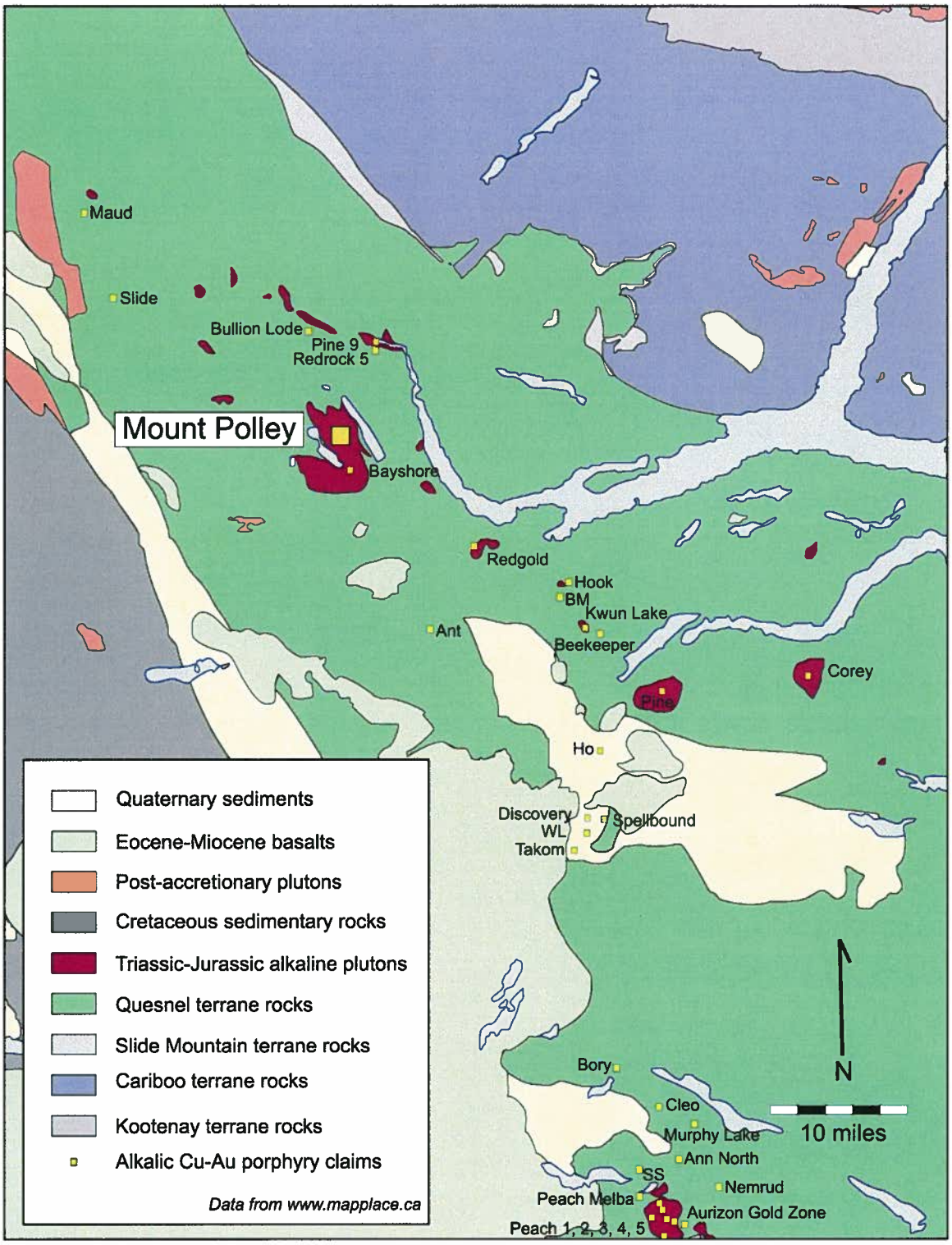

Figure 1.4- Terrane map showing Triassic-Jurassic alkalic intrusions and porphyry Cu-Au deposits and prospects in the Mount Polley Area; redrafted from www.mapplace.bc.ca

The porphyry system at Mount Polley involves a number of discrete ore zones within a post-mineralization north-plunging syncline (Hodgson et al., 1976; Fraser, 1994a, b; Fraser et al, 1995; Rees et al., 2005, 2006; Logan and Mihalynuk, 2005, Tosdal et al., 2008). The area is highly faulted, but it is possible that the ore zones represent different stratigraphic levels of a series of spatially related porphyry-style deposits (Logan and Mihalynuk, 2005). Cu:Au:Ag:Mo ratios differ from ore zone to ore zone, as does alteration, petrology, and the role of hydrothermal and igneous cemented breccia (Rees et al., 2005 and 2006). Average grades, alteration, and host rock types vary as well. If true, each center may have formed at slightly different crustal depths. This supposition is supported by the relative positions of the ore zones with respect to the regional stratigraphy. The Nicola Volcanic group rocks closest to the Northeast Zone are substantially higher in the section than those adjacent to the Southeast zone.

The Northeast Zone has the highest Ag content of the ore zones and shows the most clearly hydrothermal features in the breccia. The Northeast zone is the only ore zone in the cluster with widespread sericite-bearing alteration assemblages. In the deepest observed portions of the Northeast zone, K-feldspar constructive alteration is similar to that reported in the central ore zones (Fraser et al., 1995, Panteleyev et al. 1996, Rees et al., 2005).

The Cariboo-Bell and Springer zones in the center of the group contain hydrothermal and intrusion-cemented breccia- and vein-hosted sulfide minerals associated with roughly concentric alteration assemblages around a Cu-Au–rich core (Fraser et al., 1995). The central potassic (including albite, biotite, and actinolite subfacies) core is surrounded by an intermediate garnet-epidote zone and an outer propyllitic zone (Figure 1.5).

Chalcopyrite and minor bornite are the main sulfide minerals. Sparse pyrite is present distal to the core of the deposit, and magnetite is abundant in the central and deep portions of the orebody. Sulfide deposition accompanies K-feldspar veins and wall rock replacement. Alteration and sulfide deposition can be sequenced by multiple K-feldspar phyric porphyry intrusions (Figure 1.6). Cu:Au:Ag ratios are intermediate between the Northeast and Southeast zones.

Fraser (1994a, b; Fraser et al., 1995) divided the hydrothermal breccias in the Cariboo-Bell and Springer deposits into four types, based on dominant silicate cement mineralogy: biotite, actinolite, albite and magnetite. Albite-cemented breccia in the Springer ore zone is characterized by the presence of tabular albite and lesser biotite, magnetite and sulfides as breccia cement. Clast boundaries are diffuse and albite has extensively replaced the clasts. Biotite- and actinolite-cemented breccia characterize the Cariboo and Bell zones. The actinolite-cemented breccia dominates the Bell ore zone, whereas the biotite-cemented breccia dominates the Cariboo zone (Figure 1.5). Fraser et al. (1995) reported that the transition between the two breccia cements is gradational. Actinolite or biotite forms the dominant breccia cement and contains Cu-Fe sulfide minerals in varying amounts. In the actinolite breccia, K-feldspar replaces breccia clast margins and also forms alteration selvages around actinolite-sulfide veins that cut the country rock and breccia. In the biotite-cemented breccia, the clasts are moderately to completely replaced by K-feldspar (Fraser, 1994b). Albite-cemented breccia overprints actinolite-cemented breccia in the northern part of the Bell pit.

Magnetite-cemented breccias are uncommon (Fraser, 1994b). Where present, however, they are commonly associated with elevated Cu concentrations (Imperial Metals

Corporation, 2007b). Clasts in these breccias are also partially replaced by K-feldspar. Sulfide and sparse pyroxene are also present as breccia cement.

Another notable feature which supports this zoning is the unconformity present at the northern end of the Mount Polley property. This unconformity juxtaposes 205.2 ± 1.2 Ma Mount Polley Intrusive Complex Monzonite with a 196.7 ±1.7 Ma clastic-infill dominated breccia of unknown origin (Bailey and Archibald, 1990; Mortensen et al., 1995; Logan et al., 2007). The Northeast Zone is the closest (<500 m), spatially and stratigraphically, to this unconformity, and the Southeast zone is the farthest (3.5 km) (Figure 1.2).

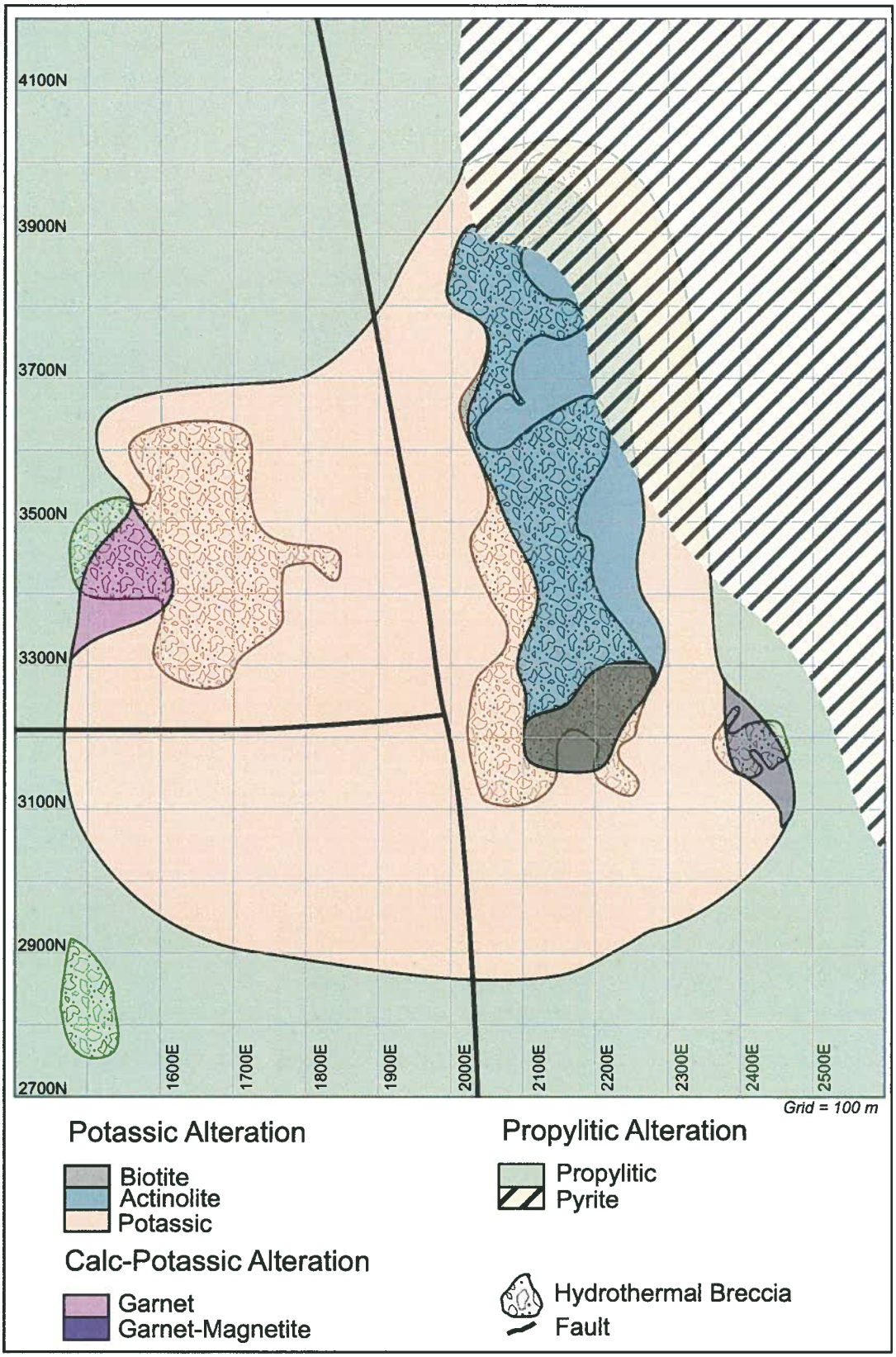

Figure 1.5-Alteration in the Central Zone at Mount Polley, redrafted from Fraser, 1995.

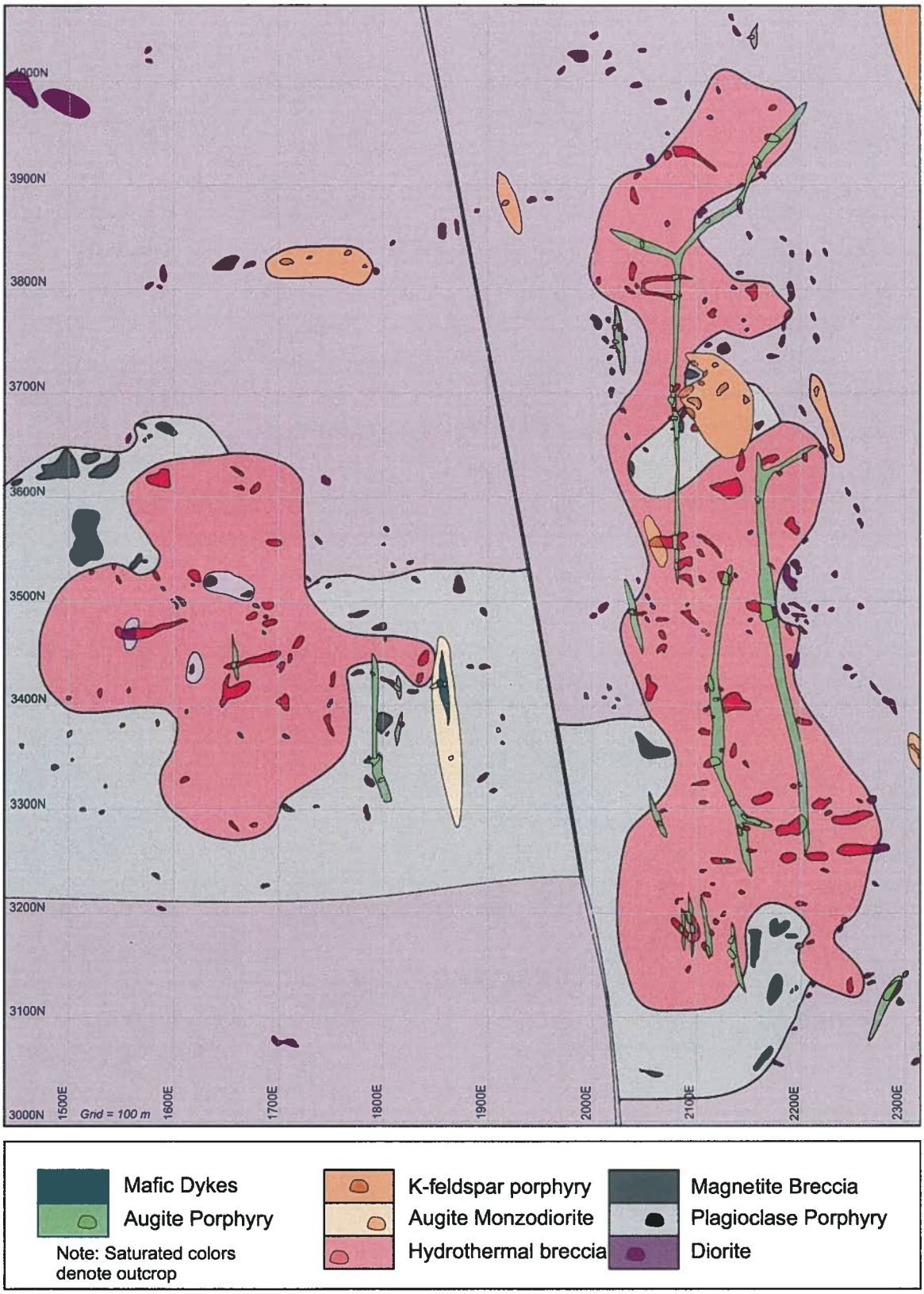

Figure 1.6-Lithology of the Central Zone at Mount Polley, redrafted from Fraser, 1995.

The inferred vertical positions of the ore zones are also based on their positions relative to regional stratigraphy (Panteleyev et al., 1996; Logan and Mihalynuk, 2005). The regional volcanic stratigraphy is folded into a moderately dipping post-mineral syncline plunging to the north-northwest (Logan et al., 2007). Extending this structure into the MPIC, the Northeast zone is located stratigraphically high within the regional syncline, and the Southeast zone is located the deepest within the regional syncline (Rees et al., 2005). Alteration characteristics of each ore zone, as discussed above, are consistent with this structural reconstruction and with alteration zoning observed at other Cu-Au porphyry deposits (Holliday and Cooke, 2007; Lickfold et al., 2007; Logan et al., 2005).

Alteration zonation in alkalic porphyry systems is relatively consistent worldwide (Jensen and Barton, 2000; Holliday and Cooke, 2007) (figure 1.5, 1.7). Mineralization is commonly associated with potassic and calc-potassic alteration assemblages within and surrounding small volume alkalic intrusions (Jensen and Barton, 2000, Sillitoe, 2002, Deyell and Tosdal, 2005). Mineralization is associated with hematite dusting of the feldspars in the rock, negative S isotopes, increased magnetic susceptibility, and anomalous Pb-Zn (Holliday and Cooke, 2007 and references therein). Mineralization is surrounded by a propyllitic halo featuring albite-actinolite (inner) and albite-epidote (outer) zones. Argillic alteration occurs above the stratigraphic level of ore deposition and along structures penetrating the ore body (Holliday and Cooke, 2007).

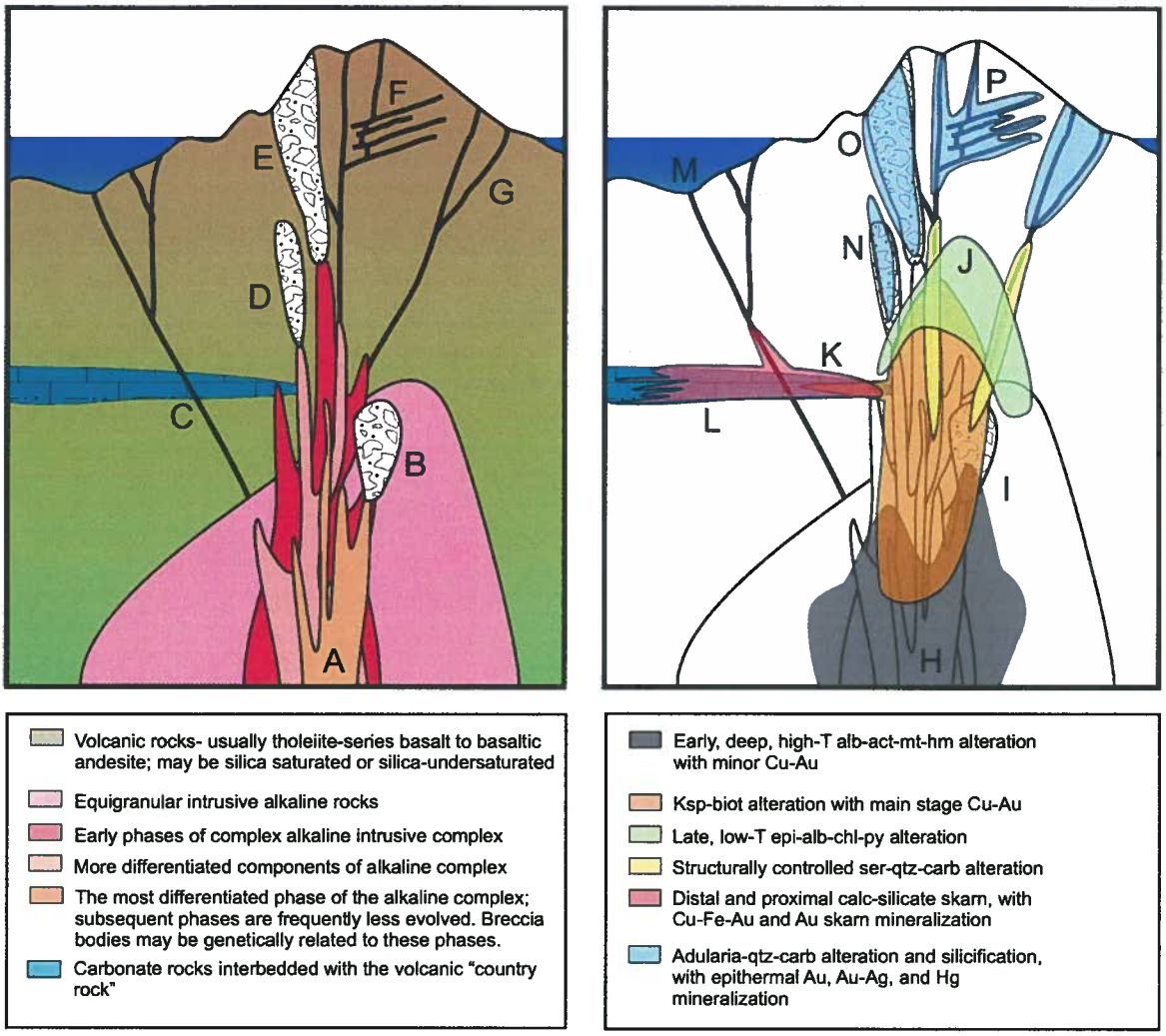

Figure 1.7- Common characteristics of mineral deposits related to alkalic intrusions. A: Complex, small volume alkaline intrusions (Cadia/Ridgeway, Goonumbla, Skouries, Mount Polley); B: Hydrothermal and magmatic breccias (Mount Polley, Galore Creek); C: Fault and vein systems (Nogal-Bonito, NM); D: Subvolcanic breccia systems that fail to breach the surface (Bessie G, CO); E: Shallow, large volume volcanic and subvolcanic breccia systems, including intracaldera structures (Cripple Creek, CO, Ladolam, PNG); F: Flat lying intra volcano and intracaldera vein and fracture systems (Emperor, Fiji); G: Steep vein and fracture systems (La Plata, CO); H: Deposits with magmatic and near-magmatic sulfide textures (Lorraine, BC, Bootjack Stock, BC); I: Deposits with both hydrothermal and magmatic characteristics (Lorraine, BC); J: "Typical" alkalic porphyry deposits associated with potassic and propyllitic alteration (Mount Polley, Galore Creek, Mt. Milligan, Cadia-Ridgeway); K: Proximal skarn deposits developed in carbonate or reactive volcanic rocks (Pond Zone at Mount Polley, Galore Creek); L: Distal skarn and carbonate replacement deposits, 'telethermal' deposits related to alkalic magmatism M: Alkalic-related VHMS deposits N: Epithermal mineralization infilling subvolcanic breccias (Bessie G., CO); O: Epithermal mineralization infilling diatreme breccias (Cripple Creek, CO) P: Low-sulfidation epithermal systems with sericite-roscoelite-fluorite-carbonate assemblages (Ladolam, Emperor, Porgera)

Describing the alteration, mineralization and brecciation processes which formed the Northeast Zone orebody at Mount Polley will provide clues to what may be the shallowest depths of an alkalic porphyry system. Analysis of this portion of the system, its relationship to the deeper portions of the same system (represented by the other ore zones in the group), and how it compares to and contrasts with similar portions of calc-alkalic systems, will increase understanding of the upper portions of alkalic orebodies as a class. Analysis of the uppermost levels of the porphyry system may also provide clues to the linkage between porphyry and epithermal ore deposition environments, aiding exploration for epithermal systems in porphyry districts and vice versa.

Thesis objectives

The Northeast Zone at Mount Polley presents an unusual view of an unusual type of porphyry deposit. This thesis describes previous work performed on the Mount Polley deposit, its regional setting, and the ore deposit itself. The igneous rocks that surround and cut the hydrothermal breccia body, which hosts mineralization, are described, and the characteristics and internal architecture of the breccia body are presented. Description of the breccia body yields insights into the physical evolution of the fluid system; description of the associated alteration assemblages yields insights into the chemical alteration of the fluid system. Finally, a hypothesis is advanced to explain the relationship between intrusion, brecciation, alteration, and mineralization.

Chapter 2-Background and Previous Work

Introduction

The Mount Polley deposit has been known since the 1960s, and since that time a considerable mass of work has been produced addressing the geology and geologic setting of the deposit. This chapter addresses the previous body of geologic literature dedicated to the Mount Polley area, the exploration and production history of the Mount Polley mine, and summarizes the regional and local geology of the Quesnel and adjacent terranes in which the Mount Polley deposit formed. Research carried out by other workers on the Mount Polley deposit and internal research undertaken by Imperial Metals and the Mount Polley Mining Corporation is summarized here to provide a deposit-scale and regional-scale context for discussion of the Northeast Zone.

This chapter introduces the magmatic evolution of the igneous rocks spatially, genetically and temporally associated with the Mount Polley deposits. This magmatic evolution is more fully developed in Chapter 3.

Previous Work

Literature review

Placer gold localities in the Quesnel Lake/Cariboo Mining district were documented as early as 1877 (Dawson, 1877; Bowman, 1895), describing activity beginning in around 1859. The volcano-sedimentary package in the Quesnel River area was first described and ascribed a Mesozoic age by Bowman (1889). Studies in the 1950s and 1960s, conducted mainly by the Geological Survey of Canada, formalized and refined this stratigraphy, recognizing that the "Quesnel River Beds" defined a volcanic belt that was

nearly contiguous throughout the Canadian Cordillera (Tipper, 1959, 1978; Campbell, 1961, 1963; Campbell and Campbell, 1970; Campbell, 1978). The regional-scale syncline in which the Mt. Polley deposit sits was first described as the "Quesnel Trough" by Roddick et al. (1967).

The relationship between the Quesnellia terrane and adjacent accretionary terranes at the latitude of Mount Polley has been extensively studied (Campbell, 1971; Montgomery, 1978; Fillipone, 1985; Elsby, 1985; Montgomery, 1985; Ross et al, 1985, 1989; Carye, 1986; Struik, 1986, 1988a and b; Bloodgood, 1985, 1987; Rees 1981 and 1987; Rees and Ferri, 1983 Radloff, 1989). The alkaline nature of the volcanic and intrusive rocks of the Quesnellia terrane was first recognized by Fox (1975). Studies by Hodgson et al. (1976), Bailey and Hodgson, (1979), Fraser et al., (1995), and Wild, (1999) examined the central ore zones of the deposit. More recent regional-scale work in the Mount Polley area has been completed by Logan and Mihalynuk (2005), Logan and Bath (2005, 2006), and Bath and Logan (2006), and Logan et al., (2007).

Panteleyev et al. (1996) compiled a comprehensive study of the geology and mineral deposits of the Mount Polley area. Fraser (1994) a; b, and Fraser et al. (1995), investigated the alteration and mineralization of the "central zone" deposits of the Mt. Polley complex. Bailey and Hodgson (1979) examined breccias of the Cariboo-Bell area. Deyell (2005) and Deyell and Tosdal (2005) investigated S isotope variations for the southern area of the then-newly discovered Wishbone (now Northeast Zone) orebody. Rees et al. (2005, 2006) summarized the geology of the district, showing the spatial relationship between the host volcanic rocks, intrusions, and breccia. Lang et al. (1995)

examined the alteration and igneous fertility of the intrusive rocks associated with the Mount Polley deposits in comparison with those of other alkalic porphyries in BC.

History of the Mount Polley Deposit

Property Discovery

Although placer gold was known in the Mount Polley area in the 19th century and hydraulic mining was widespread and productive (Cockfield and Walker, 1932; Cockfield, 1948; Levson and Giles, 1993), heavy cover, both vegetative and fluvioglacial (Blackwell and Stubley, 2005; Levson, 2001; Tipper, 1971), inhibited the discovery of lode deposits despite known copper occurrences. A follow-up prospecting study conducted after a government airborne magnetic survey map issued in 1963 showed an aeromagnetic anomaly and demonstrated the existence of the Mt. Polley/Cariboo-Bell Cu-Au deposit (Panteleyev et al., 1996).

Exploration

Initial development and prospecting on the property was done by Mastodon Highland Bell Mines Limited and Leitch Gold Mines, which merged to form Cariboo-Bell Copper Mines Limited in 1966. In 1969, control of the property was taken by the Teck Corporation, and work continued intermittently until a Teck affiliate, Highland Crow Resources, acquired control in 1978 (Rees et al., 2005). In 1981, the property was optioned by E&B Explorations, which acquired 100% interest in 1982. Imperial Metals Corporation and Geomex Partnerships joined the project as joint venture partners in 1987, but intensive evaluation work on the property did not begin until 1990 (Caldwell, 2005). In 1990, a feasibility report on the property was completed by Wright Engineers,

proposing a 5 million tonne/year plant. E&B Explorations merged with Mascot Gold Mines, which in turn merged with Corona Corporation and ultimately became Homestake Canada. Between 1987 and 1992, Imperial Metals bought out the interest held in the Mt. Polley property by Homestake Canada and others, acquiring Geomex partnerships in 1992 to become the sole owner of the deposit. A downturn in metals prices resulted in the project being furloughed. In 1994, Imperial Metals merged with Bethlehem Resources, which had a long-standing relationship with Sumitomo Corporation (Rees et al., 2005; Caldwell, 2005).

Development

The decision to pursue further development of the Mt. Polley property was made in 1996, and financing was arranged through the Sumitomo Corporation. Imperial Metals retained 55% interest and operational control over the project, and Sumitomo retained 45% interest (Caldwell, 2005). This joint venture, incorporated as the Mt. Polley Mining Corporation, commenced mining activities in 1997. Between 1997 and 2001, mining from the Cariboo and Bell pits produced 133 million pounds of copper and 370,000 ounces of gold from 27.7 million tones of ore milled (Rees et al., 2005). In 1998, Imperial Metals merged with Princeton Mining Corporation, thus assuming operational control over the Huckleberry Mine, near Houston, BC (Rees et al., 2005). In 2001, Sumitomo Corporation sold its interest in the Mount Polley property to Imperial Metals for $11 million. Shortly thereafter, having exhausted the reserve in the Cariboo pit and facing a $15 million pre-strip on the Springer pit, Mount Polley was placed on care and maintenance pending a rebound in metals prices (Caldwell, 2005).

Discovery of the Northeast zone

In 2003, on-site exploration resumed and a small, high-grade Cu-Au-Ag resource was discovered 1.5 km northeast of previously known mineralization (Rees et al., 2005). The area was previously mapped as volcaniclastic rock and included with the post-mineral cover located farther to the north and west (Figure 1.2), (Bailey and Hodgeson, 1979, Fraser et al., 1995). In 2003, reconnaissance exploration aimed at identifying possible oxide-ore reserves discovered an area of high grade oxidized float. Tracing this float back to its origin, an outcrop of breccia grading 3% Cu was discovered. The first hole drilled in this zone intersected 57 meters grading 2.54% Cu, 1.15 g/t Au, and 17 g/t Ag. This hole was located 2 km northeast of the existing mill. The discovery of the Northeast Zone and subsequent expansion of proven and probably reserves under the Springer pit prompted an influx of capital in the project and into the company, bringing the operation back into active status. This deposit, initially called the Northeast zone or the Wishbone, is in the process of being developed as the Wight Pit. Pit development began in March, 2005.

Development of the Northeast zone

In 2005, the Mount Polley mine milled 4,814,084 tonnes of ore from the Wight Pit, the Bell pit, and low-grade stockpiles (Imperial Metals, 2007a). Separated statistics for the Wight pit alone are not available; the mill in place at Mount Polley was designed for the lower-grade ore produced by the Cariboo, Bell and Springer pits, and ore from the higher-grade Wight pit was diluted for metallurgical reasons. This milled tonnage resulted in the recovery of 30,328,771 lbs Cu, 30,635 oz Au, and 234,355 oz Ag in 2005. In 2006, 6,235,221 tonnes were mined, again dominantly from the Wight Pit, but

augmented from the Bell Pit and low-grade stockpiles. This milled tonnage resulted in the recovery of 55,548,194 lbs Cu, 38,164 oz Au, and 422,588 oz Ag (Imperial Metals, 2007a and b). As of the date of writing, production has not been announced for 2007.

Reserves and resources at Mount Polley

Overall, the various deposits constitute proven and probable reserves of 59.9 Mt of ore containing 0.36% Cu, 0.27 g/t Au and 0.73 g/t Ag (Imperial Metals, 2007a) (Table 2.1). Measured and indicated resources include 73.570 Mt of ore at 0.356% Cu, 0.302 g/t Au, and 1.426 g/t Ag. The Northeast zone orebody, the focus of investigation during this project, contains a proven and probable reserve of 4.31 Mt of ore at 0.829% Cu, 0.268 g/t Au, and 5.929 g/t Ag. Measured, indicated and inferred resources outside the planned pit in Northeast zone total 17.520 Mt of 0.8% Cu, 0.2 g/t Au and 4.4 g/t Ag (Imperial Metals, 2007). This resource excludes the results of two years of production, totaling 11.049 Mt of 0.438% Cu and 0.278 g/t Au.

Table 2.1: Reserves and resources for the Mount Polley orebody, from www.imperialmetals.com

PROVEN AND PROBABLE RESERVES, BY MODELED PIT					
Zone/Pit	Wight	Bell	Springer	Southeast	**Total**
Tonnes Ore	7,935,000	6,675,500	24,266,000	2,100,402	**40,976,902**
Copper %	0.871	0.297	0.367	0.273	**0.448**
Copper (lbs)	152,323,086	43,768,815	196,270,751	12,641,391	**405,004,043**
Gold g/t	0.282	0.316	0.313	0.514	**0.318**
Gold (oz)	72,040	67,773	244,458	34,710	**418,980**
Silver (oz)	1,621,772	n/s*	n/s*	81,238	**1,703,010**

MEASURED, INDICATED AND INFERRED RESOURCES, BY ZONE (excludes pit reserves)					
Zone	**Tonnes**	**Copper Equivalent**	**Copper %**	**Gold g/t**	**Silver g/t**
Northeast					
Measured	14,297,702	0.779	0.609	0.190	4.384
Indicated	1,387,308	0.830	0.636	0.221	4.616
Inferred	1,835,195	0.773	0.600	0.197	4.160
Bell					
Measured	9,562,373	0.420	0.233	0.238	n/s*
Indicated	976,160	0.376	0.227	0.190	n/s*
Inferred	828,312	0.372	0.236	0.174	n/s*
Springer					
Measured	20,033,640	0.554	0.342	0.270	n/s*
Indicated	12,865,244	0.531	0.318	0.272	n/s*
Inferred	23,055,896	0.519	0.282	0.302	n/s*
C2					
Measured/Indicated	5,891,159	0.475	0.236	0.304	n/s*
Inferred	1,448,995	0.450	0.223	0.288	n/s*
Southeast					
Measured/Indicated	14,229,738	0.622	0.247	0.462	1.338
Total Resource					
Measured/Indicated	79,243,324	0.584	0.352	0.287	n/s*
Inferred	27,168,398	0.528	0.299	0.290	n/s*

ns*-Silver only economically significant in the Northeast Zone

Regional geology

Geology of Quesnellia

The Quesnel terrane is an accreted island arc terrane characterized by alkalic and lesser calc-alkaline volcanism and magmatism that extends from south of the U.S. border to north-central British Columbia (Lang et al, 1995). Quesnel rocks range in age from 230 to 180 Ma (Bailey and Archibald, 1990; Mortensen et al., 1995; Logan et al., 2007). The latter date may reflect the date of docking with the North American craton (Mortensen et al., 1995). The characteristic components of Quesnellia are Middle Triassic to Early Jurassic volcanic, sedimentary and plutonic assemblages, which formed in an island arc volcano-plutonic tectonic setting. The Quesnel arc is similar in age and chemistry to the Stikine arc to the west.

Quesnellia hosts several major porphyry copper deposits of both alkaline and calc-alkaline affinity, such as Highland Valley, Copper Mountain, Afton-Ajax and Mount Milligan, all generated by early Mesozoic, island-arc magmatism (McMillan et al., 1995).

Extrusive rocks of the Mount Polley Area

The regional and district scale lithology at and around Mount Polley has been examined in detail by Panteleyev et al. (1996), Logan and Mihalynuk (2004), Logan and Bath (2005 and 2006), and Bath and Logan (2006). The subdivision of the stratigraphic units as described here is that of Panteleyev et al (1996), as modified by Rees et al. (2005) based on Imperial Metals mapping of the Mount Polley property (Figure 2.1, Table 2.2). The regional 'basement' in the Mount Polley area consists of the Nicola Group.

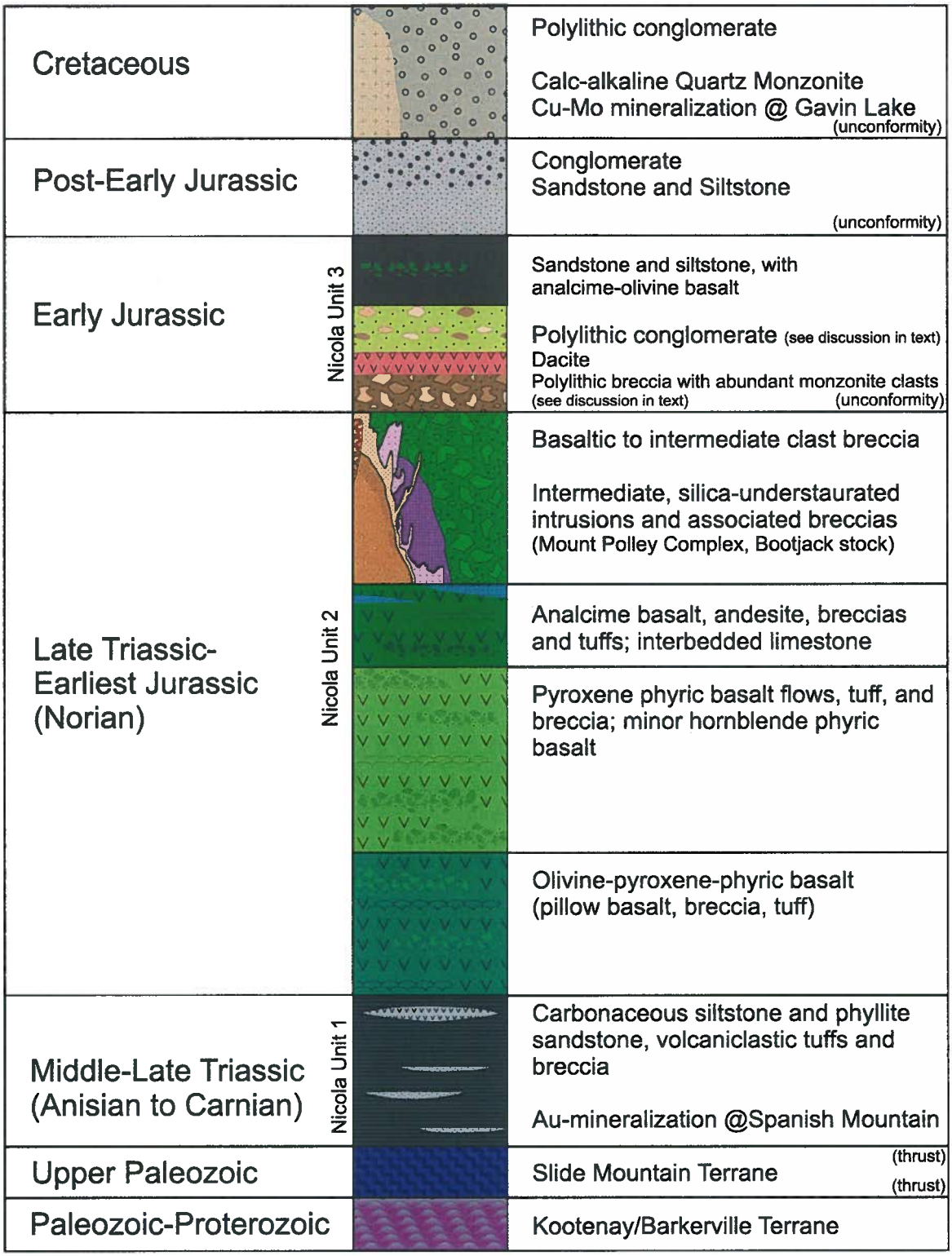

Figure 2.1-Stratigraphy of the Mount Polley Area; from Logan et al., 2007; Logan and Bath, 2005 and 2006; Rees et al, 2005; Logan and Mihalynuk, 2004; Panteleyev, et al., 1996; Bloodgood, 1990; Bailey, 1978

Table 2.2- Selected geochronology of the Nicola group, MPIC, and associated rocks; timescale in accordance with Okulich, 2001

UNIT	ROCK TYPE	DATE	DATING METHOD	SOURCE
1	Limestone	Anisian-Ladinian	Conodonts	Orchard, 1995; Bloodgood, 1990
1a	*	*	*	Panteleyev et al., 1996
2	Limestone	Norian	Fossils	Orchard, 1995
2a	Pyroxene basalts	Carnian-Norian	Fossils	Panteleyev et al., 1996
2b	*	*	*	Rees et al., 2005
2c	*	*	*	Rees et al., 2005
2d	*	*	*	Rees et al., 2005
2e	*	*	*	Rees et al., 2005
MPIC	Diorite	201.7±4 Ma	U-Pb zircon	Mortensen et al., 1995
	Plagioclase Porphyry	204.7±3 Ma	U-Pb zircon	Mortensen et al., 1995
	Pyroxene Monzonite	165.2±1.8 Ma	$^{40}Ar/^{39}Ar$	Logan et al., 2007
	K-feldspar syenite porphyry	205.01±0.3 Ma	U-Pb zircon	Logan et al., 2007
	Misc.	Upper Triasic	U-Pb zircon	Palfy et al., 2000
Bootjack Stock	C.g. Syenite	203.1±2.0 Ma	$^{40}Ar/^{39}Ar$	Bailey and Archibald, 1990
	Orbicular syenite	202.7±7.1 Ma	U-Pb zircon	Mortensen et al., 1995
	Psuedoleucite syenite	200.7±2.8 Ma	Pb-Pb titanite	Mortensen et al., 1995
Other local stocks	Shiko Lake stock	196±7 Ma	K/Ar	Panteleyev et al., 1996
		192±10 Ma	K/Ar	Panteleyev et al., 1996
		182±6 Ma	K/Ar	Panteleyev et al., 1996
	Woodjam stock	193.0±1.2 Ma	$^{40}Ar/^{39}Ar$	Logan et al., 2007
		192.2±1.1 Ma	$^{40}Ar/^{39}Ar$	Logan et al., 2007
	Gavin Lake stock	161.77 ±0.99 Ma	$^{40}Ar/^{39}Ar$	Logan et al., 2007
		162.5±0.86 Ma	$^{40}Ar/^{39}Ar$	Logan et al., 2007
		160.0±2.3 Ma	U-Pb zircon	Logan et al., 2007
3	*	*	*	Rees et al., 2005
3a	*	*	*	Rees et al., 2005
3b	Dacite	196.7±1.3 Ma	U-Pb zircon	Logan et al., 2007
3c	*	*	*	Rees et al., 2005
4	Limestone	Sinemurian	Fossils	Bailey, 1988

*-Most units within the Nicola Group have not been dated near the latitude of Mount Polley.

The basal unit of the Nicola Group (unit 1) is a 2,500-4,000 m thick sequence of fine grained graphitic to quartzose sedimentary rocks, which grade upwards into the basal unit of the overlying volcanic sequence. Unit 1 is referred to as the "basal black phyllite" and is dominated by black phyllites, siltstones, and shales. Locally, near the contact between the Quesnel terrane and the eastward Cariboo-Kootenay terrane rocks, this unit is highly deformed. The basal black phyllite hosts gold-bearing quartz-pyrite veins at the Spanish Mountain prospect, owned and operated by Skygold Ventures Ltd. The basal black phyllite is described in more detail by Bloodgood (1987a-c, 1988, 1989 and 1990), Rees (1987) and Panteleyev et al. (1996). The unit 1 sedimentary rocks are deposited onto ocean floor rocks of the Slide Mountain terrane. They are interpreted to reflect sedimentation into a low-energy, comparatively deep-water sedimentary environment, probably a restricted marginal basin environment (Rees et al., 2005).

The basal black phyllite is conformably overlain by and grades into mafic hornblende and pyroxene volcaniclastic breccia, conglomerate and tuffaceous argillite. Clasts of the volcanic rocks are found within the uppermost sedimentary beds of unit 1, suggesting that earliest volcanic activity occurred during latest sedimentation. Logan and Bath (2005) identify this unit as unit 1A. The rocks of unit 1A, referred to by Logan and Bath (2005) as the Eastern arc basalt, are petrochemically and stratigraphically distinct from the other volcanic rocks in the sequence (Panteleyev et al., 1996). Unlike the later rocks in the sequence, the volcanic rocks of unit 1A are tholeiitic rather than alkaline in composition. These rocks are interpreted to represent the onset of arc volcanism in a marginal basin setting (Logan and Bath, 2006). The rocks of unit 1A are found entirely within the sedimentary rocks of unit 1.

Conformably overlying the rocks of unit 1 and 1A is a 3,000 m sequence of subaqueous and lesser subaerial volcanic and volcaniclastic rocks (Panteleyev, 1987 and 1988; Panteleyev and Hancock, 1989). These rocks are defined by Logan and Bath as unit 2 and subdivided by Rees et al. (2005) as units 2a-e. The base of this sequence is dominated by fine- to medium-grained volcaniclastic rocks with lesser volcaniclastic breccia. Coherent fine to medium grained volcanic flows are volumetrically minor. Compositionally, this unit is dominated by green and maroon olivine-pyroxene phyric basalt. Pillow basalt is locally present, but the unit is dominated by fine- to medium-grained volcaniclastic breccias and fine-grained basaltic tuffs. The olivine-pyroxene units (unit 2A, figure 2.2) are conformably overlain by pyroxene-phyric flows, tuffs, and breccias, with minor hornblende-bearing basalt. This sequence is subdivided by Panteleyev but that subdivision was abandoned by Rees et al. (2006) and Logan and Bath (2006), who preferred the general term "pyroxene basalt". The pyroxene basalt has a higher proportion of flows and coherent rocks than the breccia-dominated olivine-pyroxene basalt, and less abundant volcaniclastic breccias. Pillows are rarer in the pyroxene basalt than in the underlying pyroxene-olivine basalt. The pyroxene basalt is conformably overlain by analcime basalt and basaltic-andesite. The upper units of the analcime basalt are interbedded with and locally capped by thin lenses of limestone, which locally form mappable units (Logan and Mihalynuk, 2004; Logan et al., 2007). The analcime basalt (unite 2e, Panteleyev et al., 1996) is dominated by subaqueous flows with minor pillows, volcaniclastic breccia, and tuffs. The analcime basalt is defined as unit 2e by Panteleyev et al (1996).

The volcanic succession is cut by a series of intrusions, most notably the Mount Polley Intrusive Complex (MPIC), which will be reviewed in more detail below, and the Bootjack stock. The Bootjack stock, as described by Bath and Logan, 2006, is a complex intrusion dominated by coarse-grained nepheline syenite with lesser K-feldspar syenite and fine-grained melasyenite. Both suites and their relationship to each other will be discussed in more detail below. The Bootjack stock, the MPIC, and the basalt sequence of Panteleyev's unit 2 are truncated by an unconformity juxtaposing 205 Ma intrusive rocks with 196 Ma breccia of unknown origin (Logan et al., 2007). This sequence, from the onset of olivine-pyroxene basalt volcanic activity through the end of analcime-basaltic andesite volcanic activity, is interpreted to reflect the main stage of arc activity. These rocks are alkaline in composition and share petrogenetic affinities (Logan and Bath, 2005).

Unconformably overlying the analcime basalt and the intrusive suites is a breccia of uncertain origin. Panteleyev et al. (1996) identify it as a volcaniclastic unit, unit 3A. The breccia is maroon in color, matrix-dominated and polylithic. It contains both volcanic- and intrusion-derived clasts and the geometry and contract relationships of the unit are still unclear (Logan et al. 2007). This breccia unit is conformably overlain by a thin unit of dacite tuff, which is in turn conformably overlain by a unit of volcaniclastic conglomerate containing rounded clasts of monzonite and underlying volcanic units. These two units are defined by Panteleyev et al. (1996) as units 3B and 3C. The conglomerate unit is similar in composition and internal organization to the breccia underlying the dacite, with the exception of having rounded rather than angular clasts (Panteleyev et al., 1996).

These units are believed to reflect the mature stage of arc formation and to be related to the erosion and redistribution of volcanic-derived material (Panteleyev et al., 1996). The conglomerate grades into a series of sandstones and siltstones interbedded with thin beds of analcime basalt. This unit is in turn overlain by a series of sedimentary conglomerates, sandstones and siltstones.

Mount Polley Intrusive Complex

All known mineralization in and around the Mount Polley property is located within 2-3 km of Mount Polley Peak, and is associated with the igneous rocks and breccias of the Mount Polley Intrusive Complex (MPIC) (Imperial Metals, 2007a). This study uses the term MPIC as advocated by Rees et al. (2006) in preference to the term Mount Polley Stock used by other workers (Panteleyev et al., 1996), as it better reflects the complex construction of this multi-generational pluton. The MPIC is a compound intrusion dominated by nepheline-normative monzonites, monzodiorites, diorites and syenites. Outside this intermediate to felsic volcanic center, the geology is dominated by intermediate to mafic volcanic rocks as summarized previously. Rees et al. (2006) divided the complex into a number of subunits (Figure 2.2). These subunits range from diorites through K-feldspar and psuedoleucite porphyries.

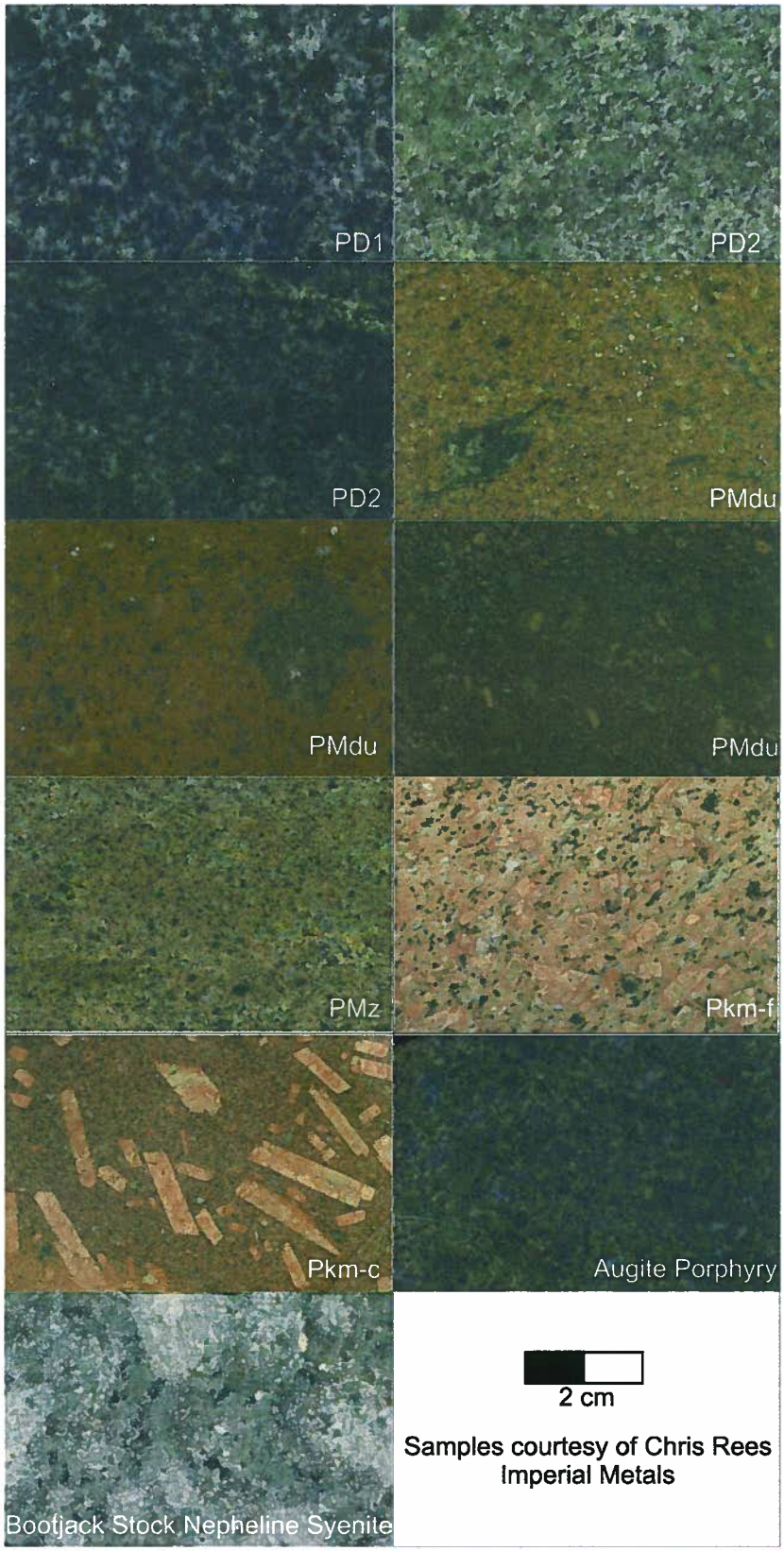

Figure 2.2-Intrusive rocks of the Mount Polley Intrusive Complex. Abbreviations explained below.

Augite-biotite diorite (PD1)

The oldest generation of intrusive units is an equigranular augite-biotite diorite dominated by augite and plagioclase but containing up to 20 vol. % K-feldspar (figure 2.3). Minor biotite, hornblende, and magnetite are present, generally composing <5 vol. % of the rock. This unit may be equivalent to the augite monzonite of Fraser (1994), although the profusion of augite-bearing equigranular monzonites and monzodiorites of various relative ages throughout the complex make direct correlation difficult. Disseminated pyrite is present in the PD1 but not common, and sparse disseminated chalcopyrite in present in the unit within the Springer pit and adjacent to the Bell pit.

K-feldspar-bearing diorite (PD2)

A more feldspar-rich diorite unit (PD2) is inferred to intrude PD1. The unit contains rocks with varying textures, all of dioritic, leucodioritic to monzodioritic composition (figure 2.3). Intrusive contacts with other units are not observed. Instead, PD2 contacts are gradational with intruding units, especially with the Polley monzodiorite (PMDu) (see below). PD2 is distinguished from PMDu by its lower K-feldspar content. Overall, PD2 rocks are variable, ranging from fine to coarse grained, and dominantly inequigranular, with slightly coarser plagioclase phenocrysts in a finer grained groundmass. Plagioclase phenocrysts are generally not more than 2-3 mm long. Slightly more mafic xenoliths, possibly of PD1, are common in the PD2 and contribute to the textural and compositional heterogeneity of the unit. Some xenoliths have gradational contacts with the bulk of the rock, whereas others are resorbed, suggesting reaction between xenoliths and magma.

Locally, PD2 is contains up to 5 vol % pyrite in leucodiorite. Distinguishing the PD2 from the PMdu is complicated by the presence of K-feldspar alteration, which alters plagioclase to K-feldspar, giving the rocks a creamy pink color.

Undifferentiated Monzodiorite (PMdu)

Polley monzodiorite (PMdu) represents the bulk of the igneous complex. Equigranular augite-bearing monzonite dominates the unit, with lesser K-feldspar-bearing diorite, monzodiorite, and K-feldspar-phyric monzonite porphyry. The PMdu is differentiated from the PD2 by the presence of primary K-feldspar, although K-feldspar is usually less abundant than plagioclase where this rock is comparatively unaltered. The PD2 and the PMdu are juxtaposed by the East Cariboo fault (Fraser, 1994). In the Springer area, PMdu intrudes PD1, establishing the igneous chronology.

The PMdu is extremely variable and encompasses rock units defined by other workers as diorites, monzodiorites, or "plagioclase porphyry" (Fraser, 1994). The PMdu is creamy grey to pinkish grey where least altered. The PMdu is equigranular to microporphyritic, and can range from fine- to coarse-grained. Albite-constructive alteration and weathering of this unit can cause plagioclase phenocrysts to stand out, resulting in the identification of this unit as plagioclase porphyry by other workers (e.g. Fraser, 1993). Augite is the most common mafic mineral in the PMdu, with hornblende locally abundant along with sparse primary, euhedral biotite. Locally, hornblende is more abundant than augite.

Xenoliths of more mafic rock are common in PMdu. These locally compose up to 25% of the rock. Inclusions are most commonly angular or irregular in shape, although smaller inclusions are frequently rounded or even amoeboid. Most inclusions are fine-grained to

aphanitic and pyroxene-rich. They may be glomerocrysts of mafic minerals, enclaves of mafic material, or xenoliths of fine-grained mafic rock. Other medium- to coarse-grained inclusions contain plagioclase and/or K-feldspar. Texturally and mineralogically, these inclusions resemble the PD1 and PD2 units. Disseminated pyrite and thin (<1 mm) pyrite veins are common in the PMdu, generally composing <1% of the rock.

Monzonite (PMz)

More homogenous, less-inclusion-rich monzonite (PMz) intrudes PMDu. These rocks are grey to pale pink, locally stained red or reddish orange. They are medium- to coarse-grained, generally coarser grained than PMdu, and contain more abundant mafic minerals (>10% augite and some primary biotite) than older rocks. Hornblende is not reported in PMz rocks. Where contact relationships are observed, PMz cuts PMdu.

K-feldspar monzonite porphyry (Pkm)

Locally, PMz and PMdu rocks are cut by dykes and irregular bodies of K-feldspar-phyric porphyry, known as Pkm. These bodies are generally elongate and less than a few tens of meters in map dimension. They trend NNW and dip steeply, often near-vertical. Pkm rocks are divided by Rees and Ferriera (2006) into two groups, the "coarser" Pkm and the "finer" Pkm.

The coarser Pkm is distinguished by K-feldspar phenocrysts 1-4 cm long. The K-feldspar phenocrysts are notably stubby or blocky in appearance and set in a coarse to medium grained groundmass. Phenocrysts are frequently aligned parallel to the margins of the intrusive bodies; in smaller dykes the texture is strongly trachytic. Phenocryst content varies markedly. In some areas, Pkm only contains 1-2% phenocrysts and appears to grade into the PMdu, especially in the Southeast zone. The groundmass of the coarser

Pkm contains plagioclase subequal to K-feldspar where least altered. The main mafic mineral in the Pkm is augite with lesser hornblende. Biotite commonly forms crystals up to 5 mm across.

The Pkm is almost always strongly altered; K-feldspar-constructive alteration with disseminated hematite is most common. Disseminated pyrite is common as is fine-grained disseminated chalcopyrite. Chalcopyrite is locally present, but is never abundant enough to constitute ore grades.

The finer Pkm is distinguished by phenocrysts ranging from a few mm to 1 cm in length. Phenocrysts are generally more abundant than those in the coarser Pkm, rarely composing more than 30% of the rock. Alignment of phenocrysts is common. Plagioclase phenocrysts are rare and generally smaller than K-feldspar phenocrysts where present (1-2 mm vs. 3-5 mm). The groundmass is finer than that of the coarser Pkm, and K-feldspar constructive alteration may make the ground mass appear finer still. As in the coarser Pkm, K-feldspar alteration is associated with hematite dusting, coloring the rock red or red-orange. In least-altered examples of this rock type, the groundmass of the rock is creamy to pinky grey and K-feldspar phenocrysts are pale pink. In most examples, the rock is red orange with pale orange or pink phenocrysts. The finer Pkm generally contains more xenoliths than the coarse Pkm. Lithic fragments resembling PMdu are most common, but medium- and coarse-grained lithic fragments resembling PD1 and PD2 are present as well. Fine-grained mafic inclusions such as those common in the PMdu are rare; local mafic inclusions are present within monzonitic xenoliths.

Augite Porphyry (AP)

Mafic to intermediate augite-phyric porphyry dykes are widespread in the Mount Polley complex (Rees et al., 2005; Ross, 2004a and b; Gillstrom, 2004). These dykes crosscut mineralized breccias and are generally unaffected by hydrothermal mineralization (Rees et al., 2005). The augite porphyry dykes vary more in orientation than any other dykes in the MPIC, and are generally controlled by faults. The augite porphyry dykes are characterized by a fine-grained, pale-green to pinkish-green groundmass containing 20-60% euhedral black augite phenocrysts. Sparse olivine phenocrysts have also been reported, typically replaced by iddingsite (Rees et al., 2005).

Bootjack Stock

To the south of the MPIC, the Bootjack stock is dominated by psuedoleucite syenite, orbicular psuedoleucite syenite, and melasyenite (Bath and Logan, 2005). The Bootjack stock is more silica-undersaturated than the MPIC, but U-Pb dates are within the error of dates from the MPIC (Table 2.2; Bath and Logan, 2005; Logan et al., 2007). The Bootjack stock is not spatially associated with economic Cu-Au mineralization or extensive hydrothermal alteration (Rees et al., 2005).

Summary

Regional volcanic rocks surrounding the MPIC reflect a trend of increasing differentiation (Logan et al., 2007). This pattern is continued within the MPIC, with the most mafic rocks (PD1 and PD2) occurring early in the development of the complex and the most feldspathic (Pkm) occurring closest to the time of brecciation and mineralization.

Chapter 3-Intrusive Rocks of the Northeast Zone

Introduction

The most salient feature of the Mount Polley deposit is the hydrothermal breccia (Rees et al., 2005; Bailey, 1978). This breccia hosts the majority of economic mineralization and presents the most striking visual feature of the deposit (Fraser, 1993, 1994 a and b; Fraser et al., 1995; Tosdal et al., 2008). The breccias at Mount Polley are, however, the product and the reflection of igneous as well as hydrothermal processes (Burnham, 1979 and 1985; Sillitoe, 1985; Jebrak, 1997; Cox et al., 2001; Gonnerman and Manga, 2003). These rocks reflect a physical and chemical evolution from the volcanic rocks into which the intrusive complex was emplaced, the intrusive complex itself and the intrusions that triggered brecciation, to the post-breccia and post-mineral intrusions which cut the breccia.

The rocks that make up the bulk of the Mount Polley Intrusive Complex (MPIC) were summarized in Chapter 2. Here, physical characteristics and cross-cutting relationships of the igneous rocks for the Northeast zone are presented, based on observations in core and hand sample. The physical and chemical evolution of the igneous rocks in the Northeast zones highlights the unusual nature of the syn-breccia intrusive phase, as well as the continuity of evolution from the earliest to the latest intrusive rocks.

Northeast Zone

Field relations

Igneous rocks examined in the Northeast zone are divided into four broad groups, according to their timing relative to the mineralized breccia (Table 3.1). The oldest rocks,

as determined by field relationships, were xenoliths observed as inclusions in the various igneous rocks. Xenoliths are included within pre-breccia rocks. This group includes the various rock types, which were observed as angular, mechanically-derived clasts within the breccia. The syn-brecciation group includes those rocks that were ductile or fluid at the time of the brecciation event. Post-breccia rocks cut the breccia. In some cases, particular rock types were observed both as dykes cutting the breccia and as clasts within the breccia (equigranular augite-bearing monzonite and equigranular hornblende-bearing monzonite). Despite their similarities, these rocks were considered as separate units based on their contact relations. In other cases, substantial intercepts of a single rock type which occurred both pre- and post-breccia were observed in core. Where these intercepts showed fine-grained or chilled margins against the breccia, they were considered to be post-breccia; where no obvious intrusive contact was observed, the intercept was assumed to reflect the presence of an oversized clast.

Table 3.1- Timing of rock types observed in the Northeast zone

TIMING	ROCK TYPES	EVIDENCE
Xenoliths in pre-breccia rocks	Fine-grained mafics, hornblende mafics, diorite, monzodiorite	Xenoliths in breccia clasts, syn-breccia clasts, and post-breccia dykes
Pre-breccia rocks	Equigranular monzonite, equigranular hornblende monzonite	Breccia clasts
Syn-breccia rocks	Megacrystic K-feldspar monzonite porphyry	Juvenile clasts in breccias
Post-breccia rocks	Multiple post-breccia dykes	Chilled/fine grained margins against breccia and other post-breccia dykes

Xenoliths

Four distinct xenolith types are present within pre-breccia rocks. The most common are angular, rounded and irregular "mafic" xenoliths as described by Rees et al. (2005, 2006) in the undifferentiated monzonite unit. Diorite and monzodiorite xenoliths are less

common. Hornblende-bearing mafic porphyry xenoliths were observed only in two locations. The xenoliths are most common in the pre-mineral equigranular monzonite, although they occur in the megacrystic monzonite porphyry as well. A few xenoliths are observed in the crowded K-feldspar porphyry. Xenolith abundance varies from absent to 5-7%, averaging around 1%. There is no systematic variation with depth or location; xenoliths occur in clusters throughout the pre-mineral equigranular monzonite and equigranular monzonite clasts within the breccia.

Biotite-magnetite "mafics"

"Mafic" xenoliths are common in the equigranular monzonite rock, which formed the majority of breccia clasts and of breccia country rock (figure 3.1). These xenoliths are most commonly angular to subrounded and 1-3 cm in diameter; in rare cases xenoliths up to 20 cm in diameter were observed. Irregular and ellipsoidal xenoliths were also observed; some of the xenoliths are tabular (figure 3.2). The mafic xenoliths are fine-grained and magnetic. In thin section, the xenoliths are composed of polycrystalline aggregates of secondary biotite, chlorite and magnetite, with rare pyrite (figure 3.3). The original mineralogy of the xenoliths, although certainly mafic, has been obscured by alteration.

The origin of the mafic xenoliths is unknown.

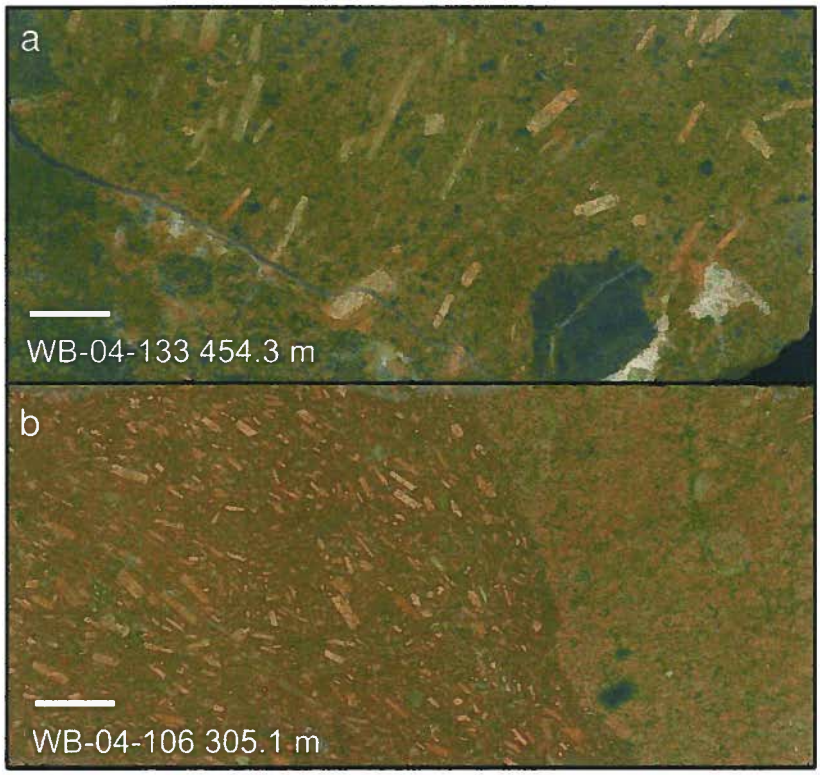

Figure 3.1; Photographs of mafic xenoliths in equigranular monzonite clasts in breccia (a) and in equigranular monzonite xenoliths in post-breccia K-feldspar porphyry dykes (b).

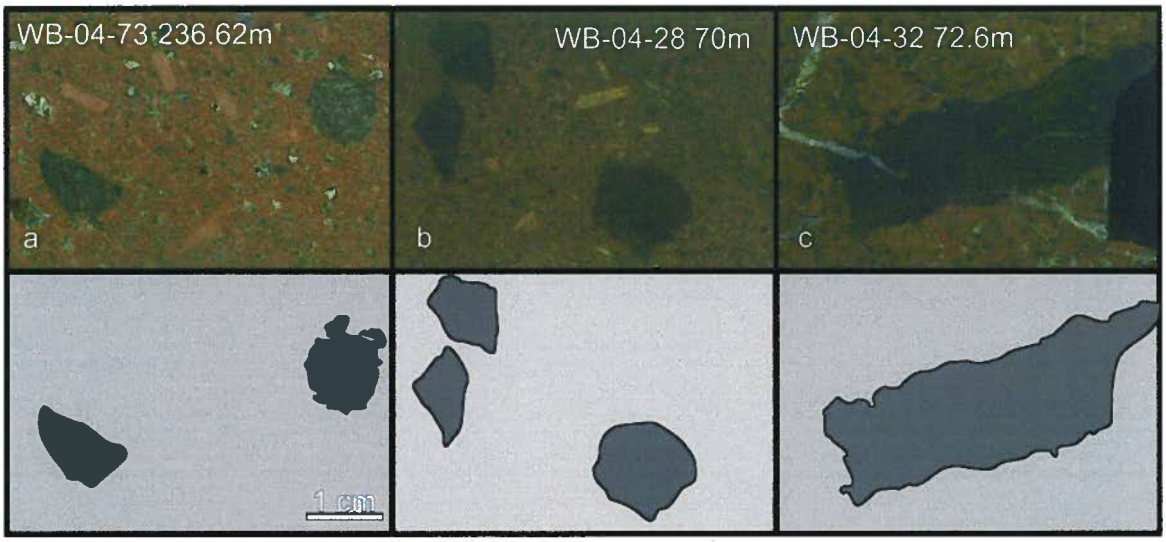

Figure 3.2-Photographs of angular (a,b) rounded (a.b) and tabular (c) mafic xenoliths. Line drawings included to highlight xenolith shapes. Scale bar equals 1 cm.

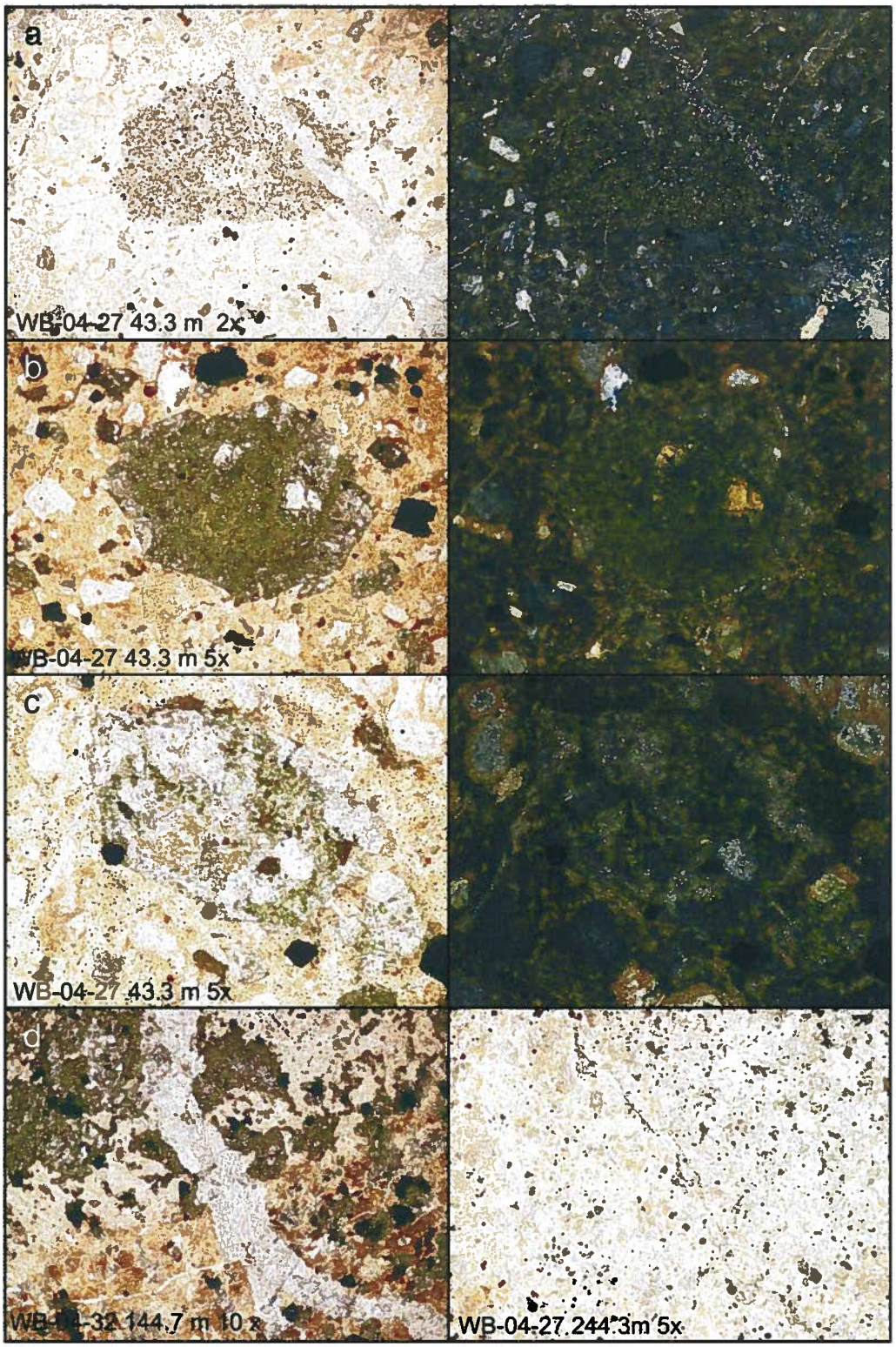

Figure 3.3-Photomicrographs of xenoliths in plane (left) and cross (right) polarized light. A; xenoltih replaced by chlorite and pyrite and crosscut by a post-mineral carbonate vein; b; Xenolith replaced by chlorite, with reaction rim between xenolith and host rock; c; partially replaced xenolith with some remnant plagioclase; d; higher magnification image of xenolith rim showing raggedness caused by polycrystalline replacement of orginal mafic minerals by chlorite and magnetite.

Diorite

A much rarer group of xenoliths are coarse grained, with 40-50% mafic minerals and 50-60% plagioclase that resemble Diorite 1 (figure 2.2). A few xenoliths show variable alteration, which might be truncated veins (figure 3.4a,b). In some cases, xenoliths show reaction rims against the surrounding rock (figure 3.4c,d). These features suggest that the xenoliths were not in chemical equilibrium with the host rock.

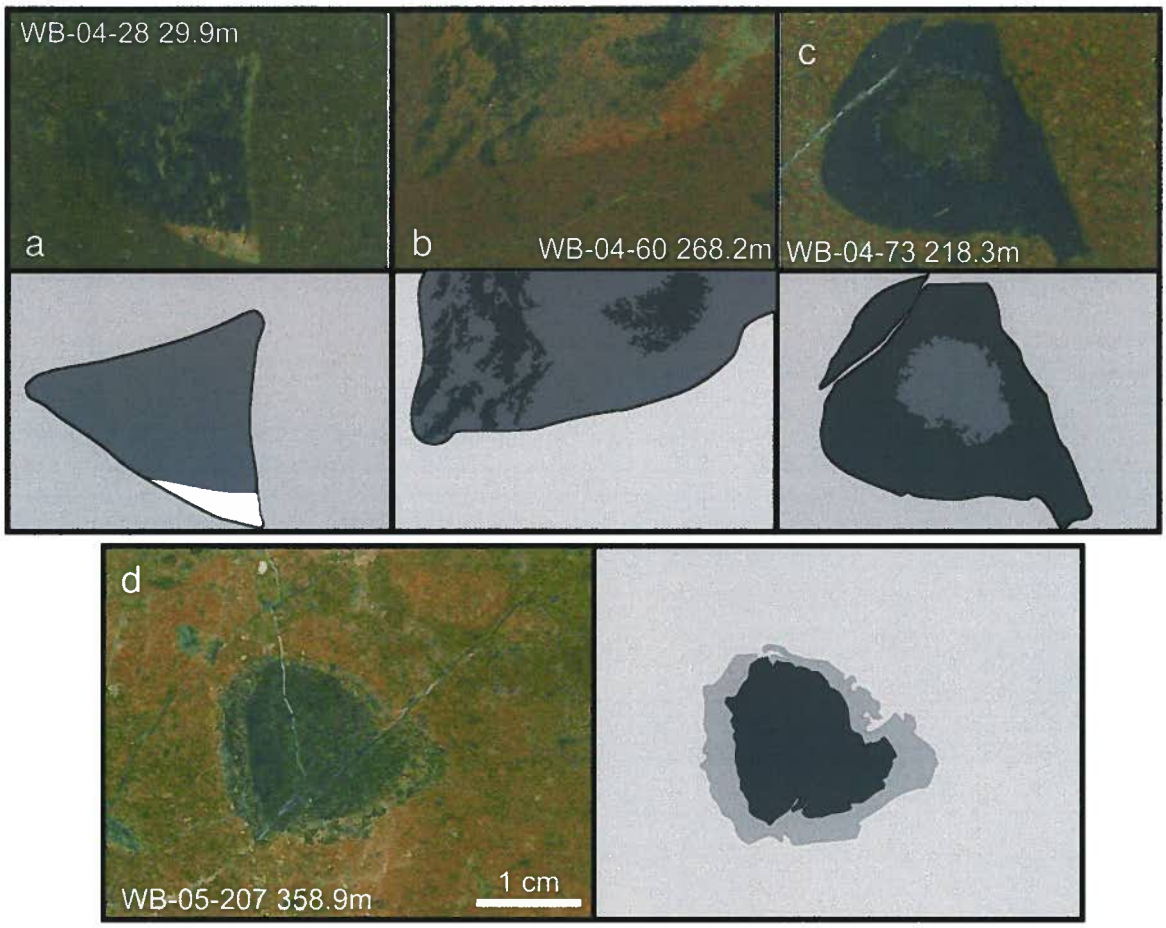

Figure 3.4-Photographs of diorite xenoliths. a; Diorite xenolith with truncated K-feldspar vein; b; diorite (?) xenolith with K-feldspar alteration; c; Diorite xenolith with mafic rim; d; diorite xenolith with reaction rim against monzonite.

Monzodiorite

A minority of coarse grained xenoliths contain K-feldspar as well as plagioclase. These monzodiorite xenoliths closely resemble Diorite 2 (figure 2.3 b-c). These xenolith usually contain 30-40% mafic minerals, 30-50% plagioclase, and ~20% interstitial K-feldspar (figure 3.5).

Figure 3.5-Photograph of monzodiorite xenolith

Hornblende mafic porphyry

The rarest xenoliths are dark green hornblende mafic porphyry. Only two hornblende mafic porphyry xenoliths were found. The groundmass of these xenoliths is fine-grained, dark blue-green, and crowded with 2-3 mm hornblende phenocrysts. These xenoliths were found only within syn-breccia megacrystic K-feldspar porphyry. The hornblende mafic xenoliths have coarse grained equigranular reaction rims against the K-feldspar porphyry (Figure 3.6).

Figure 3.6-Photograph of hornblende mafic porphyry xenolith in megacrystic monzonite porphyry dyke. Note the reaction rim around the xenolith on the right side of the image.

Due to the small size of these xenoliths, and their small volumetric contribution to the ore body, no chemical analyses were done on xenoliths.

Pre-breccia rocks

Equigranular Monzonite

Approximately 90% of the clasts in the hydrothermal breccia (Figure 3.7) consist of xenolith-bearing equigranular monzonite derived from the surrounding country rock. This monzonite is very similar to the PMdu and PMz units, and to some post-breccia dykes. The equigranular monzonite clasts consist of ~90% K-feldspar, and <10% mafic minerals, mostly altered to chlorite, magnetite, and pyrite. This rock is described here as a monzonite rather than a syenite due to the presence of widespread K-feldspar constructive alteration in the MPIC.

Figure 3.7-Photograph of variably altered equigranular monzonite clasts in breccia

Like the undifferentiated monzonite of the MPIC in general, the equigranular monzonite described here shows significant textural variation. K-feldspar microporphyry or fine-phenocryst K-feldspar porphyry forms <5% of breccia clasts, but locally can form 40-50% of clasts (Figure 3.8). There are two distinct subtypes of this rock. The K-feldspar microporphyry contains 20-30% 1-2 mm K-feldspar phenocrysts in a fine-grained K-feldspar and plagioclase groundmass. The phenocrysts are not substantially larger than the average crystal size in the groundmass, but they are visually distinct as euhedral phenocrysts among the subhedral groundmass grains. In fine-phenocryst porphyry, the K-feldspar phenocrysts are ~3 mm in length and typically <1 mm wide, giving them an elongate aspect. The groundmass is fine-grained (<2mm). The equigranular monzonite, microporphyry and the fine-phenocryst porphyry grade into each other, even within a single clast. In thin section, monzonite, which appears equigranular in hand sample, shows microporphyry textures (Figure 3.9) and as such they are considered here as a single rock type.

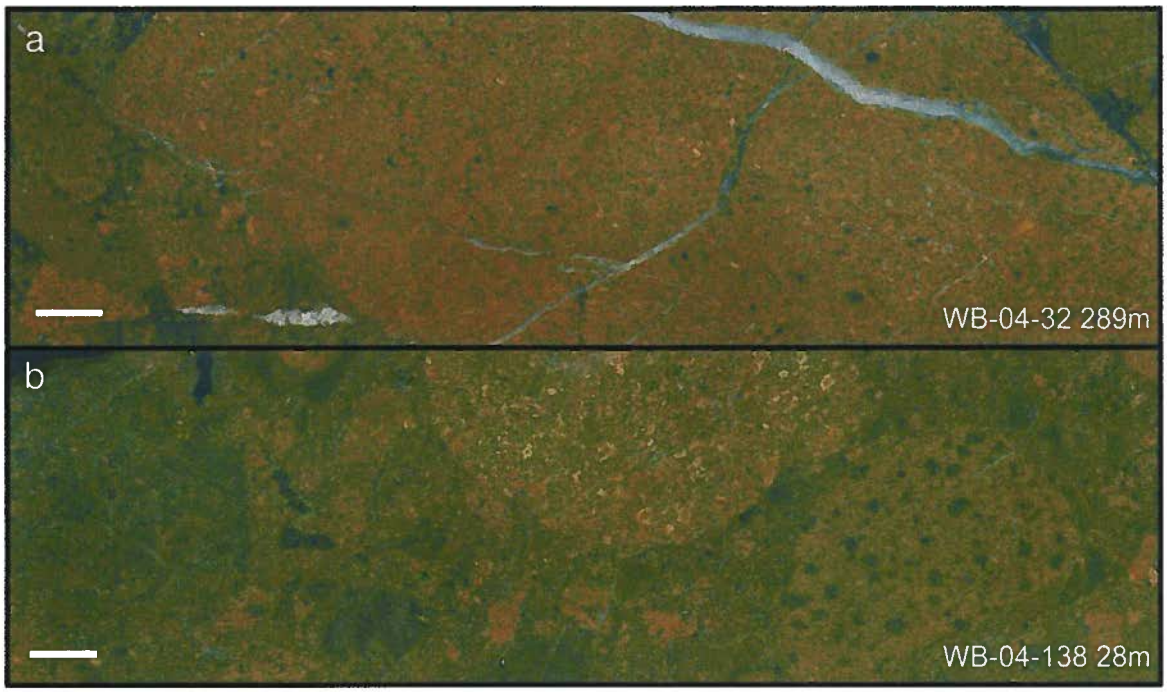

Figure 3.8-Photographs of fine-phenocryst porphyry (a) and microporphyry (b) clasts in breccia. Scale bar equals 1 cm.

No systematic variation in grain size, porphyryitic or trachytitic nature of the equigranular monzonite was observed within the breccia body. Petrography examination also shows Carlsbad twinning in the feldspar phenocrysts, indicating that the K-feldspar is primary, not potassic alteration of albite or another feldspar (Figure 3.9). The groundmass of the equigranular monzonite was too fine-grained to distinguish K-feldspar alteration from primary K-feldspar, especially given the presence of abundant hematite staining. Hematite staining was most distinct along grain boundaries, suggesting that it is of hydrothermal rather than magmatic origin (Figure 3.9). Zoning of hematite staining within K-feldspar phenocrysts suggests control of hematite staining by compositional banding within the grains. Hematitic alteration is discussed more fully in Chapter 5.

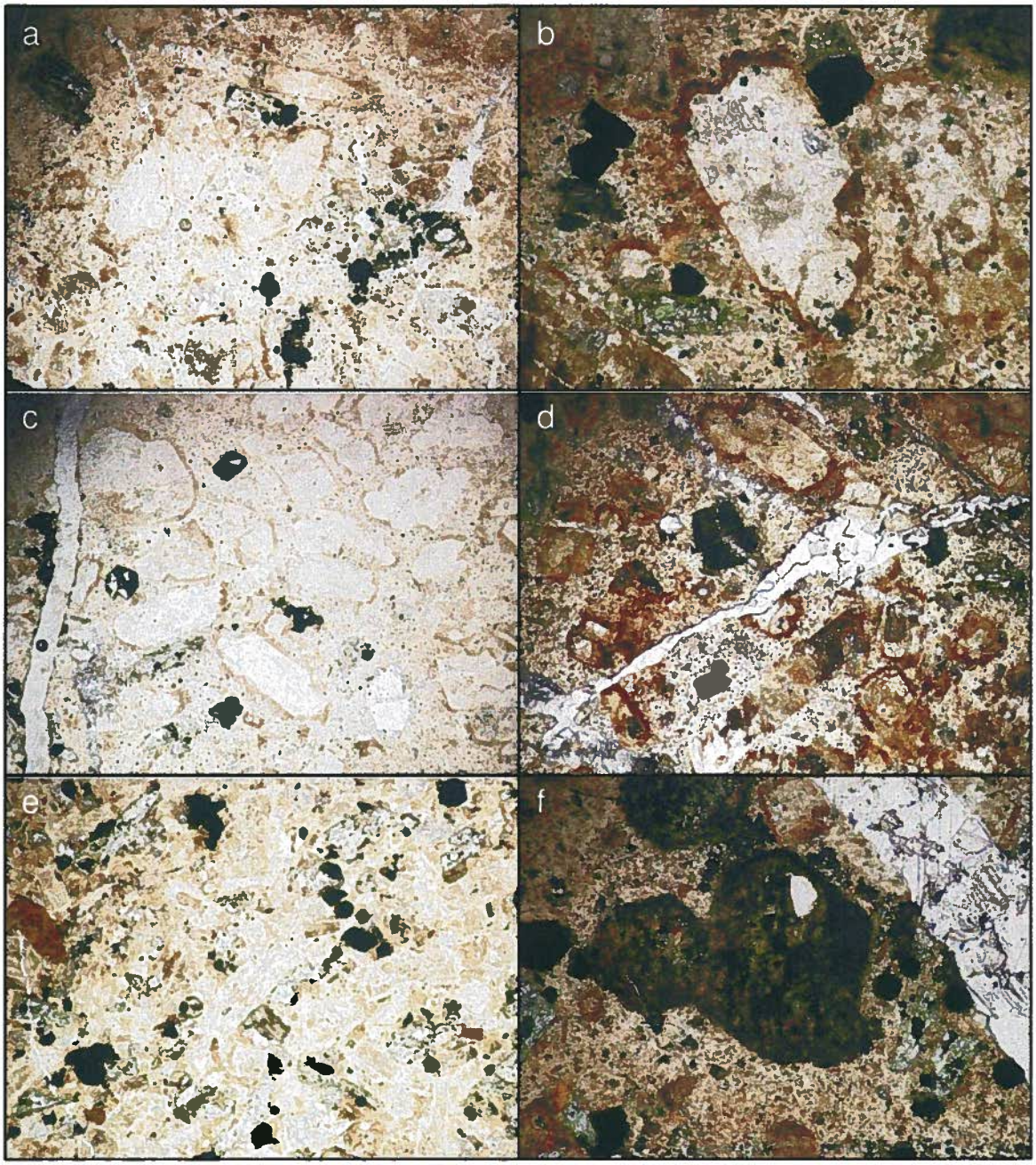

Figure 3.9-Photomicrographs of equigranular monzonite showing microporphyry textures (a). Note the hematite staining on the crystal margins (b,c,d), and Carlsbad twinning of microphenocrysts (b,d), indicating that the K-feldspar composition is original and not the effect of post-intrusion K-feldspar constructive alteration. Images e and f show chlorite altered and biotite-altered augite phenocrysts.

Monzonite clasts in the breccia are generally angular to subangular. Locally rounded clasts are present (see Chapter 4). The lack of globular or fluidal clast shapes or chilled or fine grained margins indicate that the monzonite was crystalline prior to brecciation.

Coherent equigranular augite monzonite surrounding the breccia is locally mineralized, usually as crackle-breccia infill (figure 3.10).

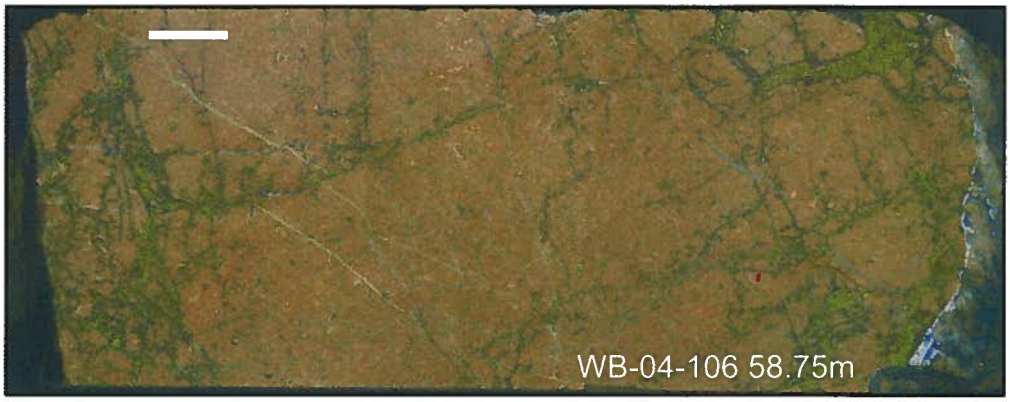

Figure 3.10-Chalcopyrite and bornite mineralization in equigranular monzonite. Scale bar equals 1 cm.

Mafic

Mafic clasts, very similar to the mafic xenoliths described above, are also observed within the breccia. Composing 1-2% of breccia clasts, these clasts locally composed up to 20% of the breccia (figure 3.11). The mafic clasts in breccia are generally smaller than clasts of other rock types, usually less than 2 cm in length. They are dark in color, fine-grained, and typically preferentially altered (see Chapter 5). Mafic clasts are most common where the average clast size of the breccia is smallest (see Chapter 4). The mafic clasts may represent re-worked xenoliths originally included within the monzonite clasts.

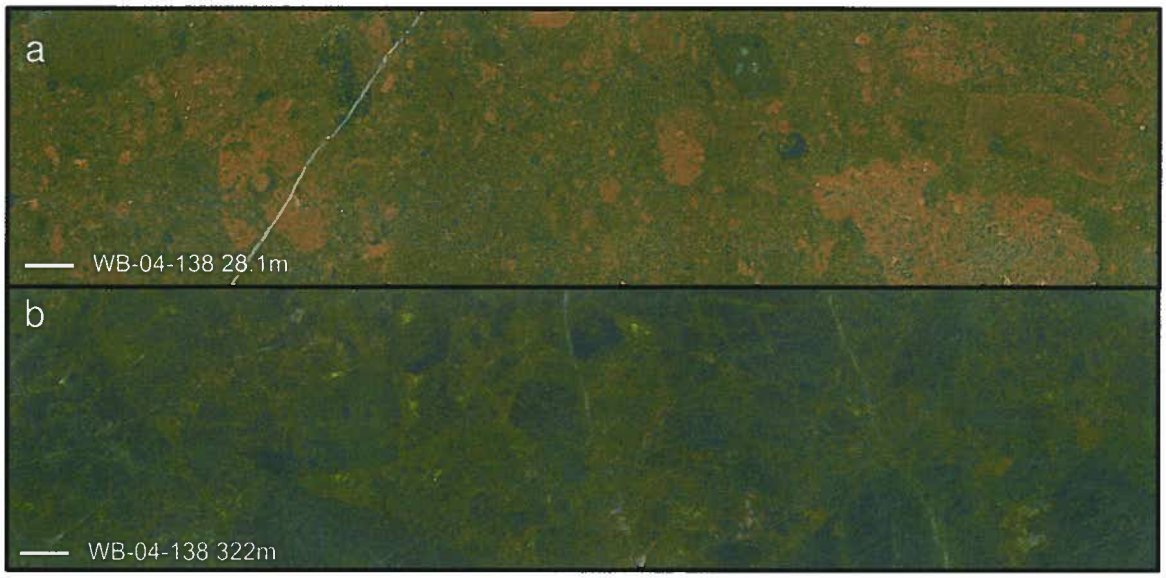

Figure 3.11-Mafic clasts in breccia. A; mafic clasts with equigranular and monzonite microporphyry clasts; b; predominantly mafic clasts. Note replacement of mafic clasts by chalcopyrite.

Altered mafic

The most distinctive group of clasts within the breccia are altered green to green-grey mafic clasts. Alteration has obscured the primary mineralogy of the clasts (the clasts are composed of secondary actinolite, albite, and minor epidote). They contain magnetite and K-feldspar veins truncated at the clast boundaries, indicating the presence of a pre-breccia hydrothermal system (figure 3.12).

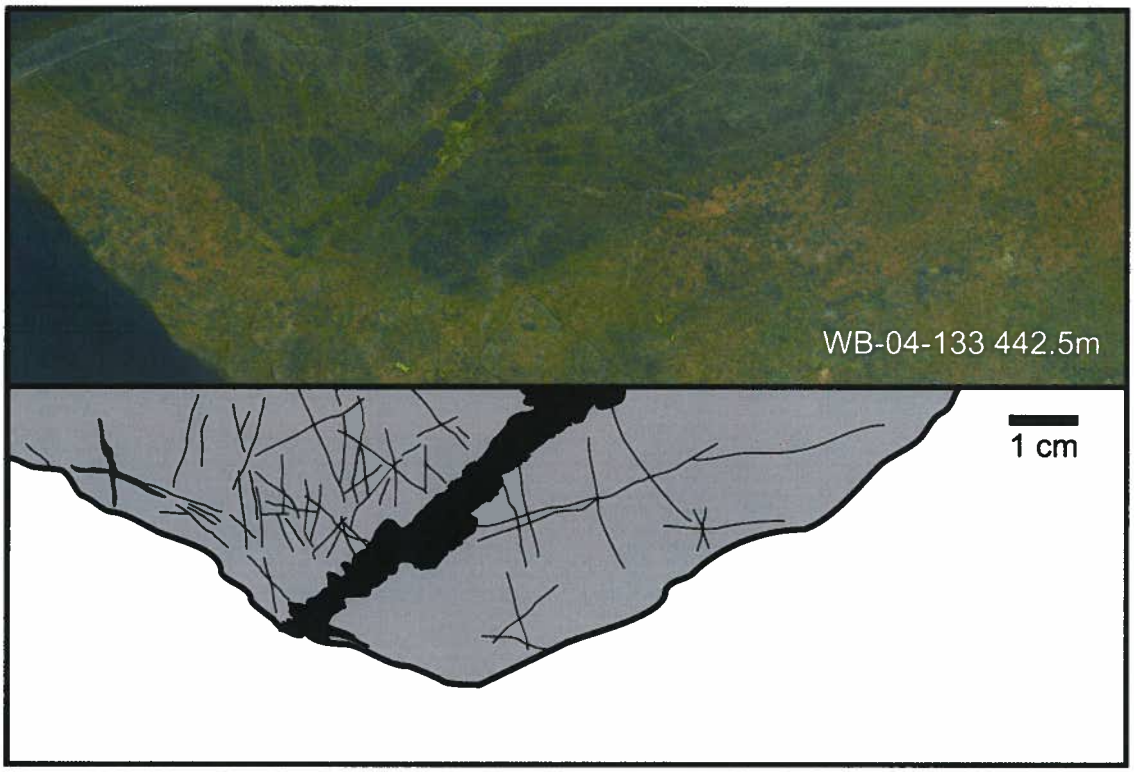

Figure 3.12-Altered mafic clast within the breccia; some magnetite ahs been replaced by chalcopyrite after the inclusion of the clast in the breccia. The magnetite vein is truncated by the clast margin, showing that the vein event pre-dated brecciation.

Although the edges of these magnetite veins are in some cases replaced by Cu-sulfides, no primary Cu-sulfides were observed associated with this generation of veins.

The tabular distribution of the altered mafic clasts within the breccia (figure 3.13) suggests that the altered mafic clasts may be the disaggregated remains of a sill-like body within the monzonite. This tabular geometry is well defined, with no altered mafic clasts outside the margins of the body shown, and up to 90% altered mafic clasts within it.

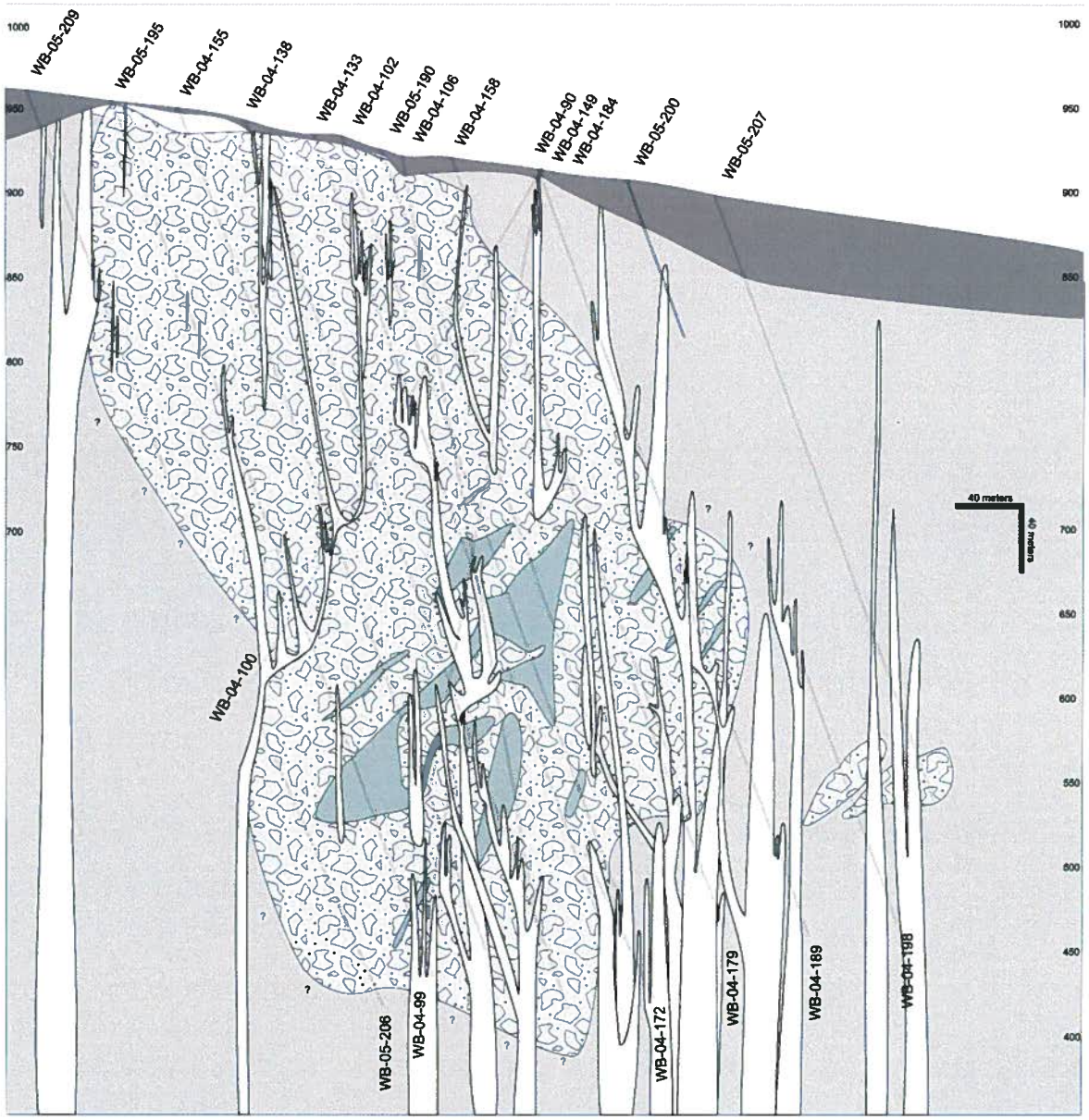

Figure 3.12-Distribution of altered mafic clasts on section 29. Altered mafic clasts were not observed on Section 18.

Syn-breccia

Between 10 and 20% of the clasts within the breccia, locally ranging from 1% to >90%, are composed of megacrystic (>1.5 cm phenocryst) K-feldspar monzonite porphyry. These clasts are most commonly angular to subrounded, but also occasionally include

complex clast shapes indicating that the unit was plastic when brecciated (Figure 3.14a and b).

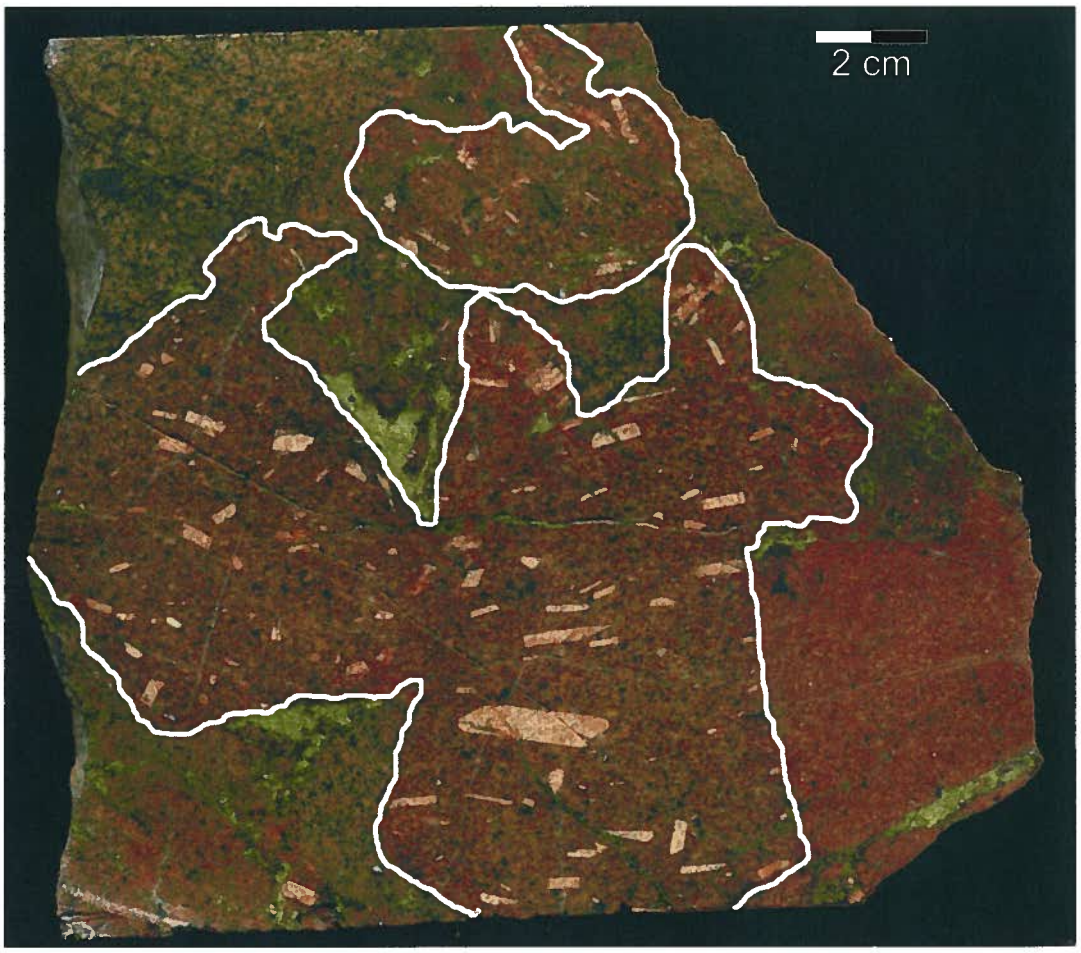

Figure 3.14a-Juvenile megacrystic porphyry clasts. Image courtesy of Dr. Kirstie Simpson.

Figure 3.14b- Juvenile megacrystic monzonite porphyry clast. Note how the clast has been squeezed between several equigranular porphyry clasts. Hole WB-04-99, 444.5 m. Field of view equals 2 cm.

Megacrystic K-feldspar monzonite porphyry clasts contain 10-15% euhedral K-feldspar phenocrysts, commonly with starburst-shaped agglomerations of phenocrysts and irregular glomerocrysts (figure 3.15). The phenocrysts are commonly broken (figure 3.15). In thin section, phenocrysts show patchy hematite dusting and oikocrystic textures (figure 3.16). The groundmass of the megacrystic K-feldspar monzonite porphyry is fine- to medium-grained, containing <5% mafic minerals. Mafic minerals within the K-feldspar monzonite porphyry are blocky in shape, suggesting that the original mineral

may have been biotite or augite, but mafic minerals are mainly altered to chlorite. The groundmass feldspar appears to be mainly K-feldspar, but the original mineralogy has probably been modified by syn- and post-breccia K-feldspar-stable alteration. Very similar megacrystic K-feldspar porphyry intrusive bodies are cut by drillholes outside the area of the breccia (figure 3.17). Cu-Au mineralization is not spatially associated with the K-feldspar monzonite dykes which cut breccia.

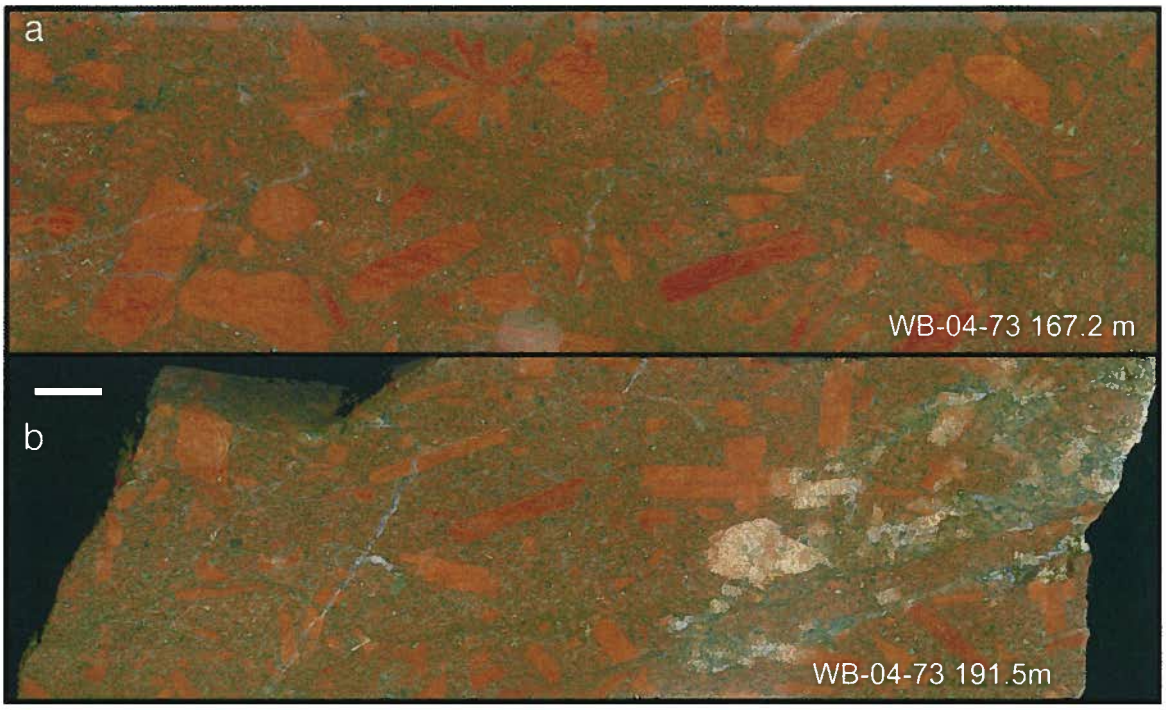

Figure 3.15-Broken phenocrysts (a, bottom left) and glomerocrysts (a and b) of K-feldspar in the megacrystic monzonite porphyry; phenocrysts are stained with hematite and locally altered to albite.

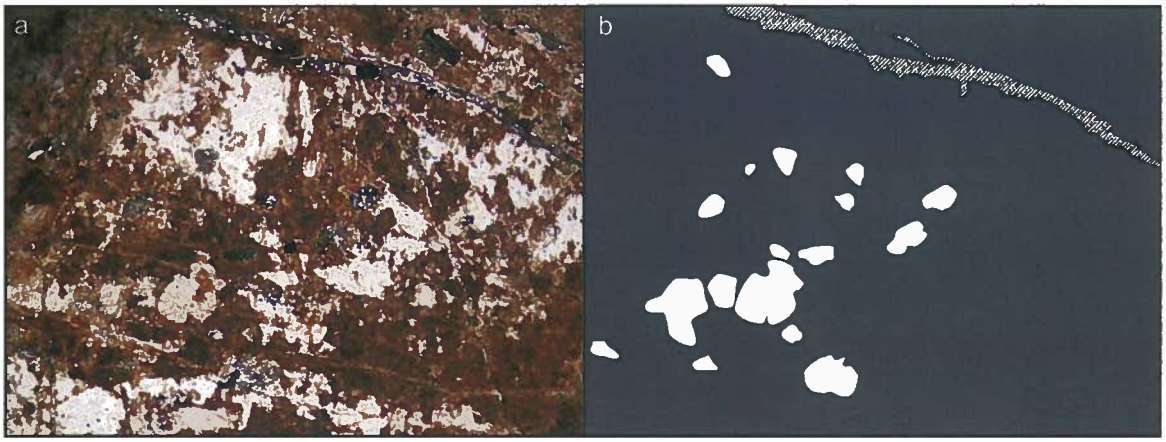

Figure 3.16-Photomicrographs of a single K-feldspar megacryst showing K-feldspar chadacrysts within the K-feldspar oikocryst, and patchy hematite dusting concentrated along fractures. Image on the right traced to show detail; vein at upper right is post-mineral calcite.

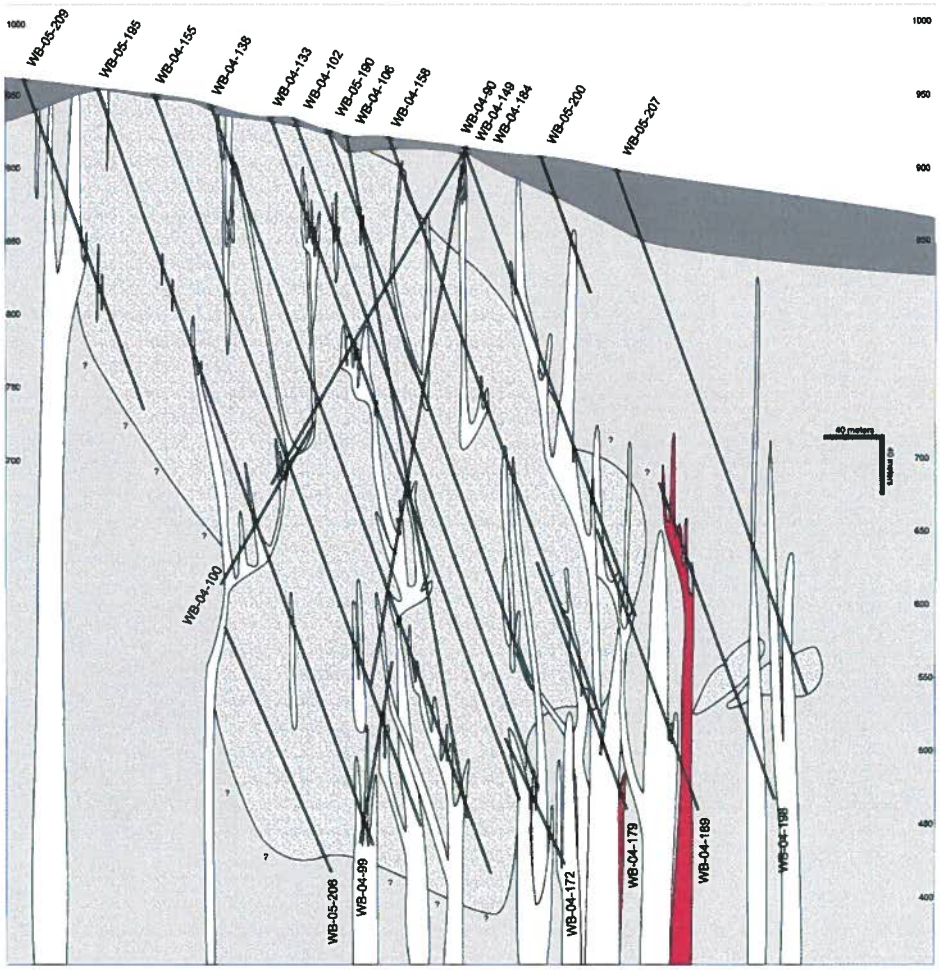

Figure 3.17a-Distribution of megacrystic porphyry dykes on Section 29.

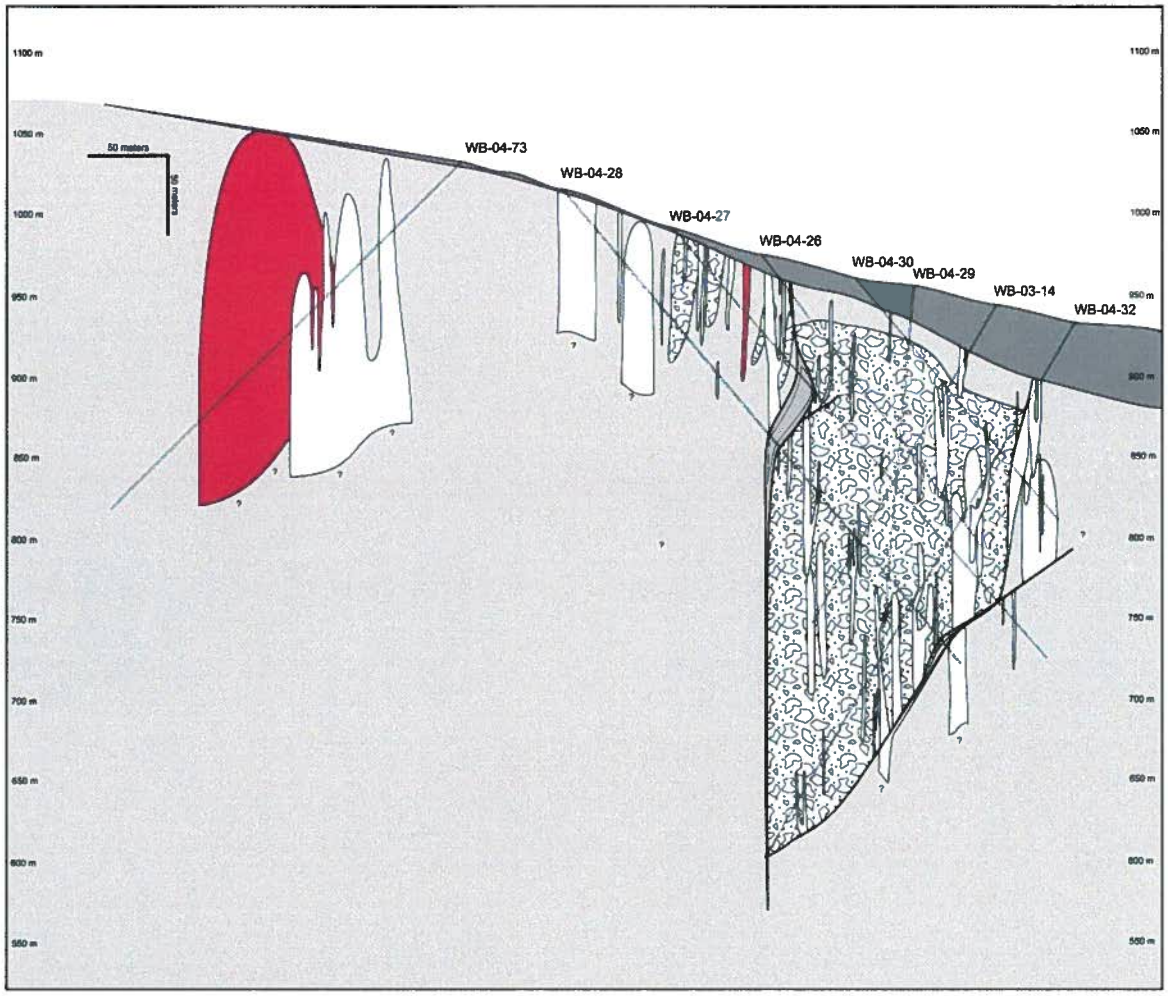

Figure 3.17b-Distribution of megacrystic porphyry intrusions on Section 18. The geometry of the large body cut by drill hole WB-04-73 is unknown.

Post-breccia Intrusive rocks

The hydrothermal breccias are cut by a host of post-breccia dykes. All the units addressed in this section have intrusive margins against the breccia or against each other. The dykes are presented in chronologic order, based on cross-cutting relationships either by direct intrusive contacts or by the presence of xenoliths of one unit in another.

The post-breccia intrusive rocks can be subdivided into compositional groups with sequential timing (Table 3.2). These dykes document chemical and physical changes both

within and between compositional groups, reflecting an overall trend of increasingly mafic compositions and decreasing grain size for each generation of dykes.

Table 3.2a: Trends in the composition and texture of post-mineral dykes

COMPOSITIONAL GROUP	DYKES	TRENDS WITHIN THE GROUP
Equigranular augite monozonite	Mineralized equigranular augite monzonite Post-mineral equigranular augite monzonite	Decreasing grain size with time
K-feldspar porphyries	Syn-breccia megacrystic monzonite porphyry Post-mineral crowded K-feldspar monzonite porphyry Post-mineral moderate K-feldspar monzonite porphyry Post-mineral sparse K-feldspar monzonite porphyry Post-mineral K-feldspar trachyte porphyry	Decreasing phenocryst size and abundance over time Increasing phenocryst aspect ratio over time
K-feldspar and plagioclase porphyry	Post-mineral K-feldspar and plagioclase porphyry	
Hornblende-bearing equigranular monzonite	Hornblende and augite-bearing equigranular monzonite Hornblende-bearing equigranular monzonite Hornblende and biotite-bearing equigranular monzonite Biotite trachyte	Increasing proportion of hydrous minerals over time Decreasing grain size
Plagioclase (diorite) microporphyry	Plagioclase (diorite) microporphyry	

Table 3.2b: **Trends in the composition and texture of post-mineral dykes**

COMPOSITIONAL GROUP	DYKES	TRENDS WITHIN THE GROUP
Mafic dykes	Plagioclase-phyric mafic microporphyry Plagioclase and augite-phyric mafic microporphyry Augite-phyric mafic microporphyry Augite and olivine-phyric mafic microporphyry Olivine-phyric mafic microporphyry	Increasingly mafic composition
Augite porphyry	Augite porphyry	Exploits faults; often highly deformed and gougy on at least one contact.

Equigranular augite monzonite

The oldest generation of post-breccia dykes is equigranular augite-bearing monzonite very similar to the country rock of the breccia. These dykes occur repeatedly throughout the sequence of dykes, generally becoming finer grained over time. The oldest of these dykes are presumed to be the oldest post-breccia dyke generation because they are the only dykes that contain chalcopyrite as veinlets and replacing mafic minerals (figure 3.18).

The equigranular monzonite dykes were to numerous and difficult to distinguish from clasts within the breccia to be shown on cross sections.

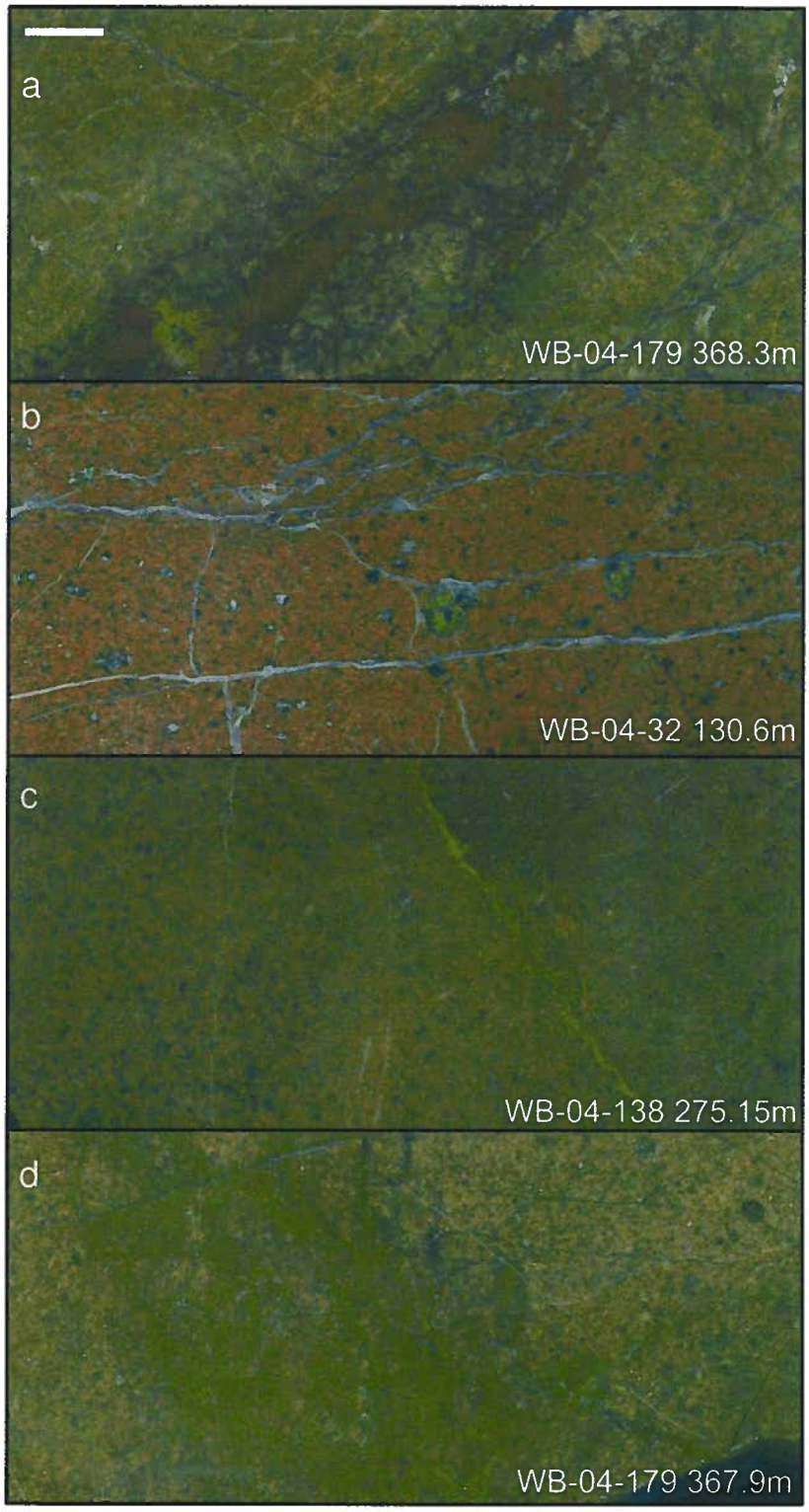

Figure 3.18-Chalcopyrite and bornite mineralization in post-breccia equigranular augite-bearing monzonite. A; Bornite-chalcopyrite vein-breccia, b; chalcopyrite replacing mafic minerals, c; chalcopyrite vein crosscutting finer-grained equigranular monzonite, and d; a diffuse chalcopyrite vein with replacement of mafic sites by chalcopyrite. Scale bar is 1 cm.

K-feldspar phyric monzonite porphyry

The equigranular augite monzonite dykes are cut by K-feldspar-phyric monzonite porphyry dykes (figure 3.19). These dykes generally have phenocrysts between 5 and 7 mm long in a fine-grained to aphanitic groundmass. This family of dykes contains no visible plagioclase either as phenocrysts or in the groundmass. The K-feldspar-phyric monzonite porphyry dykes can be divided into three subtypes based on the phenocryst percentage. Generally, the greater the percentage of phenocrysts in the porphyry, the larger and blockier the phenocrysts and the greater the amount of disseminated pyrite in the groundmass of the dyke.

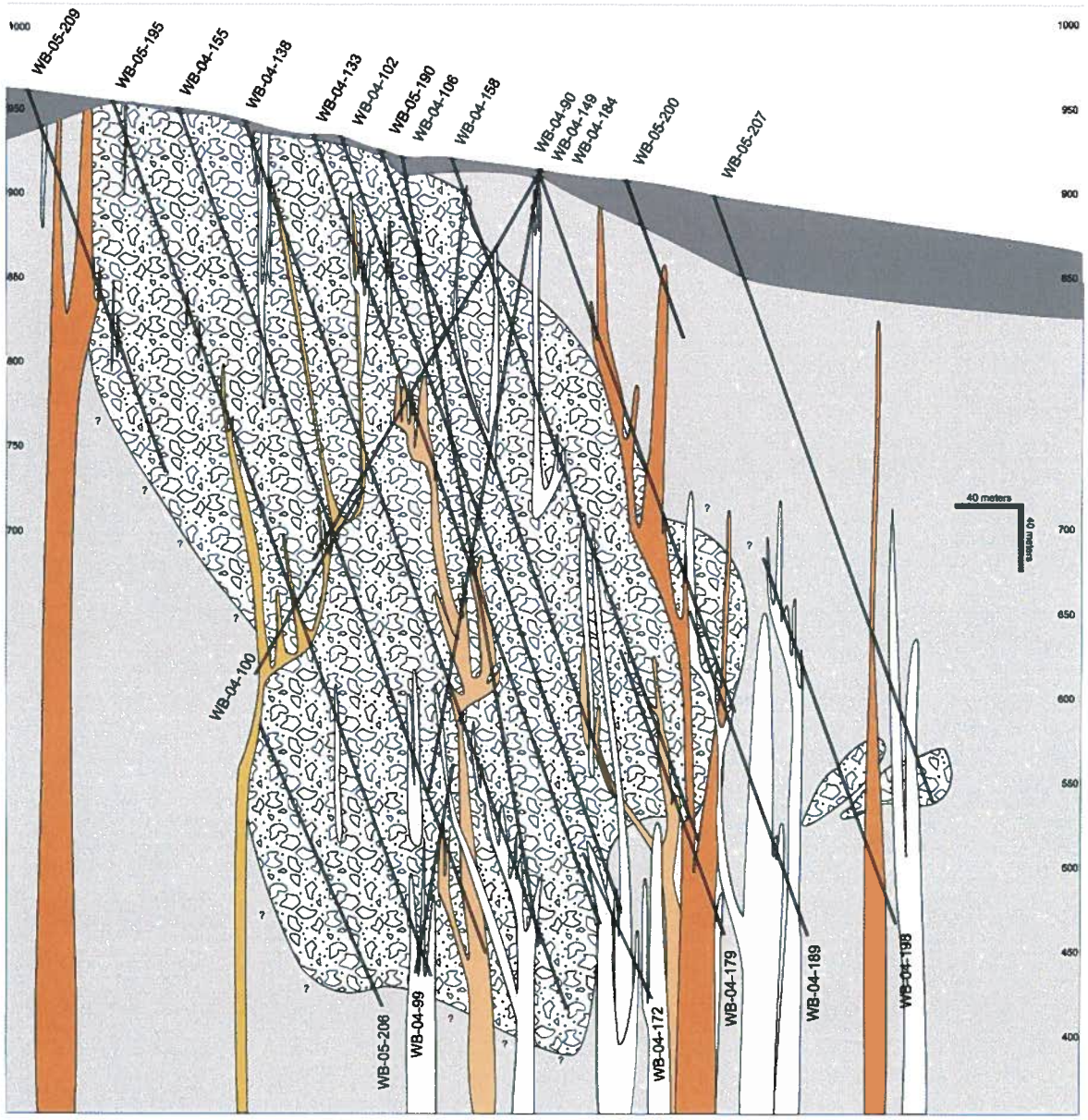

Figure 3.19a-Distribution of K-feldspar-phyric monzonite porphyry dykes on section 29

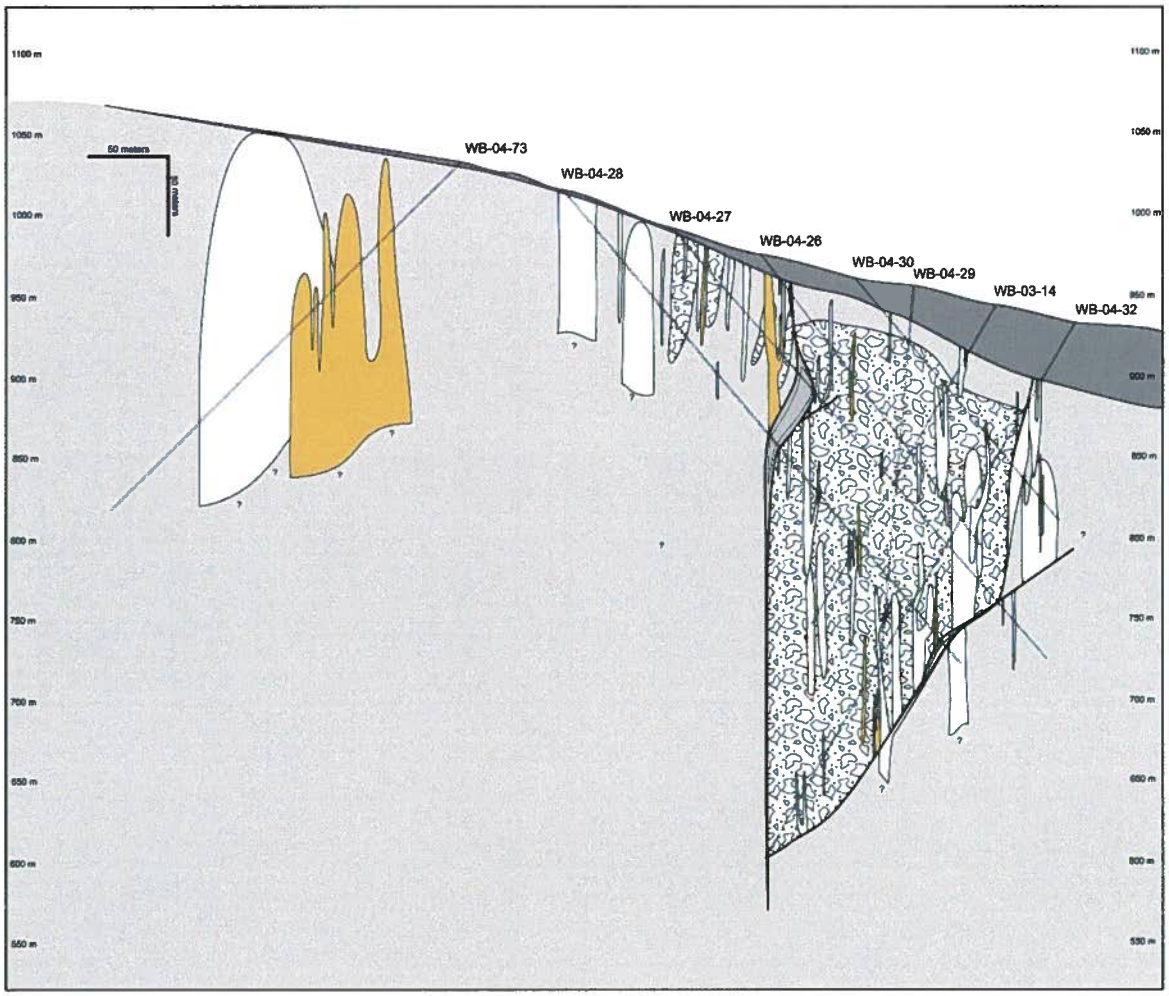

Figure 3.19b-Distribution of K-feldspar-phyric monzonite porphyry dykes on Section 18.

The dykes generally have a branching morphology and are interpreted to be approximately vertical. They are more common, and more varied, in Section 29 than Section 18.

The oldest K-feldspar porphyry is phenocryst-crowded, with >30% phenocrysts. Flow alignment of phenocrysts is common, especially around xenoliths and at the dyke margins (figure 3.20). The dykes have chilled margins against the breccia and against equigranular monzonite. They contain xenoliths of equigranular monzonite and fine-grained mafic rock.

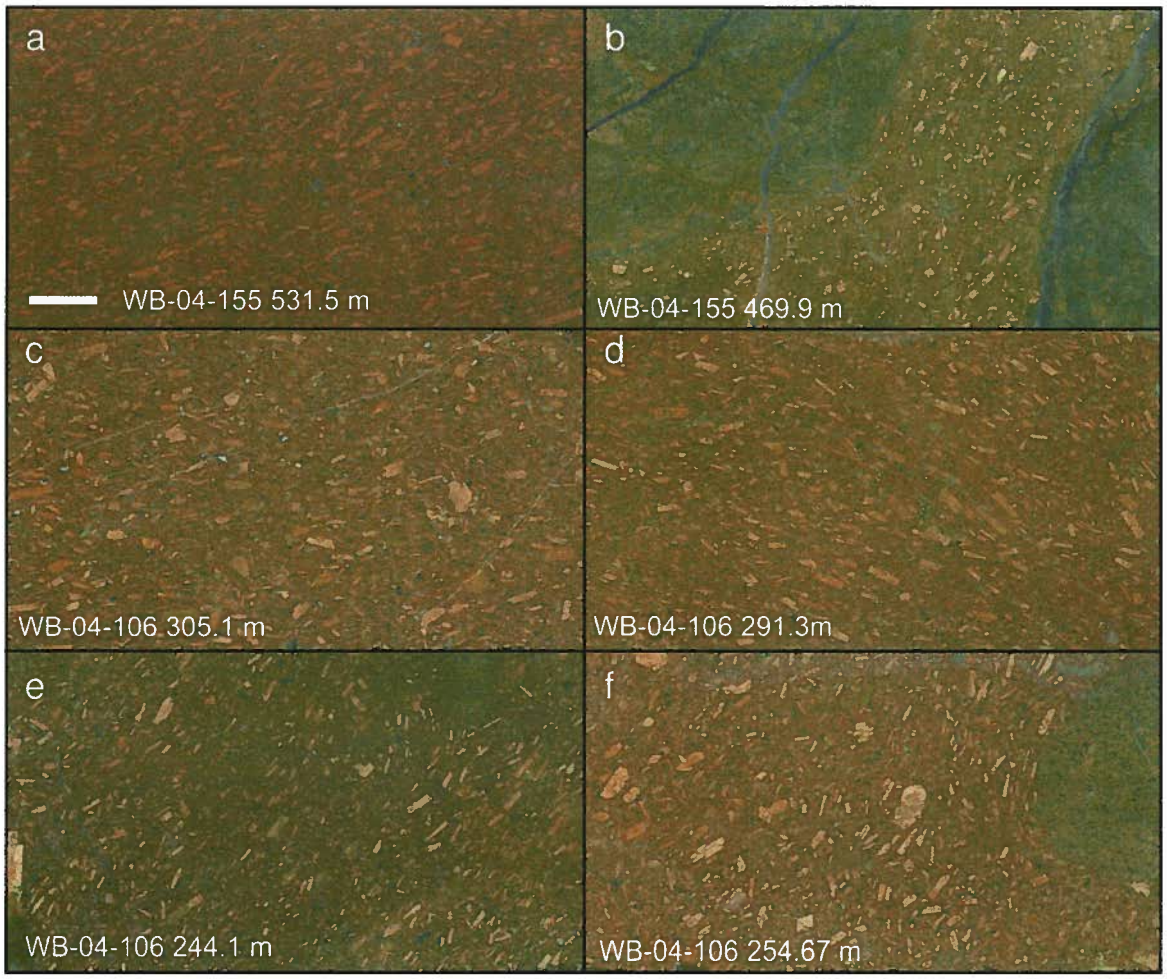

Figure 3.20-Crowded K-feldspar-phyric monzonite porphyry showing flow alignment of phenocrysts. A. flow alignment in "normal" phenocrysts; b. alignment of phenocrysts between equigranular xenoliths; c. alignment in glomerocrysts; d. change in direction of phenocryst; e. phenocryst alignment diverging around a xenolith; f. phenocryst trails "wrapped" around a monzonite xenolith. Scale bar equals 1 cm.

Although no direct crosscutting relationships were observed in core, a family of K-feldspar-phyric monzonite porphyry dykes containing 15-20% K-feldspar phenocrysts are assumed to be the next generation of dykes cutting the breccia. This conclusion is based on the apparent regular progression of decreasing phenocryst percentage in the K-feldspar porphyries. The phenocrysts in these dykes are more elongate than those in the phenocryst-crowded dykes. Disseminated pyrite was less abundant, and fewer equigranular monzonite xenoliths were observed. Some flow textures are present in these

dykes. In contrast to the crowded K-feldspar-phyric dykes, which generally had uniformly sized, shaped, and distributed phenocrysts throughout the dyke, the moderate K-feldspar-phyric monzonite porphyry dykes showed significant variation in phenocryst size and aspect ratio. Generally, phenocrysts are sparser, larger and blockier toward the center of the dykes, and more common, smaller, and more elongate toward the dyke margins. The margins of the crowded K-feldspar-phyric porphyry were also typically smooth, whereas the margins of the moderate K-feldspar-phyric porphyry are in many cases highly irregular, in many cases with apparently disaggregated fragments. Glomerocrysts and starburst-shaped phenocryst clusters are less common in the phenocryst-moderate dykes than in the phenocryst crowded ones, but still present (figure 3.21).

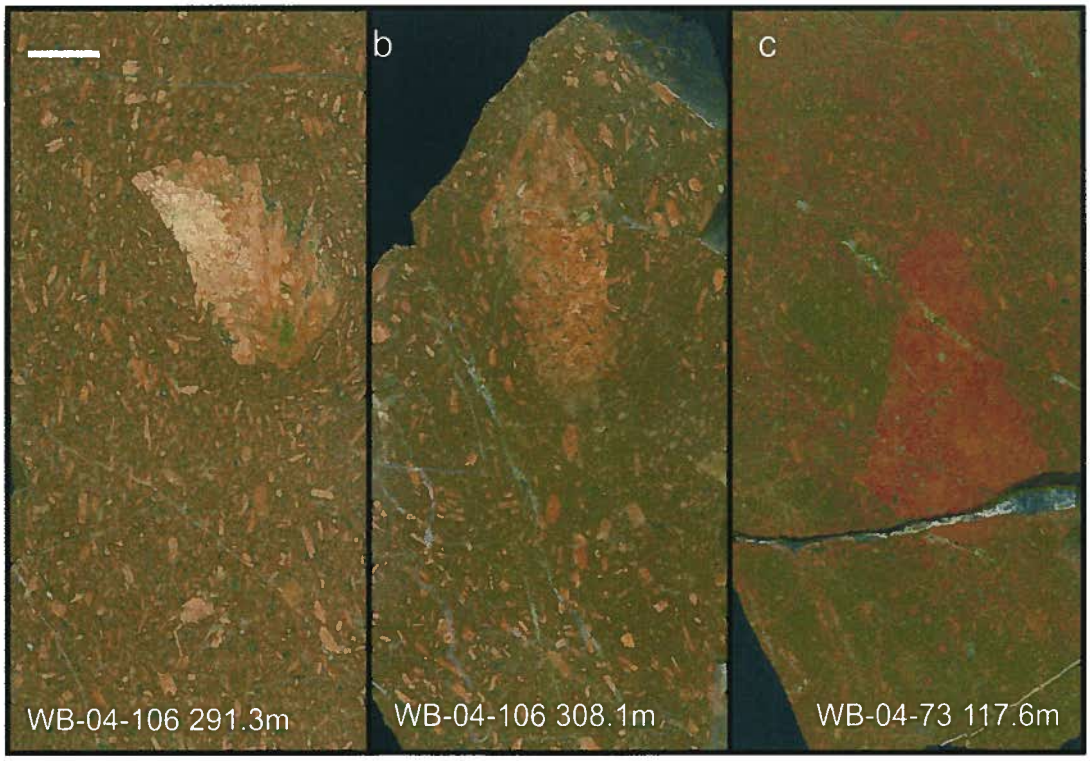

Figure 3.21-K-feldspar glomerocrysts in moderately K-feldspar-phyric monzonite porphyry. A; glomerocryst made up of larger crystals than the surrounding phenocrysts; b; glomerocryst made up of crystals the same size as the surrounding phenocrysts; c; glomerocryst overprinted by hematite-carbonate alteration. Scale bar equals 1 cm.

The youngest and most common group of K-feldspar-phyric monzonite porphyry dykes contains less than 5% phenocrysts. These are volumetrically the largest dykes in the system. The phenocryst-poor K-feldspar-phyric monzonite porphyry dykes are notably darker in color than the other dykes of the group, with a finer grained groundmass and more pronounced chilled margins. The phenocrysts in the dykes are generally more elongate than those in the moderate or the crowded K-feldspar-phyric monzonite porphyry.

Another dyke included within this larger family is the trachyte porphyry dyke observed in Section 18. Although its position on the far side of the Green Giant fault and its lack of cross-cutting relationships makes establishing the timing of this dyke problematic, the apparent trend in dyke character (finer grained groundmass, sparser and more elongate phenocrysts) suggest that the trachyte porphyry is the latest in the series. The trachyte porphyry has an aphanitic groundmass and contains 2-3% extremely elongate (1-2 mm wide by 7-15 mm long) phenocrysts. In contrast to the dark red to orange fine-grained groundmass of the other K-feldspar-phyric monzonite porphyry dykes, the groundmass of the trachyte porphyry dyke is aphanitic and dark brown in color, closely resembling the chilled margins of the phenocryst poor K-feldspar-phyric monzonite porphyry dykes. Starburst and cross-shaped phenocryst clusters were observed in the trachyte porphyry, but more complex glomerocrysts were not.

As a group, the K-feldspar phyric-dykes show a progression over time of decreasing phenocryst size and abundance, and increasing phenocryst aspect ratio (figure 3.22). This trend will be discussed in more detail below.

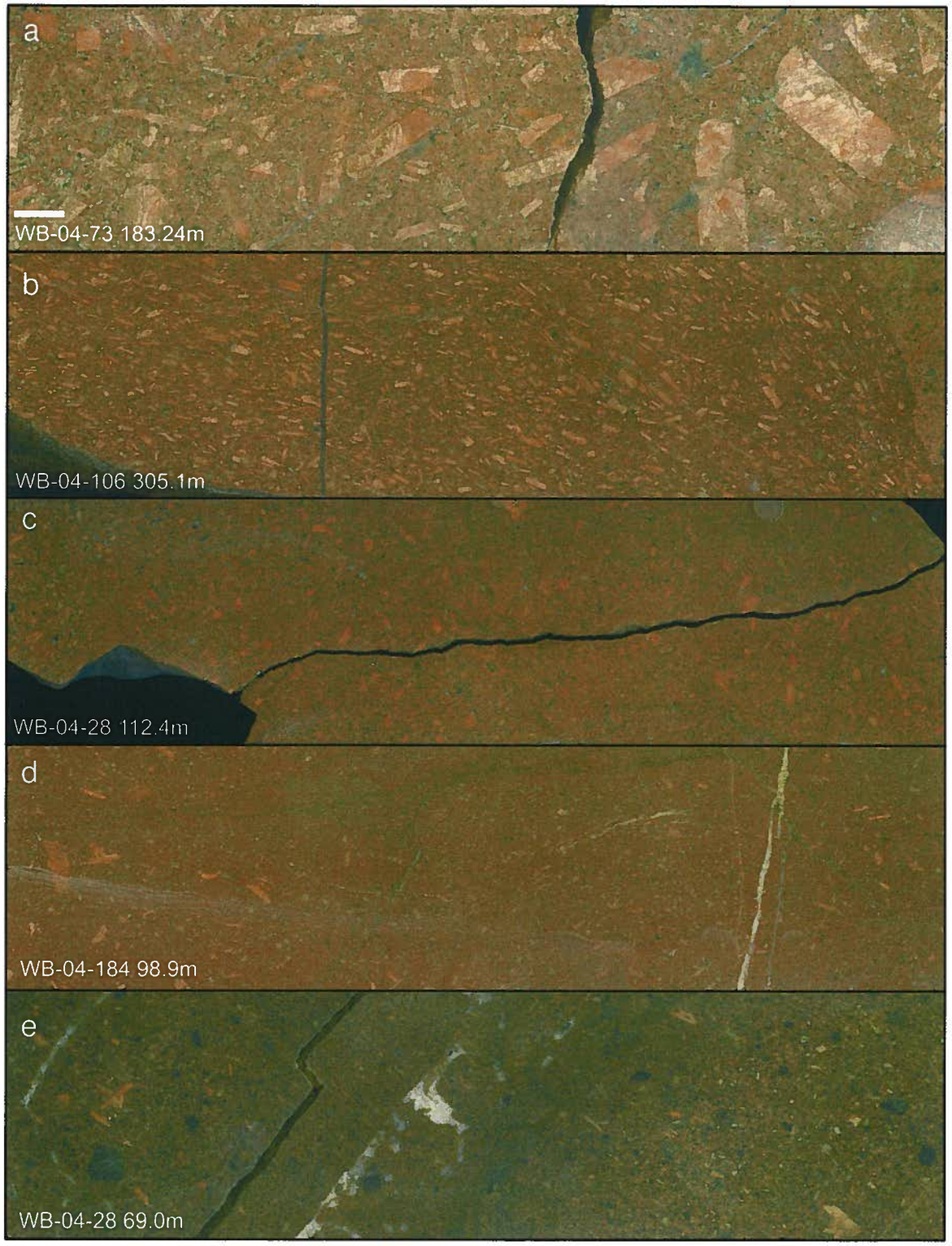

Figure 3.22-Progressive changes in dyke texture over time. A; Megacrystic K-feldspar phyric monzonite porphyry, b; crowded K-feldspar-phyric monzonite porphyry, c; moderate K-feldspar - phyric monzonite porphyry, d; sparse K-feldspar-phyric monzonite porphyry, and e; K-feldspar - phyric trachyte porphyry. Scale bar equals 1 cm.

K-feldspar- and plagioclase-phyric monzonite porphyry dykes

Cutting the K-feldspar-phyric porphyry dykes are K-feldspar- and plagioclase-phyric monzonite porphyry dykes. These dykes have 10-15% 5-8 mm orange K-feldspar phenocrysts and 5-10% 3-5 mm grey or cream-colored plagioclase phenocrysts in a fine-grained to aphanitic dark red groundmass (Figure 3.23). These dykes have a conspicuous "two-toned" appearance, but the presence of plagioclase may be the result of preservation rather than original compositional distinctiveness. The dominant mafic mineral in the dykes is biotite. It is possible that the K-feldspar-phyric dykes in which plagioclase is not observed may have simply experienced pervasive K-feldspar constructive alteration, converting plagioclase to K-feldspar, and that the biotite is secondary and replacing augite. The plagioclase- and K-feldspar-phyric monzonite porphyry dykes, like the dykes with only K-feldspar phenocrysts, commonly have disseminated pyrite in the groundmass of the rock. Although encountered in three drillholes, this rock type is probably a single dyke (Figure 3.24). This rock type was not encountered in section 18.

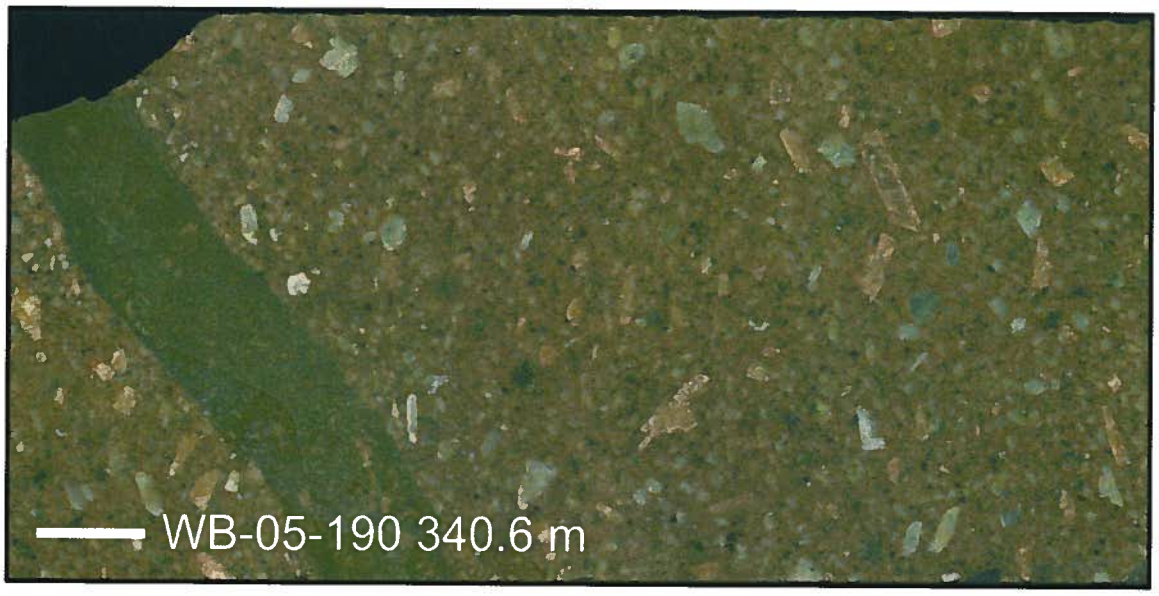

Figure 3.23-Plagioclase- and K-feldspar-phyric monzonite porphyry, cut by a multi-generation pyrite vein. Scale bar equals 1 cm.

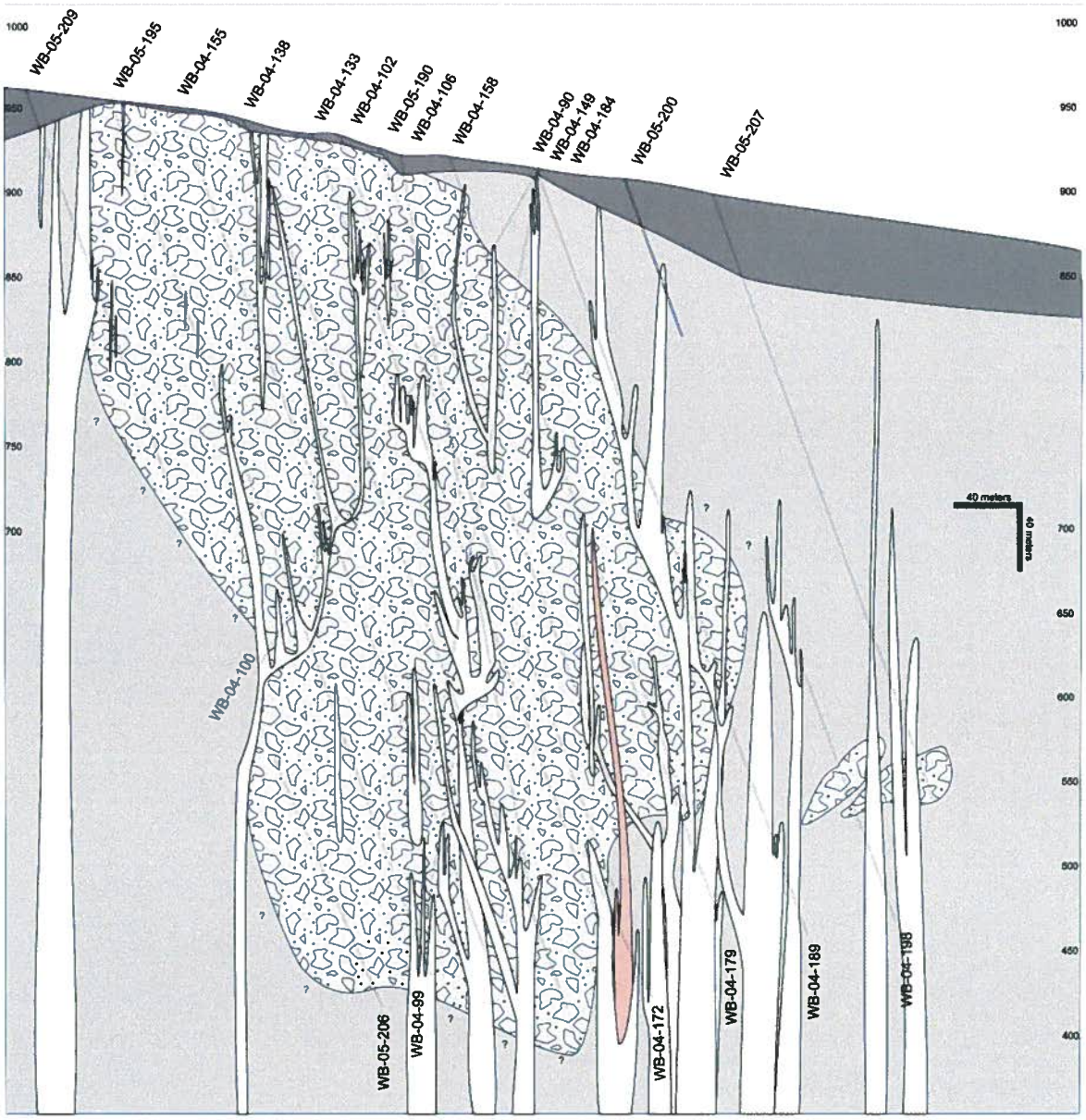

Figure 3.24-Plagioclase- and K-feldspar-phyric porphyry dyke in section 29.

Equigranular hornblende and hornblende-biotite monzonite

Equigranular augite-bearing monzonite dykes occur sporadically throughout the igneous sequence of the Northeast zone, locally with small amounts of hornblende. In a few dykes deep in Section 29, equigranular monzonite containing no visible augite and an abundance of hornblende were observed. These dykes cut K-feldspar constructive alteration, which overprints the K-feldspar-phyric and the K-feldspar- and plagioclase-phyric dykes in both Section 29 and Section 18 (figure 3.25 a and b), so they are assigned a post-K-feldspar- and plagioclase-phyric dyke timing, although direct cross-cutting relationships were not observed.

This family of dykes contains 2-5% <3mm euhedral hornblende laths in a fine grained K-feldspar and plagioclase groundmass (figure 3.26). Disseminated pyrite is not observed in these dykes, but fine-grained disseminated magnetite is present. The hornblende bearing equigranular monzonite is cut by a second generation of hornblende-bearing equigranular monzonite, distinguished from the first by the presence of 1-2% primary biotite. Primary biotite forms <2mm euhedral crystals. Secondary biotite forms felty black or green-black crystalline aggregates replacing augite or hornblende. The biotite and hornblende-bearing monzonite also contains xenoliths of biotite-free hornblende-bearing monzonite, confirming the timing relationship between biotite-bearing and biotite-free hornblende monzonite. In section 18, hornblende-bearing monzonite forms a larger body than those observed in Section 29. In section 18, hornblende monzonite is cut by trachyte and diorite dykes and by faults exploited by augite porphyry dykes.

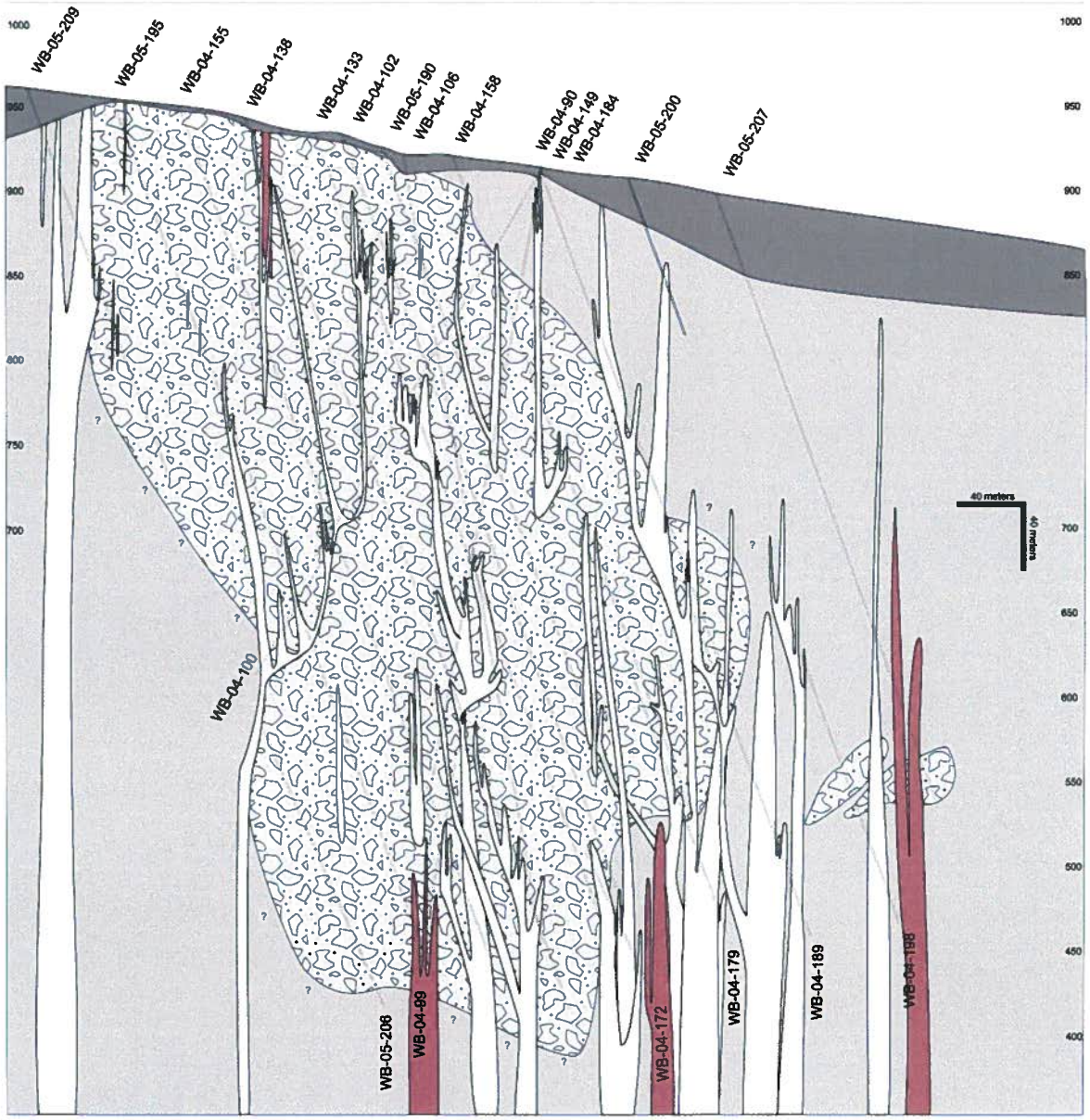

Figure 3.25a-Hornblende and hornblende-biotite dykes in Section 29.

Hornblende and hornblende-biotite dykes in section 29 cut K-feldspar constructive alteration, but are cut by albite-epidote alteration. This suggests that the hornblende-biotite dykes occurred late in the development of the hydrothermal system, and were post-mineral, but were not post-hydrothermal. Minor pyrite is present replacing mafic minerals in these dykes (figure 3.26).

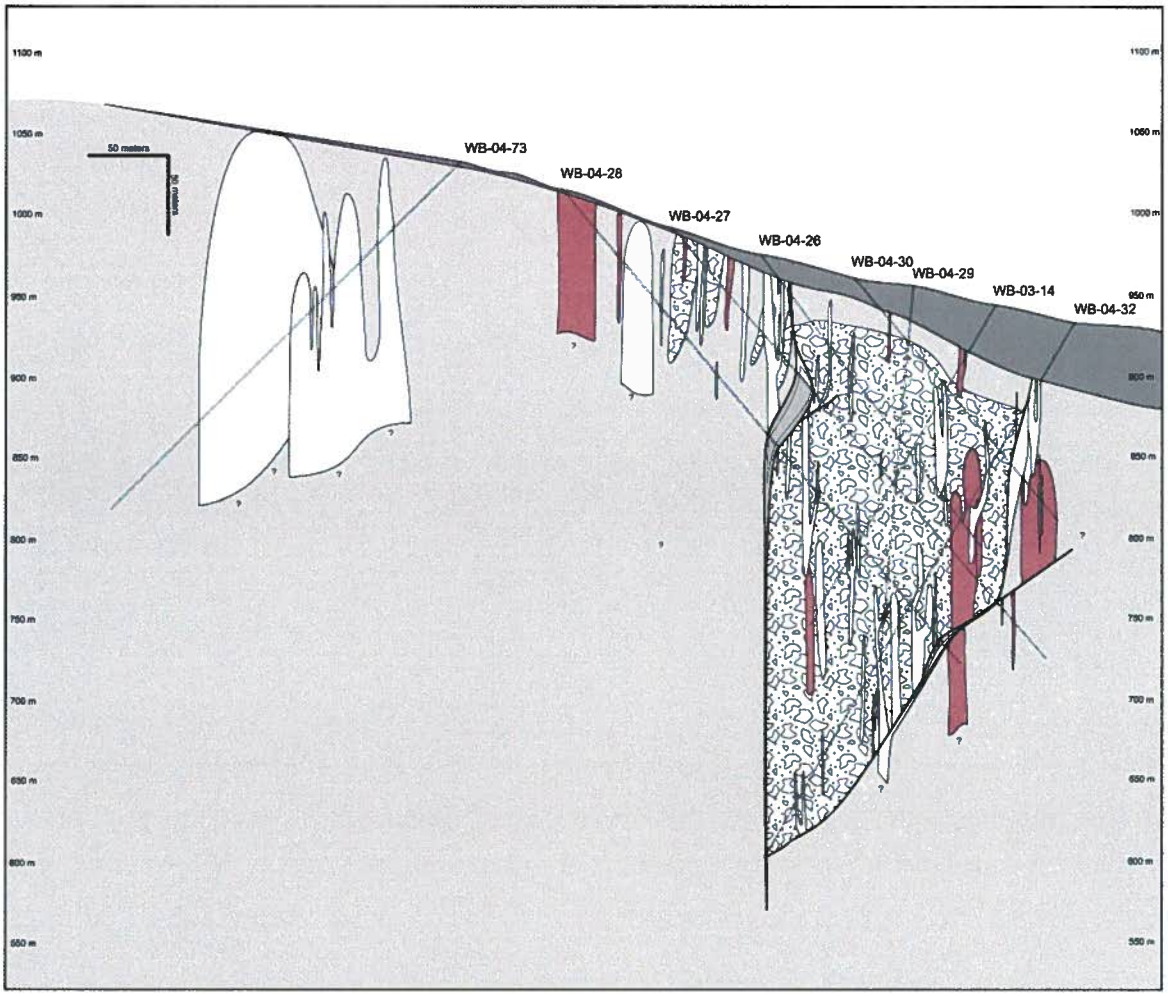

Figure 3.25b-Hornblende and hornblende-biotite bearing equigranular monzonite on section 18.

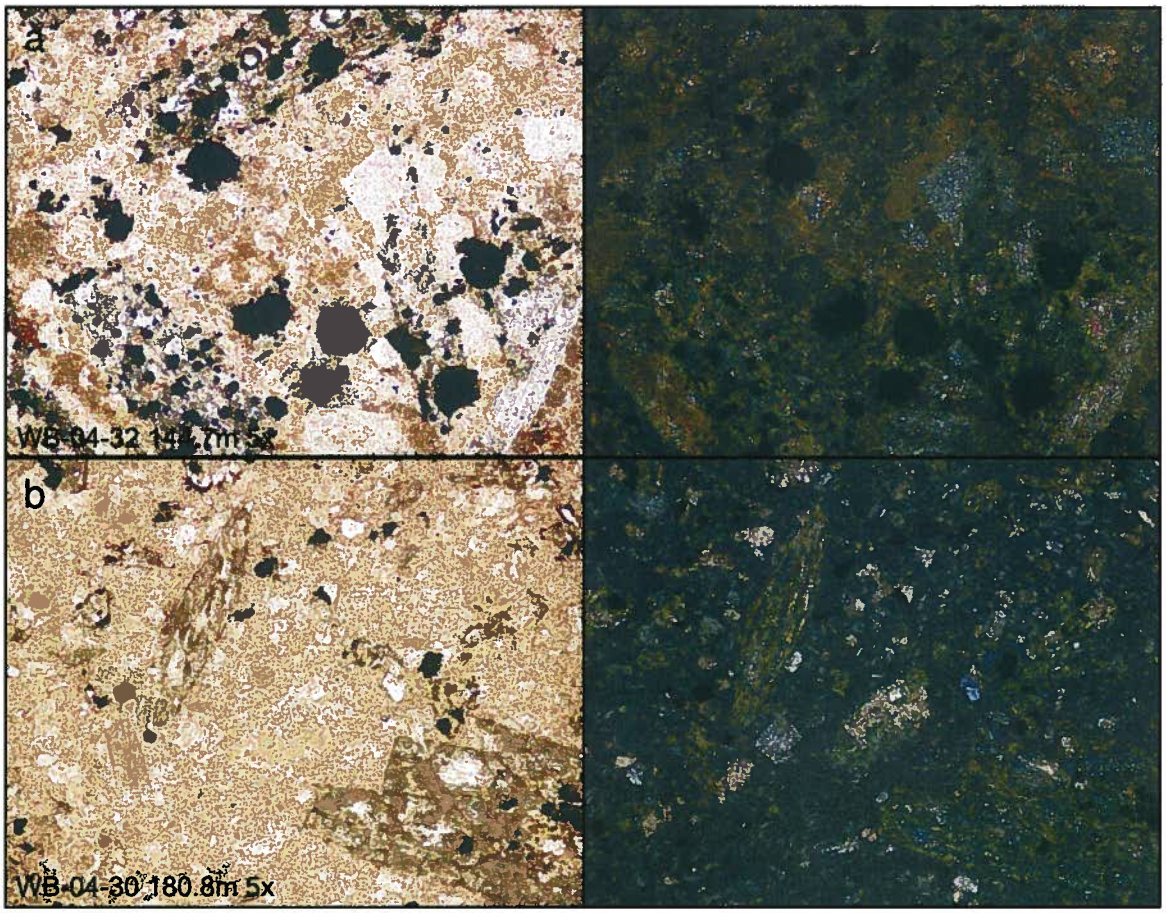

Figure 3.26- Photomicrographs of hornblende in equigranular hornblende monzonite. Note the replacement of mafic minerals by chlorite in both samples. Opaques (both pyrite and magnetite) are common (a); where opaques are less abundant, the shape of the primary hornblende is more apparent (b).

The most common, although not the most voluminous, dykes in the Northeast zone are trachyte dykes (figure 3.27). No trachyte dykes of mappable scale were observed in section 29, but they were abundant in section 18. These dykes are dark brown in color, aphanitic, and are observed cross-cutting all but the mafic and augite porphyry dykes. The term "trachyte" is used here in the sense of an aphanitic equivalent of monzonite, not as a textural term denoting flow alignment of phenocrysts (Bateman et al., 1989). They commonly form 2-5 cm 'microdykes' cutting other units (figure 3.28). These dykes are commonly vesicular or amygdaloidal (figure 3.29). The trachyte also commonly forms local intrusive infill breccias where it cross-cuts breccia or fractured

monzonite units (figure 3.30). The trachytes also frequently form the clasts of carbonate and gypsum-cemented mosaic and jigsaw breccias related to the latest stages of hydrothermal activity in the Northeast zone (figure 3.31, see chapter 5).

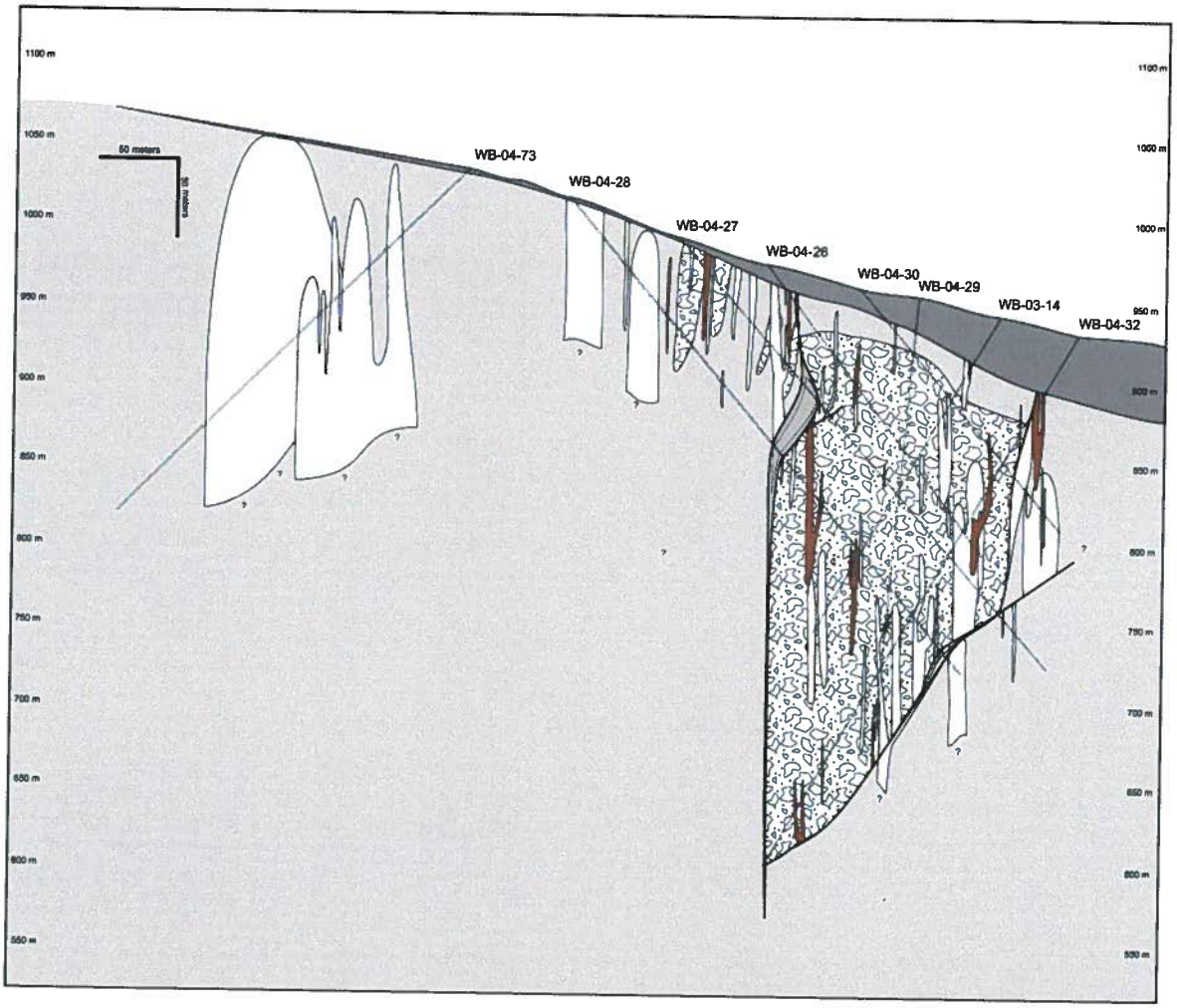

Figure 3.27-Trachyte dykes on Section 18.

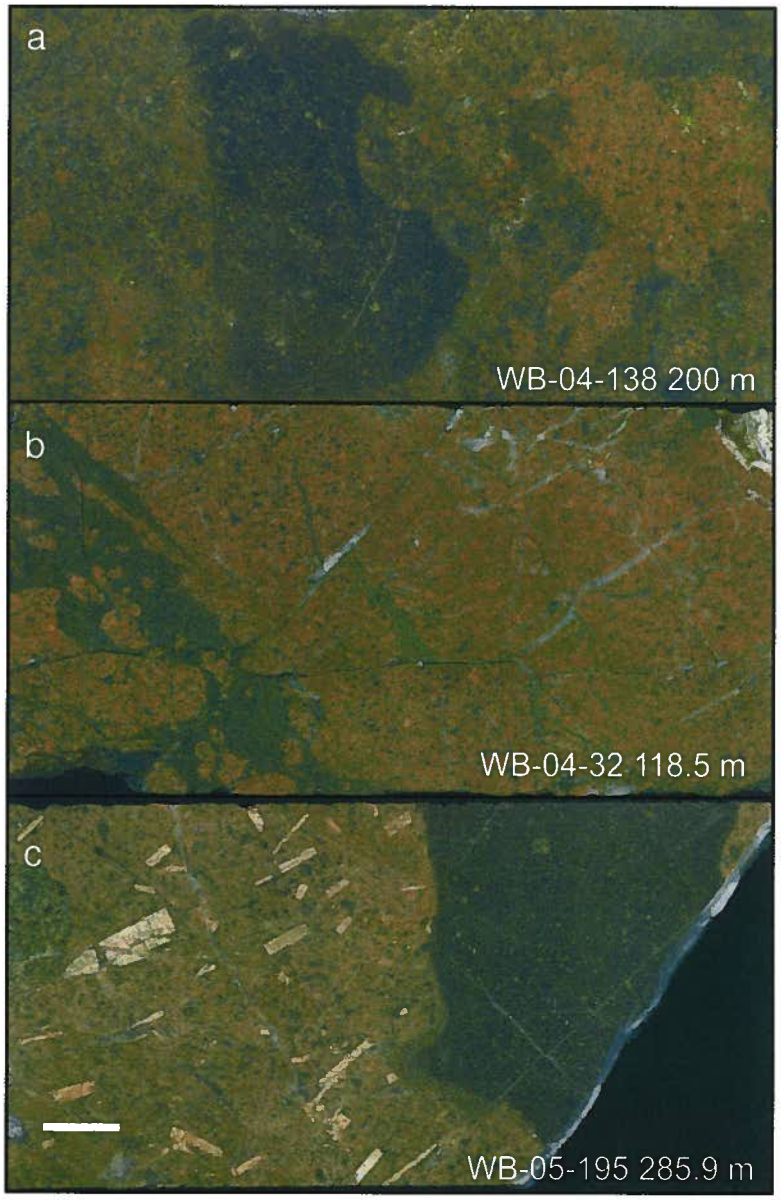

Figure 3.28-Trachyte microdykes cutting hydrothermal breccia. a; trachyte microdyke cutting breccia; note the irregular margin on the right controlled by the breccia texture. b; irregular trachyte microdyke controlled by fractures in coherent equigranular monzonite. c; trachyte microdyke with chilled margin against megacrystic monzonite porphyry. Scale bar equals 1 cm.

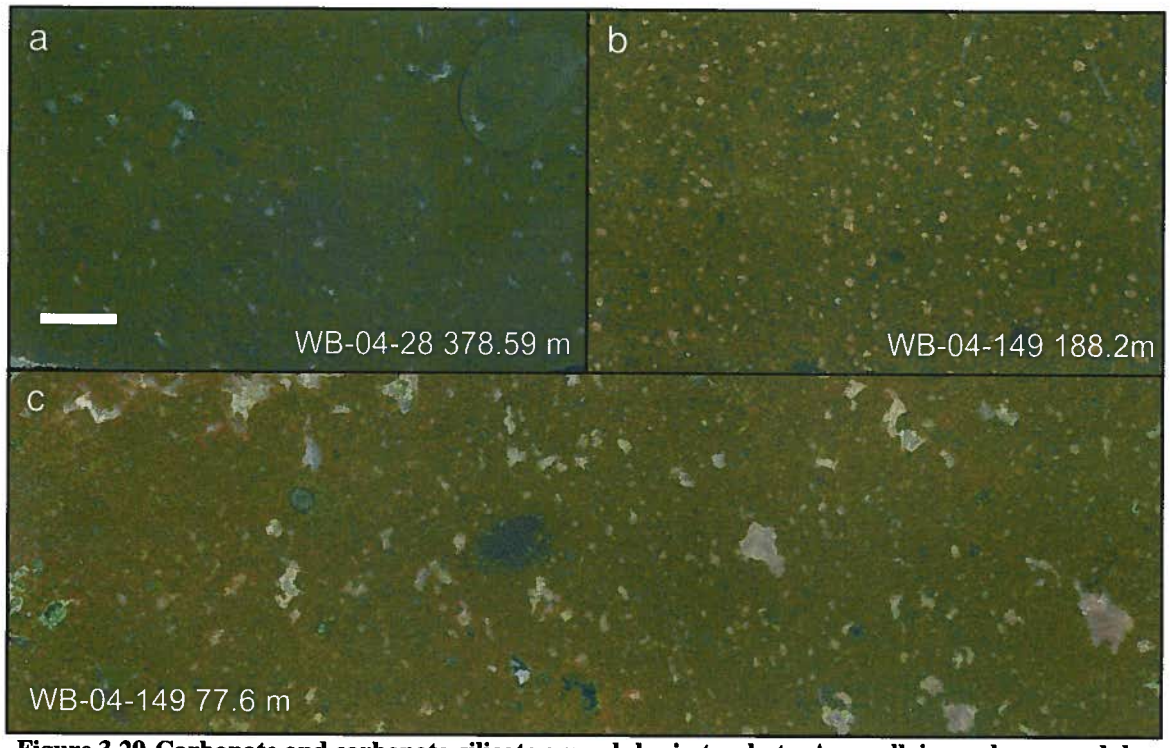

Figure 3.29-Carbonate and carbonate-silicate amygdules in trachyte. A; small, irregular amygdules in even-textured, aphanitic trachyte; b; small, rounded amygdules in even-textured, fine-grained trachyte; c; large, irregular amygdules filled with multiple minerals. Scale bar equals 1 cm.

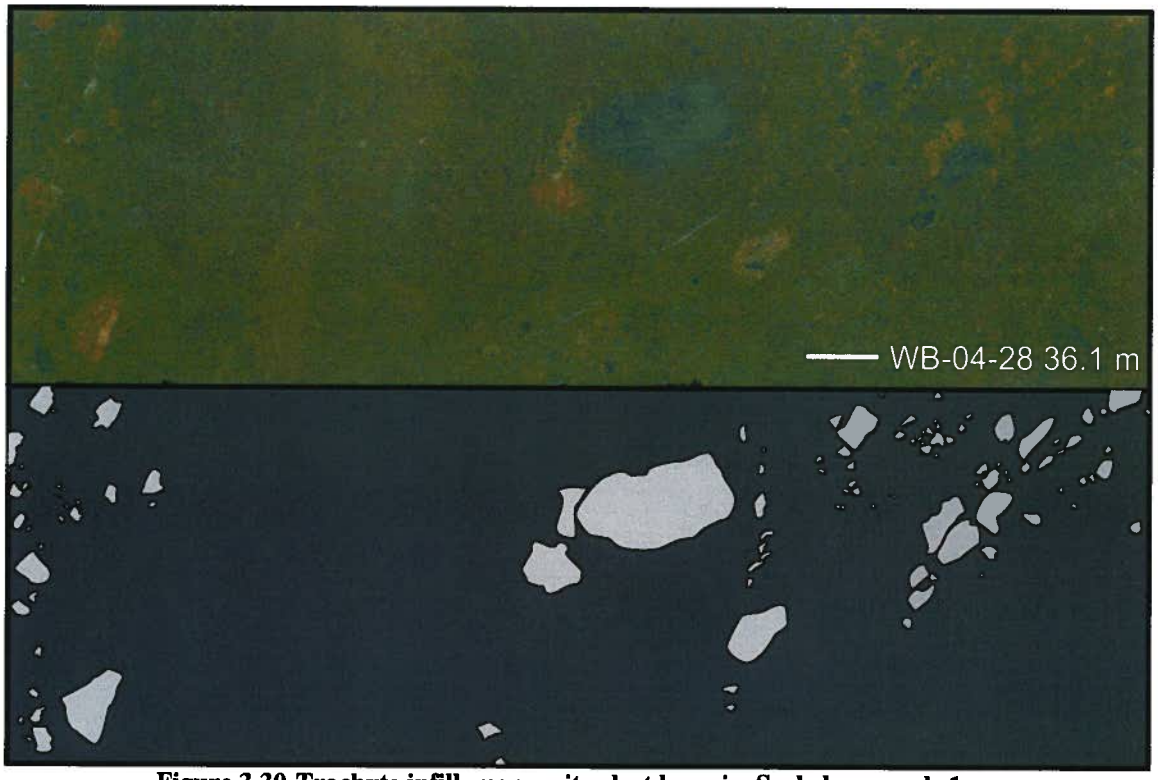

Figure 3.30-Trachyte infill, monzonite clast breccia. Scale bar equals 1 cm.

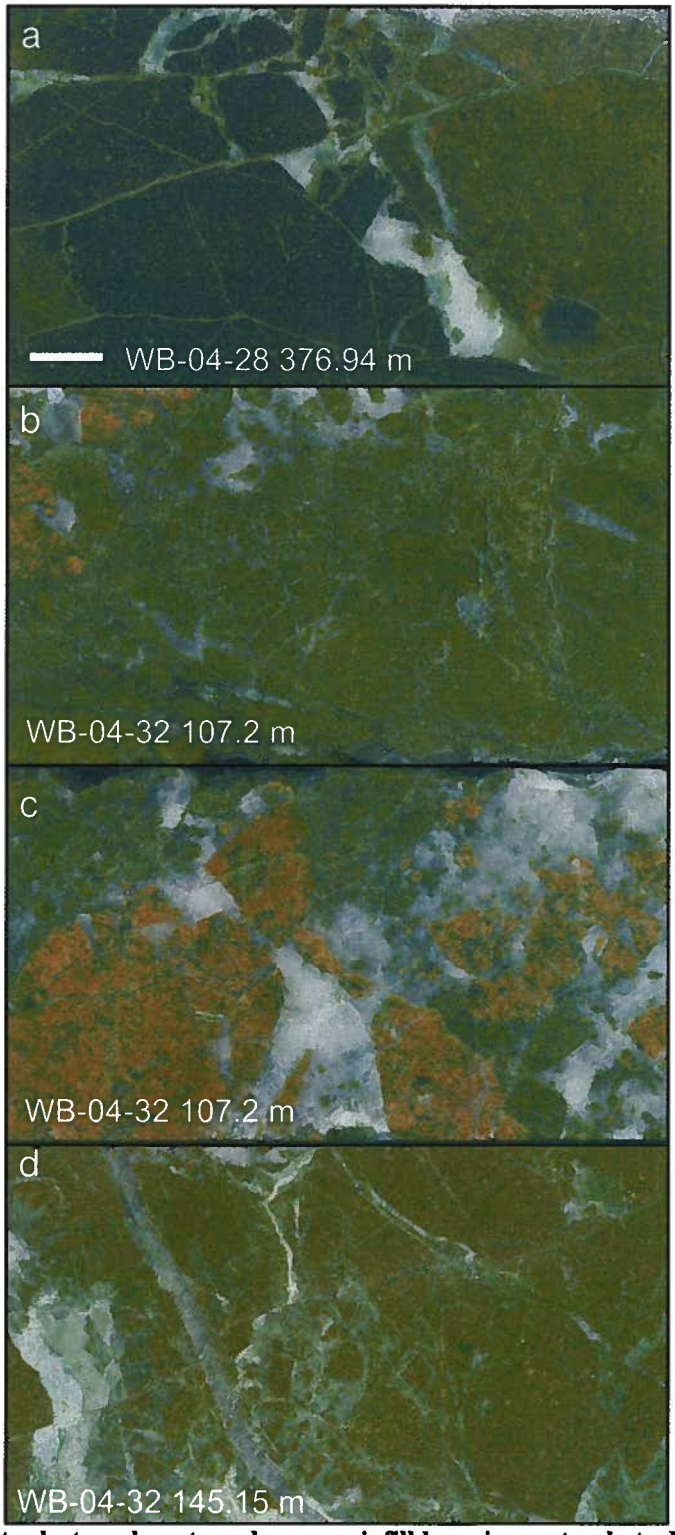

Figure 3.31-Trachyte clast, carbonate and gypsum infill breccias; a; trachyte dyke cut by fluorite-carbonate infill breccia; b; carbonate-infill crackle breccia; c; carbonate infill breccia crosscutting equigranular monzonite/trachyte contact; d; carbonate-infill, trachyte-clast breccia crosscut by gypsum vein. Scale bar equals 1 cm.

In thin section, the trachyte dykes contain 70-80% fine-grained biotite (figure 3.32). They are considered the end-member of the hornblende- to hornblende- and biotite-bearing equigranular monzonite. This family of dykes shows a trend of increasing mafic content and increased hydrous mineral content over time.

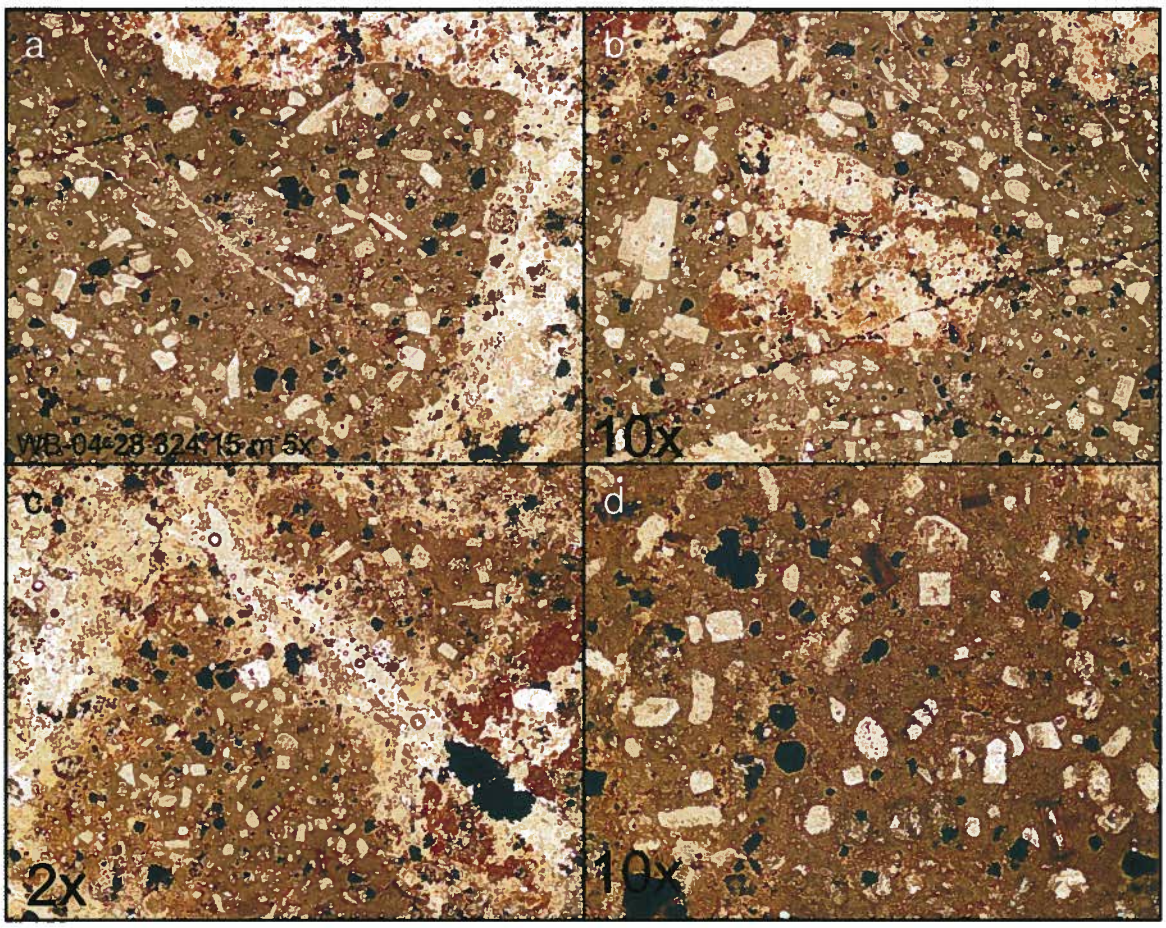

Figure 3.32-Photomicrographs of a trachyte microdyke. The dominant groundmass mineral in the microdyke is biotite. A; margin of the microdyke; b; K-feldspar phenocryst in the microdyke; c; carbonate vein crossing the microdyke margin; d; euhedral and resorbed phenocrysts in the microdyke. Field of view 5 mm.

Diorite and plagioclase porphyry

Two distinct units in the Northeast zone compose the diorite group. The plagioclase porphyry observed in Section 29 consists of an aphanitic dark brown or green-brown groundmass crowded with 2-3 mm plagioclase phenocrysts which make up

>60% of the rock. The 'dark monzonite' is an equigranular fine-grained dark brown rock, also dominated by plagioclase, which forms larger bodies in section 18. The timing relationship between them is ambiguous, as the "dark monzonite" was only observed in Section 18 and the plagioclase microporphyry was only observed in Section 29 (figure 3.33).

Both units appear to post-date most alteration and all mineralization. They are cut only by the mafic dykes described below.

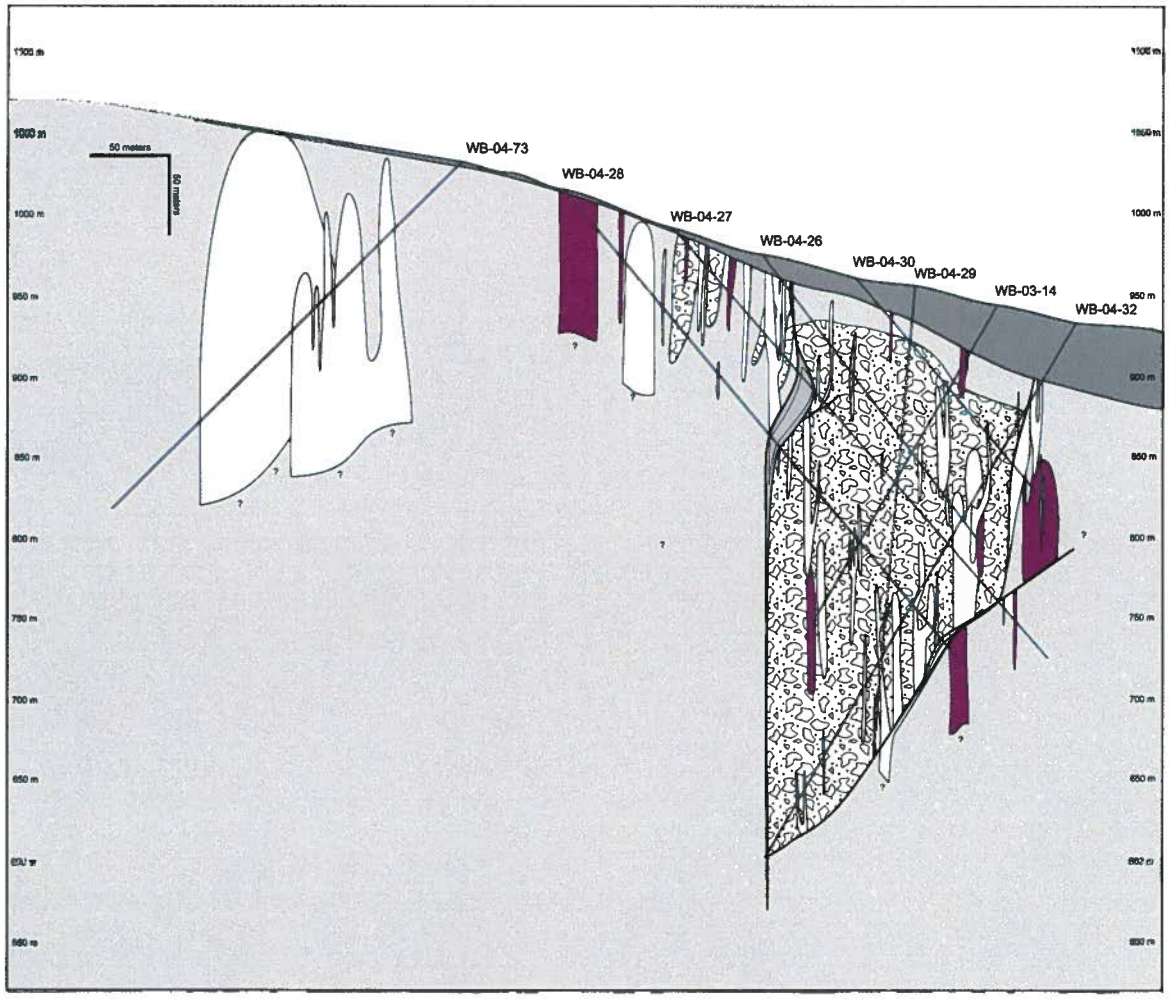

Figure 3.33a-Dark monzonite dykes on section 18.

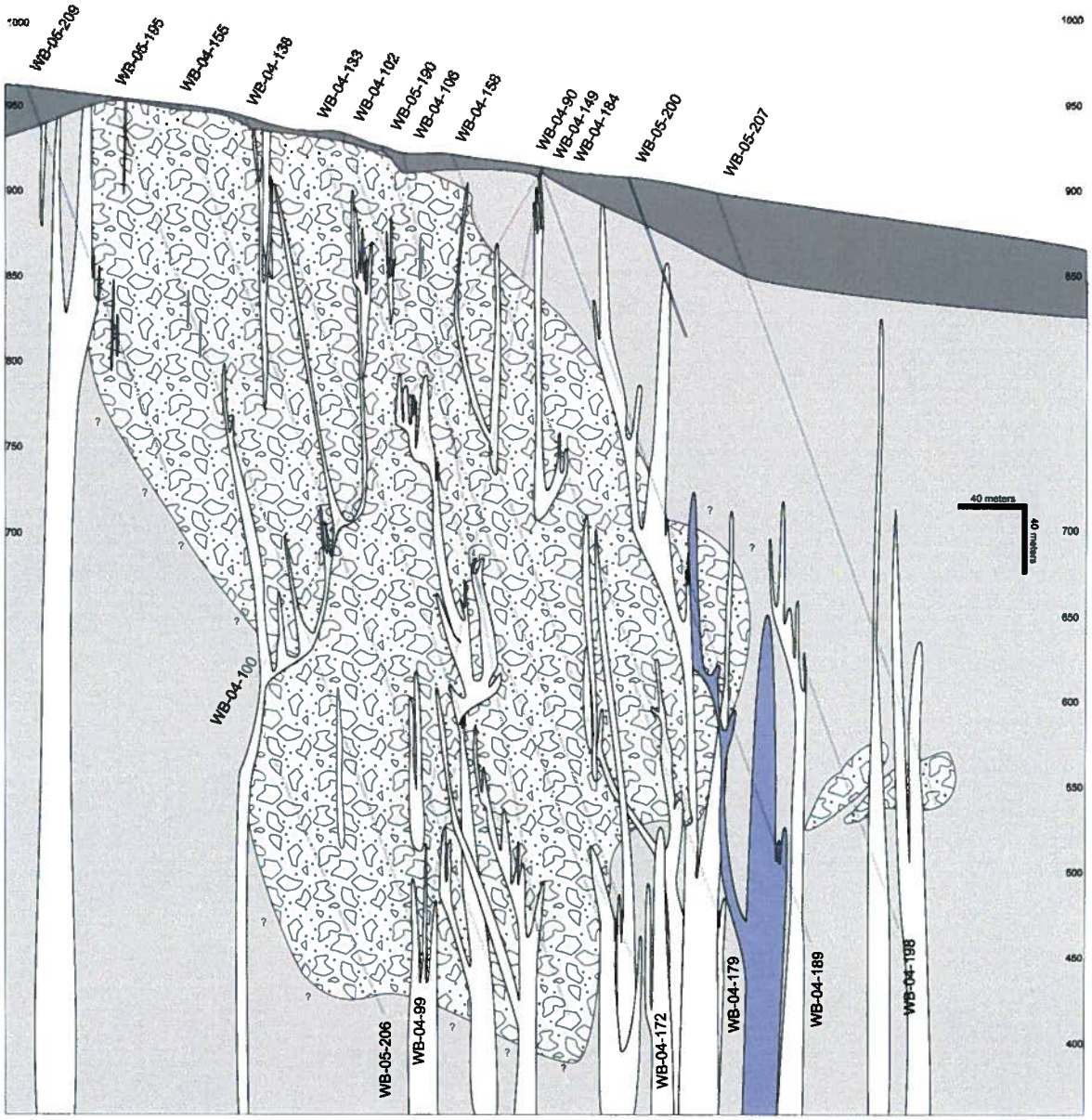

Figure 3.33b-Plagioclase porphyry dyke on section 29.

Mafic dykes

Aphanitic, green-black mafic (alkali basalt) dykes are the most distinctive dykes in the Northeast zone (figure 3.34). The mafic dykes have complex intrusive margins against other units, showing distinct chilled margins. In many cases the dyke material infiltrates the breccia, forming intrusive cement breccias. In a few cases, these intrusive cement breccias show grading parallel to the dyke margins. (figure 3.35). The mafic dykes can be

subdivided into a three subtypes: augite-phyric, plagioclase-phyric, and olivine-phyric. All three dyke types have fine-grained, plagioclase-dominated groundmasses with augite and/or olivine phenocrysts (figure 3.36). All three dyke types contain local carbonate and carbonate-silicate amygdules.

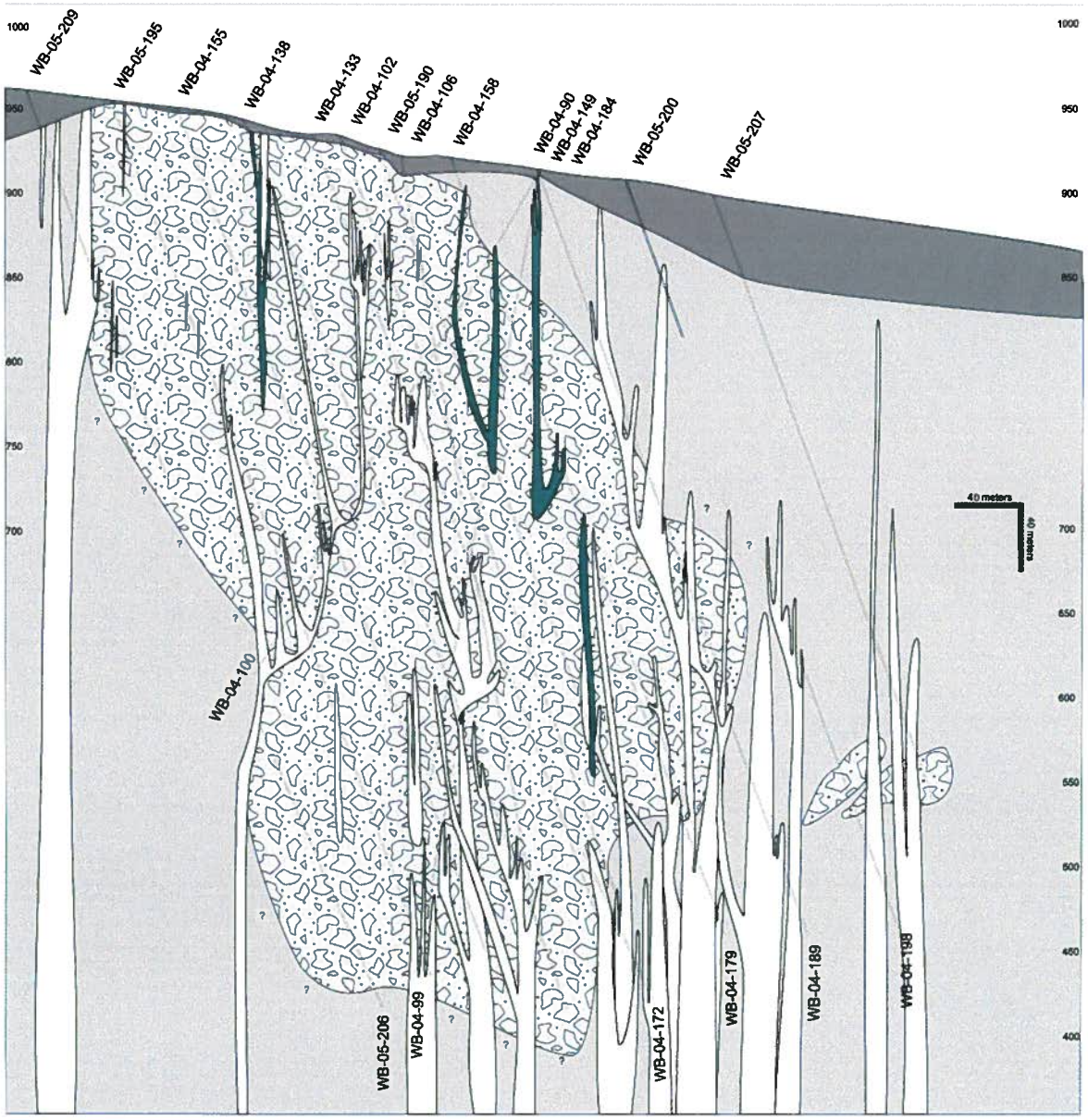

Figure 3.34-Mafic dykes on section 29.

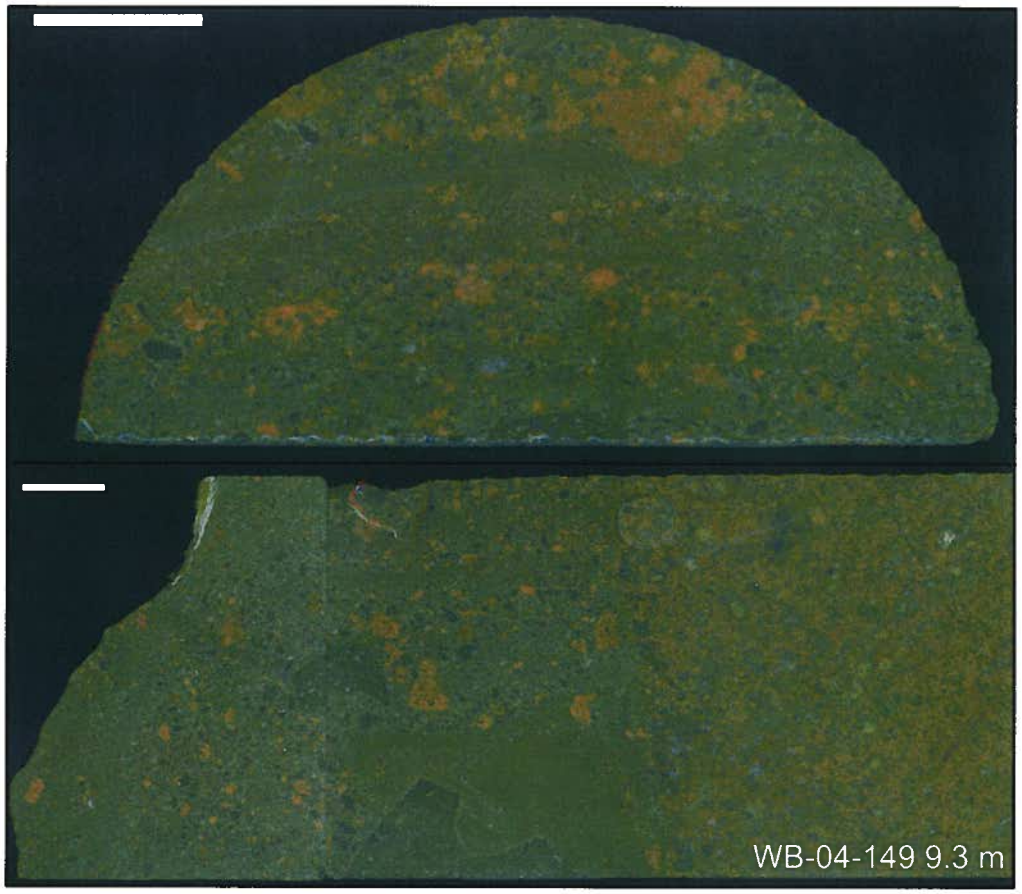

Figure 3.35-Grading of clastic material parallel to mafic dyke margins. Scale bars both equal 1 cm.

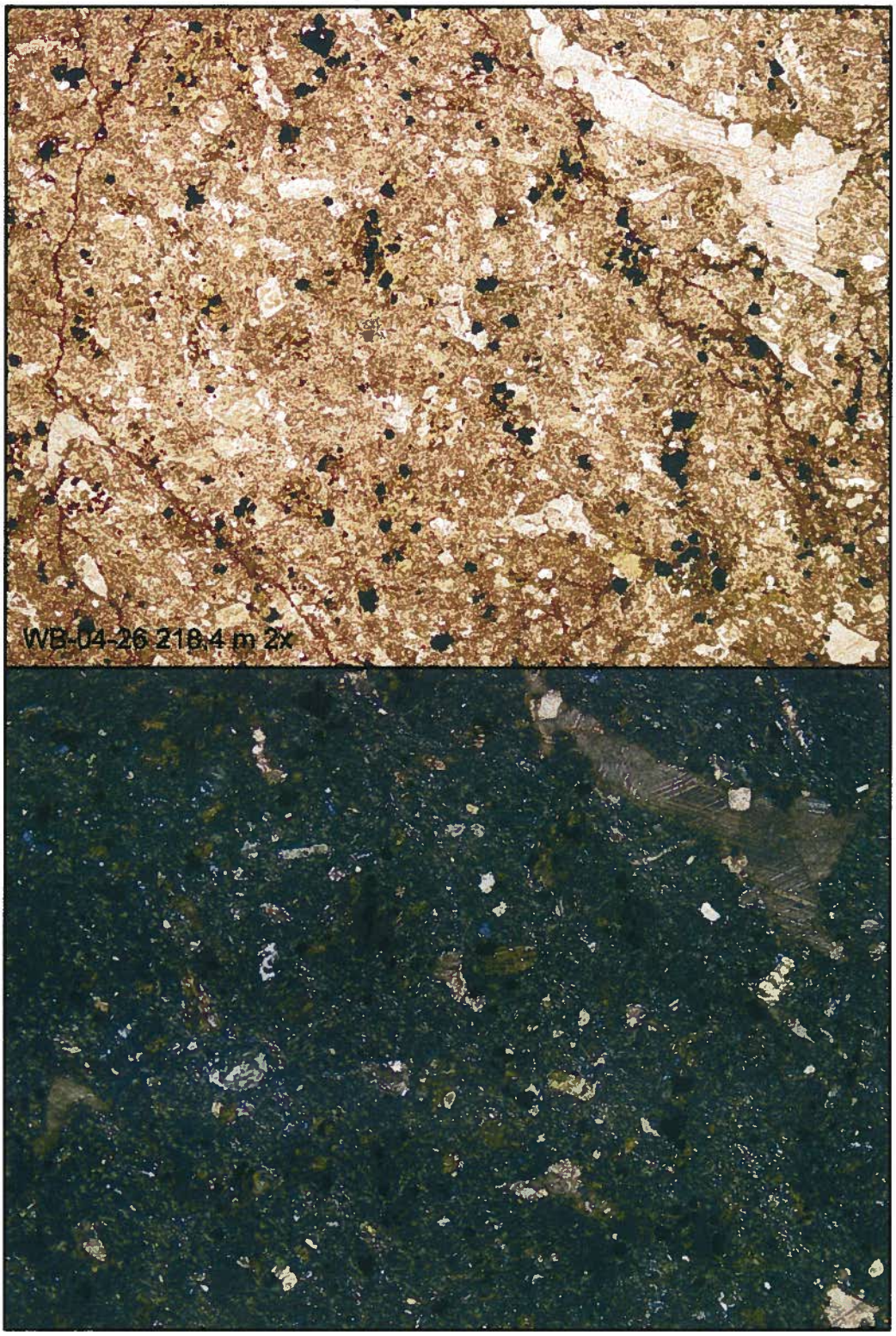

Figure 3.36- Photomicrographs of a mafic dyke, including a carbonate amygdule (top right). Top; plane polars; bottom; crossed polars. Field of view 5 mm.

Augite-phyric mafic dykes are the most difficult to recognize in hand sample, as the <2 mm black augite phenocrysts blend into the aphanitic black groundmass of the dyke. The phenocrysts make up <5% of the rock, and are most visible where the rock has been partially altered to late sericite. The augite-phyric mafic dykes are cut by plagioclase-phyric mafic dykes (figure 3.37). The contacts between the plagioclase-phyric and augite-phyric mafic dykes are commonly indistinct, but the presence of 3-5% very fine, white, elongate plagioclase phenocrysts distinguish the former unit. The plagioclase phenocrysts are <2 mm long and <0.5 mm wide, and show flow alignment along the margins of the dykes (figure 3.38). The plagioclase-phyric mafic dykes are distinguished from the plagioclase porphyry by their finer grain, darker color, and less abundant phenocrysts.

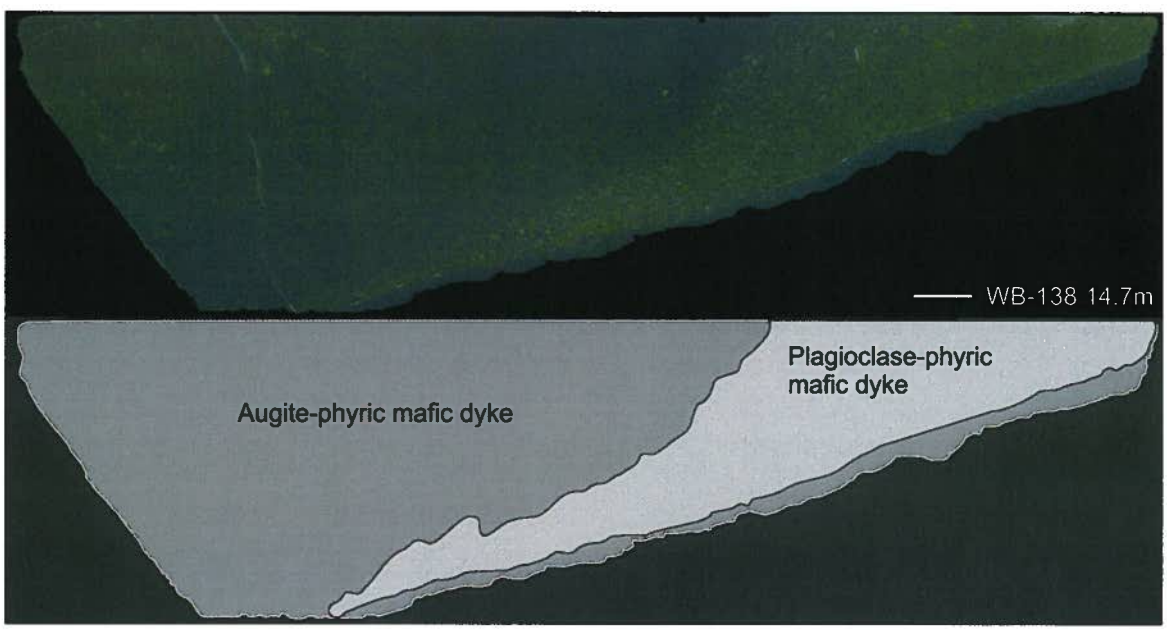

Figure 3.37-Plagioclase-phyric mafic dykes cutting augite-phyric mafic dyke. Scale bar equals 1 cm.

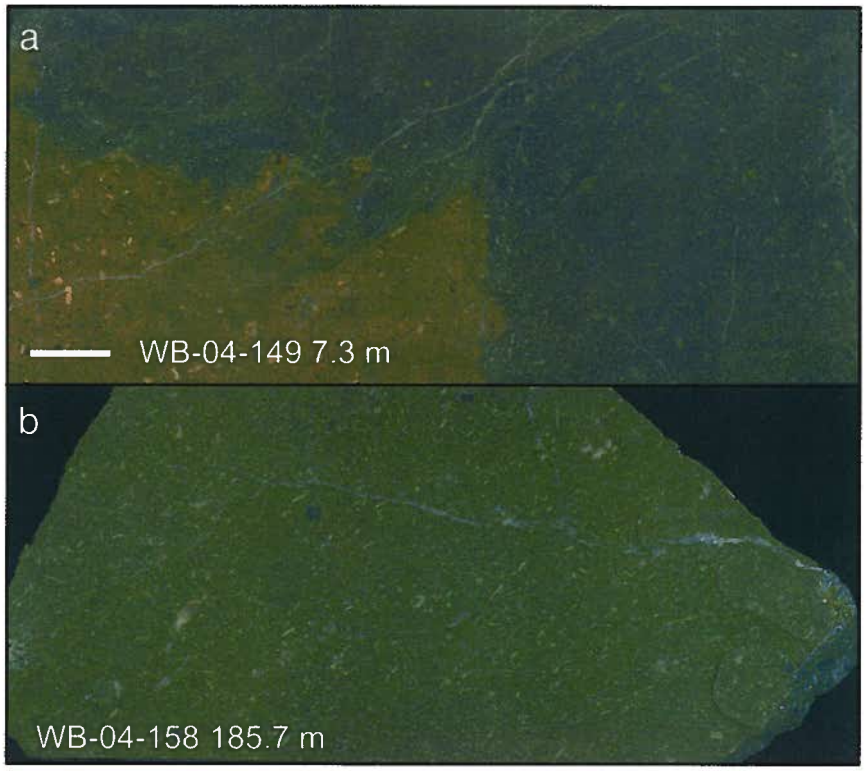

Figure 3.38-Plagioclase-phyric mafic dykes showing flow alignment of phenocrysts. A; aligned phenocrysts along the dyke margin; b; aligned phenocrysts within a dyke. Scale bar equals 1 cm.

Emplacement of the augite- and olivine-phyric mafic dyke with respect to the other mafic dykes is ambiguous due to the rarity of the olivine-bearing unit. Olivine forms 5-7% of the rock, as euhedral phenocrysts typically rimmed by bright red iddingsite (figure 3.39). Augite forms 2-3% of the rock as more subtle, blocky black phenocrysts in the dark groundmass of the dyke. The presence and preservation of olivine in these dykes suggests that the olivine-phyric dykes post-dated all hydrothermal activity except that responsible for the sericite-quartz-carbonate alteration assemblage (see Chapter 5).

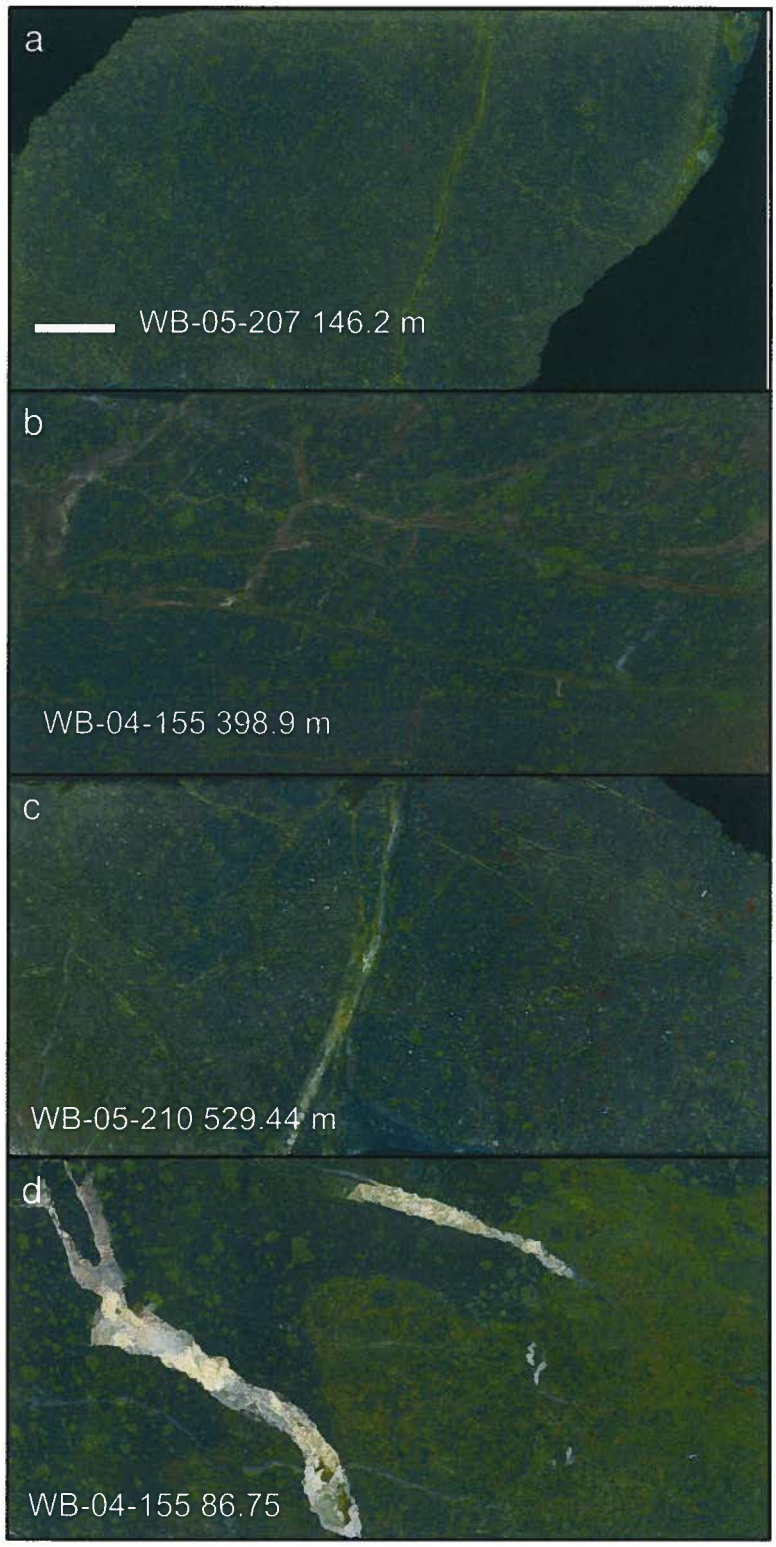

Figure 3.39-Olivine-phyric mafic dykes. A; Variably-sized olivine phenocrysts; b; carbonate veins cutting olivine phenocrysts; c; olivine phenocrysts altered to dark red iddingsite; d; complex dyke margins.
Scale bar equals 1 cm.

Augite Porphyry

Unlike the mafic dykes described above the augite porphyry has a fine-grained, bright green groundmass with conspicuous, blocky, 2-3 mm black augite phenocrysts (figure 3.40). Direct cross-cutting relationships between the augite porphyry and aphanitic mafic dykes were not noted. The augite porphyry dykes have a notably different habit and distribution than the other dykes in the system; rather than being fairly planar or branching and steeply dipping, the augite porphyry dykes exploit or are exploited by fault surfaces (figure 3.41). They are irregular in width and orientation. Where observed in core, the dykes commonly display chilled margins on one edge, with gouge indicating reactivation of the other contact. On the basis of this unique habit, the augite porphyry dykes were assigned the latest timing in the igneous sequence.

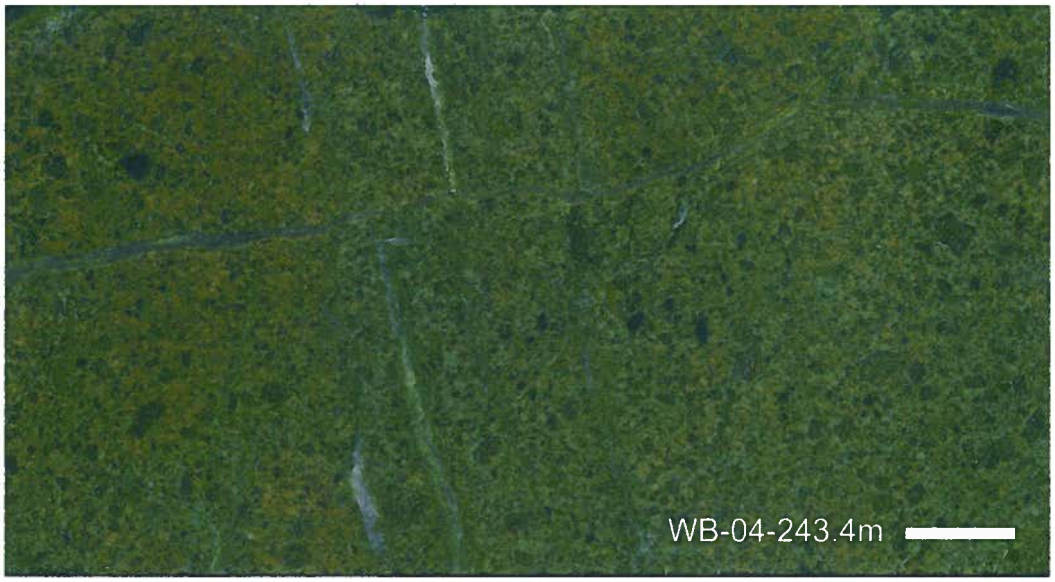

Figure 3.40-Augite porphyry. Scale bar equals 1 cm.

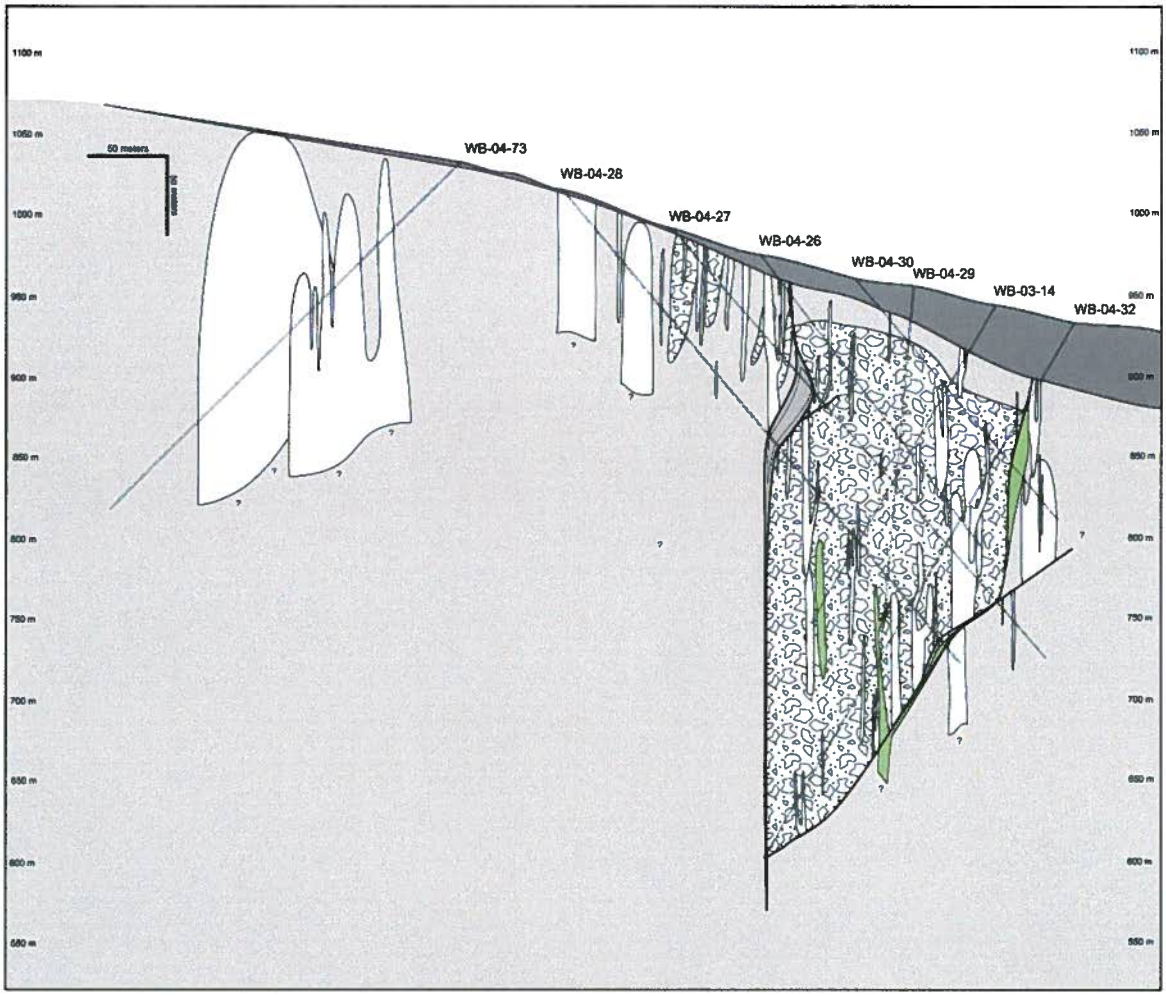

Figure 3.41a-Augite porphyry dykes on section 18.

In thin section, the augite porphyry consist of 60-70% fine-grained elongate plagioclase crystals, 25-35% large euhedral augite phenocrysts, and <5% small subhedral olivine phenocrysts (figure 3.42). The augite porphyry is distinctly coarser grained than the members of the mafic dyke family. Ross (2004a and b) noted that the augite porphyry is also chemically distinctive; this will be addressed in more detail below.

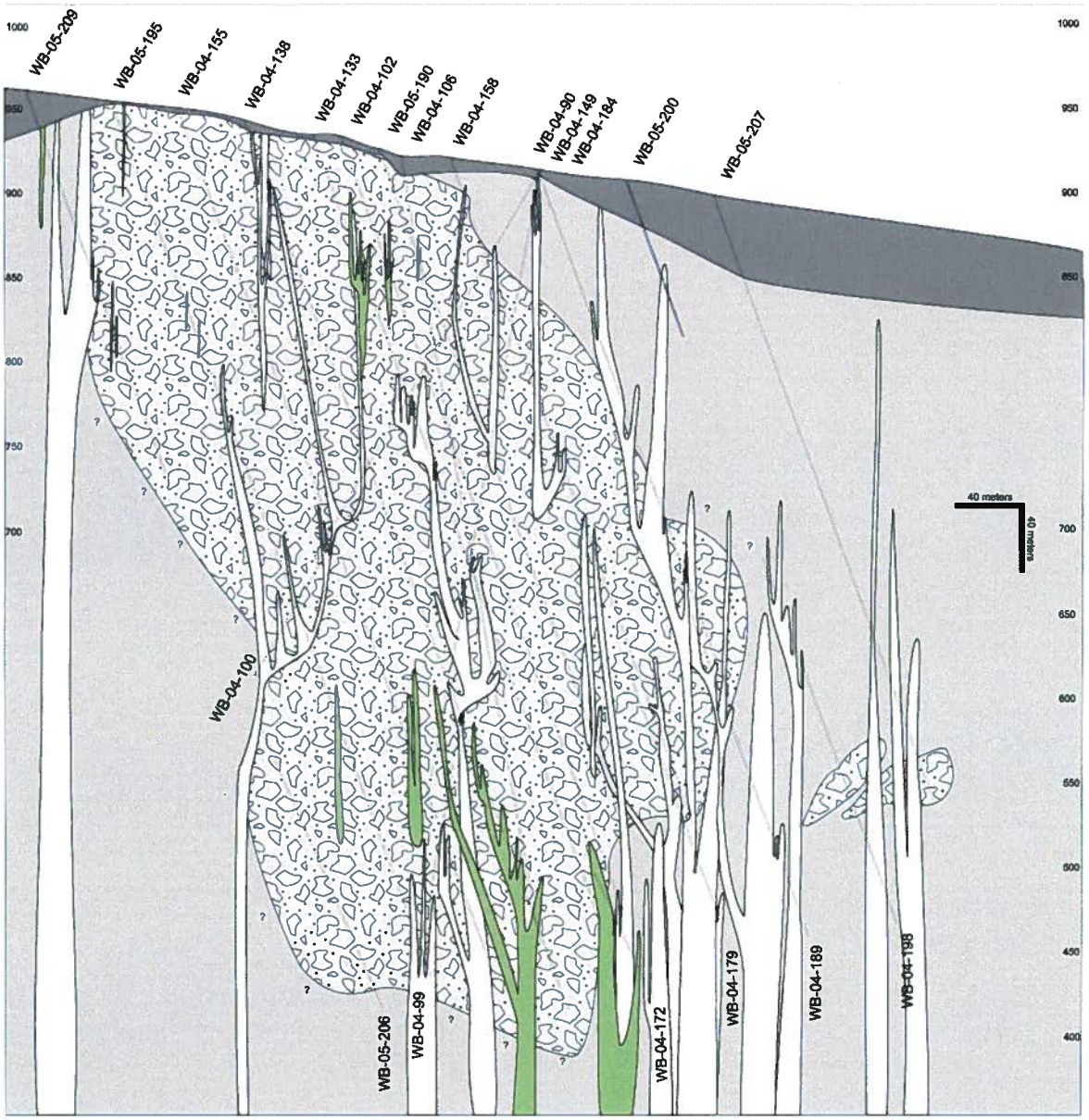

Figure 3.41b-Augite porphyry dykes on Section 29.

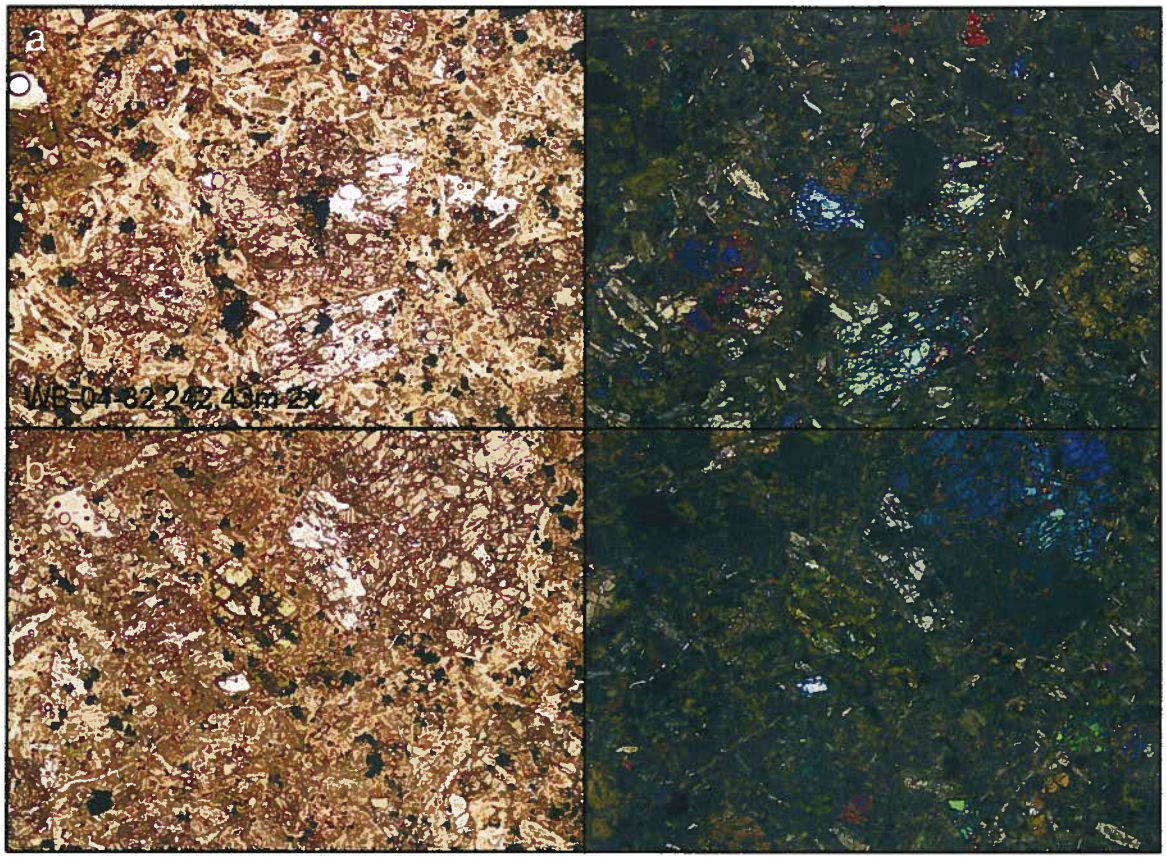

Figure 3.42-Photomicrographs of augite porphyry, showing polycrystalline augite phenocrysts in a dominantly plagioclase groundmass. A; monocrystalline and polycrystalline augite phenocrysts; note the two dominant orientations of the plagioclase grains in the groundmass. B; polycrystalline prismatic augite phenocryst, top right. Field of view 2.5 mm.

Conclusions

The intrusive rocks of the Northeast Zone appear to reflect a trend of increasing differentiation and increasing residence time culminating with the syn-breccia K-feldspar monzonite porphyry. Following brecciation and the intrusion of the syn-breccia K-feldspar monzonite porphyry, this trend is reversed, as the post-breccia dykes become increasingly mafic, hydrous, and fine-grained.

Chapter 4 -Characteristics of the Northeast Zone Breccia

Introduction

Magmatic-hydrothermal breccias

Hydrothermal and magmatic-hydrothermal breccias are common in porphyry copper deposits (Lowell and Guilbert, 1970; Gustafson and Hunt, 1975; Sillitoe, 1985; Laznicka, 1988; Corbett and Leach, 1996 and 1998). Depending on their timing relative to mineralization and the nature and genesis of the breccias, they can provide either preferential sites for mineralization and high-grade zones, or they can provide fluid barriers that retard movement of fluids, causing the ponding of mineralizing fluids adjacent to low-grade or barren zones (Burnham, 1979; Burnham, 1985; Sillitoe, 1985; Bushnell, 1988; Zweng and Clark, 1995; Serrano et al., 1996). Late breccia formation can dilute ore by mixing fragments of variably mineralized rock, or by erupting, venting potentially mineralizing fluids to the atmosphere and diluting the grade of the rock mass. Establishing those relations are important as breccia can have strong influences on distribution of metals and the economics of the deposit.

At Mount Polley, the relationship between breccia and economic mineralization is strong (Barr et al., 1976; Bailey, 1976; Fraser, 1993, 1994 a and b; Fraser et al., 1995; Read, 1997; Bailey, 2004a and b; Gillstrom, 2004; Rees et al., 2005 and 2006). Nearly all Cu-sulfide minerals are confined to breccia bodies, but not all areas within the breccia are mineralized (Fraser et al., 1995; Rees et al., 2005 and 2006). Understanding the interaction between brecciation and mineralization processes is important to distinguishing prospective from less prospective volumes of breccia, and to recognizing possible potential for economic mineralization in areas which may not show evidence for

brecciation at present erosional levels (Burnham, 1979; Burnham, 1985; Sillitoe, 1985; Bushnell, 1988; Zweng and Clark, 1995; Serrano et al., 1996). Clarifying the origins and architecture of the breccia can also assist in structural reconstruction of the district as a whole, and to recognition of further mineral potential.

"Classic" breccia-associated porphyry deposits

Sillitoe (1985) estimates that 50-60% of porphyry orebodies are spatially related to breccias. These breccias take a variety of roles in the localization of ore. For example, pre- or syn-mineral breccia could have acted as a permeability control on fluid flow or a chemical trap, which caused deposition of ore and gangue minerals (e.g. the Maria breccia, La Cananea, Mexico (Bushnell, 1988)), or the formation of a breccia can drastically change the nature of the ore deposition environment (e.g. the collapse of the Louise Volcano at the Ladolam deposit, Lihir, Papua New Guinea (Mueller et al., 2002, Carman, 2003) and the Kelian deposit, Borneo (Davies, 2002; Davies and Cooke, 2000)). Conversely, a post-mineral breccia body could excise portions of the sulfide ore body system (e.g. the Braden pipe at the El Teniente deposit, Chile (Skewes et al., 2002, Cannell et al., 2005).

Review of classification and processes

Breccias are produced by a wide variety of geologic processes and combinations of processes (Laznicka, 1988). The formation of a breccia requires varying degrees of breakage, transport, comminution, and cementation (Jebrak, 1997). The processes involved can be sedimentary/diagenetic, volcanic, tectonic, magmatic, or hydrothermal (Davies, 2002). Even within the subset of hydrothermal, magmatic, and volcanic ore-associated breccias common in porphyry deposits, breccias have been defined and

classified via a wide variety of descriptive and genetic schemes (e.g. Bryner, 1961 and 1968; Sillitoe, 1985; Baker et al., 1986; Laznicka, 1988; McPhie et al., 1993; Taylor and Pollard, 1993; Corbett and Leach, 1998; Davies, 2002). Most schemes have been intended to discriminate between breccias formed by different genetic processes or combinations of processes. Some sources distinguish between processes of breakage, transport, and comminution, whereas others do not.

In order to comprehend the relationship between brecciation and mineralization, the process of "brecciation" is divided into four approximately sequential subprocesses (Jebrak, 1987):

I. Breakage

II. Transport

III. Comminution and sorting

IV. Cementation

In attempting to assign semi-quantitative parameters to these processes, conceptual work done by Burnham (1985) and Fournier (1999) on brecciation in calc-alkaline rocks was restated to consider the different physical, mechanical, and chemical properties of the silica-undersaturated rocks in which the Mount Polley breccias formed. Minimum prerequisites for brecciation are: 1) energy and 2) open space (Jebrak, 1997; Ross et al., 2001 a and b; Ross, 2002). Energy is consumed by fragmentation and creation of new surface area (fracture energy, or energy required to overcome the work strength of the rock), plasticity (friction) and elastic wave energy dispersion (Cummins and Given, 1973). Open space must be sufficient to accommodate the difference between the volume of the original rock mass and the volume of open packing of the fractured rock mass

(Cummins and Given, 1973). This amount of open space probably never existed as single opening or in aggregate at any one point during breccia development. Instead the open space formed is filled via the bulking effect of rock mass fracturing nearly simultaneously (Locke, 1926).

Descriptive classification

Despite the abundance of literature on breccias and brecciation processes, no generally agreed upon descriptive terminology has emerged. For purposes of this study, the descriptive terminology advocated by Davies, (2002) has been slightly modified. Davies described breccias using five elements: alteration, internal organization, components, grain size, and body geometry. With minor changes, this convention will be followed here (Table 4.1).

The five elements can be further subdivided. Alteration includes pre-, syn-, and post-breccia alteration. Internal organization includes dilation, grading, and sorting. The components, which are most commonly described in breccia bodies, include clasts, clastic infill, chemical infill, and open space. Grain size involves both grain size and grain size range and size distribution. Body geometry describes both the shape of the overall breccia body and distribution of the other characteristic within that volume.

Table 4.1-Breccia Descriptive scheme

BRECCIA DESCRIPTIVE SCHEME

5	+	4	+	3	+	2	+	1
Alteration		Internal Organization		Components A+B+C+D		Grain size		Body Geometry

1. Body Geometry
   - a. Geometry
     - i. Pipe
     - ii. Cone
     - iii. Dyke
     - iv. Irregular
     - v. Tabular
   - b. Orientation
     - i. Strike and dip of principle axes
     - ii. Strike and dip of irregular branches
   - c. Contacts
     - i. Sharp
     - ii. Gradational
     - iii. Irregular
     - iv. Faulted
     - v. Planar
   - d. Contact relationships
     - i. Concordant
     - ii. Discordant

2. Grain size
   - a. Mud (<1/16 mm)
   - b. Sand (1/16 - 2 mm)
   - c. Breccia / conglomerate
     - i. Fine-grained (2 - 4 mm)
     - ii. Medium-grained (4 - 64 mm)
     - iii. Coarse-grained (64 - 256 mm)
     - iv. Very coarse-grained (256 mm to 1 m)
     - v. Megabreccia (>1 m)
   - d. Grain size distribution
     - i. Normal
     - ii. Slightly bimodal
     - iii. Extremely bimodal

3. Components
   - a. Clasts
     - i. Monomict or polymict
     - ii. Lithology
     - iii. Shape
       - 1. Angular, subangular, subrounded, rounded, tabular, faceted, equant
   - b. Clastic infill
     - i. Rock flour
     - ii. Lithic fragments
     - iii. Crystal fragments
     - iv. Vein fragments
   - c. Chemical infill
     - i. Crystalline igneous rock
     - ii. Chemical
       - 1. Mineralogy
       - 2. Paragenesis
       - 3. Texture
         - a. massive
         - b. layered
         - c. drusy
         - d. bladed
         - e. cockade
   - d. Open space or vugs

4. Internal Organization
   - a. Dilation
     - i. Crackle
     - ii. Mosaic
     - iii. Rotated
     - iv. Transported

5. Alteration
   - a. Clast alteration
   - b. Matrix alteration
   - c. Textural destruction

Alteration

Alteration in breccias may be pre-, syn-, or post-brecciation (Beane and Titley, 1981; Gustafson and Hunt, 1975; Lowell and Guilbert, 1970). Alteration may take different forms in clasts than in infill; it may form veins which either transverse or are truncated at clast margins (Davies, 2002). Alteration assemblages may rim clasts, or they may be confined to either clasts or infill, subject to differences in reactivity, surface area, and fluid residence time or reactivity (Gifkins et al., 2005). Also, as per normal in coherent rocks, alteration may be stable with respect to some mineral phases in a rock and destructive with respect to others (Gifkins et al., 2005; Barnes, 1997). Assigning a single alteration classification to a breccia may thus be inaccurate and uninformative. Alteration was not used as a major criterion for subdividing breccia units at Mount Polley; it is discussed as a separate characteristic of the rocks, as Chapter 5.

Internal organization

Davies (2002) defines the internal organization of the breccia as a number of subsidiary characteristics including clast abundance (clasts greater than or less than infill), clast distribution (in situ, rotated, or chaotic), graded or non-graded, and stratified or unstratified. At Mount Polley, mineralogy and alteration made clast/infill boundaries locally difficult to pinpoint, making clast abundance difficult to define. For this reason clast abundance was seldom quantified, but described qualitatively.

Clast distribution, on the other hand, was found to merit more detailed subdivision. At Mount Polley a gradient was observed from intact ('coherent') country rock into chaotic, mixed and transported breccias (figure 4.1, Table 4.2). In order to capture this variability, breccias were described ranging from 'crackle breccias' (<1 mm infill between clasts,

jigsaw-fit, no visible rotation or transport), to 'mosaic breccias' (>1 mm infill between clasts, jigsaw fit clasts, no visible rotation or transport), rotated breccias (variable infill, visible rotation, but no mixing of clast types), chaotic breccias (variable infill, clasts cannot to be visually returned to their original positions, but all clasts represent a single rock type) and transported breccias (variable infill, clasts cannot be visually returned to their original positions and rock types are mixed) (Table 4.2).

These classifications are arbitrary, based on units which could be consistently defined from core-scale onservations. Mixtures of clasts of the same rock type but different alteration types presents a problem. Differences in alteration between clasts may be related to variation in susceptibility to post-breccia alteration, or to the syn-breccia mixing of clasts from different zones of alteration. Grading and stratification are not observed at Mount Polley.

Table 4.2-Breccia internal organization

BRECCIA INTERNAL ORGANIZATION					
Breccia type		**~%dilation**	**Infill**	**Alteration**	**Lithology**
Jigsaw	Crackle	<5%	Chemical	Uniform	Monomict
	Mosaic	5-10%	Chemical	Uniform	Monomict
Chaotic	Rotated	10-25%	Chemical or clastic	Uniform or mixed	Monomict
	Transported	>25%	Chemical or clastic	Mixed	Monomict or polymict

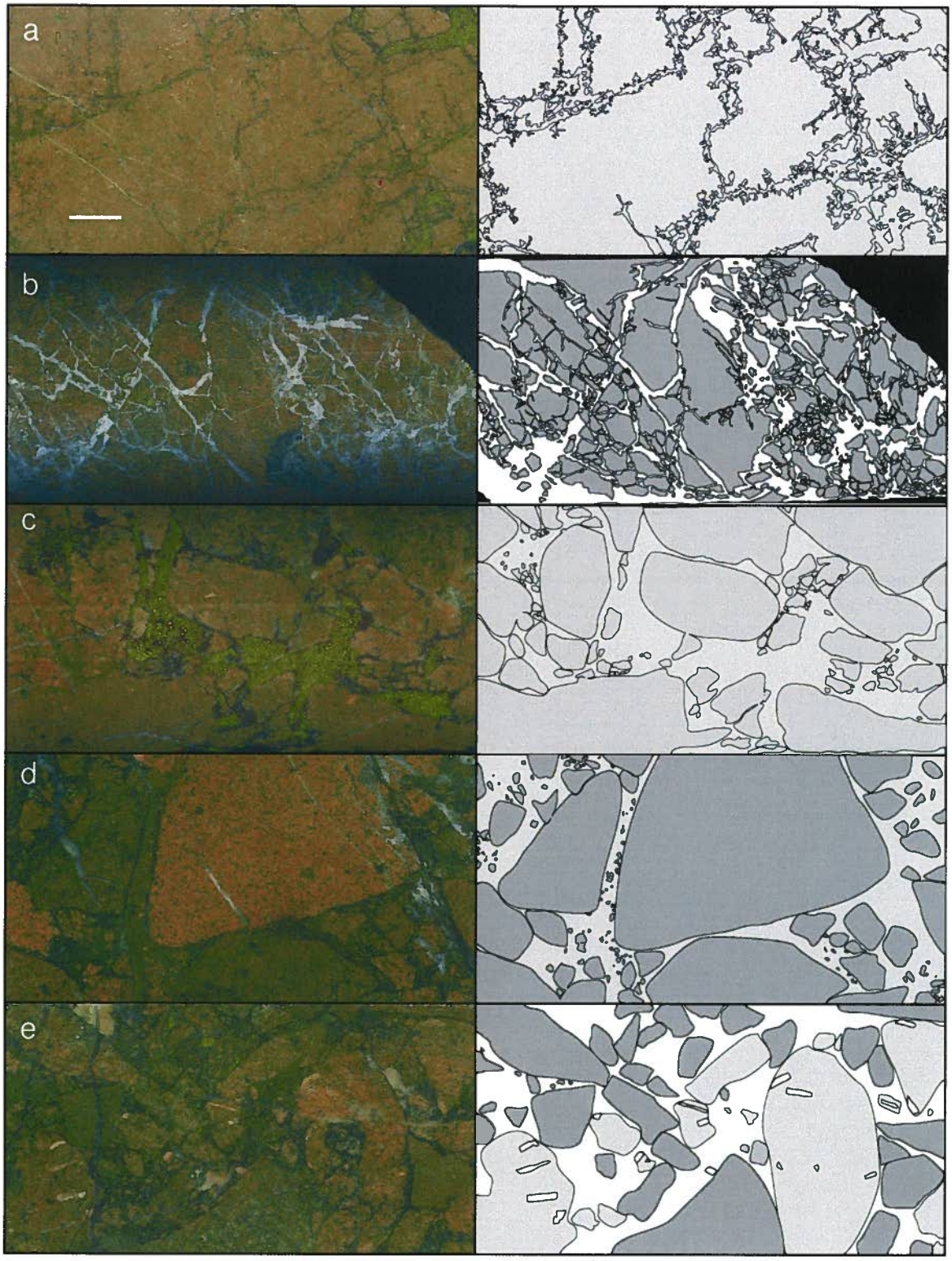

Figure 4.1-Breccia internal organization. A; crackle breccia, b; mosaic breccia, c; rotated breccia, d; transported monolithic and e; transported polylithic breccias. Scale bar =1 cm

Components

The components of the breccia are subdivided into clasts and infill. In the majority of breccia literature related to economic geology, infill is referred to as "matrix" without regard to its composition or origin (Bryner, 1961 and 1968; Sillitoe, 1985; Baker et al., 1986; Laznicka, 1988). Davies (2002) reserves the term "matrix" for clastic infill, and uses the term "cement" to denote chemically precipitated infill, in accordance with general practice in volcanology and sedimentology (McPhie et al., 1993). However, retention of a common term creates confusion. As such and to clarify the issue, infill is herein subdivided into open space, clastic infill, chemical infill, and igneous infill, avoiding the terms "matrix" and "cement" entirely. Open space preserved within breccias can be described on the basis of the size, percentage, and shape of voids or vugs. Clastic infill denotes material with a grain size of less than 2mm between clasts. This material is referred to elsewhere as rock flour matrix, milled matrix, hydrothermal sandstone, or 'mud' (Farmin, 1937; Emmons, 1938; Bryner, 1961 and 1968; Sillitoe, 1985; Baker et al., 1986; Laznicka, 1988; Kwak, 1990; McPhie et al., 1993; Taylor and Pollard, 1993; Serrano et al., 1996; Corbett and Leach, 1998; Davies, 2002; Jensen, 2003). The term 'clastic infill' is the most free of genetic connotation and potential confusion, especially in cases where there is no clear break between the grain size of the clasts and the grain size of the infill. Clastic infill also avoids confusion in situations where the material described includes lithic fragments, vein fragments, and crystal fragments. The texture of the clastic infill can also be described. Clastic infill can show laminated, graded, banded or draped textures (McPhie et al., 1993). It can be well or poorly graded, or massive (McPhie et al., 1993; Davies, 2002). At Mount Polley the great majority of clastic infill is massive. The grain size of the clastic infill is also an important characteristic, but this

becomes problematic when there is no clear size distinction between the clasts and the infill material. At Mount Polley, an arbitrary cutoff of 2 mm was selected. This decision will be discussed at more length below.

Chemical infill, also called cement, hydrothermal cement, or precipitate (Davies, 2002; Davies and Cooke, 2000; McPhie et al., 1993), involves any mineral that is precipitated by hydrothermal solutions in the spaces between settled clasts or onto the surfaces of clasts in suspension. In many cases, infill is an intimate mixture of clastic and chemical infill (figure 4.2). Chemical infill is described by mineralogy, paragenesis, grain size, habit (cockscomb, drusy, laminated, massive, etc.), just as it would be in a vein. At Mount Polley, where clastic and chemical infill are normally intermixed (figure 4.3) and where igneous infill is normally restricted to the margins of dykes cutting breccia, it was found to be useful to consider the three as end members of a ternary system (figure 4.4), thus separating igneous infill into its own category rather than including it within a broader ('cement') category.

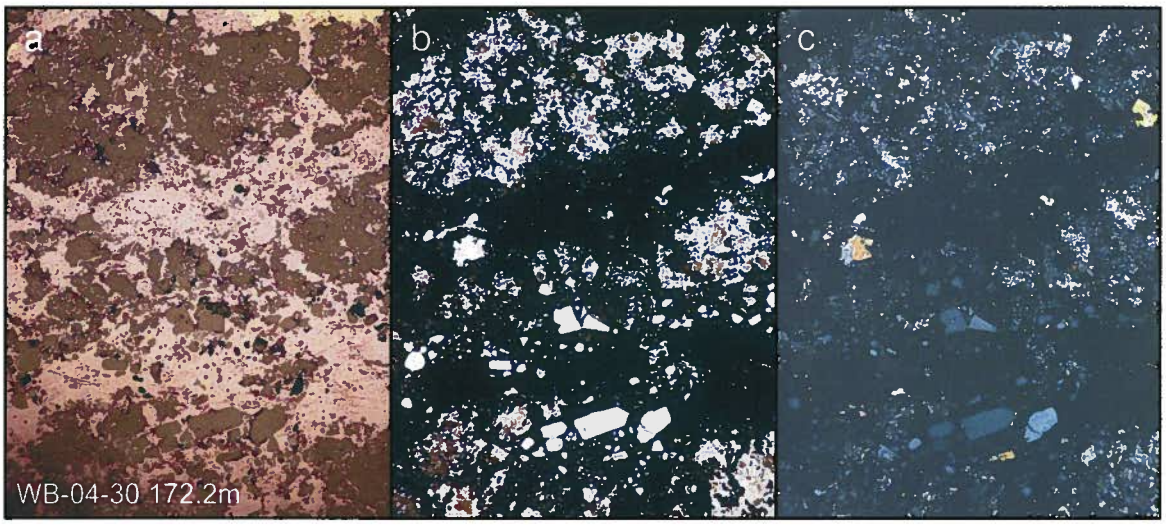

Figure 4.2-Photomicrographs showing the intimate mixture of clastic and chemical infill. Field of view is 3.5 mm; a; reflected light, b; transmitted light with plane polars, and c; transmitted light with crossed polars. Note that the clastic infill includes both crystal and lithic fragments; the chemical infill is bornite.

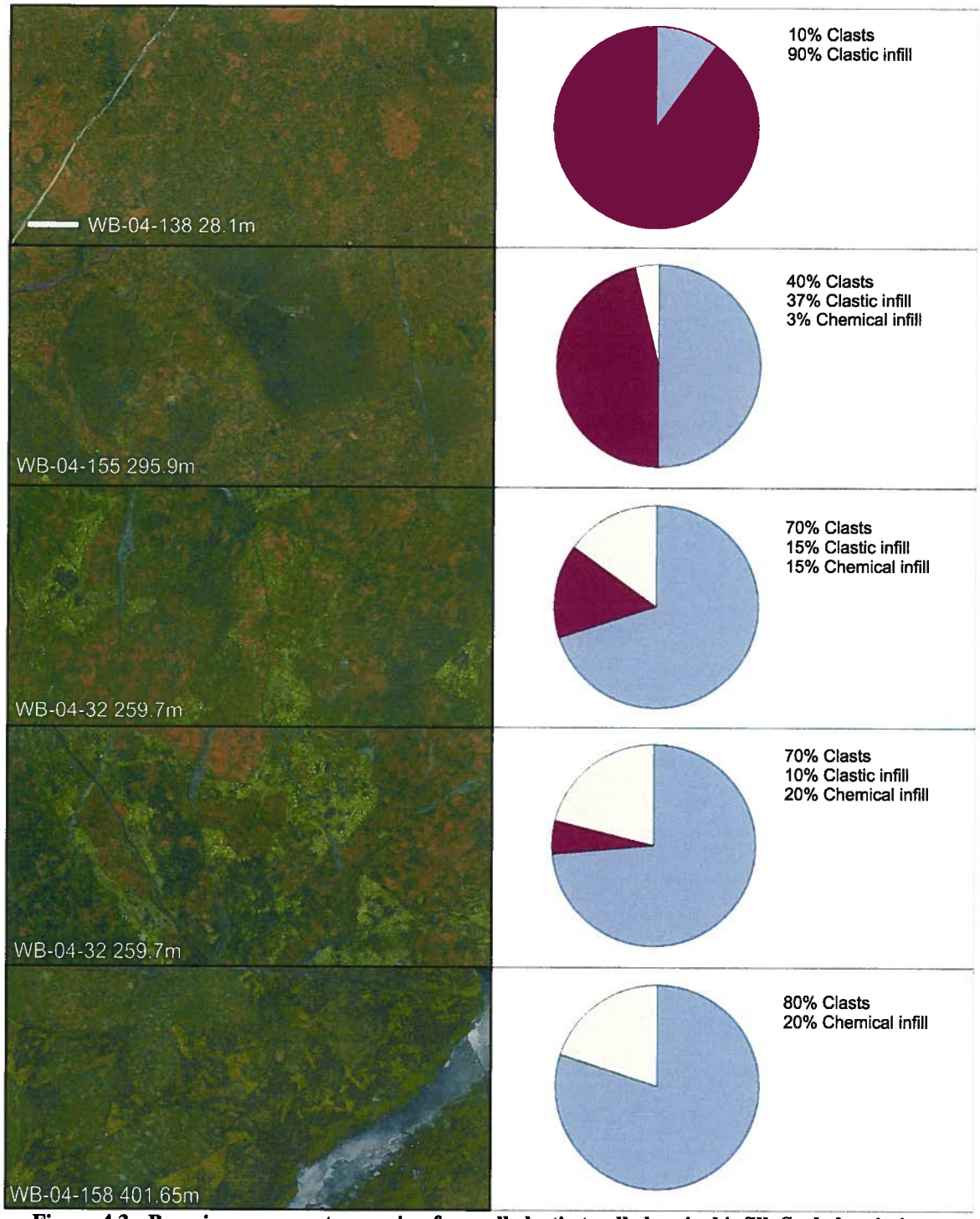

Figure 4.3a-Breccia components, ranging from all clastic to all chemical infill. Scale bar is 1 cm.

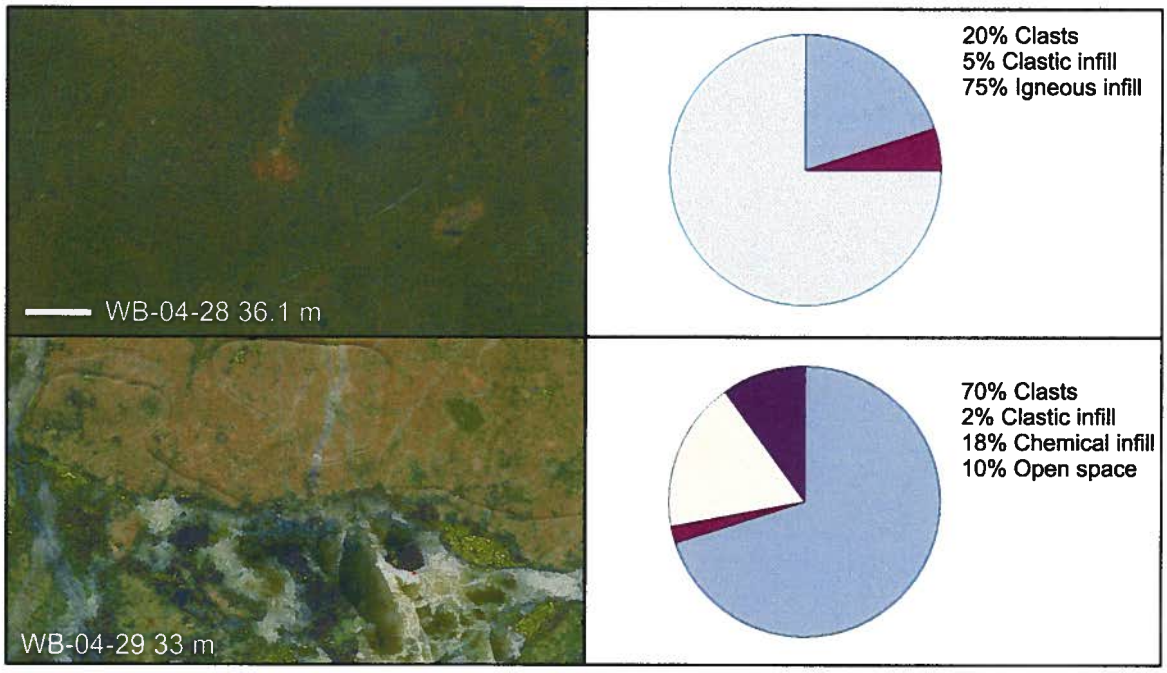

Figure 4.3b-Breccia components, showing igneous infill and open space. Note the bladed textures of the silica (chalcedony?) infill in the lower sample. Scale bar equals 1 cm.

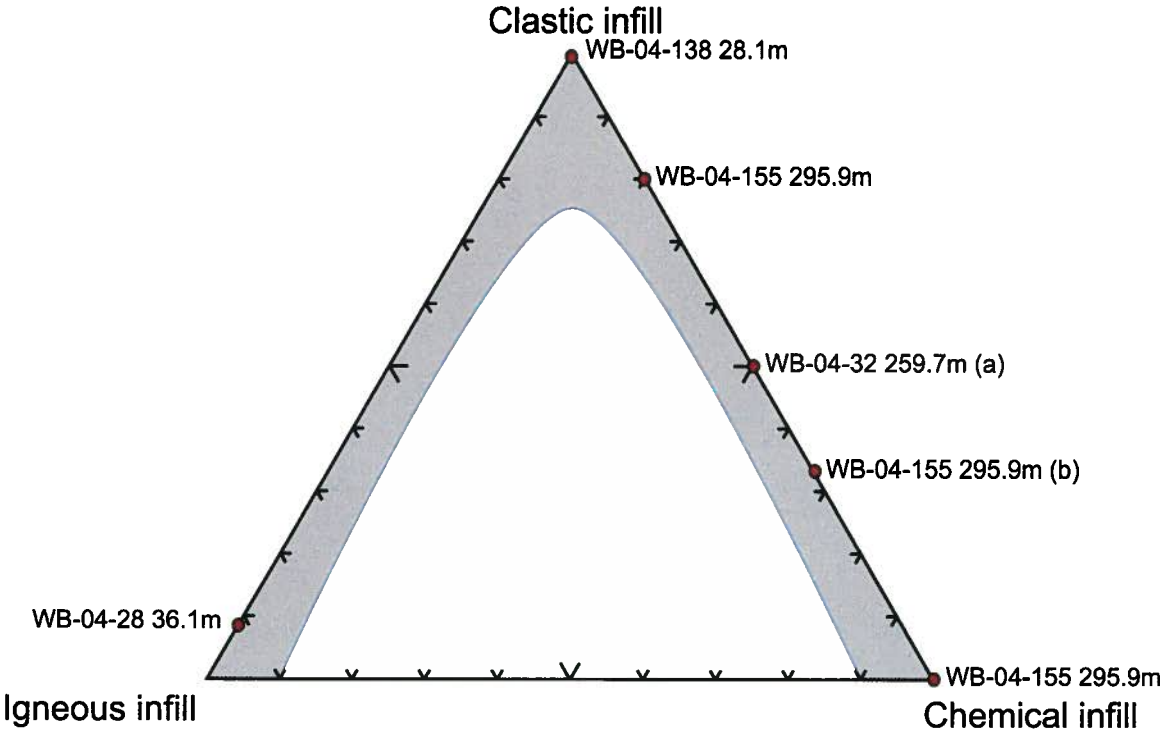

Figure 4.4-Ternary plot showing the relationship between clastic, chemical, and igneous infill. Shading indicates probable range observed in magmatic-hydrothermal settings. Samples shown in figure 4.3.

There is no consensus in the literature regarding methods for distinguishing silicate mineral infill from alteration (McPhie, et al., 1993; Barnes, 1997; Gifkins et al., 2005). Clastic infill can be modified by pre-, syn- or post-breccia alteration. Clasts and clastic infill can be modified by syn-breccia or post-breccia alteration, resulting in difficulty distinguishing clasts from infill, clastic infill from chemical infill, and pre- from syn- and post-breccia changes in mineralogy. Here, silicate infill, with a few exceptions clearly distinguishable as syn- and pre-breccia assemblages, is considered mostly under the heading of 'alteration'. Modifications of clastic material, and chemical infill, which resulted from infiltration of fluids into the breccia after the breccia body had formed and settled, may be related to the same fluids that formed the breccia or to different ones, and thus should be considered alteration rather than primary breccia characteristics (Sillitoe, 1985; Barnes, 1997; Gifkins, 2005).

Description of the infill of the breccia lends crucial insight into the processes that formed the breccia, but description of the clast population is somewhat more ambiguous. Clast population reflects the original distribution of rock types in the body of rock disturbed by brecciation processes, the mixing or transport involved in those brecciation processes, and, for certain clast types, they can indicate the sources of energy or fluids, and in some cases the nature of fluid flow (Burnham, 1985; McCallum, 1985; Taylor and Pollard, 1993; Jebrak, 1997; Link et al., 2006; Mukherjee and Mishra, 2007). Clasts are described on the basis of range of lithology (monolithic vs. polylithic), and clast lithology (rock types, vein fragment, breccia clasts, mineralized and altered clasts) (McPhie et al., 1993; Davies, 2002). Where the stratigraphy of the surrounding rock is well understood, the distribution of clast lithologies can be used to constrain the motion of clasts within the

breccia in striking precision (Bryant, 1968). Unusual clast types which are particularly useful for genetic interpretation include accretionary lapilli, indicating high velocity gas streaming, and juvenile magmatic clasts, identified by their globular, peperitic, or fluidal clast shapes, which indicated juvenile magmatic input into the breccia (McPhie et al., 1993; Davies, 2002). The morphology of the clasts can also be useful; it may be angular, rounded, faceted, tabular or equant (Jebrak, 1997; Ross et al., 2001a and b; Ross, 2002). The morphology of clasts may vary with rock type, due to the mixing of clasts which have been transported different distances.

Grain size

The grain size of the breccia is an important, but problematic aspect of breccia description. Average grain size is important, but grain size distribution and differences in grain size between different lithologies also yield valuable information about brecciation processes (figure 4.5). At Mount Polley, it was useful to identify if the distribution of clast sizes was normal, meaning that there was no break in grain size distribution between the smallest and largest clasts observed, or if it was bimodal, with two distinct clast size populations. In some cases, the average clast size was different for some lithologies than others. The presence of 'outlier' or 'outsize' clasts, or clasts substantially larger than the average, was also noted. The distinction between clasts and clastic infill is ignored for this descriptive tool, with clastic infill simply considered as a volume of < 2mm clasts. Clast size distribution was determined by visual estimate, rather than by quantitative means.

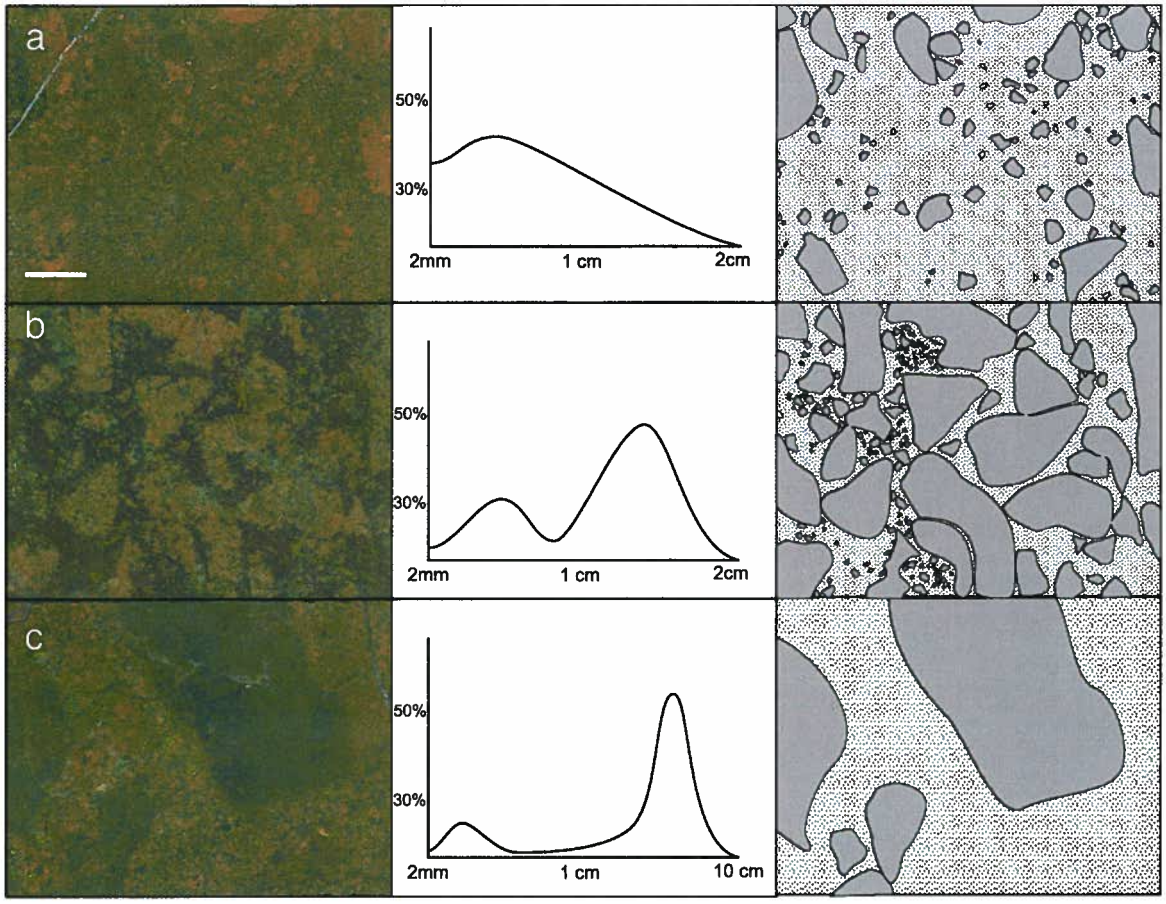

Figure 4.5-Normal (a), slightly bimodal (b), and extremely bimodal (c) grain size distributions. Scale bar equals 1 cm. All three samples have significantly smaller grain sizes than the average for the Northeast Zone breccia body.

Geometry

Davies (2002) emphasizes that understanding the geometry of a breccia body is very important to any determination of breccia genesis. Breccias can be pipelike, tabular, irregular, conical, vein-like or dyke-like (Sillitoe, 1985; Jebrak, 1997; Bryant, 1968; Bushnell, 1988; Ross, 2002). They can also be concordant or discordant. Where the top of a breccia is preserved it may be gradational or abrupt, domal, conical, convex, concave or planar (Sillitoe, 1985; Jacobsen et al., 1976; Norton and Cathles, 1968). Fluid escape structures may emanate from the tops of breccias in the form of veins, radial or concentric fracture networks, 'breccia dykes' or 'pebble dykes' (Farmin, 1934; Baker and Andrew, 1991; Gustafson and Hunt, 1975). A breccia can terminate downward into a

fault, a vein, or an intrusive body (Bushnell, 1988; Gustafson and Hunt, 1975; Norton and Cathles, 1973). The nature of the lateral contacts of the breccia is also informative. They may be gradational, abrupt, faulted, irregular, or planar.

General

Breccia geometry

The drill program at Mount Polley concentrated on the breccia body that hosts ore. Limited condemnation drilling was completed around the margins of the breccia body. From the data available, however, the breccia appears to be geometrically divisible into two segments (figure 4.6). The southern segment is fault-bounded, forming a discordant wedge defined by three major faults: the Green Giant Fault, the Brown Wall fault, and an inferred fault. The northern segment of the breccia appears to be conical, narrowing with depth and overprinted by post-breccia dykes. Whether or not this shape reflects the original geometry of the breccia body can not be confirmed.

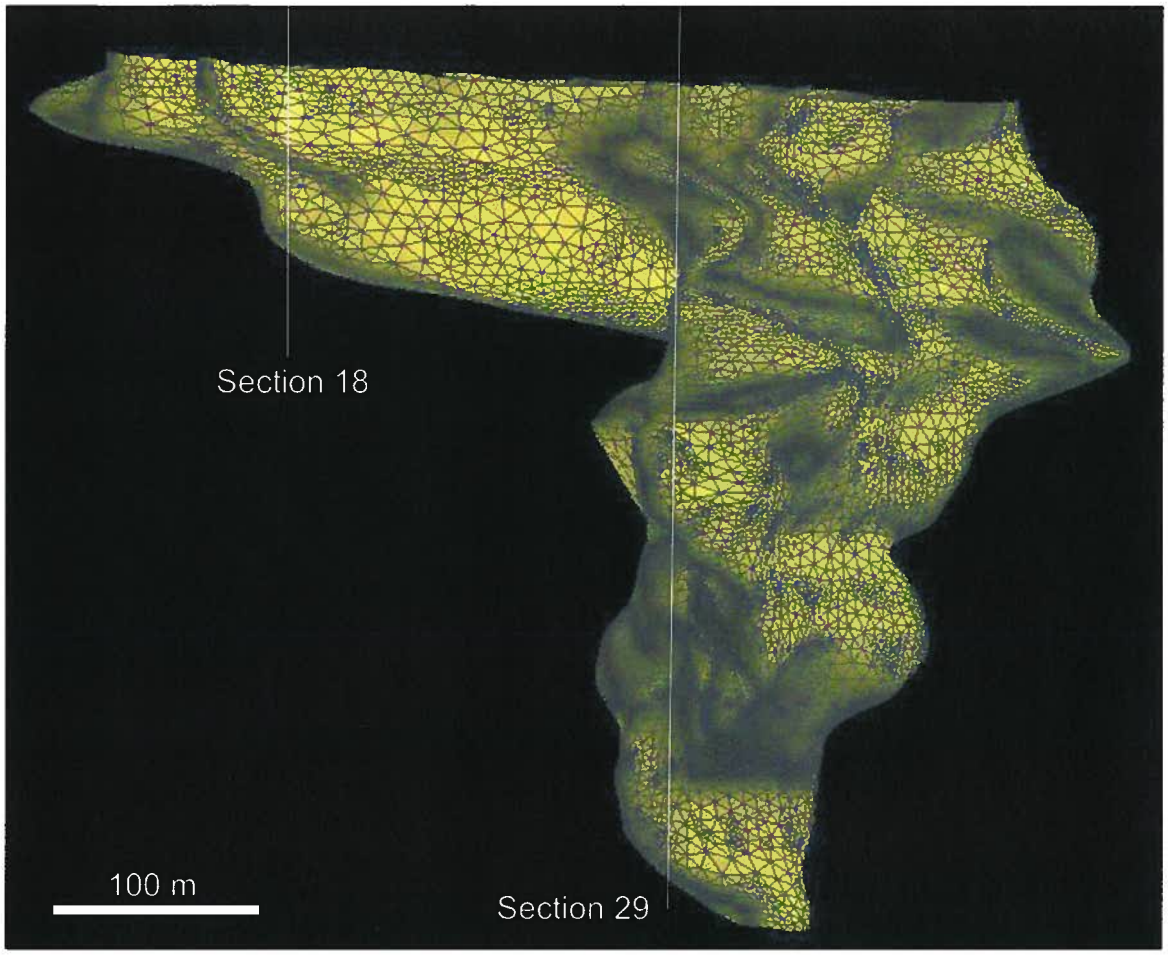

Figure 4.6-Three dimensional view of the breccia, viewed from the east-northeast. Data courtesy of Imperial Metals.

Section 18 and Section 29 relative to the breccia body as a whole

The two cross-sections chosen for this project cut both segments of the breccia (figure 4.6, 4.7). Section 18 cuts the southern segment of the breccia at an azimuth of 120, intersecting both the Brown Wall fault and the Green Giant fault. Section 29 is parallel to section 18, cutting the northern segment of the breccia near its widest point.

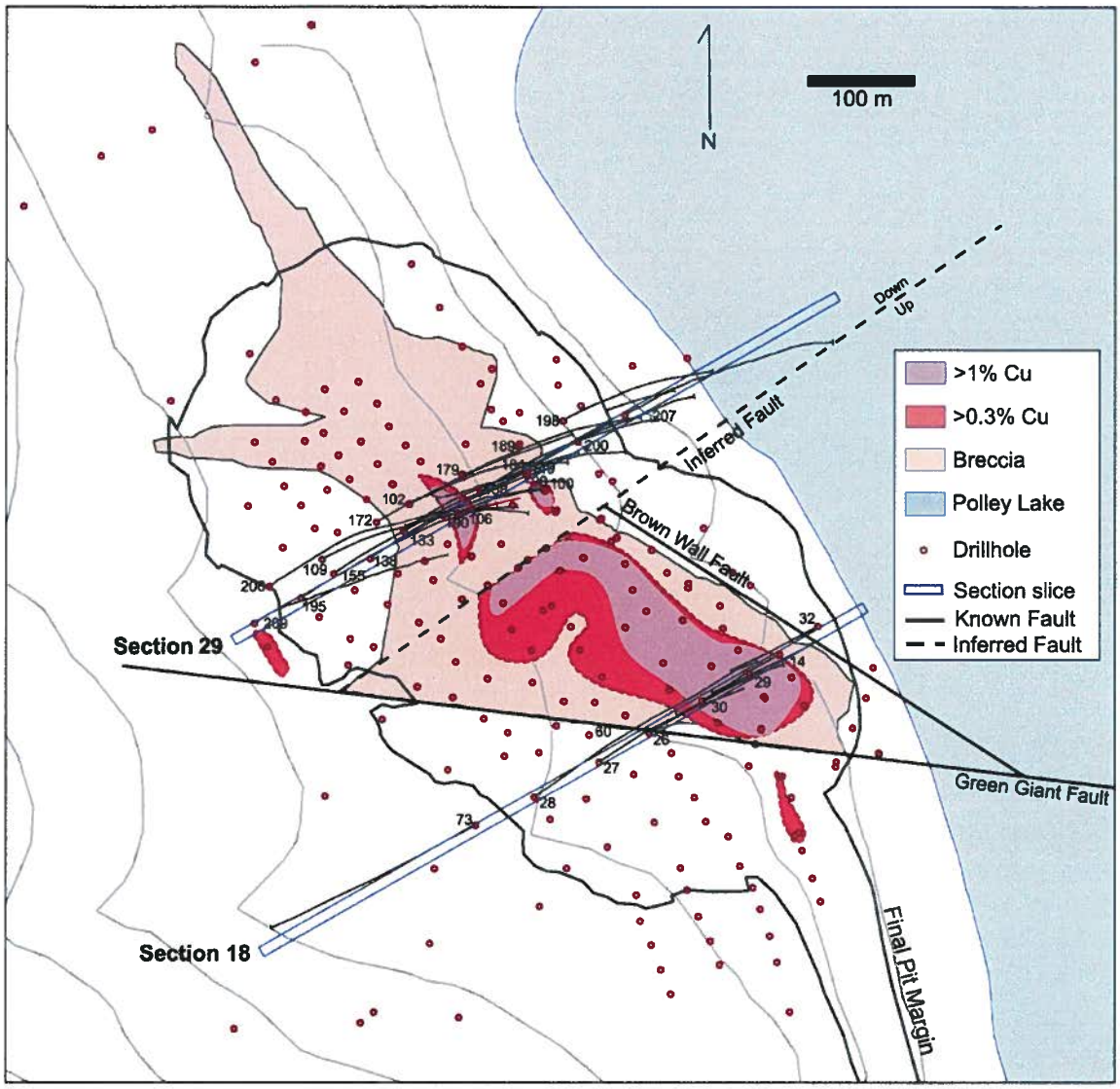

Figure 4.7-Location of the cross sections relative to the breccia body as a whole. Locations of faults are approximate. Data courtesy of Imperial Metals.

Breccia types

Subunits within the breccia body were divided on the basis of clast populations, infill character, grain size, grain size distributions, clast shape, and internal organization. Clast populations were defined by 'key clast types' which are particular rock types concentrated within restricted volumes within the breccia body as a whole. Key clast

populations are the altered mafic clasts, and megacrystic porphyry clasts (see Chapter 2) (figure 4.8 and 4.9).

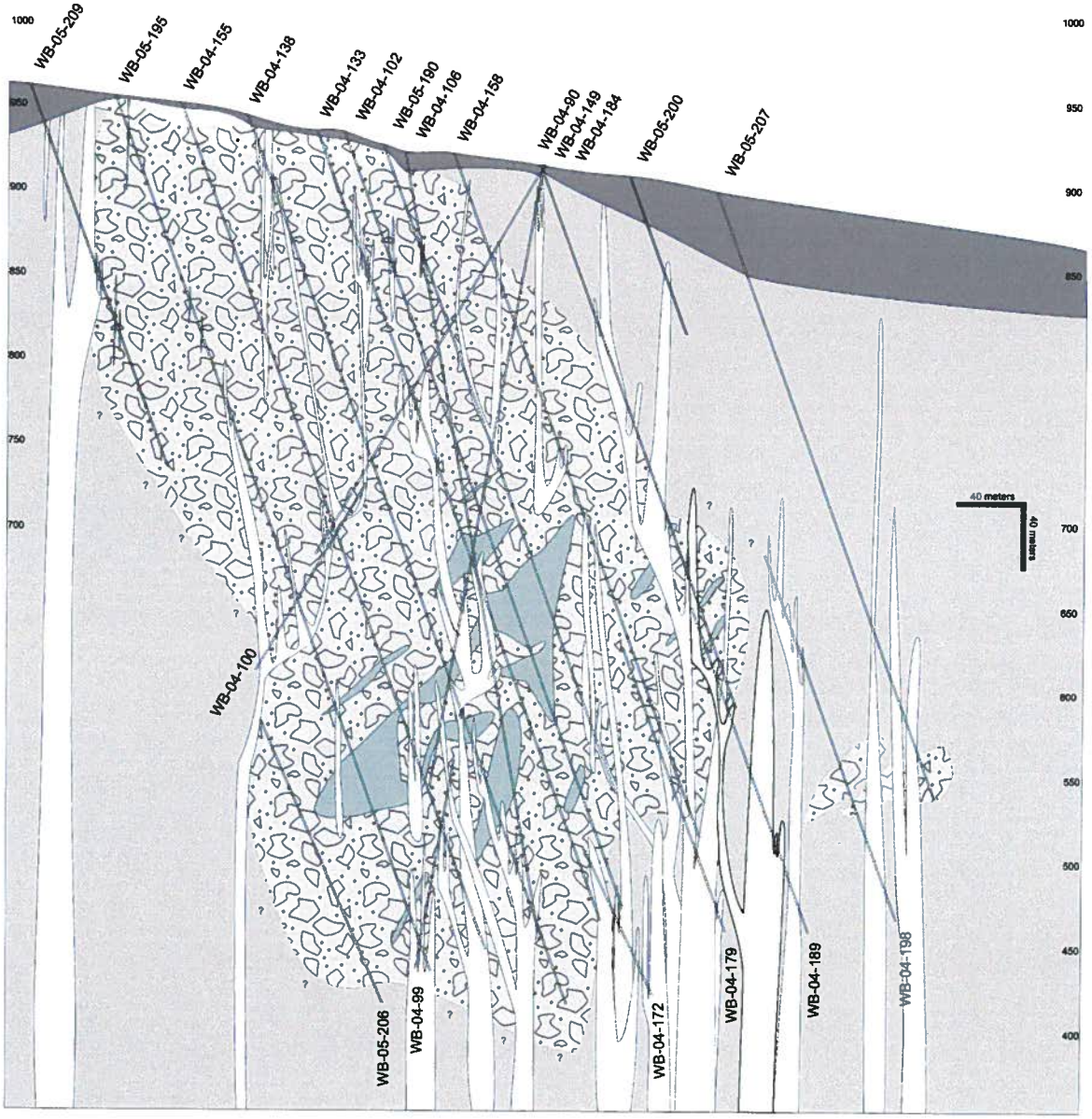

Figure 4.8-Distribution of altered mafic clasts on Section 29. No altered mafic clasts were observed on Section 18.

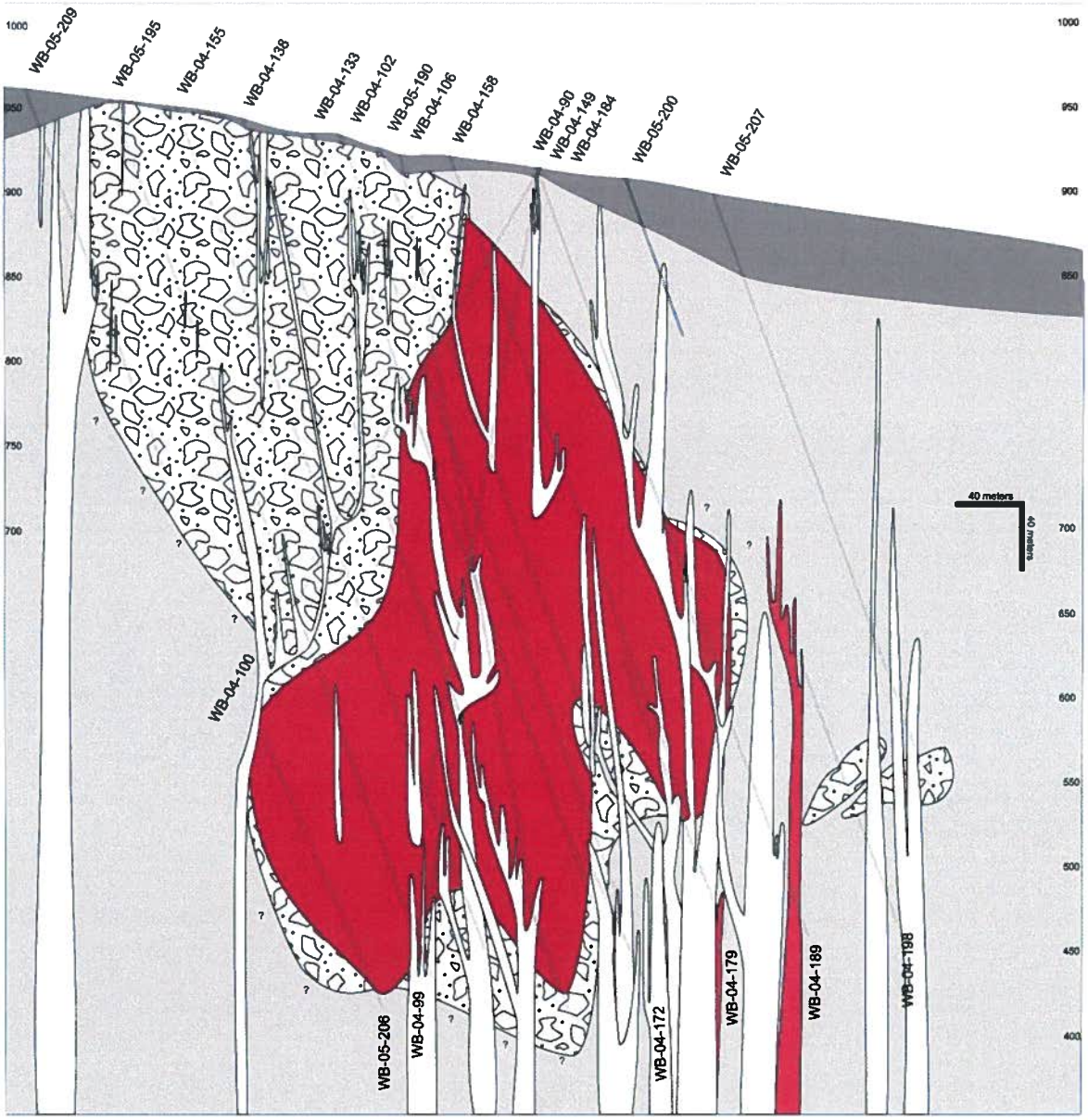

Figure 4.9-Distribution of megacrystic clasts on Section 29.

Infill character was divided into chemical infill only, chemical infill exceeding clastic infill, clastic infill exceeding chemical infill, and clastic infill only (figure 4.10). Chemical infill exceeding clastic infill dominated in section 29. Chemical infill only was most prevalent near the base of the preserved breccia body. Clastic infill and clastic infill greater than chemical infill dominated in the upper, western portion of the breccia.

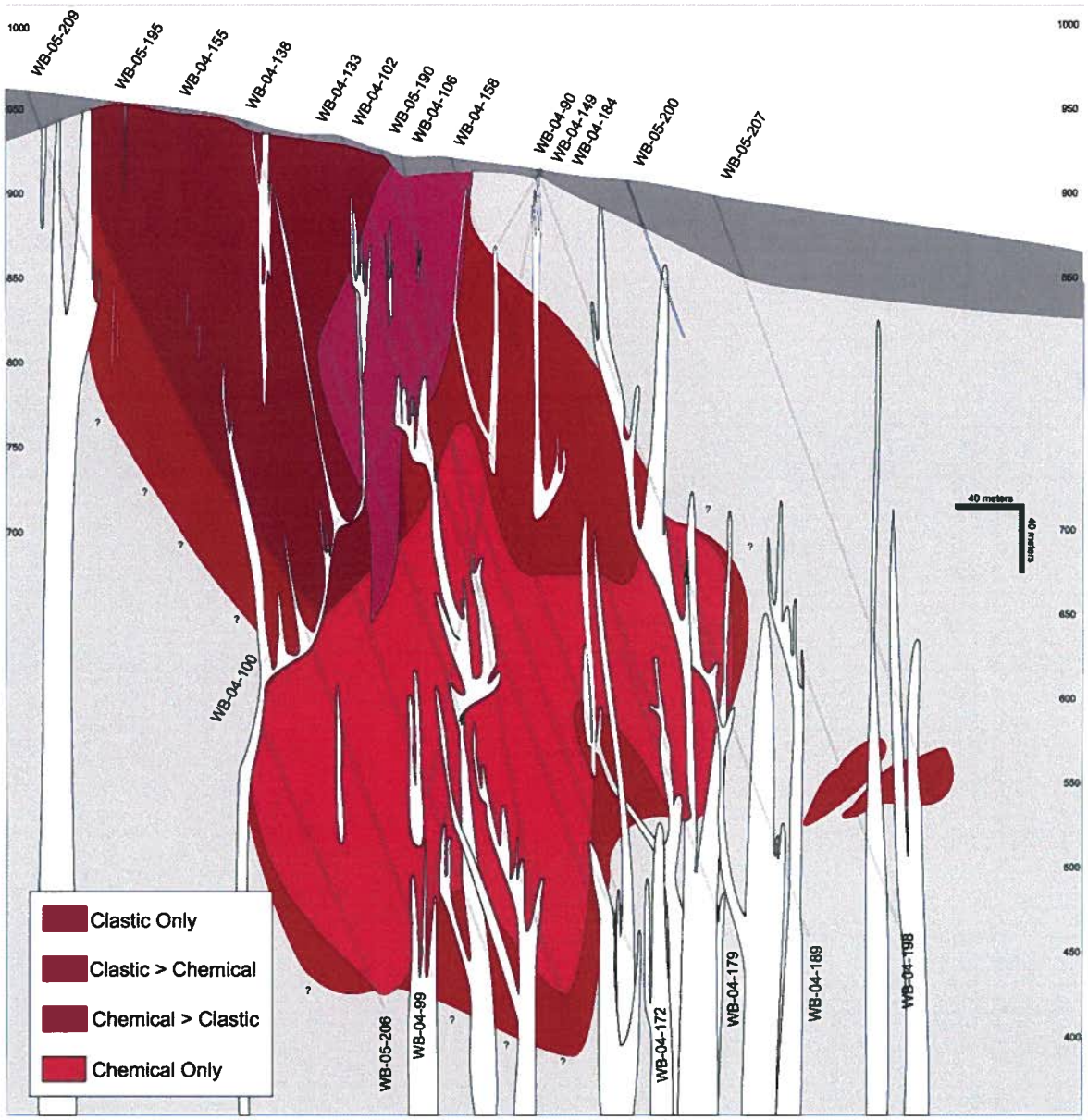

Figure 4.10-Infill types on section 29.

Grain size and grain size distribution in the breccia is problematic, due to the fact that in much of the breccia, average clast size exceeds the diameter of the core. Thus, grain size estimates are approximate, and, in areas where grain size was considerably larger than core diameter, outsize clasts may significantly skew estimates. Alteration also complicates estimates of clast size. Where alteration was intense or texture destructive,

the margins of clasts are usually obscured. Excluding outsize clasts (clasts >2x core diameter), the average clast size is between 6 and 25 cm except in a discrete zone on the western side of Section 29 (figure 4.11).

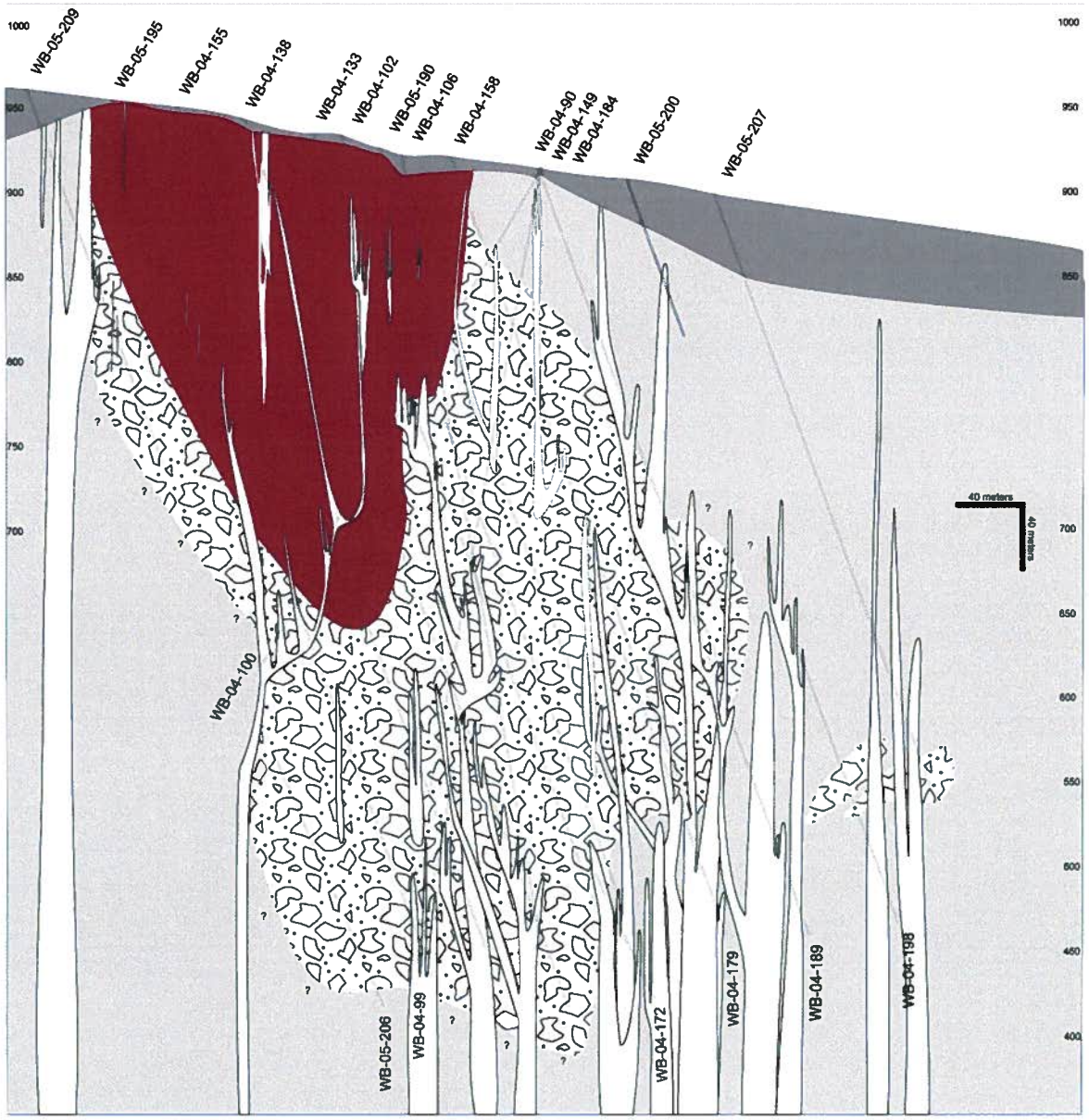

Figure 4.11-<4 cm clast zone on Section 29.

Grain size distribution was normal, slightly bimodal, and extremely bimodal. In normal clast size distributions, there is no clear break in grain size between the largest and the smallest clastic fragments in the breccia. Bimodal clast size distributions are further subdivided into slightly versus extremely bimodal distributions. Slightly bimodal grain size distributions were those in which the two populations of grains were less than an order of magnitude different in mean grain diameter. For example, clasts averaging over 10 cm in diameter in clastic infill averaging less than 2 mm in diameter would be extremely bimodal, whereas a breccia with clasts averaging 4 cm in diameter in a clastic infill averaging 1 cm in diameter and grading smoothly down to <2mm would be classed as a slightly bimodal grain size distribution(figure 4.5). Extremely bimodal clast size distributions, with 6-25 cm clasts and <2mm matrix, dominated (figure 4.12), with a zone of normal clast size distribution in Section 29 and a transitional slightly bimodal zone between the two.

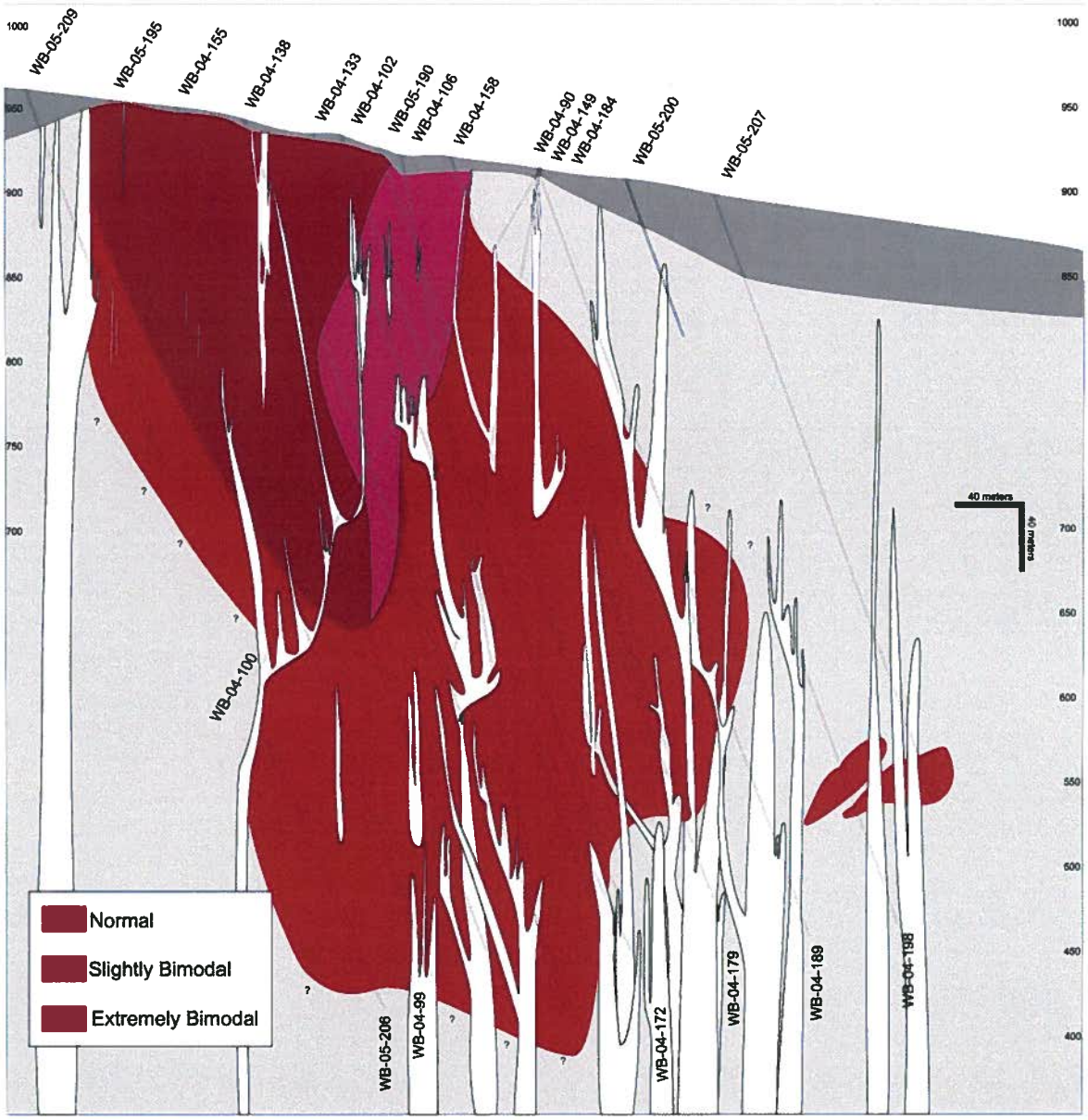

Figure 4.12-Clast size distribution in section 29

Clast shape was qualitatively assessed. Clasts were generally subrounded to subangular. Angular clasts were more common in the crackle and rotate breccia at the margins of the body, and rounded clasts more common in the fine grained portion of the body (figure 4.13).

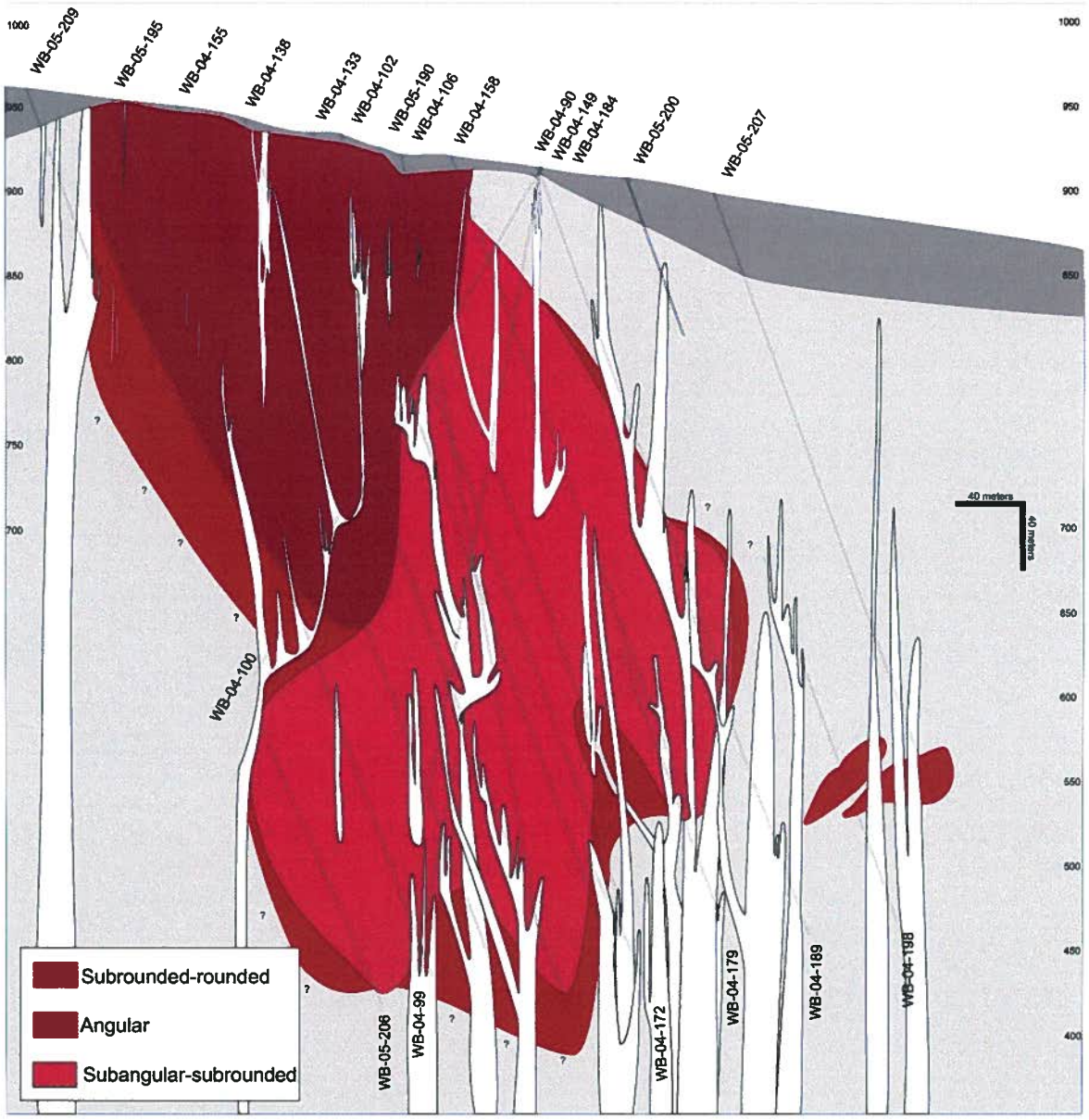

Figure 4.13-Clast shape distribution on section 29.

The breccia was divided into crackle, mosaic, or rotated breccias, referred to collectively as non-transported breccias and transported breccias (figure 4.14). The majority of the breccia body is dominated by chaotic, polylithic breccias. The margins of the chaotic breccia were rotated with limited or absent transport, and the contact between the breccia and the coherent equigranular monzonite on its margins grades from mosaic to crackle

breccia. Most mineralization originally described (Rees et al., 2005, 2006) as being hosted in monzonite is in fact hosted in the crackle breccia transitional between the chaotic breccia and the equigranular monzonite host rock.

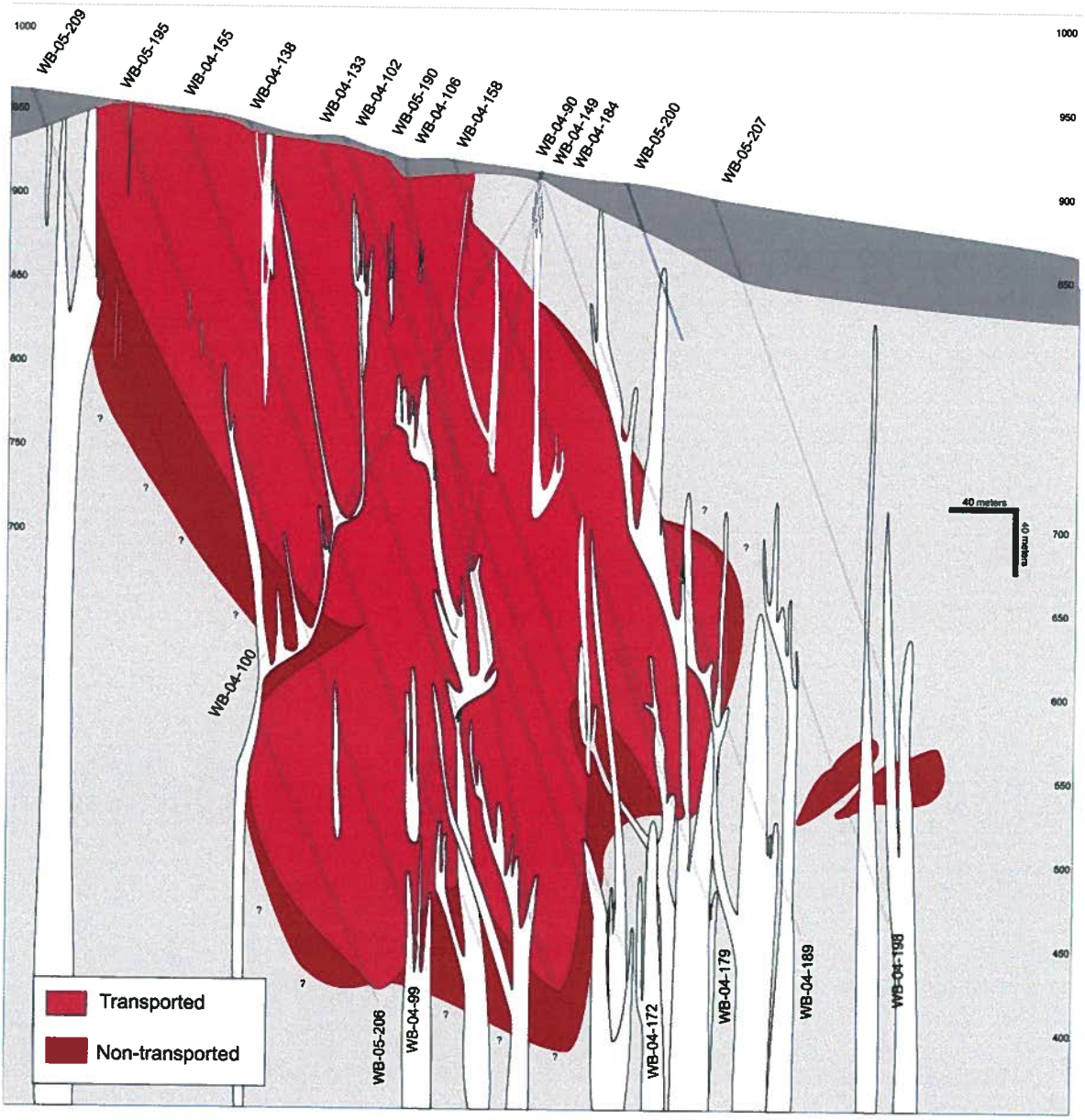

Figure 4.14-Transported versus non-transported breccia units on section 29.

Margins and nature of margins of breccia body

Most margins of the breccia are truncated by faults or are intruded by post-breccia dykes. Where original breccia margins are preserved (drillholes WB-04-90 and WB-04-149), there is a gradation from coherent country rock to crackle breccia, mosaic breccia and into rotated, transported and chaotic breccias. The original breccia margins are poorly known overall, thus hindering a coherent view of the original volume and geometry of the body.

Breccia subunits

Based on the primary characteristics described above, the breccia body was divided into five major subunits (Figure 4.15, Table 4.3). The peripheral subfacies of the breccia consist of monolithic equigranular augite-bearing monzonite clasts, generally angular to subangular, with little infill. Clastic infill is far subordinate to chemical infill, clast size distribution is generally normal, and breccia internal organization ranges from crackle breccias to transported breccias. Clast size is varied.

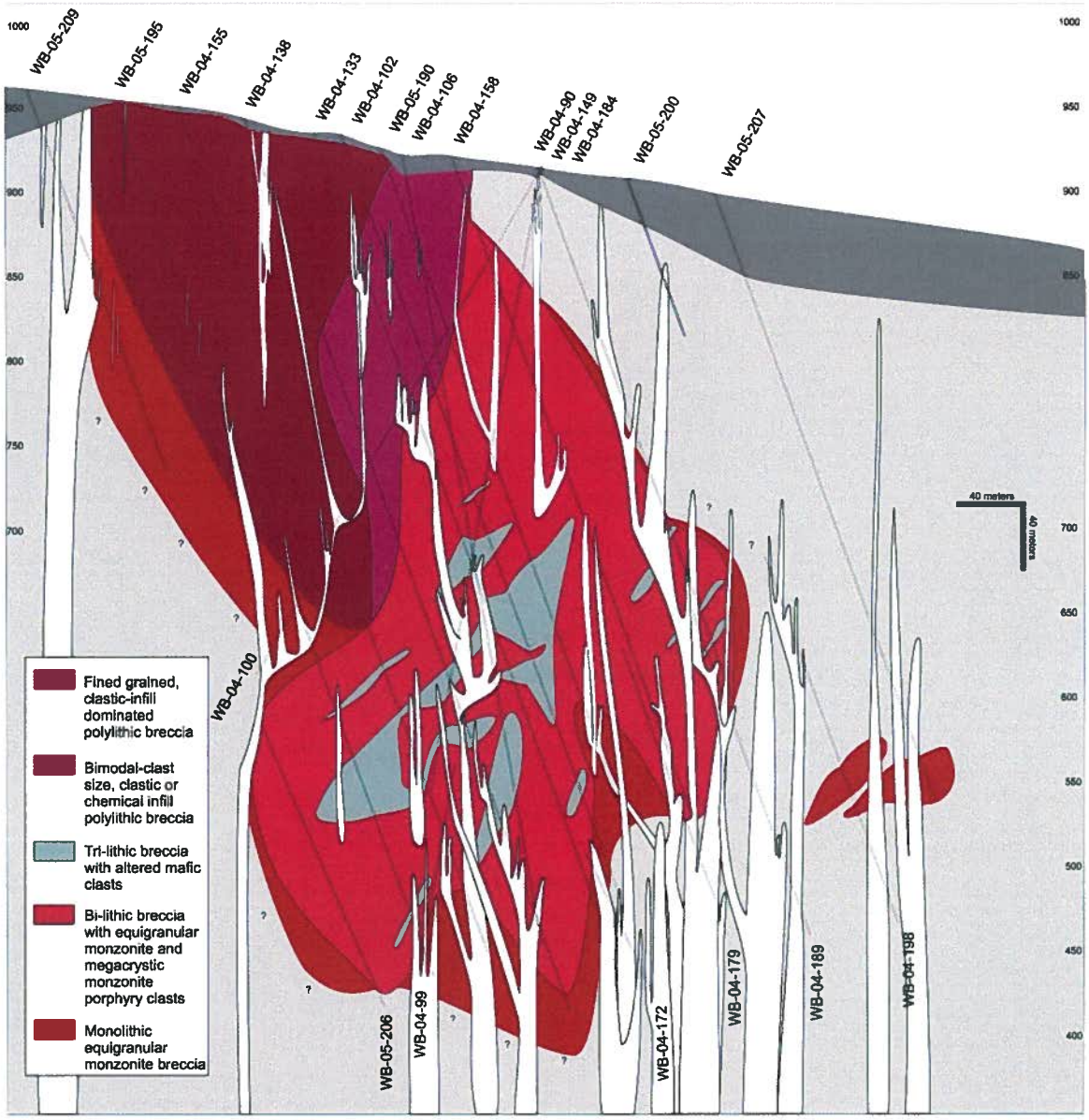

Figure 4.15-Units within the Northeast zone breccia, Section 29.

Table 4.3-Characteristics of breccia subunits.

BRECCIA SUBUNITS							
Unit	**Internal organization**	**Clast size**	**Clast size distribution**	**Clast shape**	**Clast lithology**	**Infill**	**Contacts**
Monolithic breccia	Jigsaw or rotated	2mm->1 m	Normal	Ang. to sub-ang.	Eq. Monz	Chemical	Grad.
Bilithic breccia	Transported	4-25 cm	Extremely bimodal	Sub-ang. to sub-rounded	Eq. Monz and mega. porphyry	Clastic to chemical	Grad.
Trilithic breccia	Transported	4-25 cm	Extremely bimodal	Sub-ang. to sub-rounded	Eq. Monz, mega. porphyry, and alt. mafic	Clastic to chemical	Grad.
Bimodal breccia	Transported	1-10 cm	Lith. dependent bimodal	Sub-ang. to rounded	Eq. monz and mega. porphyry	Clastic>chemical	Grad.
Fine grained breccia	Transported	1-4 cm	Normal	Sub-rounded to rounded	All lith.	Clastic	Grad.
Breccia units unrelated to the main breccia body							
Vein breccia	Crackle to mosaic	<2 cm	Normal	Ang.	All lith.	Chemical	Sharp
Fault breccia	Transported	<1 cm	Normal	Ang.	All lith.	Clastic	Faulted
Igneous infill	Jigsaw to transported	<1 cm	Normal	Ang. to round.	All lith.	F.g. igneous	Igneous

Lith=lithology, ang=angular, Eq. monz= equigranular monzonite, mega=megacrystic, f.g.=fine grained, grad=gradational

Inward from the monolithic breccias along the breccia margins, the bulk of the breccia body consists of polylithic chaotic breccia with subangular to subrounded clasts. This breccia contains at least 2-5% megacrystic monzonite clasts, locally grading into >90% megacrystic monzonite clasts. Clastic infill is subequal to or greater than chemical infill in Section 18, but chemical infill dominates over clastic infill in Section 29. Clast size distribution is extremely bimodal, with a clear gap in grain sizes between the <2 mm clastic infill and the 4-10 cm clasts. This breccia commonly contains outsize equigranular monzonite clasts.

The polylithic chaotic breccia with extremely bimodal clast size distribution grades into a polylithic chaotic breccia with a slightly bimodal clast size distribution, characterized by a normally distributed 4-20 cm megacrystic monzonite clast population in a normally distributed 2-20 mm polylithic clast population with up to 10% mafic clasts. This breccia subunit is observed only in section 29, where it is dominated by chemical infill.

The extremely bimodal breccia grades into a fine grained (clast sizes <2mm), polylithic chaotic breccia. Clast size distribution is normal, with no abrupt grain size change between clasts and clastic infill. The largest clasts in this breccia unit are smaller than the phenocrysts that define the megacrystic monzonite porphyry, but the presence of abundant broken K-feldspar crystals in the clastic infill suggests than megacrystic monzonite was present, but has been disaggregated beyond recognition. Mafic clasts form up to 15% of this breccia unit.

The fine-grained breccia unit appears to form a narrow, vertical sub-pipe within the overall breccia (J. Blackwell, pers.comm.), but the western margin of this body has not been drilled. Examination of Imperial Metals core logs indicates that the gradual nature of the fine-grained breccia to more 'normal' breccia transition observed in Section 29 is consistently observed around the body. This gradual transition suggests that the fine-grained breccia subunit is not a separate pipe cutting the main breccia body.

Infill

In addition to distinguishing between clastic and chemical infill, infill mineralogy and paragenesis also lend insight into the nature and origin of the breccia and the fluids which formed it and which pervaded it after formation. Infill mineralogy, however, straddles the space between primary brecciation features and the alteration features which modified the breccia after its development. Particularly where texturally destructive alteration modifies both clasts and clastic matrix, the original nature of the infill is impossible to determine. Chemical infill types were distinguished on the basis of the most volumetrically significant mineral component. A broad overview of alteration mineralogy and distribution is provided here, as is relevant to the development of the breccia body; a more comprehensive description and analysis is provided by Pass et al. (2007).

Carbonate

White and pink carbonate (calcite, dolomite, and rhodocrosite) infill is a common late component of vein breccias (figure 4.16) overprinting the main breccia body and filling relict open space in the breccias. These late minerals commonly exhibit bladed textures. Carbonate infill was more pronounced in section 18 than in section 29. In thin section, carbonate was observed intimately mixed with gypsum. In a few cases, carbonate was observed as infill in the main-stage breccias, pre-dating or coeval with sulfides. Sulfides were observed on the contact between carbonate and gypsum infill (WB-04-32 212.23).

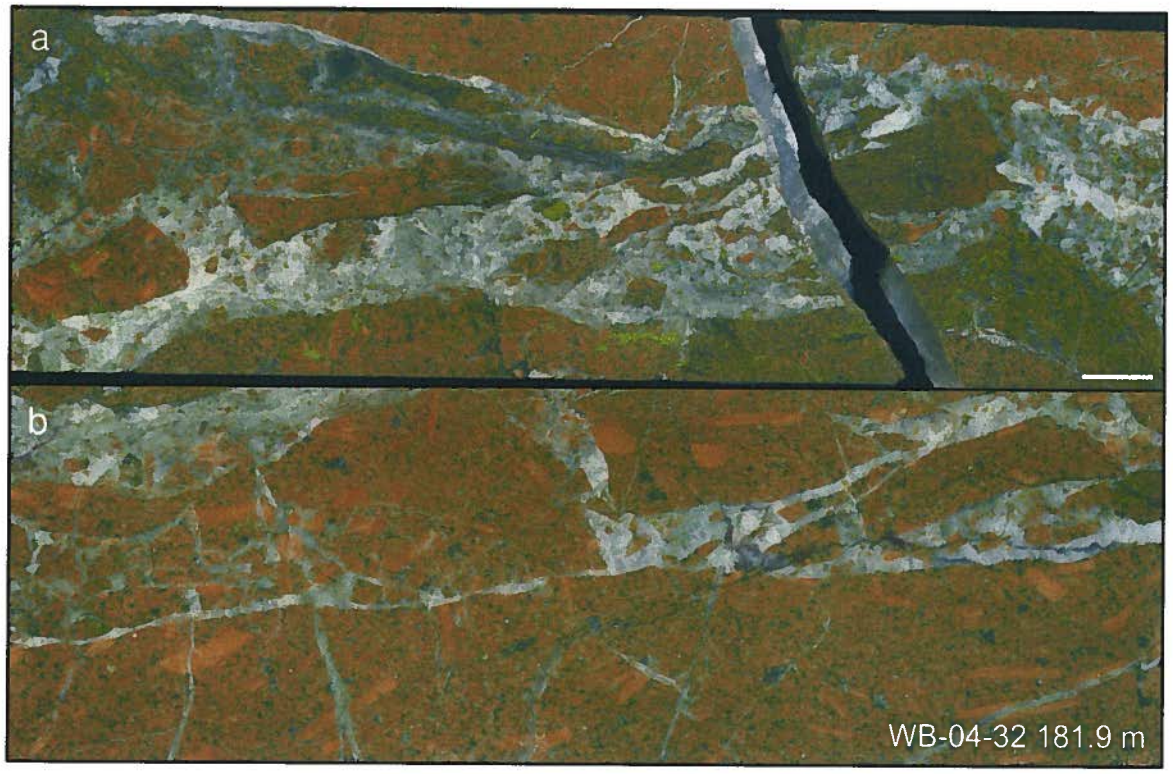

Figure 4.16- Carbonate-infill breccia overprinting sulfide+clastic infill bilithic breccias. Scale bar= 1 cm. A; Sulfide clasts in breccia; b; note jigsaw fit between clasts (left).

Chlorite

Chlorite is the most common infill mineral in the peripheral subunit of the breccia. It forms very fine-grained green to green-brown infill in crackle breccias. Chlorite infill is most common in the upper and peripheral portions of section 29 (figure 4.17). In thin section, chlorite is the most common product of the alteration of mafic minerals, particularly augite, and is also observed as rims on amygdales in coherent monzonite.

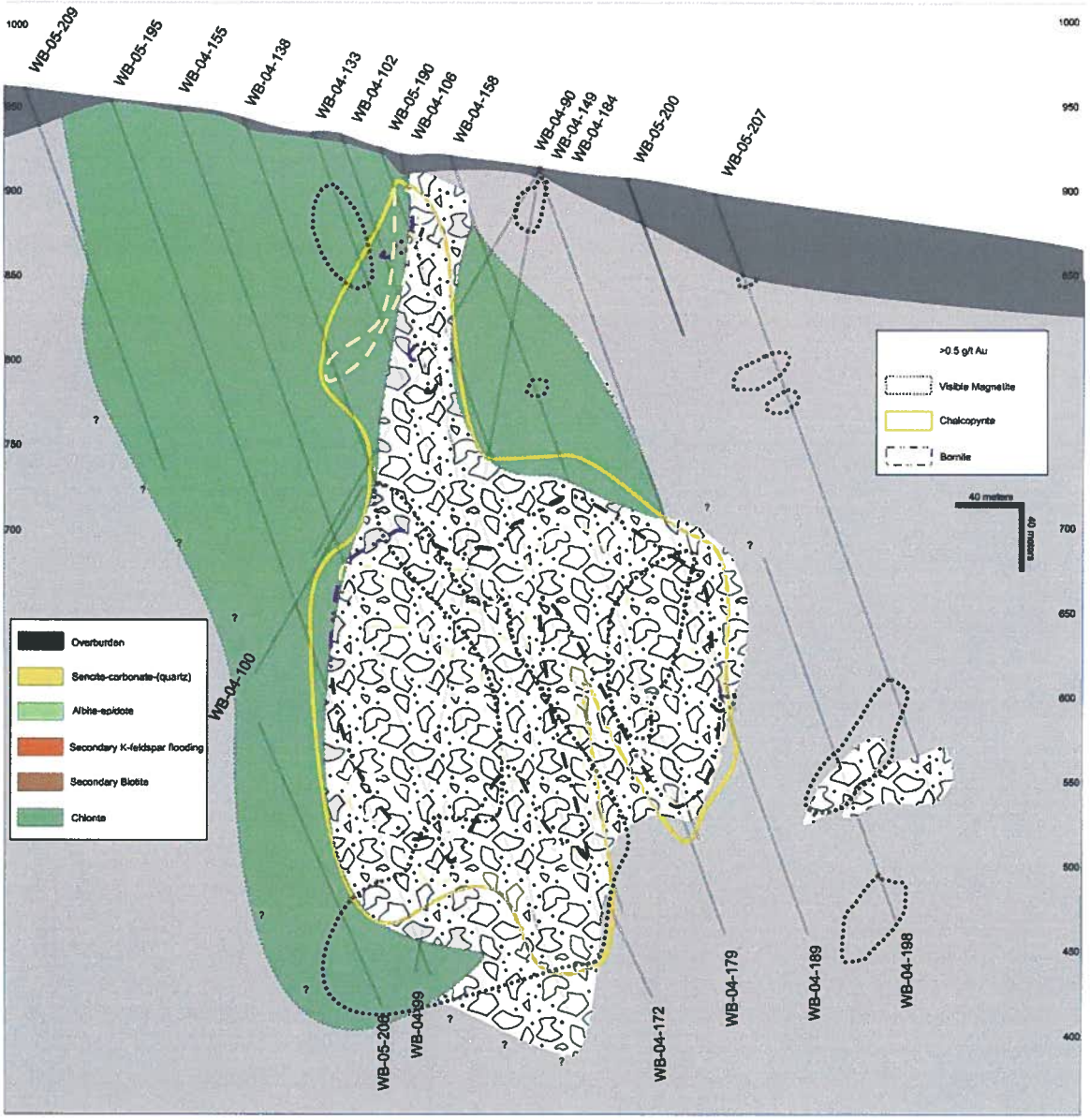

Figure 4.17-Chlorite infill on Section 29.

Biotite

The transition between chlorite and biotite infill in the breccias is subtle. The dark green color of the fine grained phyllosilicate infill becomes dark brown, and the overall color of the breccia becomes darker. Some caution must be exercised with the biotite infill, because in case where the breccia has been subject to K-feldspar flooding, clasts are commonly altered to biotite. Distinguishing biotite infill from biotite altered clasts, or

biotite altered rims on clasts, is locally difficult. Biotite infill occupies the bulk of section 29, and is coincident with the majority of sulfide mineralization (figure 4.18).

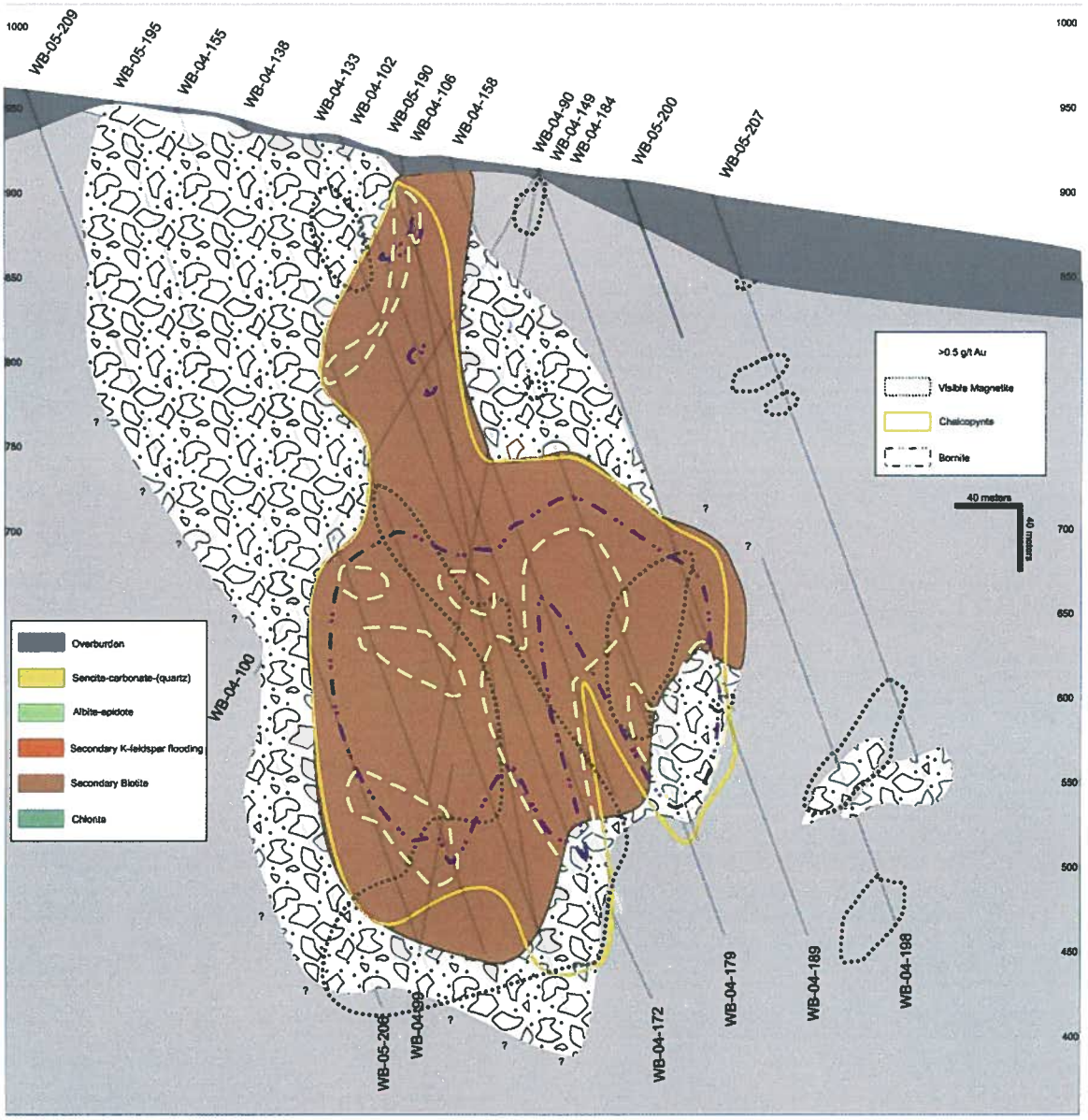

Figure 4.18-Biotite infill on section 29.

Sulfide

Sulfide is the most common infill mineral, especially in section 18. Sulfide assemblages can also be subdivided by sulfide mineralogy into chalcopyrite only, chalcopyrite-bornite, chalcopyrite-magnetite, and magnetite-pyrite assemblages (figure 4.19).

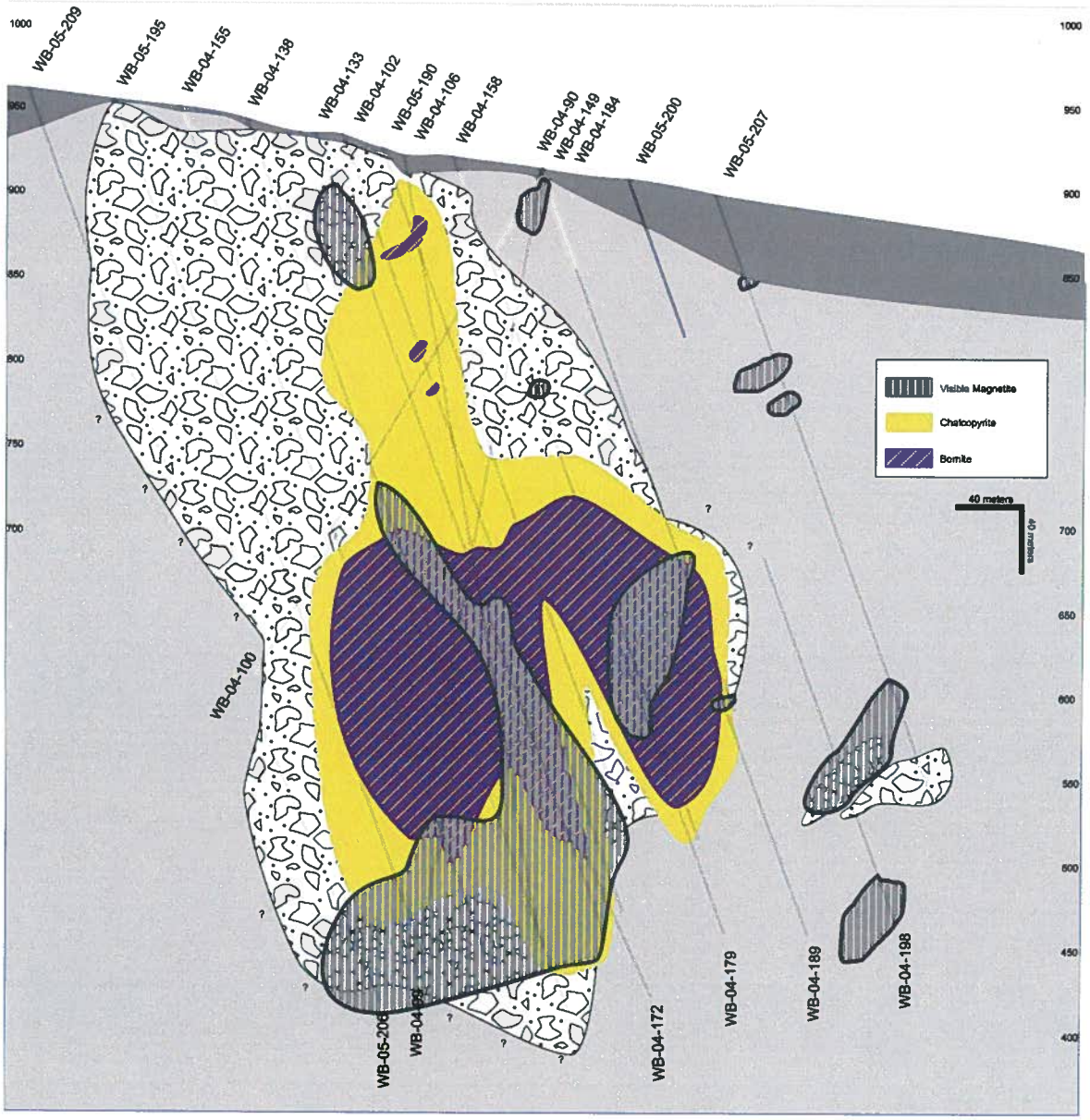

Figure 4.19-Sulfide infill on section 29.

Magnetite is the earliest mineral in the 'sulfide' paragenesis (figure 4.20a-d). It is commonly replaced by chalcopyrite (figure 4.20a), and less commonly by pyrite (4.20b-d). Where magnetite, pyrite, and chalcopyrite are present together, magnetite is replaced by pyrite and pyrite is replaced by chalcopyrite (figure 4.20c). Primary pyrite is less common (figure 4.20e). Bornite is not observed directly replacing magnetite. Where bornite and chalcopyrite co-exist, cusp-and-caries textures show chalcopyrite replacing bornite (figure 4.20g) and exsolution textures (figure 4.20f) indicating that the two minerals are co-eval. In rare cases, especially associated with sericite-carbonate alteration as described below, both chalcopyrite (figure 4.21h) and bornite (figure 4.21i) are replaced by chalcocite. Chalcocite is not abundant enough to contribute to the grade of the orebody, but their presence indicates remobilization of Cu or a late increase in the sulfidation state of mineralizing fluid.

Paragenesis of the sulfide minerals and magnetite is discussed in the context of alteration, brecciation, and intrusion events in Chapter 5.

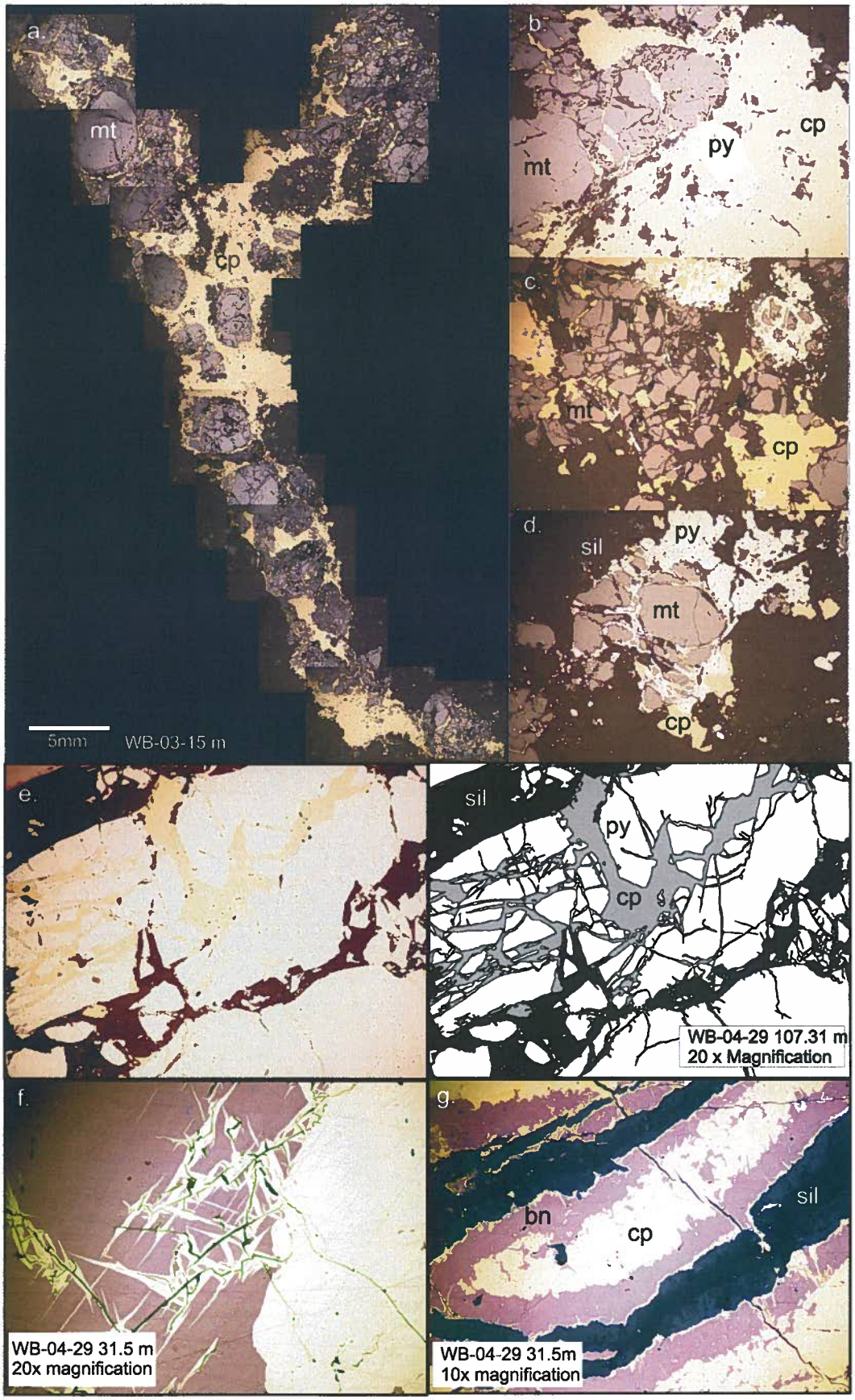
a.
mt
cp
5mm
WB-03-15 m
b.
mt
py
cp
c.
mt
cp
d.
sil
py
mt
cp
e.
sil
py
cp
WB-04-29 107.31 m
20 x Magnification
f.
WB-04-29 31.5 m
20x magnification
g.
bn
cp
sil
WB-04-29 31.5m
10x magnification

Figure 4.20-Photomicrographs of magnetite and silicate infill. A; Two generations of magnetite (euhedral and as anhedral overgrowths; overgrown and surrounded by chalcopyrite. B; magnetite and pyrite overgrown by chalcopyrite. C; magnetite replaced by pyrite replaced by chalcopyrite. D; magnetite fractured and infilled with pyrite, replaced by chalcopyrite E; primary pyrite fractured and infilled with chalcopyrite; sketch at right shows textural relationship. F; Exsolution textures in chalcopyrite and bornite. G; cusp-and caries textures showing chalcopyrite replaced by bornite. Mt= magnetite, cp=chalcopyrite, py=pyrite, bn=bornite, sil=silicate. Except as noted, field of view is 2.5 mm.

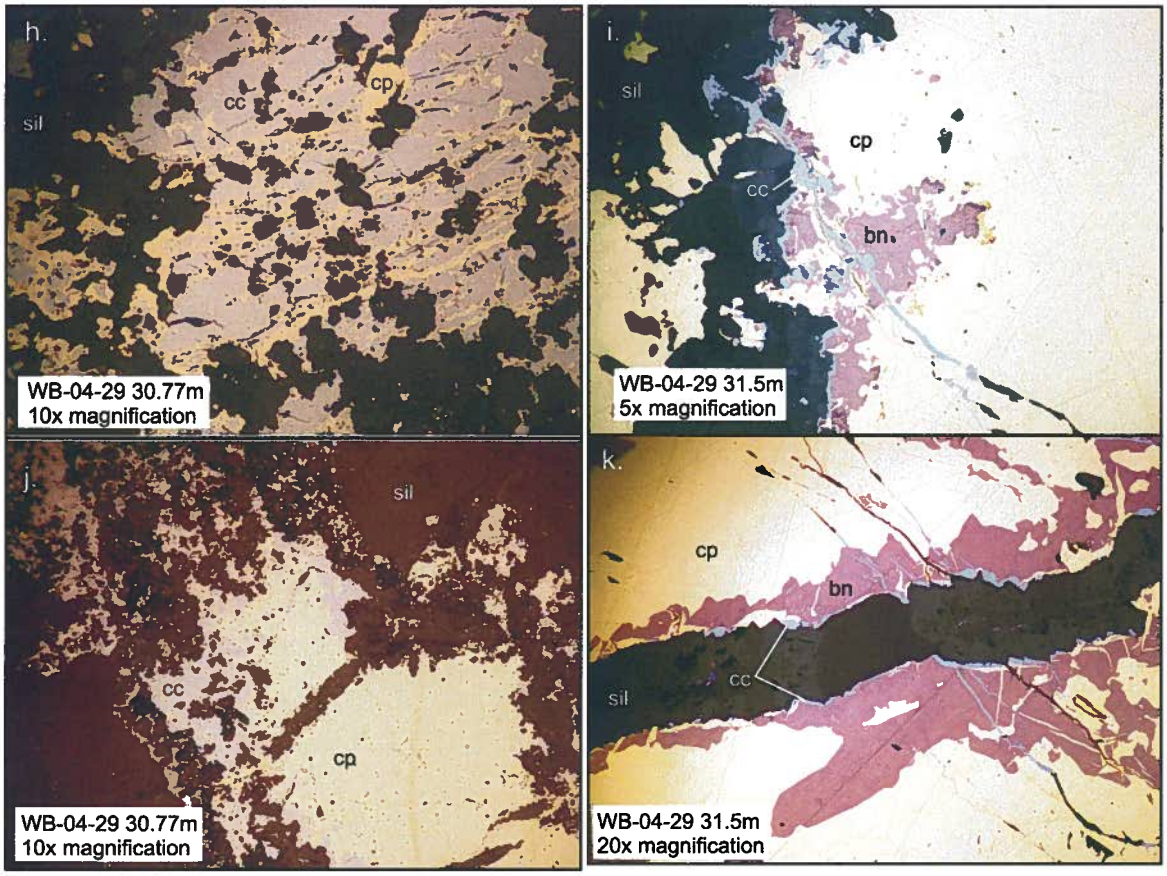

Figure 4.21-Chalcocite replacing chalcopyrite and bornite. H; Chalcocite replacing chalcopyrite along fractures. I; chalcocite replacing chalcopyrite and bornite along fractures. J; chalcocite rimming chalcopyrite. K; chalcocite rimming chalcopyrite and bornite, and along fractures. Sil=silicate, cc=chalcocite, cp=chalcopyrite, bn=bornite

Magnetite

Locally within the breccia, magnetite is the dominant or the only infill mineral (figure 4.19). In contrast with the physically separate magnetite breccia described by Fraser (1995), the magnetite breccias in the Northeast zone form an infill-based subfacies of the main body, with no distinctive differences in clast type or geometry. In thin section, magnetite infill, as distinct from magnetite-constructive alteration, is observed rimming clasts and intimately mixed with clastic infill (figure 4.22).

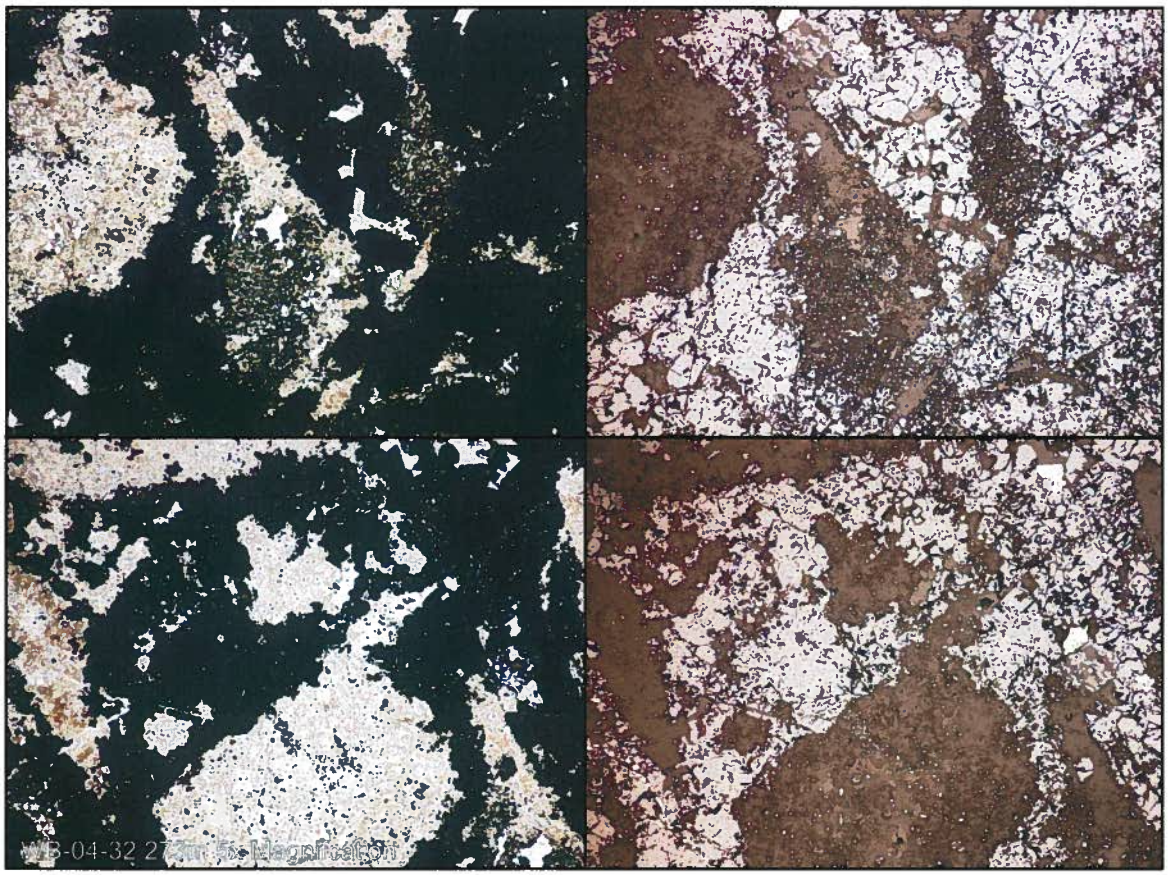

Figure 4.22- Photomicrographs of magnetite infill in transmitted light with plane polars (left) and reflected light (right). Note the complex clast boundaries. Field of view 2.5 mm.

Silicate infill

Three distinct infill types may reflect primary hydrothermal infill or post-breccia modification of infill by alteration processes. These assemblages are albite-actinolite, albite-epidote, and K-feldspar. Albite-actinolite infill is restricted to a narrow zone within the fine-grained breccia in Section 29 and to areas in Section 18 on the west side of the Green Giant fault. Albite-epidote assemblages are observed deep in Section 29, and K-feldspar infill forms a tabular zone between biotite and albite-epidote assemblages in Section 18 and a restricted zone in the center of Section 18, coinciding with the zone of highest megacrystic clast concentration (figure 4.23).

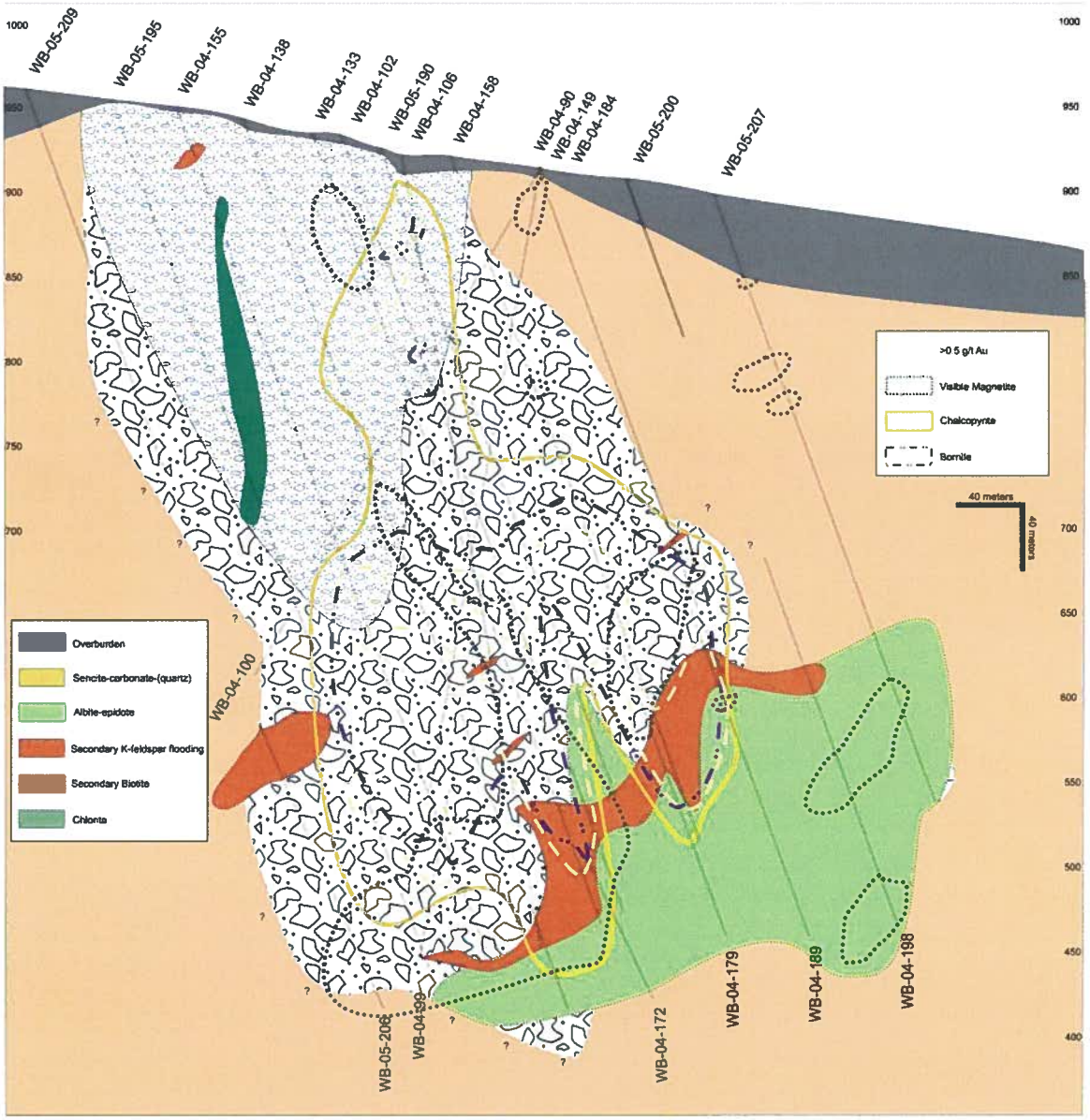

Figure 4.23-Silicate infill on Section 29.

Discussion of breccia features

The fairly uniform clast lithologies and gradational contacts between breccia subunits suggest that the Northeast Zone breccia body at Mount Polley reflects a single brecciation event (Rees et al., 2005 and 2006; Logan and Bath, 2006; McPhie et al., 1993). The lack of variation in clast lithologies between breccia subunits, and the lack of clasts of breccia in breccia or mineralized clasts, reinforces this hypothesis. Given that

the breccia represents a single event, variation in sulfide mineralization within the breccia body suggests a secondary control on mineralization. The highest grades are present in zones:

I. Where chemical infill exceeds clastic infill

II. Where clast transport was significant (mixing of lithologies)

III. Close to the highest concentration of megacrystic porphyry clasts

IV. Close to the transition between biotite and K-feldspar infill assemblages

The first and second controls are explained by permeability; mineralization occurred in the most permeable zones within the breccia body (Emmons, 1906; Davies, 2002). The third control suggests that the megacrystic porphyry was the originator of the mineralizing fluids as well as the initiator of brecciation (McPhie et al., 1993; Tosdal et al., 2008). The last control is chemical and thermal, based on the evolution of the mineralizing fluid as it infiltrated the breccia body (Gifkins et al., 2005; Barnes, 1997).

If the mineralization is both syn-breccia and controlled by permeability established by the internal structure of the breccia, then the actual process of brecciation must be examined in more detail. Brecciation cannot be dealt with as a single, instantaneous event, but as a series of sequential processes separated in space and time (Burnham, 1985; Fournier, 1999; McCallum, 1985; Zweng and Clark, 1995; Yang et al., 2007). The first prerequisite for brecciation is hydraulic or hydrothermal fracturing (Fournier, 1999; Burnham, 1985; Gonnerman and Manga, 2003; Bonafede and Danesi, 1997, Engvik et al., 2003 and 2005).

Hydrothermal fracturing occurs when a volume of rock is subjected to fluid pressure in excess of the lithostatic load and the tensile strength of the rock (Li, et al.,

2002, Lockner, 1995; Krech, 1973). Fluid overpressure can develop in a variety of ways (table 4.4), including continuous input of fluid within the rigid carapace of a cooling intrusion (Burnham, 1985), or onset of hydraulic conductivity between deeper and shallower lens-like fluid pockets of reservoirs (Fournier, 1999). Rapid spikes in fluid pressure can occur as the result of tectonic processes (Husen et al., 2004; Manga and Brodsky, 2006). Overpressure can also be induced by sudden evolution of volatiles from a melt, induced by disequilibrium degassing (Mangan and Sisson, 2000) or by injection of mafic material into a felsic magma chamber (Sparks et al., 1977 and 1993; Eichelberger, 1980; Pallister, 1992; Murphy et al., 2000; Gerbi et al., 2004; Keith et al., 1998).

Table 4.4-Mechanisms for triggering a hydraulic overpressure

MECHANISMS FOR TRIGGERING A HYDRAULIC OVERPRESSURE				
Source of overpressure	Locality	Result	Reference	Deposit type
Unloading via mass wasting	Ladolam	Transition from porphyry to epithermal environment	Carman, 1994; Gemmell et al., 2004; Moyle et al., 1990	Alkalic Cu-Au porphyry/ epithermal
	Mount St. Helens	Eruption	Dzurisin et al., 1983	Stratovolcano
Injection of mafic material into felsic magma chamber	Mt. Pinatubo, Montserrat	Eruption	Pallister, 1992; Murphy et al., 2000; Eichelberger, 1980; Gerbi et al., 2004; Keith et al., 1998	Stratovolcano
Seismicity triggered by distant earthquake	Yellowstone, Long Valley caldera	Fluid overpressure in a meta-stable hydrothermal system.	Manga and Brodsky, 2006; Husen et al., 2004; Roeloffs et al., 2003	Active geothermal system
Connectivity of fluid lenses	Theoretical	Stockwork and breccia formation	Fournier, 1999; Cline and Bodnar, 1994; Bagdassarov, 1994	Many
Accumulation of fluid within a cooled carapace	Penasquiera	Lens shaped accumulations of hydrothermal minerals	Kelly and Rye, 1979; Lange, 1994	Sn-W granitoid
Collapse of fluid-supported arch	Questa	Tabular-clast breccia	Ross, 2001 a and b, 2002; Cline and Bodnar, 1994	Porphyry Mo
Magma withdrawal	Questa	Tabular-clast breccia	Ross, 2001 a and b, 2002; Cline and Bodnar, 1994	Porphyry Mo
Mineral self-sealing	Many	Mineral deposition	Fournier, 1983; Beane and Titley, 1981	Many

Fracturing occurs when the overpressure exceeds the sum of the lithostatic load and the tensile strength of the rock mass (Fournier, 1999; Li et al., 2002; Pollard, 1998). The potential energy of the overpressure is expended via the creation of new surface area, friction (plasticity) and elastic wave energy dispersion (Li et al, 2002; Atkinson, 1987; Krech, 1973). Fracture network development, especially to the point of hydraulic conductivity, is much easier in already jointed rock (Gillou-Frottier and Burov, 2003; Janssen et al., 2001; Broek, 1982; Broberg, 1999; Boone, 1986; Pollard, 1979; Cloos, 1955).

Where these fractures become hydraulically contiguous, a fluid flux can be established, with fluid flow driven by thermal buoyancy, tectonic or hydraulic pumping, and fluid expansion via first and second boiling (Burnham, 1979; Brodsky et al., 2003). When hydrothermal fracturing is accompanied by loss of volume (via hydrothermal dissolution or magma withdrawal) or the presence of available free space (i.e. breach to the surface, regional extension, or doming), rotation of fragments becomes possible (Davies, 2002; Burnham, 1985; Segall, 1984; Pollard et al., 1983; Sillitoe and Sawkins, 1971). At this point in the development of a system of hydraulically contiguous fractures, the system can form a hydrothermal breccia (Sillitoe, 1985; Burham, 1985; Beane and Titley, 1981).

The point at which a hydrothermal stockwork becomes a hydrothermal breccia is poorly defined in the literature. The establishment of hydraulic conductivity between fractures may be the most appropriate stage to which to assign the onset of brecciation, but for practical purposes of field identification, rotation or transport of fragments may be easier to establish (Davies, 2002; Taylor and Pollard, 1993; Bryant, 1968).

Where void space exceeds 25.4% (depending on fragment geometry), the fractured rock mass can flow (Bryant, 1968). In the case of a hydrothermal breccia, which is inferred to be a relatively closed system with respect to clasts, but an open system with respect to fluids, 'flow' refers to the ability of clasts to move relative to each other, and to mix or segregate in accordance with three-phase fluid dynamics (Yang et al, 2008; Mukherjee and Mishra, 2007; Link et al., 2006; Wolfe, 1980). When flow is established, the solid mass mimics the behavior of a fluid and enabling the transport and mixing of fragments (Bryant, 1968). When the upward fluid flux exceeds the settling rate of the fragments, as a function of the fluid viscosity, fragment shape and density, and the presence and bubble size of a gas phase, fluidization can occur (Yang et al., 2008; Mukherjee and Mishra, 2007; McCallum, 1985). Fluidization enables the sorting of fragments by size (fines segregation), spouting and channeling within the fluidized pipe (Link, et al., 2007; Mukherjee and Mishra, 2007; McCallum, 1985). Fluidization, especially in a gaseous or low-viscosity medium, facilitates impact and abrasion between fragments (Link et al., 2007; Kennedy et al., 2005). The upward motion of the fluid medium, results in plucking of grains from the fragment rims, also resulting in rounding, attrition and comminution of fragments. This process is enhanced if the fluid medium is corrosive (Gonnerman and Manga, 2003; Carlson and Sawkins, 1980; Emmons, 1906).

Fragment size reduction is also aided by mutual impact between particles. Due to decreased drag forces on particles, mutual impact is a more effective mechanism for fragment size decrease when the fluid is gaseous rather than liquid (Yang et al., 2007; Alidibirov and Dingwell, 1996a and b; Anderson, 1991). Attrition and comminution create a positive feedback loop with fluidization; fluidization is dependent on fragment

size and on the viscosity of the fluid medium (Yang et al., 2008). Attrition and comminution both decrease fragment size and increase effective fluid viscosity by the addition of fines; the fluid becomes slurry as opposed to a simple fluid (Mukherje and Mishra, 2007). Accretionary lapilli may form in hydrothermal pipes, as a result of accretion of fines in a fluidized state (Davies, 2002, Gofton, 2007; McPhie et al., 1993).

Upward fluid flux also results in the sorting and mixing of clasts. Mixing and segregation are dependent on clast size, clast density, and the velocity of fluid flux (Mukherjee and Mishra, 2007); both mixing and segregation can occur in the same particle bed dependent on fluid flux velocity (Mukherjee and Mishra, 2007).

After the upward fluid flux velocity declines and particles settle back through the fluidization threshold, the sorting of particles becomes 'locked' (Yang et al., 2008). The zones in which fines were concentrated became zones of decreased permeability, 'choked', with all potential open space between the larger clasts occupied by fine grained clastic infill. In zones where the fines are depleted, 'stripped out', abundant open space between larger clasts will be available for the subsequent mineral deposition (Davies, 2002).

Aside from the availability of open space for sulfide deposition, the major prerequisite for the deposition of porphyry mineralization in the breccia is the failure of the breccia to breach directly the surface (Holliday and Cooke, 2007; Skewes et al., 2002; Cannell et al., 2005; Sillitoe, 1985). The breach of the breccia to the surface creates a diatreme, venting mineralizing fluids directly to the atmosphere without allowing adequate residence time in the fractured mass for sulfides to precipitate (Cannell et al., 2005; Emmons, 1938).

Mineralization in close proximity and directly above the highest concentration of megacrystic clasts indicates a direct relationship between mineralizing fluids and to disaggregated megacrystic dykes. The juvenile nature of the megacrystic clasts indicates that the megacrystic dykes were the breccia initiator, and relationship between the megacrystic clasts and the mineralization indicates that the megacrystic dykes were the source of the mineralizing fluids. However, the permeability control of breccia subunits on sulfide deposition suggests that sulfide deposition did not occur, or did not occur in quantity, until after the fluidized breccia mass had settled. The fluid evolution which makes the deposition of breccia cement from the same fluid responsible for fracturing the rock mass is discussed in Chapter 6.

Chapter 5-Alteration

Introduction

Primary breccia features record the energetics of the hydrothermal flux responsible for fracturing and rearranging the rock mass (Laznicka, 1988). Alteration, and especially the timing of alteration relative to the stages of breccia development, records the chemical evolution of the hydrothermal fluid before, during, and after brecciation (Gifkins et al., 2005; Barnes, 1997; Lowell and Guilbert, 1970; Meyer and Hemley, 1967). The single episode of brecciation at Mount Polley, and the genetic link between brecciation and mineralization, results in relatively simple alteration zoning.

Alteration in the Northeast zone can be divided into pre-, syn-, and post-breccia types (figure 5.1). Pre-breccia alteration is recognized by the uniform alteration of clasts, veins and vein selvages which are truncated at clast margins, and by clasts of different alteration types juxtaposed in the breccia. Syn-breccia alteration is recognized by altered rims on clasts, veins which originate in the breccia chemical infill but penetrate clasts, and alteration which modifies clastic infill but not the clasts themselves. Post-breccia infill alters clasts and clastic infill uniformly and may be breccia-texture destructive. Post-breccia alteration also modifies post-breccia dykes, and the timing of these events is constrained by the dykes (Fraser et al., 1994 a and b; Fraser, 1995).

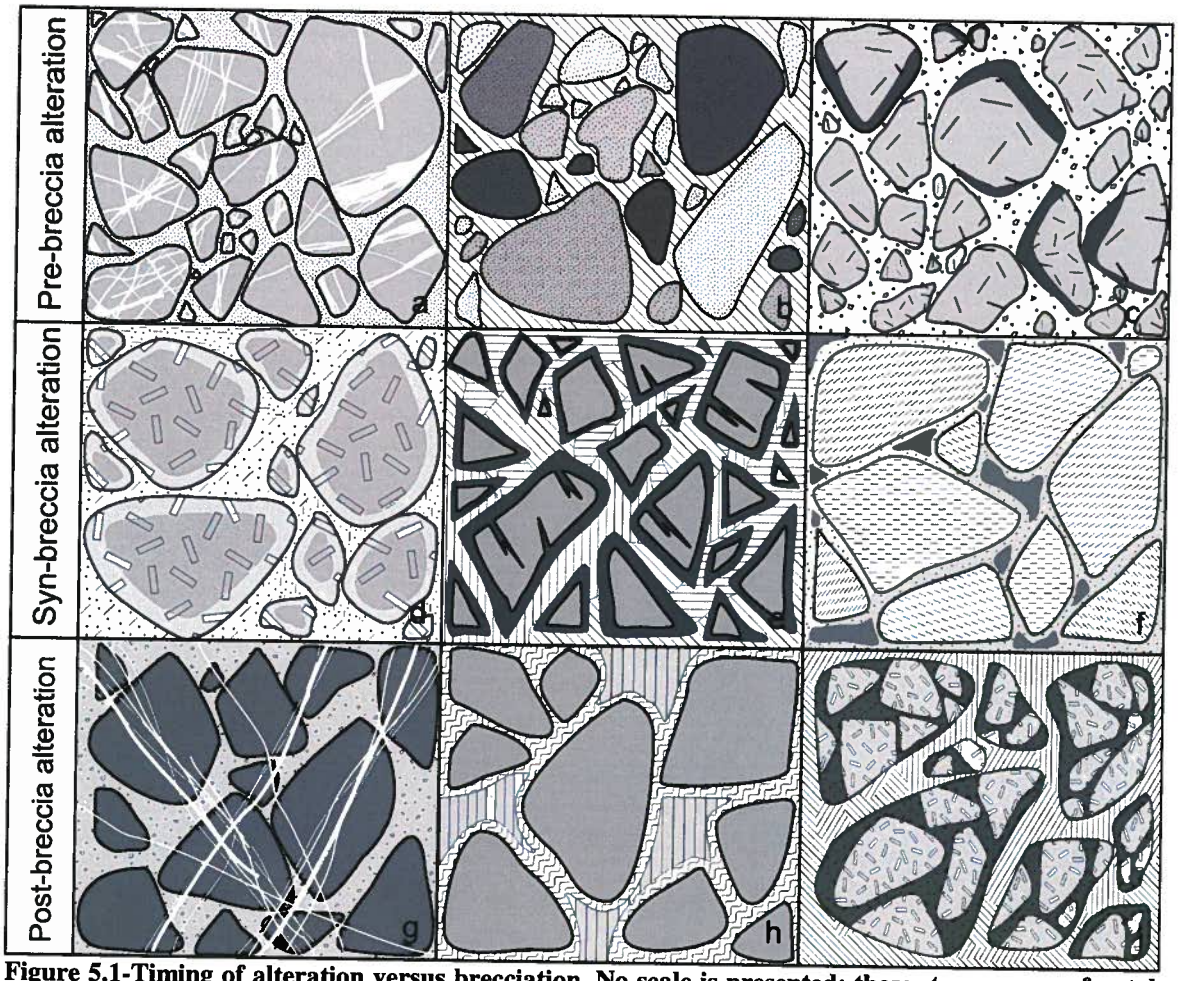

Figure 5.1-Timing of alteration versus brecciation. No scale is presented; these strucures are fractal. Pre-breccia alteration: a- Veins truncated by clast margins, **b-**Clasts of mixed alteration types, **c-**Broken altered clast rims, **Syn-breccia alteration: d-**Altered clast rims, **e-**Hydrothermal minerals armoring clasts, and syn-breccia veins, **f-**Hydrothermal mineral infill, **Post-breccia alteration: g-**Veins cross-cutting breccia textures, **h-**Hydrothermal minerals occupying re-opened breccia, **i-**Clasts of breccia in breccia, or vein fragments in breccia.

The relationship between infill, as described above, and alteration can be ambiguous, as can the relationship between syn- and post-brecciation processes. The ambiguity and complexity of this relationship is discussed in Chapter 4. For purposes of breccia description here, the 'syn-breccia' period is defined as the period from the development of a hydraulically contiguous fracture network through clast movement and potentially fluidization, until the mass has settled and been cemented with the first generation of chemical infill. This description is predicated on the assumption that there was no extended period of quiescence with unfilled permeability or open space within the

breccia between the settling of the mixed bed and mineralization, and places the end of the syn-breccia period at the point at which the breccia begins to behave as a rheological unit, rather than as a particle bed.

Pre-breccia Alteration

Pre-breccia alteration is widespread and pervasive in the Mount Polley system. Due to the lack of drilling information outside the mineralized system, the lateral and vertical extent of pre-breccia alteration is unknown. Pre-breccia alteration can be pervasive or restricted to veins and vein haloes, but the pre-breccia nature of the alteration can be determined by alteration restricted to breccia clasts or truncated by clast margins.

Altered mafic clasts

As discussed in Chapter 2, the most distinctive pre-breccia alteration is the alteration of the 'altered mafic clasts'. These clasts have been subject to texturally destructive albite- and actinolite-forming alteration of the groundmass, cut by magnetite veins with pink feldspar haloes. This overprint renders the clast protolith indistinct. The alteration style is not observed in coherent rocks, making it difficult to place the clasts in stratigraphic context, although the clustering of the clasts within the breccia suggests that the unit may have had an originally tabular geometry, somewhat disrupted by subsequent brecciation. The most distinctive feature of these rocks is the presence of magnetite and K-feldspar veins in a mottled, dark grey-green grundmass. These veins are truncated by clast margins (figure 5.2).

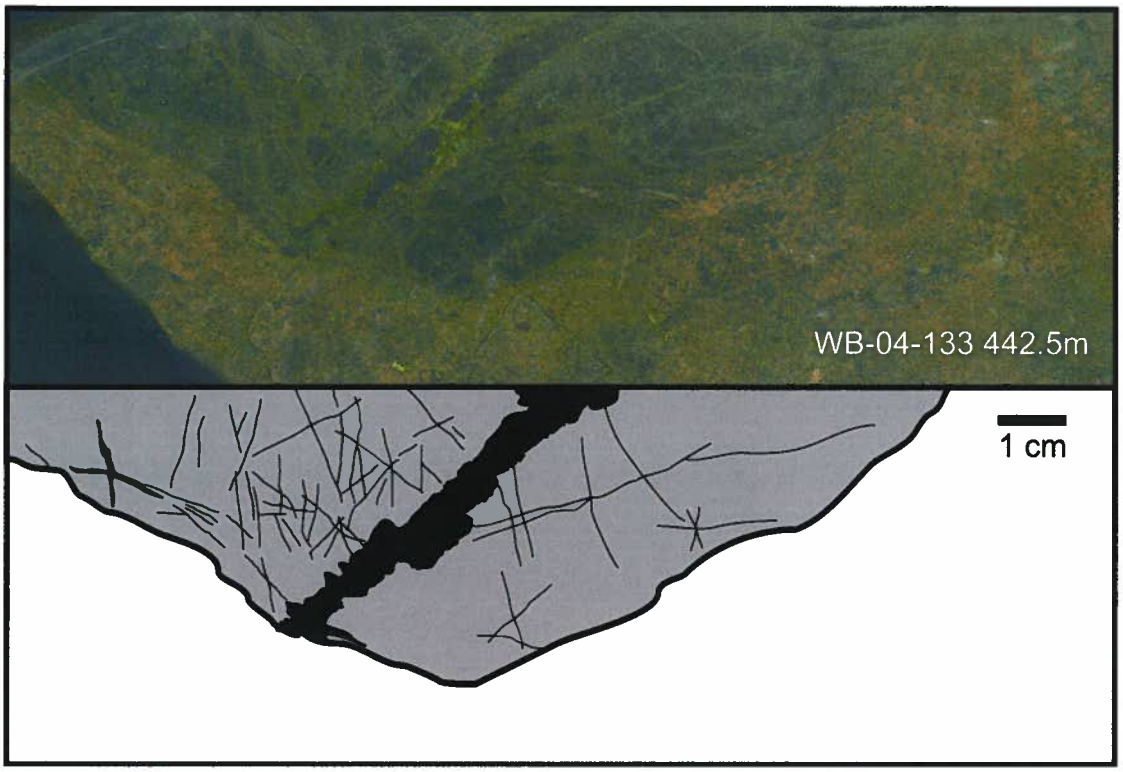

Figure 5.2-Altered mafic clast within the breccia; some magnetite ahs been replaced by chalcopyrite after the inclusion of the clast in the breccia. The magnetite vein is truncated by the clast margin, showing that the vein pre-dated fragmentation.

Hematite-carbonate

The most widespread pre-breccia alteration was a K-feldspar-stable hematite-carbonate alteration. Nearly all clasts in the breccia and much of the surrounding coherent monzonite was subject to this alteration, which resulted in a 'dusting' of hematite, lending the rock a pink to red-orange coloration. Wherever this red coloration was observed, the rock is also pervaded by small (<1 mm) clots and blebs of calcite (figure 5.3a and b).

Figure 5.3a-Hematite staining on pre-breccia monzonite. Hole WB-04-32, 111 m; Scale bar equals 1 cm. Veins are calcite (left) and chalcopyrite (right).

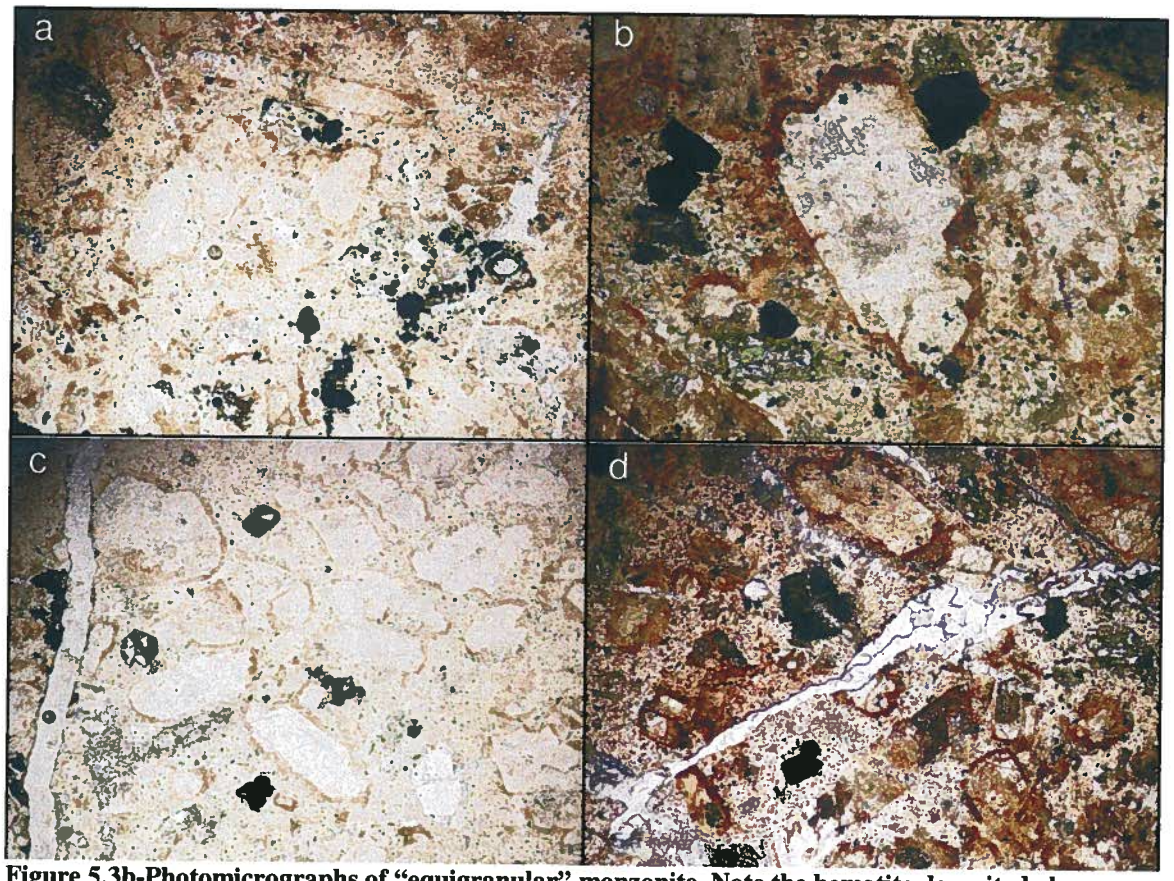

Figure 5.3b-Photomicrographs of "equigranular" monzonite. Note the hematite deposited along grain boundaries and interstitial calcite. The veins cutting all four samples are also calcite. A; note the replacement of mafic minerals by chlorite and opaque minerals. B; Carlsbad-twinned K-feldspar phenocryst rimmed with hematite (center), and partially hematite stained K-feldspar phenocryst (lower left). C; less intense hematite-staining. D; hematite staining on phenocryst rims and preferentially replacing domains within phenocrysts. Each FOV=5mm.

Hematite-carbonate alteration is also observed in the equigranular augite-monzonite, K-feldspar and K-feldspar-plagioclase porphyry dykes that cut the breccia. It

is observed less strongly in the hornblende-bearing monzonite dykes, and is absent in the plagioclase microporphyry or mafic dykes. In the K-feldspar porphyry dykes, the margins of the dykes are in some cases strongly reddened by hematite-carbonate alteration while the interiors of the dykes are not (figure 5.4). This suggests that the hematite dusting and carbonate is a secondary, fluid-related modification of the igneous rocks, rather than related to magma characteristics. The hematite-carbonate alteration is most evident modifying the feldspar site in the affected rocks. Mafic minerals in rocks affected by hematite-carbonate alteration are generally replaced by chlorite.

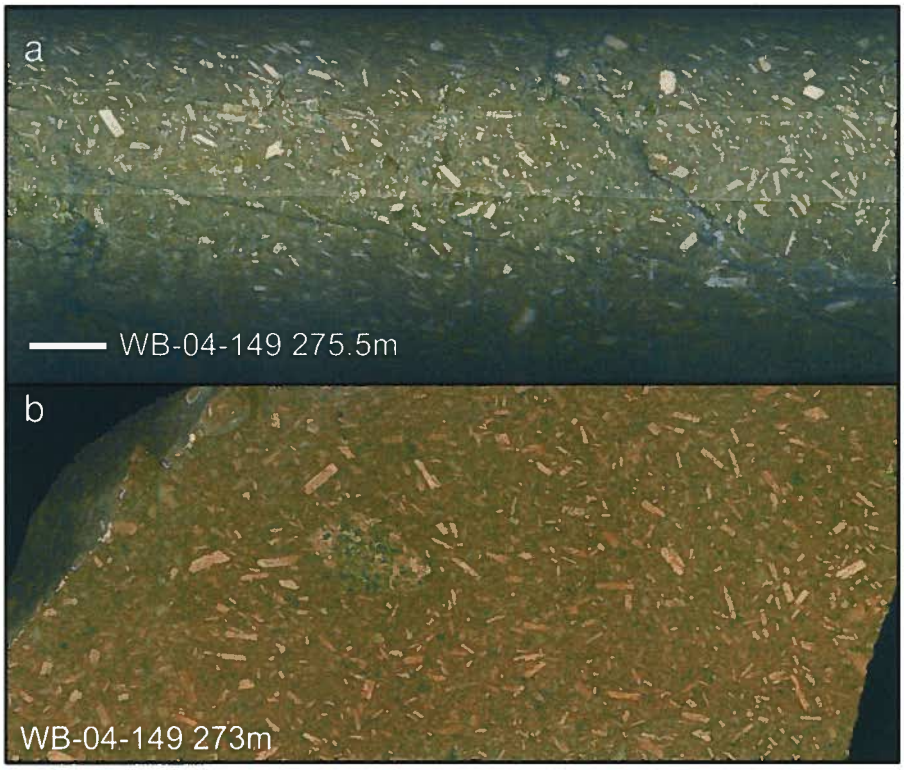

Figure 5.4-Grey interior (a) and red exterior (b) of the same crowded K-feldspar porphyry dyke. Scale bar equals 1 cm.

In most cases where the rock is modified by syn- and post-breccia alteration, some sign of relict hematite-carbonate mineralization remains, suggesting that the alteration was uniform throughout the Northeast zone prior to brecciation.

Biotite-magnetite

Biotite-magnetite alteration, as described here, applies mostly to the mafic xenoliths incorporated into the pre-breccia equigranular monzonite. Some of this alteration may be the product of reaction between the mafic xenoliths and the magma into which they were incorporated, as evidenced by the rimmed xenoliths (see figure 3.4). The xenoliths, which were probably originally dominated by pyroxene, are replaced by a texturally destructive combination of biotite and magnetite (figure 5.5).

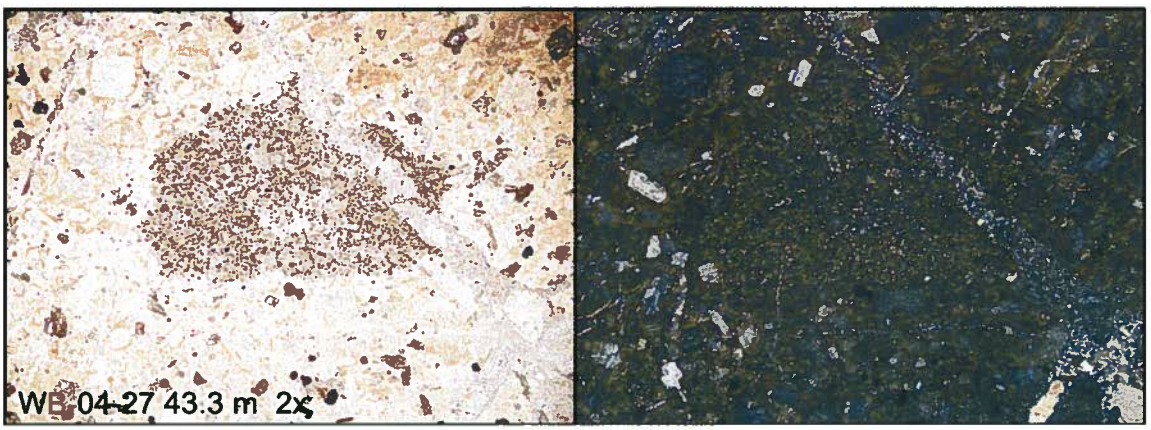

Figure 5.5-Biotite-magnetite alteration of a pre-monzonite xenolith. Plane and crossed polars. FOV=1 cm

Chlorite

The mafic sites in rocks modified by pre-breccia hematite-carbonate alteration were generally replaced by polycrystalline chlorite. Mafic minerals are still recognizable based on the shapes of the mineral sites. Chlorite completely psuedomorphs blocky, square mineral sites (originally augite), and elongate mineral sites (originally hornblende). Rare secondary biotite is also present. The euhedral nature of the psuedomorphs suggests that the mafic minerals were directly altered to chlorite, rather than being altered to secondary biotite, then to chlorite, which would result in more diffuse, irregular psuedomorphs.

Syn-breccia Alteration

Syn-breccia alteration is widespread in the Northeast zone, but is more difficult to recognize than the pre-breccia alteration.

Chlorite

Syn-breccia chlorite alteration and chlorite chemical infill are difficult to distinguish. Chlorite chemical infill is distinguished by fine, inward-pointing chlorite crystals nucleated along clear, well-defined clast margins (figure 5.6). Chlorite infill is frequently the only infill in crackle breccias, and usually completely surrounds clasts even where they are in direct contact with other clasts. Chlorite alteration, on the other hand, forms very thin rims or rinds on clasts, resulting in indistinct clast margins where the outer 1 mm edge of the clast has been replaced by chlorite (figure 5.7). Chlorite alteration is mostly observed in the shallow and peripheral parts of the breccia (figure 5.8).

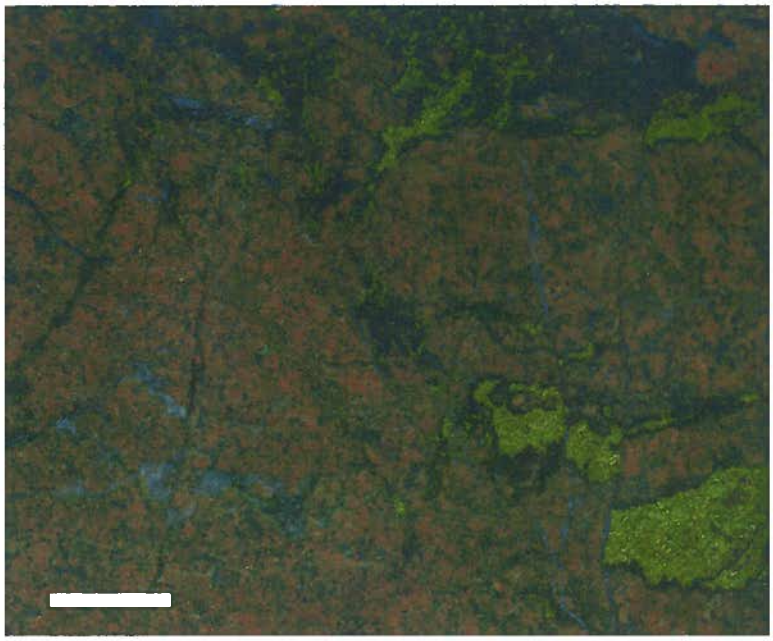

Figure 5.6-Chlorite infill followed by chalcopyrite infill; WB-03-14-88m; Scale bar equals 1 cm.

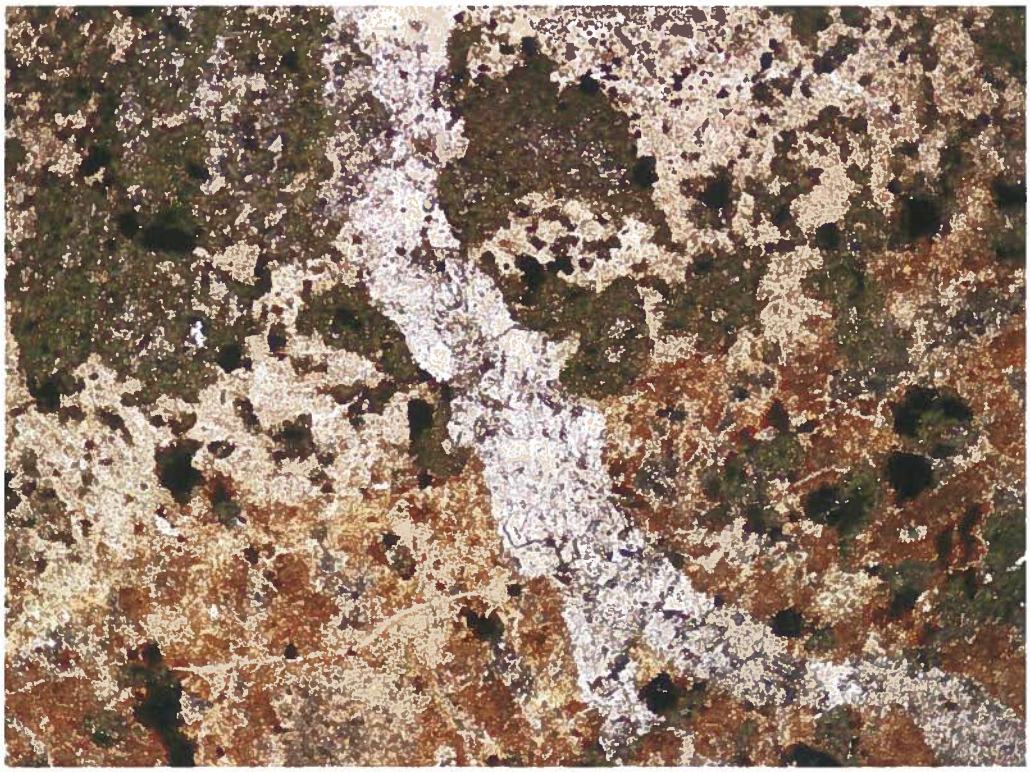

Figure 5.7-Chlorite-altered clast margin (green, top left) against K-feldspar altered infill (brown, bottom right); crosscut by late calcite vein (white, center). WB-04-32, 125.5 m FOV 2.5 mm.

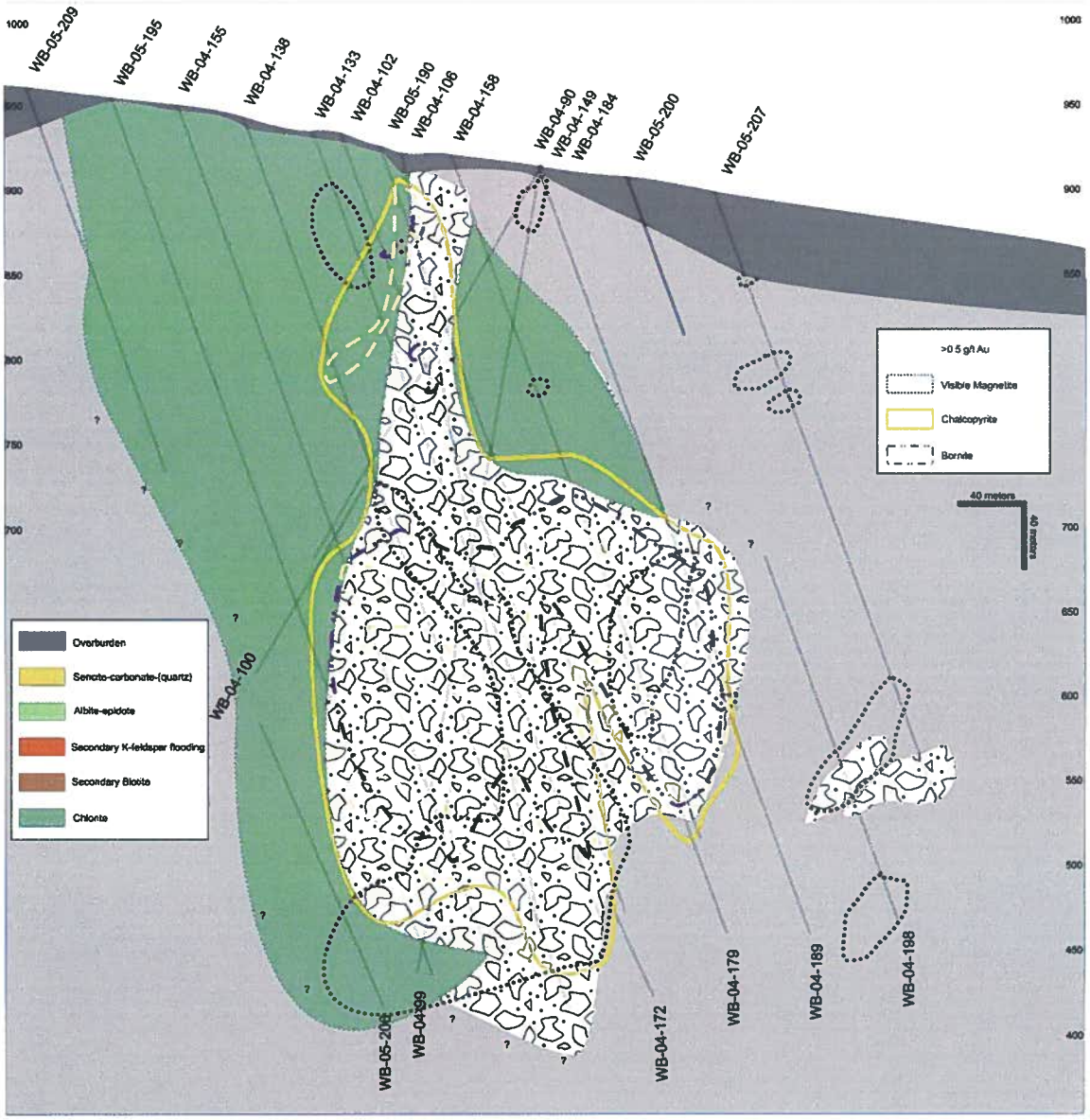

Figure 5.8-Distribution of Chlorite on section 29.

Biotite

Syn-breccia biotite alteration occupies the bulk of the breccia in the Northeast zone (figure 5.9), where it overprints the pre-breccia hematite-carbonate alteration, giving the rock a dark brown cast. Unlike chlorite alteration, biotite alteration forms distinct 1-2 cm rims on clasts and occasionally overprints clasts entirely. Biotite alteration predated K-feldspar flooding (see below) as biotite-altered 'ghost' clasts survive within pervasive, texturally destructive K-feldspar alteration (figure 5.10). Biotite alteration is directly

spatially associated with sulfide mineralization, but chalcopyrite-bearing veins with K-feldspar haloes crosscut biotite-altered clasts (figure 5.11)

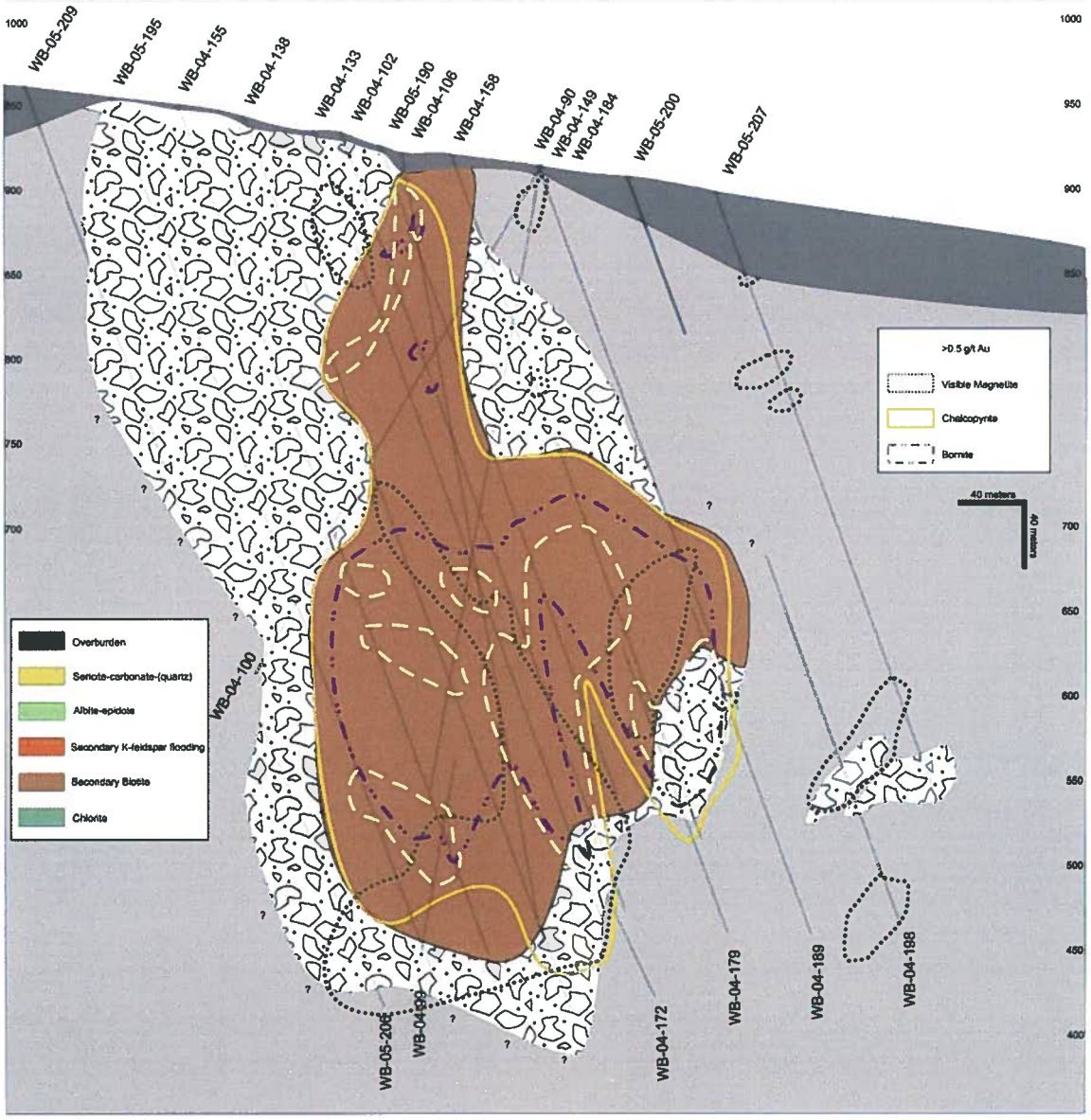

Figure 5.9-Biotite alteration on section 29

Figure 5.10-Biotite altered relict clasts in pervasive K-feldspar flooding. Scale bar equals 1 cm.

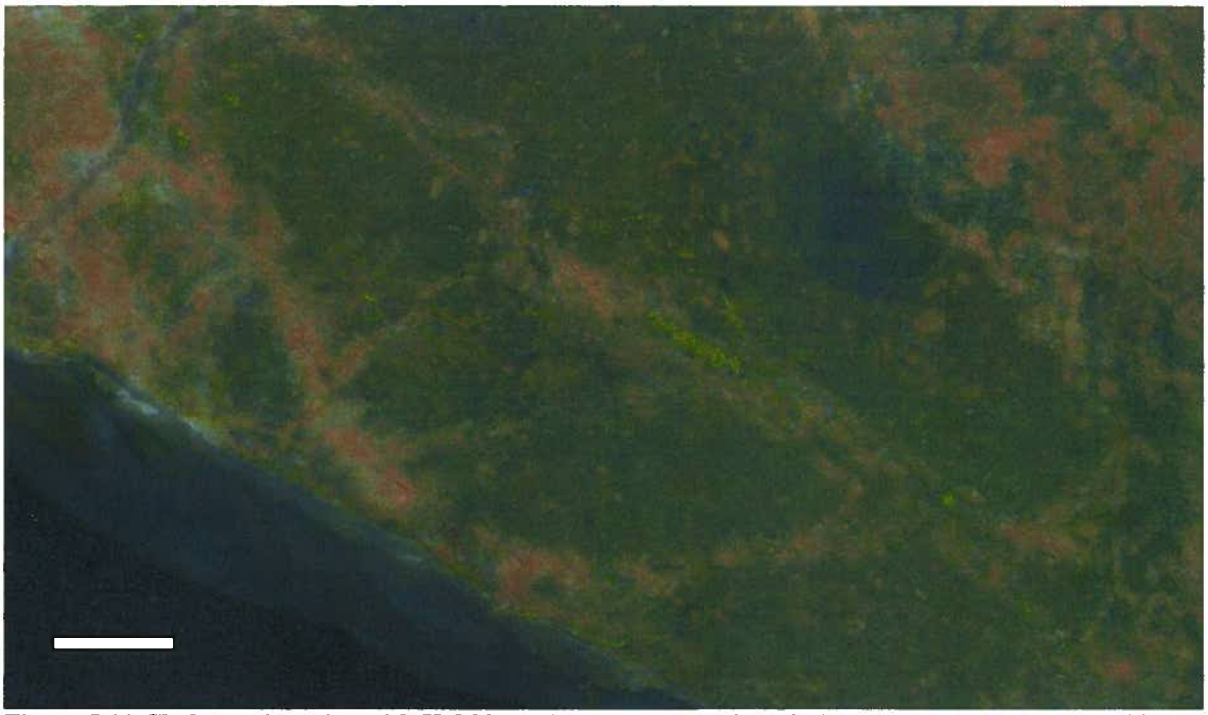

Figure 5.11-Chalcopyrite veins with K-feldspar haloes crosscutting biotite-altered clasts. WB-04-133, 310.4m. Scale bar equals 1 cm.

Sulfide replacement

In local regions of the breccia, the combination of a high percentage of mafic clasts and the presence of mineralizing fluids resulted in the replacement of mafic clasts by chalcopyrite (figure 5.12). This local relationship is the only evidence of chemical control on ore distribution at Mount Polley by wall-rock reactivity. Areas of replacement of mafic clasts are commonly high grade, but they are small and restricted such that they contribute little to the overall grade and tonnage of the mineralized body.

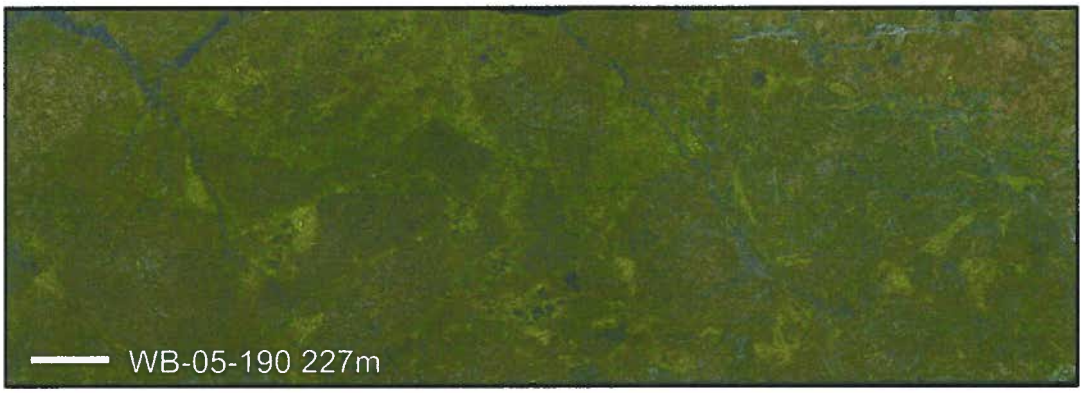

Figure 5.12-Mafic clasts replaced by chalcopyrite. Scale bar equals 1 cm.

K-feldspar

The origin and timing of the texturally destructive K-feldspar "flooding" observed in both section 18 and 29 is somewhat obscure. K-feldspar flooding post-dates biotite alteration related to sulfide deposition in most cases, but in other cases sulfide deposition appears to post-date K-feldspar. The K-feldspar flooding forms a 'blanket' at depth in section 29, and a 'bulb' in the heart of section 18 (figure 5.13). In rocks affected by this alteration, the infill of the breccia is completely or almost completely replaced by a uniform, monomineralic zone of salmon-pink K-feldspar. This alteration post-dates the biotite alteration as surviving clasts replaced by biotite are visible within the K-feldspar alteration. In megacrystic monzonite porphyry clasts, the K-feldspar phenocrysts survive within diffuse biotite aggregates largely destroyed by subsequent K-feldspar flooding

(figure 5.14). The K-feldspar flooding pre-dates and is overprinted by albite-epidote alteration at depth (figure 5.15). All of these textures might indicate that K-feldspar flooding was post-breccia, but the presence of K-feldspar rims on some clasts (figure 5.16) suggests a syn- to late-breccia timing. Likewise, the spatial relationship between K-feldspar flooding and ore (the highest grades in section 29 coincide with the upper 1/3 of the K-feldspar alteration), suggests a syn- to late-breccia provenance. Bornite mineralization appears to post-date K-feldspar deposition. In some areas, anhydrite is also present within and immediately above the K-feldspar flooded zone.

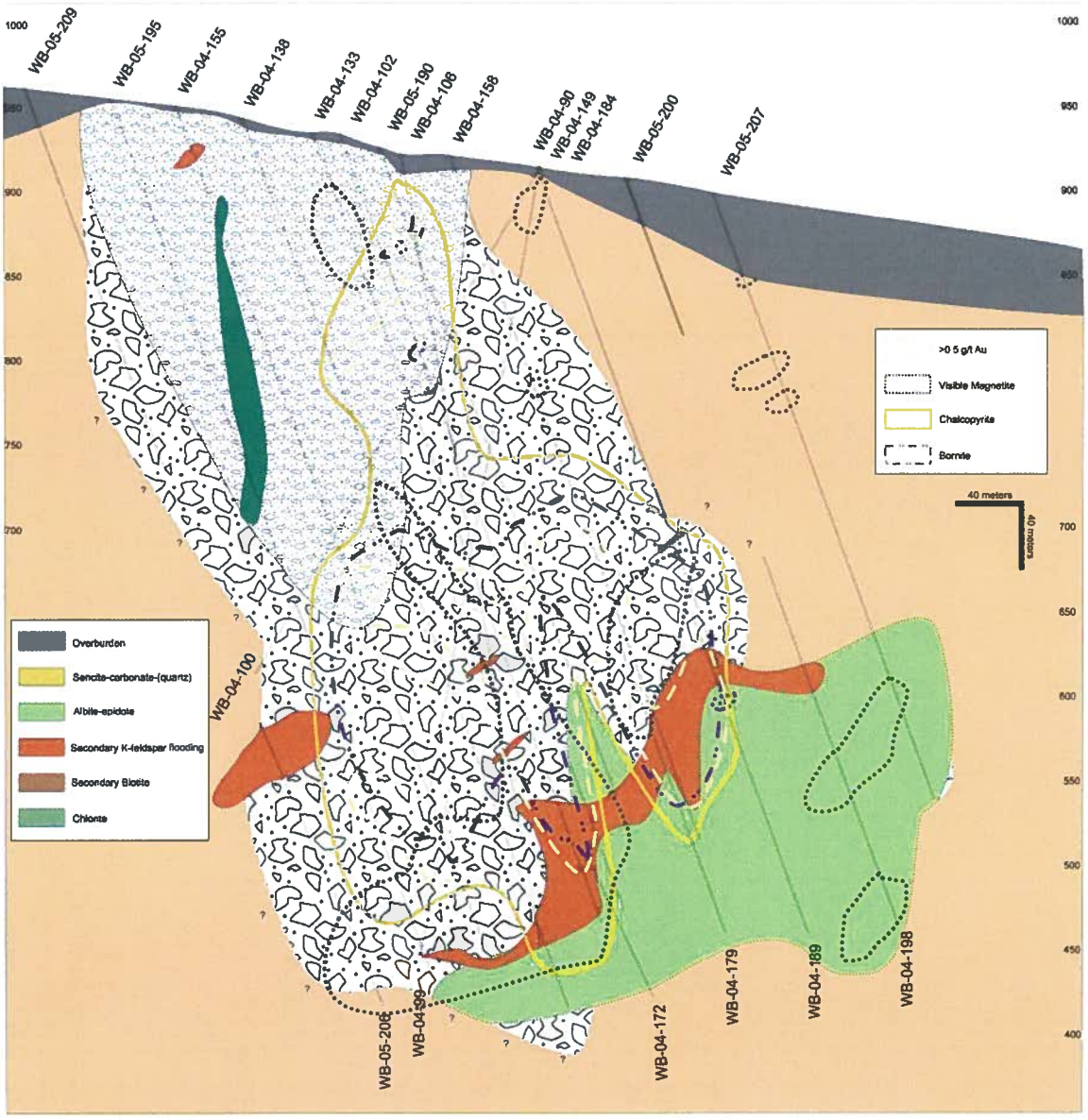

Figure 5.13-Silicate alteration on Section 29. Note the relationship between K-feldspar alteration and bornite mineralization.

Figure 5.14-Biotite-altered relict clasts in pervasively K-feldspar altered infill. Scale bar equals 1 cm.

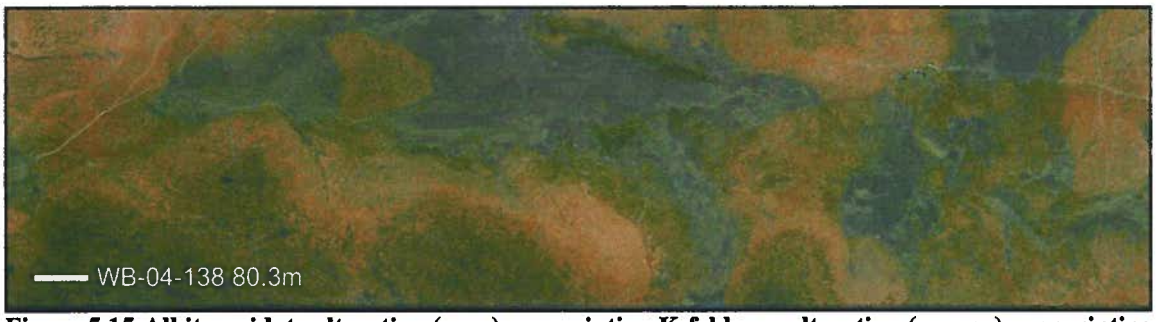

Figure 5.15-Albite-epidote alteration (grey) overprinting K-feldspar alteration (orange) overprinting biotite alteration (brown). Scale bar equals 1 cm.

Figure 5.16-K-feldspar rims on biotite-altered clasts. Scale bar equals 1 cm.

Magnetite

Magnetite alteration forms a blanket at depth in Section 29, with a distinct upward extension coinciding with the central portion of the fine-grained breccia subunit (figure 5.17). Magnetite alteration pre-dates sulfide deposition; magnetite is paragenetically early and replaced by chalcopyrite where they occur together (figure 5.18). Magnetite and bornite seldom coexist, and where they do, magnetite is extremely corroded; thin laths of what appear to be specular hematite do occur with bornite (figure 5.19). Magnetite alteration is overprinted by both K-feldspar and albite-epidote alteration. Where it is overprinted by albite-epidote alteration, magnetite is replaced by pyrite (figure 5.20). The nature and timing of magnetite alteration with respect to post-breccia albite-actinolite alteration (described below) is unknown as the two alteration assemblages have yet to be seen in contact. As both alteration styles are early and reflect high-temperature processes, they are assumed to be relatively coeval.

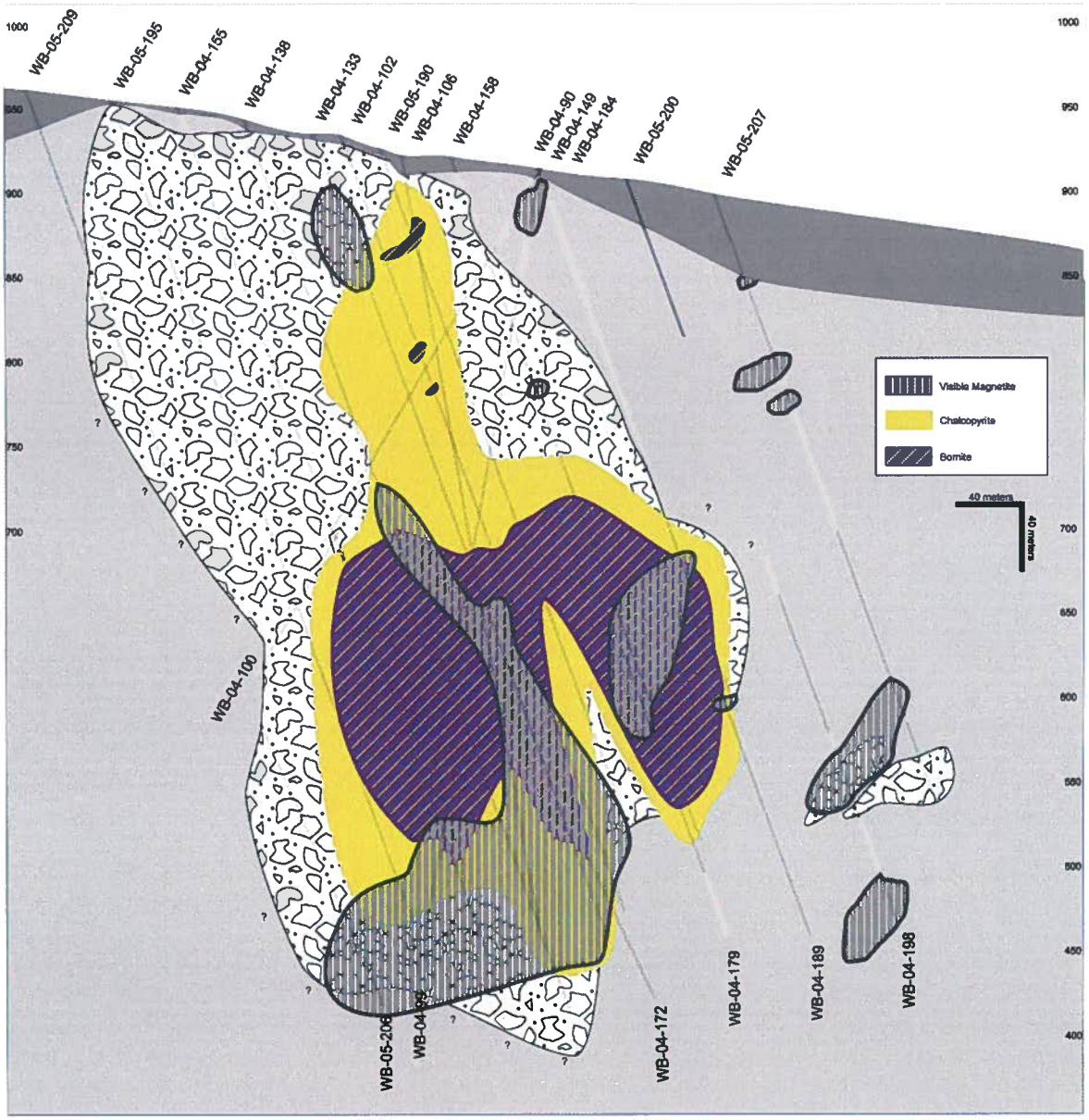

Figure 5.17-Magnetite and sulfide infill on Section 29.

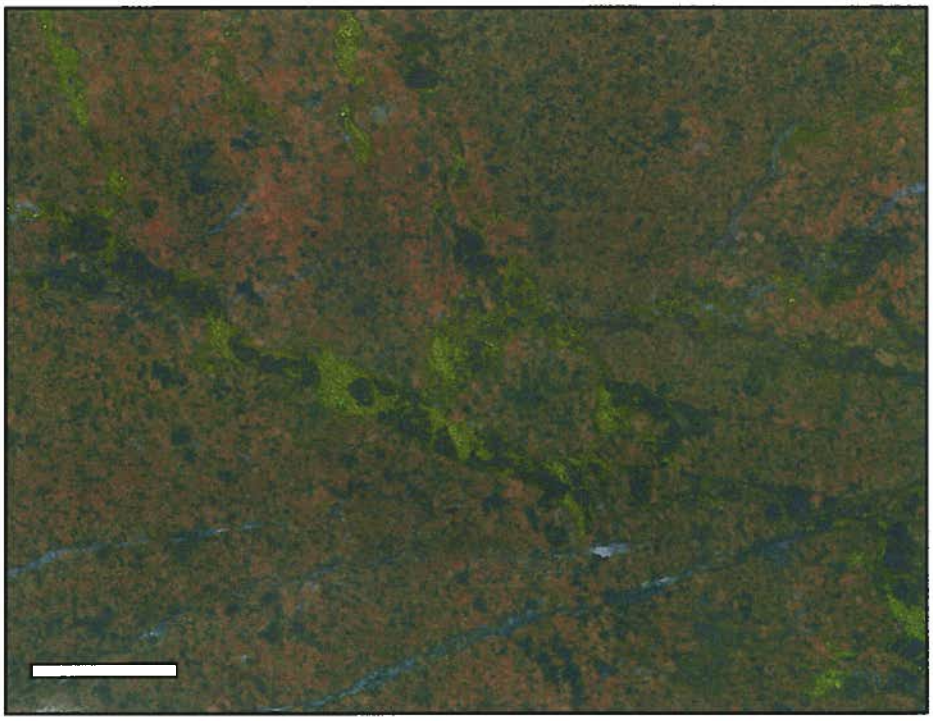

Figure 5.18-Magnetite replaced by chalcopyrite. WB-04-14 99 m; scale bar equals 1 cm.

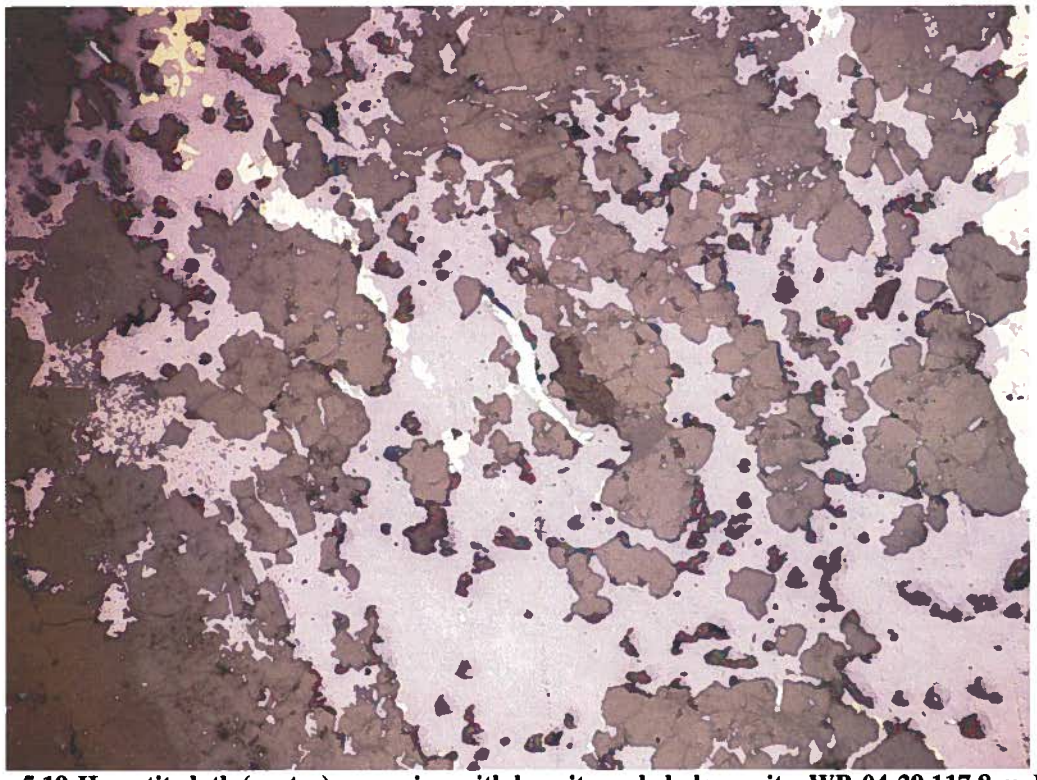

Figure 5.19-Hematite lath (center) occurring with bornite and chalcopyrite. WB-04-29 117.8 m. Field of view 1 mm.

Albite-actinolite

Albite-actinolite alteration is, at least as far as it is preserved, the least volumetrically significant of the syn-breccia alteration assemblages (figure 5.13). Albite-actinolite alteration is best preserved in the fine-grained breccia. This is unusual in that none of the other syn-breccia alteration types are well developed in the fine-grained breccia. Actinolite alteration is commonly developed as actinolite rims on clasts, with albite replacement of K-feldspar on clast rims and sometimes in the interior of clasts. Clastic infill is commonly completely replaced by albite and actinolite (figure 5.20). In some cases, actinolite alteration coincides with extremely high Cu-Au grades at the bases of the breccia (figure 5.21).

To the west of Section 18, an area of albite and actinolite alteration is interpreted as being related to the structurally deeper and temperature 'Leak Zone' area of low-grade mineralization, juxtaposed with the shallower Northeast zone by the Green Giant Fault (figure 5.22). Much of the albite-actinolite alteration related to this zone forms psuedobreccia textures, but some of it may be a texturally destructive overprint on a true breccia, with relict K-feldspar altered clasts (figure 5.23). Unlike the albite-actinolite alteration in the Northeast zone, which is associated with high-grade mineralization or with barren zones, the albite-actinolite mineralization in this zone contains small amounts of chalcopyrite, nowhere exceeding 1% of the rock.

Figure 5.20-Albite-actinolite alteration overprinting K-feldspar alteration (WB-04-73, 14.4 m) Scale bar equals 1 cm.

Figure 5.21-Biotite-altered clasts with K-feldspar rims and albite-actinolite altered clastic infill associated with bornite and chalcopyrite chemical infill, WB-04-189, 315 m. Scale bar equals 1 cm.

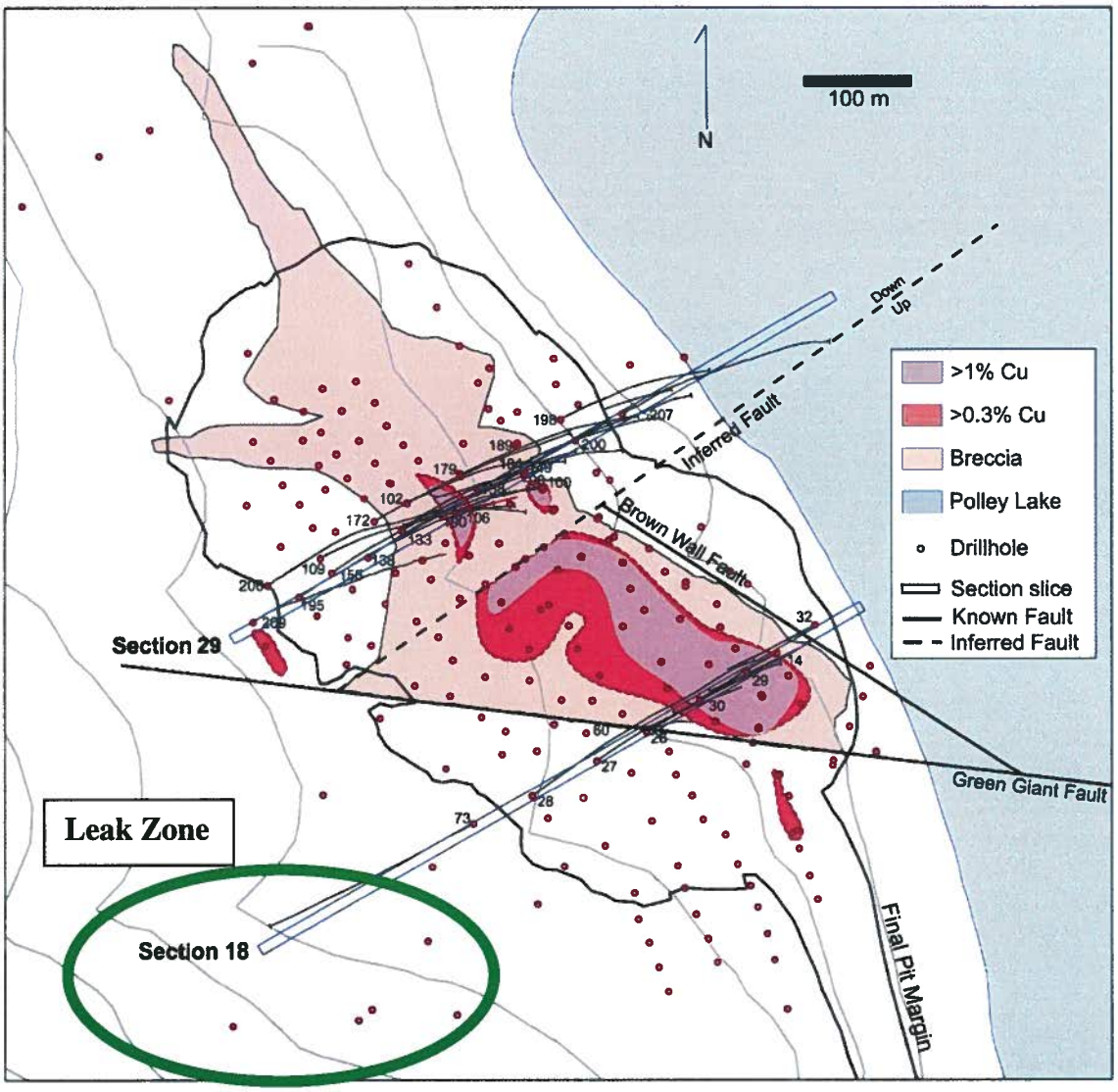

Figure 5.22-The Northeast Zone. The Leak Zone is located south and west of Section 18; Leak-zone style alteration was encountered in hole WB-04-73, WB-04-26 and WB-04-27

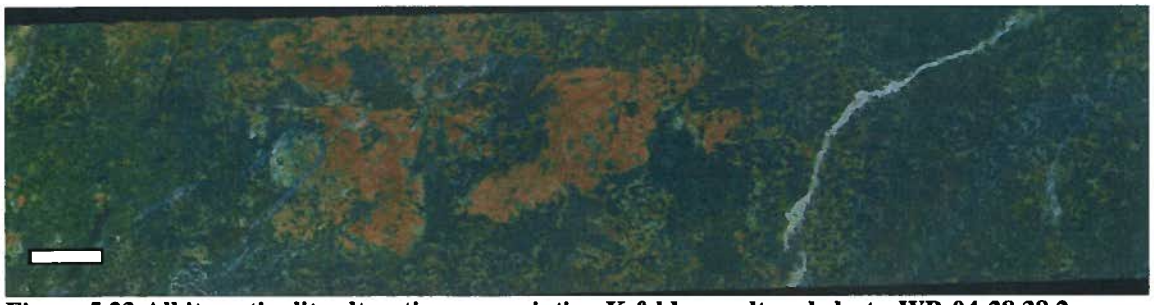

Figure 5.23-Albite-actinolite alteration overprinting K-feldspar altered clasts. WB-04-28 38.2 m. Scale bar equals 1 cm.

Post-breccia alteration

Sulfide replacement in coherent rocks

In some coherent rocks intruding the breccia, sulfides are present as blebs occupying former mafic sites within the rock (figure 5.24). The blebs are commonly associated with <1 mm white albite veins. Chalcopyrite is most common. Pyrite is commonly disseminated in the K-feldspar and K-feldspar and plagioclase phyric monzonite porphyry dykes, but it appears to be magmatic, not a replacement of mafic minerals.

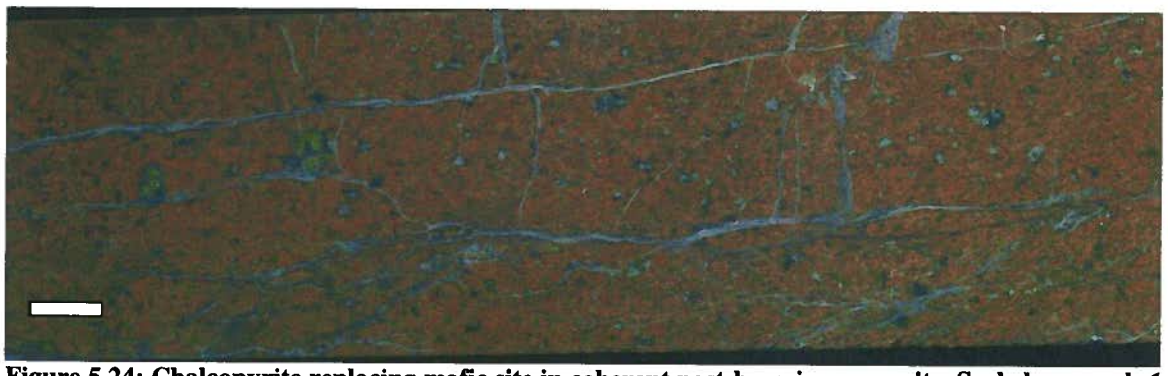

Figure 5.24: Chalcopyrite replacing mafic site in coherent post-breccia monzonite. Scale bar equals 1 cm.

Sulfide veins

Sulfide veins crosscut the breccia and the contacts between breccia and immediately-post-breccia equigranular monzonite and trachyte dykes (figure 5.25). These dykes show no macroscopic gangue or accessory minerals, except for chalcopyrite. Post-breccia chalcopyrite is minor and does not appear to have contributed significantly to the overall grade of the system, at least in the Northeast zone. It was not widespread or consistent enough to be reliably tied to any particular dyke generation.

Figure 5.25-Chalcopyrite veins crosscutting breccia textures. The chalcopyrite vein has been exploited by a later gypsum vein. Hole WB-04-106, 380.4 m

Albite-epidote

Albite epidote is common and texturally destructive in the deepest portions of Section 29 (figure 5.26). It was not observed in Section 18. Albite is more prevalent than epidote in Section 29. This proportion appears to be consistent throughout the zone. Pyrite is associated with albite-epidote alteration, and replaces both Cu-sulfides and magnetite (figure 5.27). Albite-epidote alteration post-dates the post-breccia hornblende-bearing equigranular monzonite dykes (figure 5.28). Mafic dykes cut albite-epidote alteration.

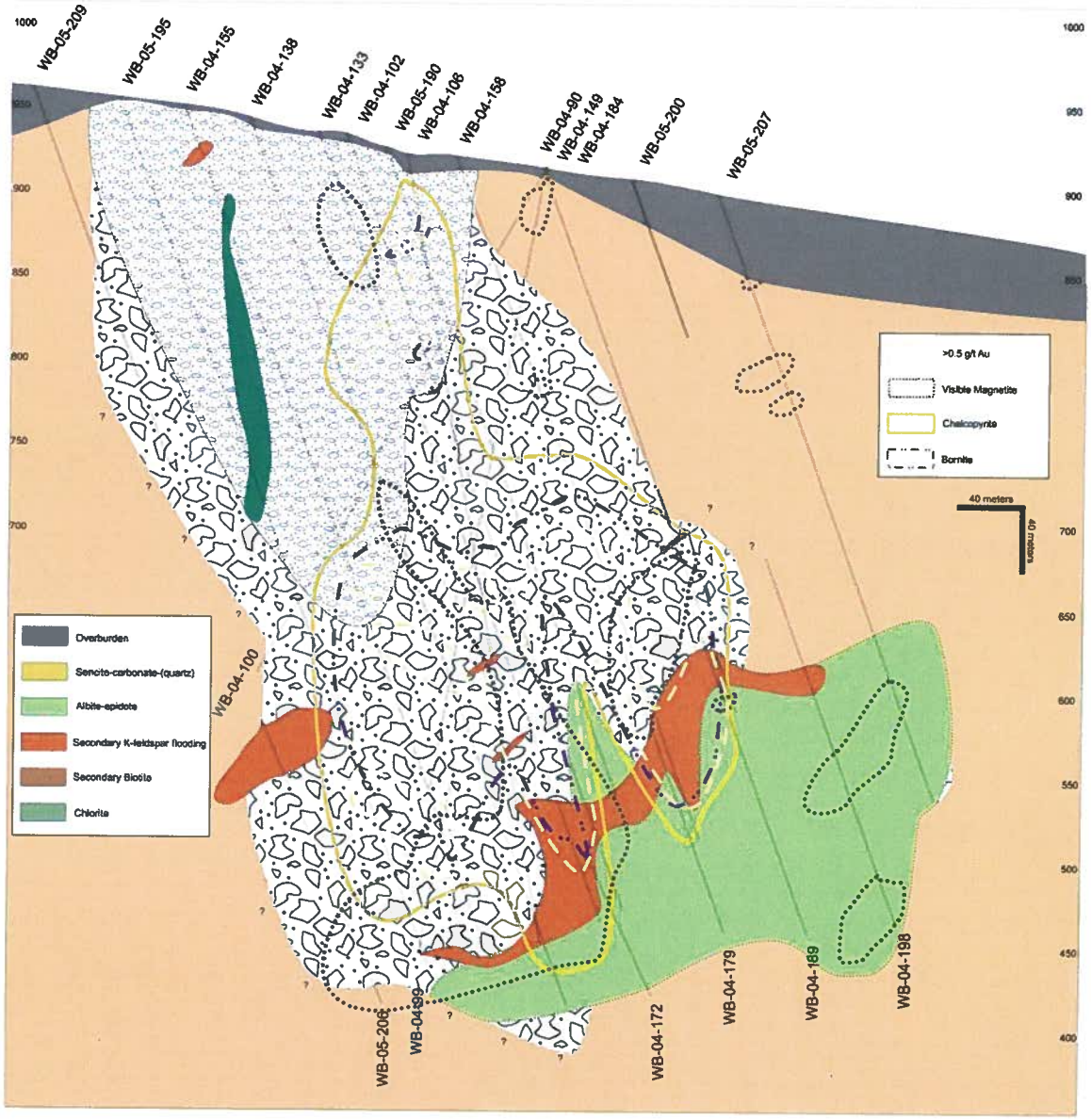

Figure 5.26-Albite-epidote alteration on section 29.

Figure 5.27-Albite-epidote alteration of a post-breccia hornblende-bearing monzonite dyke (right) cutting pre-breccia equigranular augite-bearing monzonite (left). WB-04-189, 480.8 m.

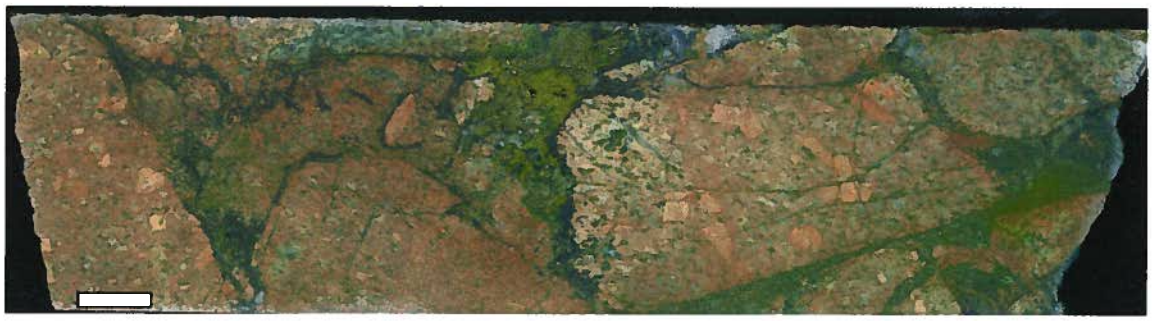

Figure 5.28-Pyrite replacing chalcopyrite, associated with albite-epidote alteration (grey mineral replacing K-feldspar). Scale bar equals 1 cm.

Sericite-quartz-carbonate

Sericite-quartz-carbonate alteration is restricted to the immediate vicinity of veins, fractures, and small faults in the Northeast Zone (figure 5.29). The alteration assemblage is texturally destructive, usually resulting in a featureless, amber-colored rock. The hardness of the rock varies greatly, from quite soft where sericite and carbonate dominate, to quite hard where disseminated quartz is dominant. Generally the rock is hardest closest to the central vein or fracture around which the alteration is developed. The center of each sericite-quartz-carbonate zone is marked by a multi-generation vein of

white, visually opaque quartz (figure 5.30). The best developed of these veins form vein breccias, with breccia clasts formed of banded vein fragments containing carbonate and quartz, sometimes with euhedral, terminated quartz crystals forming cockade clusters at the vein margins (figure 5.31). This is the only quartz observed in the Northeast Zone.

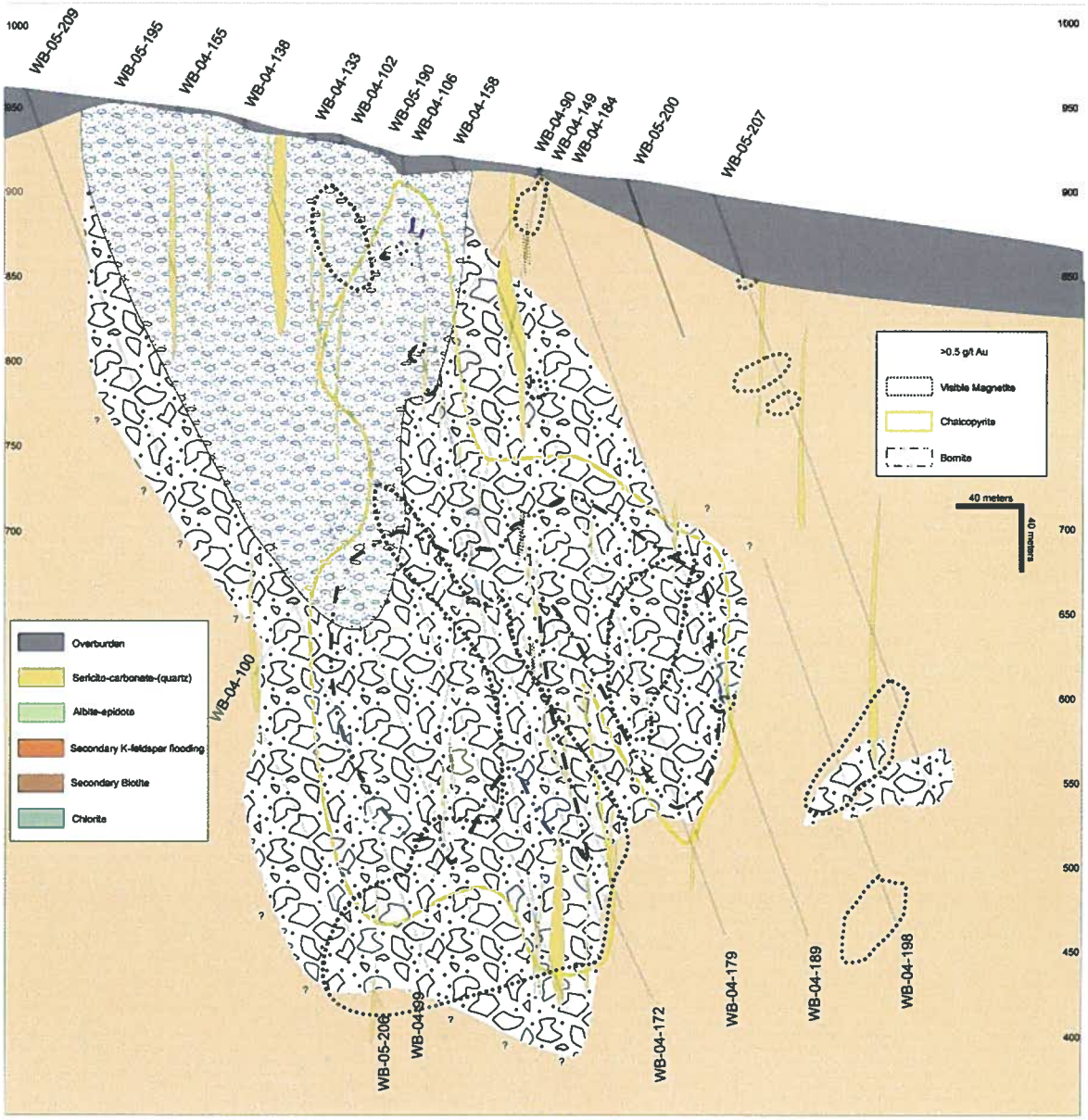

Figure 5.29- Quartz-sericite carbonate alteration on Section 29.

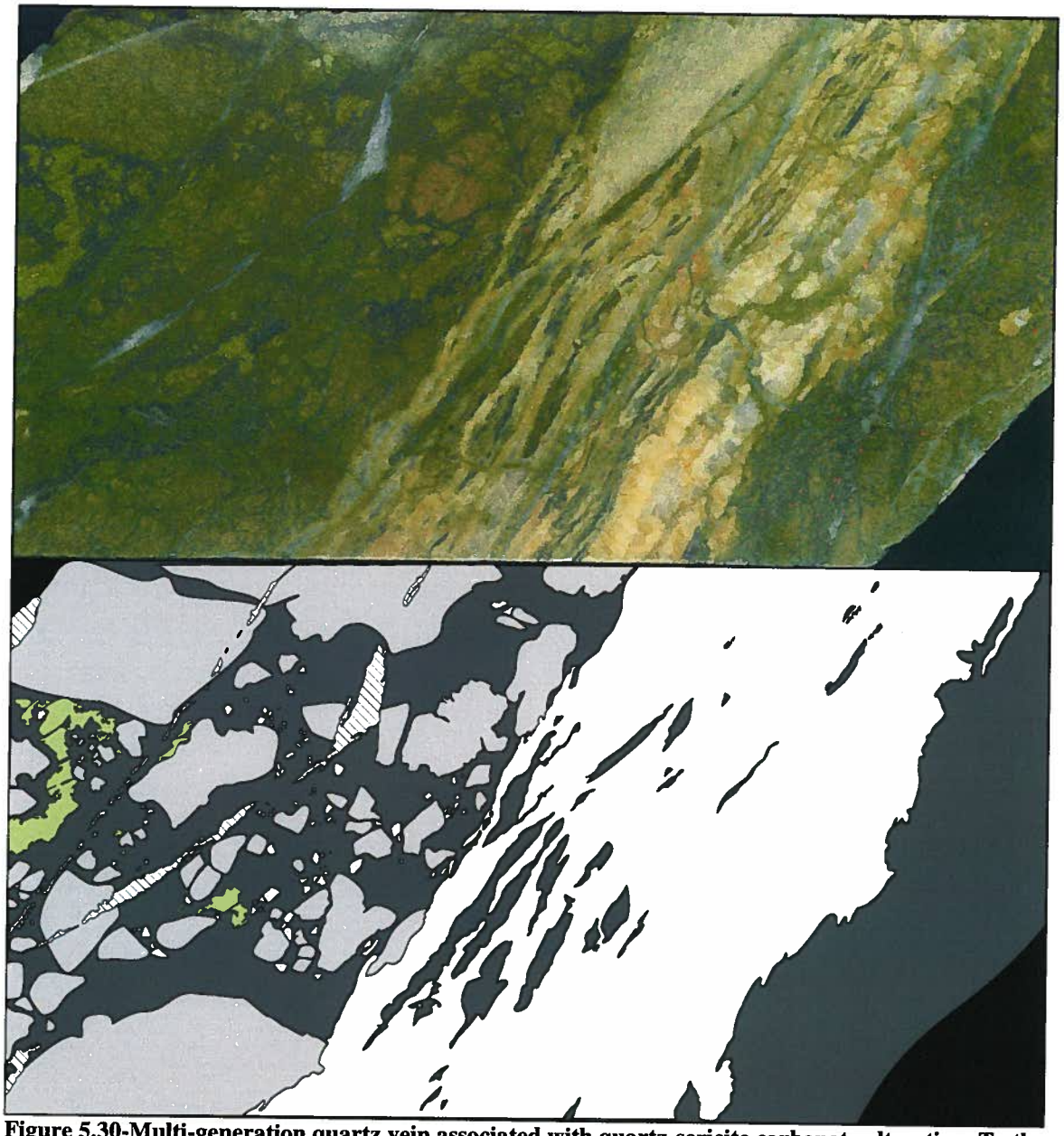

Figure 5.30-Multi-generation quartz vein associated with quartz-sericite carbonate alteration. To the right of the image, chalcopyrite is replaced by chalcocite.

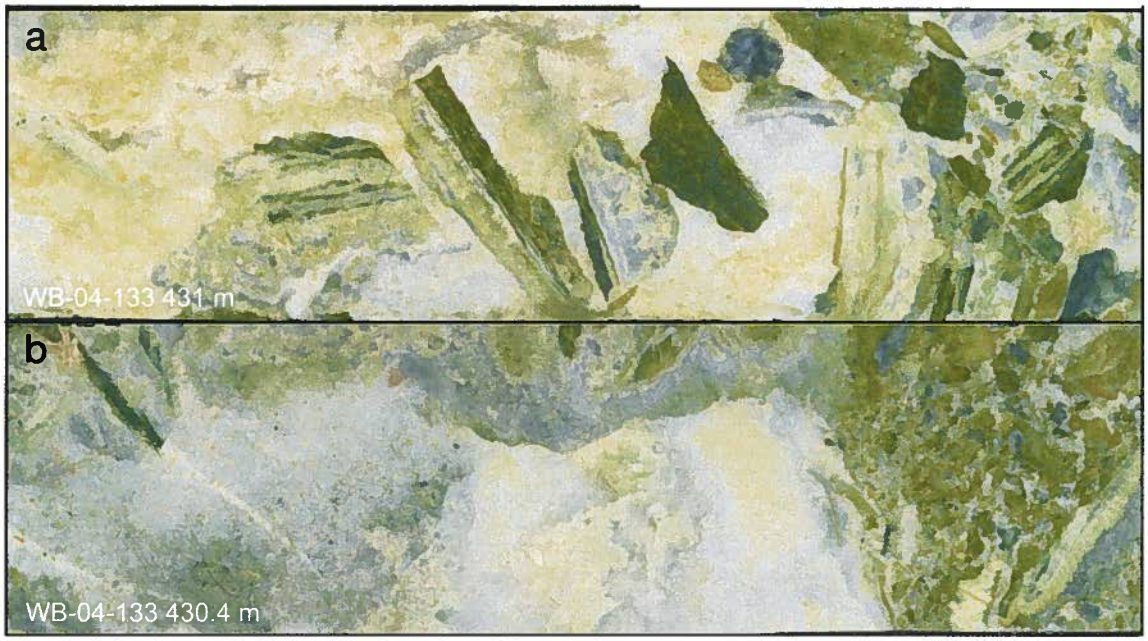

Figure 5.31-Quartz-infilled vein breccias with vein fragments as clasts. A; the cockade textures in the clasts; b; cockade textures in infill.

Although small quantities of pyrite are commonly present in the sericite-quartz-carbonate alteration as fine, disseminated grains, the alteration does not seem to destroy Cu-sulfides (figure 5.32). Chalcocite and covellite postdating chalcopyrite and bornite are only associated with this alteration assemblage, and are locally abundant (>50% of sulfides) (figure 5.33). Sericite-quartz-carbonate alteration overprints all generations and types of dykes, including the latest augite porphyry dykes (figure 5.34).

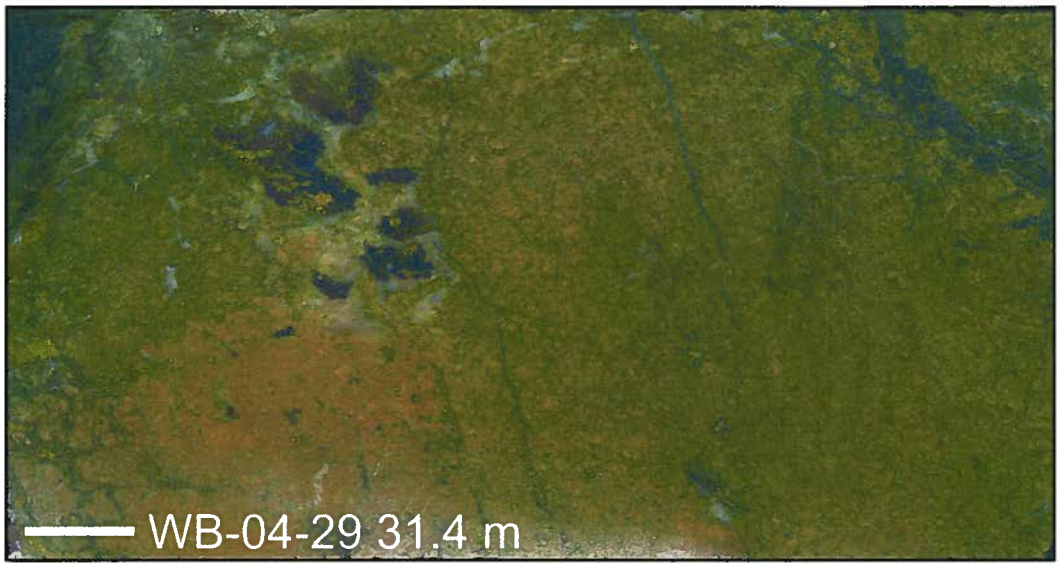

Figure 5.32-Chalcocite replacing chalcopyrite in a zone of sericite alteration (hand sample).

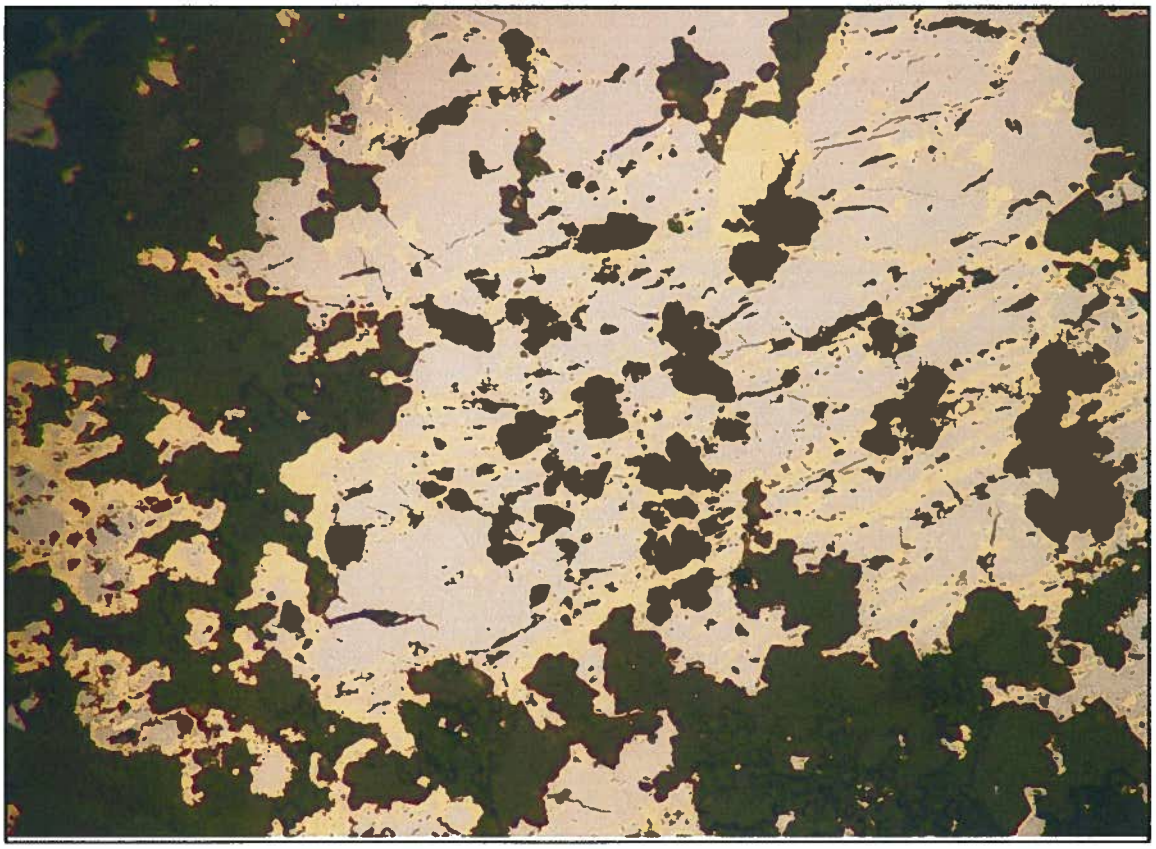

Figure 5.33-Chalcopyrite (lavender) replacing chalcopyrite (yellow) in a zone of sericite alteration (reflected light photomicrograph). FOV equals 2.5 mm.

Figure 5.34-Sericite alteration overprinting an augite porphyry dyke. Cream-colored vein at the right of the image is quartz; white vein at the center of the image is calcite.

Carbonate-gypsum-(clinozoisite-zeolite)

In Section 18, all rock types are overprinted with a network of carbonate-gypsum veins. Veins are ubiquitous in Section 18 but scarce in Section 29. Veins are composed of white calcite, gypsum, pale pink carbonate, cryptocrystalline grey clinozoisite, and salmon-pink zeolite (figure 5.35) (Ross, 2004). These minerals form vein breccias, mosaic and rotated breccias with carbonate infill around clasts of other rocks types, including sulfides (figure 5.36). Carbonate veins commonly have bladed textures indicative of boiling (figure 5.37). The bladed carbonate veins are exclusively post-sulfide.

Figure 5.35-Quartz-carbonate-zeolite vein exploiting sulfide-infilled breccia textures. WB-04-29, 33m. Scale bar equals 1 cm.

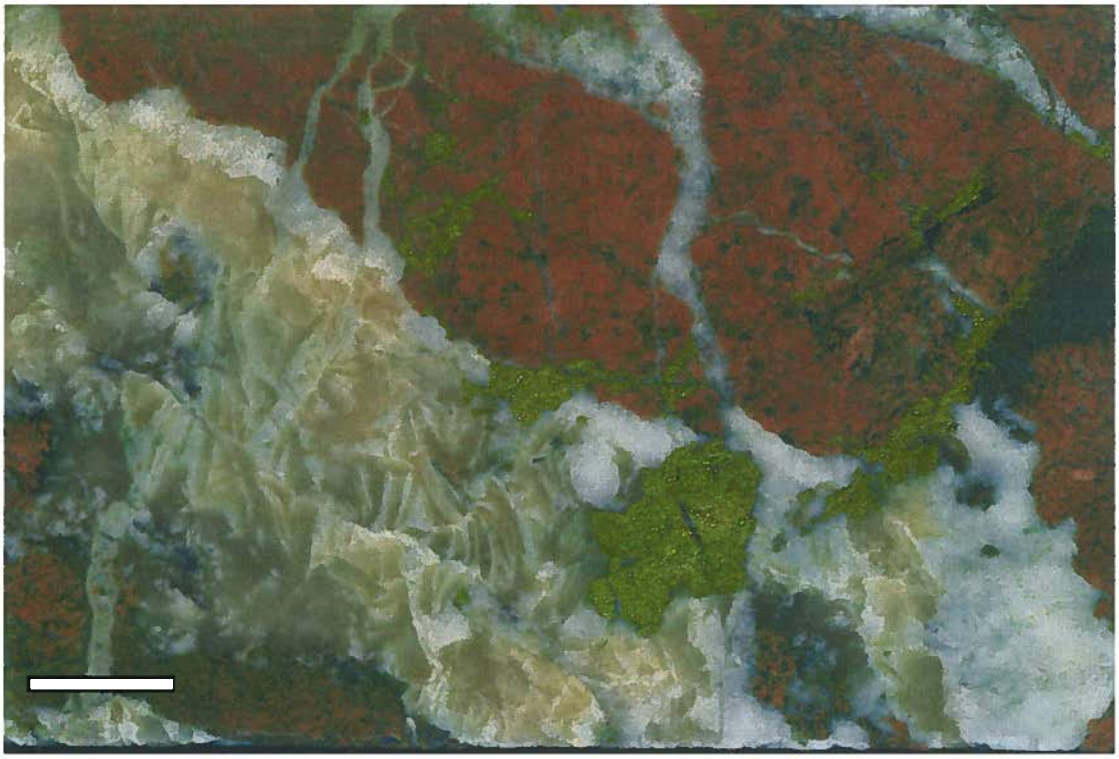

Figure 5.36-Chalcopyrite clast in a late carbonate-gypsum zeolite vein. WB-04-29, 198 m; Scale bar equals 1 cm.

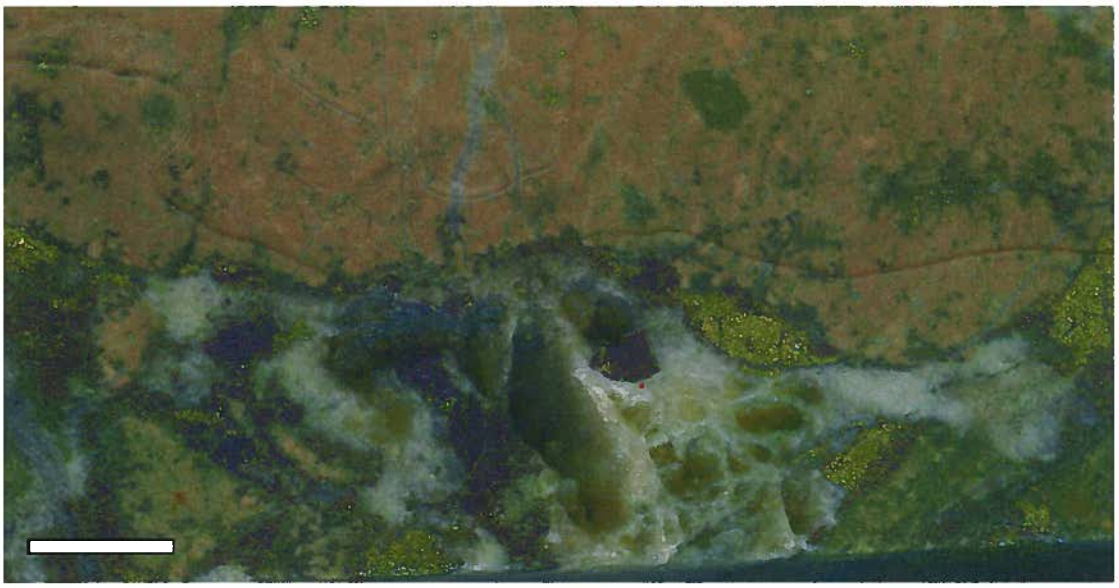

Figure 5.37-Bladed textures in post-sulfide chalcedony. WB-04-29, 33m. Scale bar equals 1 cm.

Sequence of alteration, brecciation, and intrusion

Alteration, brecciation, and intrusion establish a sequence of events recording both the physical and chemical evolution of the Northeast Zone hydrothermal system (figure 5.38). Hematite-carbonate alteration pervasively altered the monzonite before the intrusion of the megacrystic monzonite porphyry. The alteration may be related to the first pulse of fluid coming off the mineralizing intrusion. The hematite dusting and the carbonate blebs suggest that this fluid was oxidizing, near-neutral, and possibly CO_2-rich.

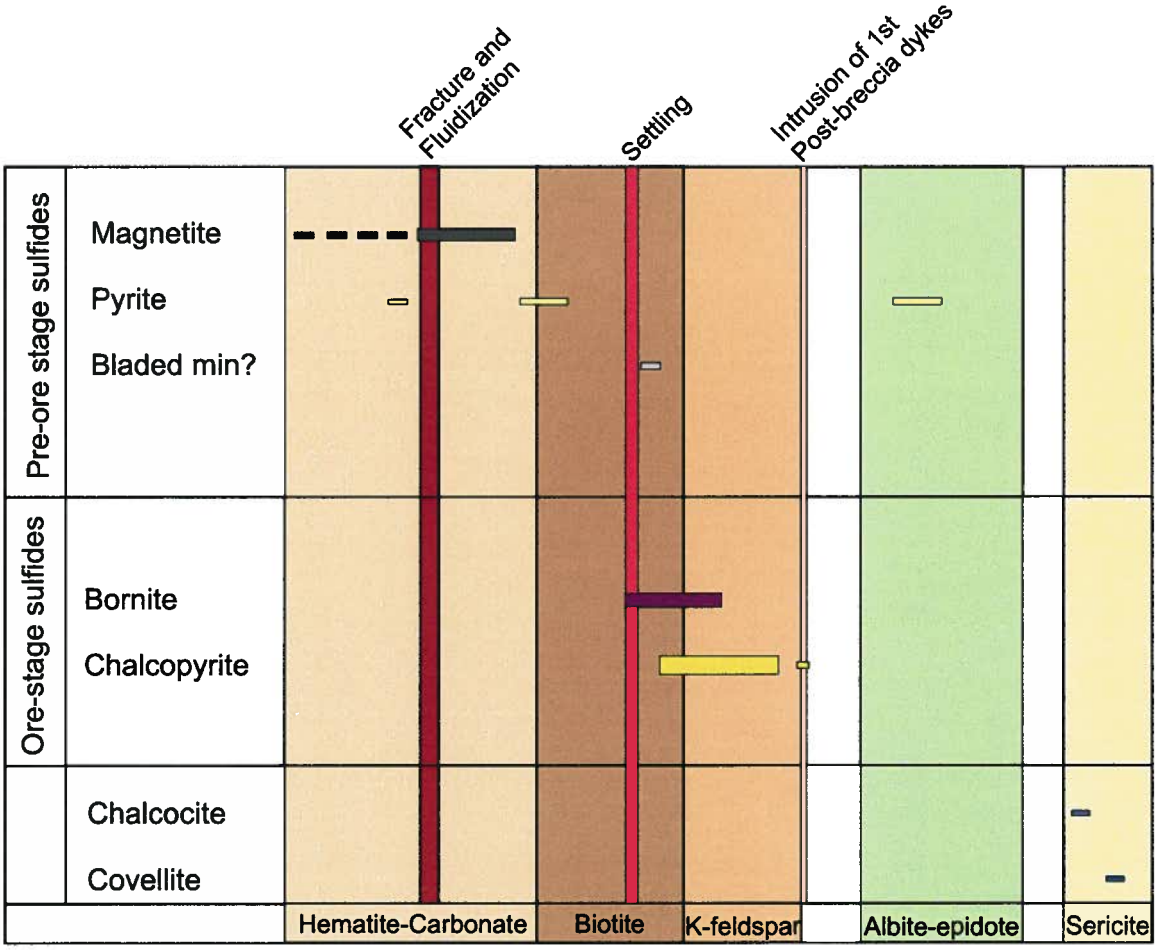

Figure 5.38-Paragenesis of mineralization and alteration relative to brecciation and intrusion in the Northeast zone at Mount Polley.

The alteration that followed, during and immediately after fragmentation, was more complex, involving a temperature-dependent zonal arrangement of chlorite, biotite,

actinolite-albite, and magnetite alteration. Chlorite alteration was the most distal alteration assemblage, forming high and peripheral within the system. Biotite alteration formed at slightly deeper depths and higher temperatures. Magnetite alteration formed at higher temperatures still, deeper in the system and proximal to the zone of highest fluid flux. This area of highest fluid flux also controlled the location of the actinolite breccia. The relationship between the magnetite alteration and the zone of fine-grained breccia are two expressions of the same phenomenon, a local area in which the most direct corridor was available between high and low hydraulic potential, between the origin and the destination of hydrothermal fluids. Due to the high fluid flux through this area, this particular pipe-within-the-pipe had a direct corridor to magmatic temperatures, hence the high temperature alteration assemblages localized along this zone.

As this initial fluid flux waned, the grain size segregation developed during breccia fluidization established permeability contrast within the breccia. Later fluids infiltrating this quiescent bed deposited K-feldspar which overlapped with the last stages of fluidization. This timing explains the existence of both K-feldspar rimmed clasts and of K-feldspar as breccia infill and overprinting the breccia. Concentration of sulfide minerals immediately above the K-feldspar flooding suggests that the two may be tied to the same evolving fluid, and that after K-feldspar had been deposited, the resulting fluids were oversaturated with respect to sulfides. Sulfides were deposited in the available open space within the most permeable breccias. Permeability control on sulfide deposition suggests that the breccia was not well consolidated at the time of mineralization. The sulfide mineralization is thus late, but still syn-breccia.

The relationship between sulfides and the gangue minerals associated with them is unclear. Anhydrite seems to be related to the zone between the K-feldspar flooding and biotite alteration, and may be related to the actual mineralizing fluids. Apatite and possibly garnet appear to be syn-sulfide. Other gangue minerals associated with the sulfide, notably magnetite, which appears to be pre-sulfide, and carbonate, which is post-sulfide, are not related to the sulfide depositing fluids.

Sealing of the system by sulfide deposition apparently resulted in, to a limited extent at least, repressurization of the system. Thus, the last of the sulfide mineralization achieved enough pressure to exceed the lithostatic pressure and form veins rather simply exploiting pre-existing open space. These veins post-date and cut the first generation of breccia-cutting dykes.

At sometime after this last generation of copper sulfides, the system experienced a lower temperature, 'retrograde' alteration event, which resulted in the Cu-sulfide destructive, deep albite-epidote overprint at the base of Section 29. This alteration assemblage shows all the hallmarks of a deep propylitic overprint on a waning system (Guilbert and Park, 1980), possibly related to the influx of meteoric fluids as the hydrothermal system waned and fluid flow collapsed back in on itself. Albite, epidote, and pyrite replaced K-feldspar, Fe- and Mg-bearing minerals, magnetite, and chalcopyrite.

The sericite-quartz-carbonate alteration is the product of conversion of K-feldspar to sericite and silica in response to acidic solutions (Barnes, 1997). The high neutralization capacity of the monzonite host rocks restricted the visible effects of alteration by acidic fluids to areas immediately adjacent to faults.

The alteration assemblages and zoning observed at Mount Polley are similar to those observed in other alkalic porphyry systems (Holliday and Cooke, 2007; Cooke et al., 2006; Deyell and Tosdal, 2005; Frei, 1995; Heithersay and Walshe, 1995; Lang et al., 1995a and b). The presence of sericite alteration suggests that the Northeast zone may represent a comparatively shallow portion of the hydrothermal system.

Chapter 6-Evolution of the Northeast Zone Breccia

Discussion

The genesis of the Mount Polley deposit, for purposes of this study, began with the intrusion of the Mount Polley Intrusive complex into the rocks of Nicola Volcanic Group. The Mount Polley intrusive complex does not differ greatly from trends expressed in the igneous evolution of the host volcanic arc. Instead, the Mount Polley Intrusive complex represents a further development in the overall evolution of the volcanic sequence into which it intruded (Logan and Bath, 2006). Logan and Bath (2006) and Logan et al. (2007) suggest that the Mount Polley intrusive complex may have formed quite high within or subjacent to a volcanic edifice. The similarities between the intrusive and extrusive rocks may support this hypothesis, although a simpler explanation may be that the intrusive and extrusive systems simply tapped the same crustal magmatic reservoirs.

In the Northeast zone, magmatic evolution continued with the intrusion of the megacrystic monzonite porphyry. The megacrystic monzonite porphyry represents a deviation in the physical, though not the chemical, evolution of the igneous system. Rather than fine-grained, relative equigranular textures indicative of relatively short super-solidus residence time, the extreme grain size contrast between phenocrysts and groundmass indicate extended storage at supersolidus temperatures (McLeod and Tait, 1999; Blake, 1984; Higgins, 1999; Cabane et al., 2001; Eberl, 2002; Higgins and Roberge, 2003).

The extended super-solidus residence time of the megacrystic magma resulted directly in the accumulation of fluids in the magma chamber presumably subjacent to the

dykes (Lickfold, 2002; Dilles and Einaudi, 1992; Burnham, 1985; Manning and Prichavant, 1984; Marsh, 1982 and 2000). The megacrystic dykes are inferred to represent the uppermost apophyses of a larger plutonic body at depth (Marsh, 1082, 1996, and 2000; McLeod and Tait, 1999). If the cores of the dykes were held as plastic, permeable crystal mush, they provide a favorable conduit for collecting or focusing fluids evolving off the underlying body by second boiling (Michioka and Sumita, 2005; Lange, 1994). The multi-stage intrusive complex preceding the intrusion of the megacrystic dykes probably aided in preheating and rheologically homogenizing the rockmass into which the dykes intruded (Belcher and Kisters, 2006).

This accumulation of fluids probably had a positive feedback relationship with the supersolidus cores of the dykes. Fluids were able to infiltrate because the crystal mush was plastic and permeable, and the presence of abundant fluid, and of direct hydraulic conductivity to the higher temperatures at depth, kept the interiors of dykes as crystal mush (Marsh, 1996; Eggleton, 1979). As fluid accumulated into the fluid-saturated zone under the chilled margin of the dyke, it formed horizontal lenses within the plastic interior of the dyke (Fournier, 1999; Marsh, 1996). These lenses propagated until they extended from the interior rheological limit of the dyke, the limit of where the material was rigid enough to sustain a fracture at the strain rate controlled by the rate of fluid influx, to the exterior limit where the dyke was too rigid to be fractured under the available overpressure (Hubbert and Willis, 1957).

The limits of the fluid lenses were controlled by a combination of crystal mush physical properties, fluid overpressure, and strain rate (Bertram and Kalthoff, 2003; Fournier, 1999; Brisbin, 1986). The vertical expansion of the fluid lenses is limited by the

same factors, but once the horizontal expansion limits of the fluid lens is reached, overpressure resulting from continued fluid input is released through the development of fractures (Li et al., 2002; Carrington, 1998; Clemens and Mawer, 1992). These fractures would link fluid-filled lenses at different topographic levels within the intrusion, possibly over a vertical extent of a kilometer or more (Gustafson and Hunt, 1975; Dilles and Einaudi, 1992; Lickfold, 2002; Sillitoe, 1973). This would result in significant hydraulic pressure in the upper reaches of the system. Alternatively, the fluid lenses could be linked or overpressured as the result of a tectonic event (Husen et al., 2006; Roman, 2005; Linde et al., 1994; Rubin, 1993 and 1995; Segall, 1984 a and b).

Through whatever process, fluids accumulated within the carapace of the megacrystic monzonite dykes until an overpressure was developed. This overpressure exceeded both the lithostatic pressure exerted by the overlying rock and the tensile strength of the dyke carapace (Li et al., 2002). The fluid overpressure at the apex of the dyke complex resulted in a cone of fracture that propagated upward from its original base and downward from its original apex, in a manner analogous to the development of diatremes (Skewes et al., 2002; Cannell et al., 2005; Lorenz, 1986, 2003 a and b; Lorenz and Kurszlaukis, S. 2006; Yakovlev, 1980).

Where overpressure exceeds the sum of the lithostatic load and the tensile strength of the rock, fractures can form and propagate (Passchier and Trouw, 2005; Li, et al., 2002). Energy is expended in the creation of new surface area (fracture propagation) (Cummins and Given, 1973; Hubbert and Willis, 1957). If these fractures are sufficiently closely spaced and accompanied by volume loss in the system, they come to define breccia clasts (Laznicka, 1988). In order for the breccia body to propagate upward,

continued energy input at least equal to the energy expended in surface area creation and transport of fragments is required to continue upward propagation of the breccia body (Vyazmensky et al., 2008; Laubscher, 2000; Suppe, 1995).

Mathematical model for breccia propagation

In constructing a simple mathematical model for breccia propagation, certain base assumptions must be made. The stress regime at the point of breccia initiation is treated here as axial. This assumption is reasonable for hydrothermal breccias formed in the shallow crust within fairly isotropic country rocks (Belcher and Kisters, 2006; Richards, 2003; Bergantz, 1991). Given these assumptions, the growing breccia can be modeled as a cone, with its axis normal to σ^3 and its apex at the point of initial rupture (figure 6.1a).

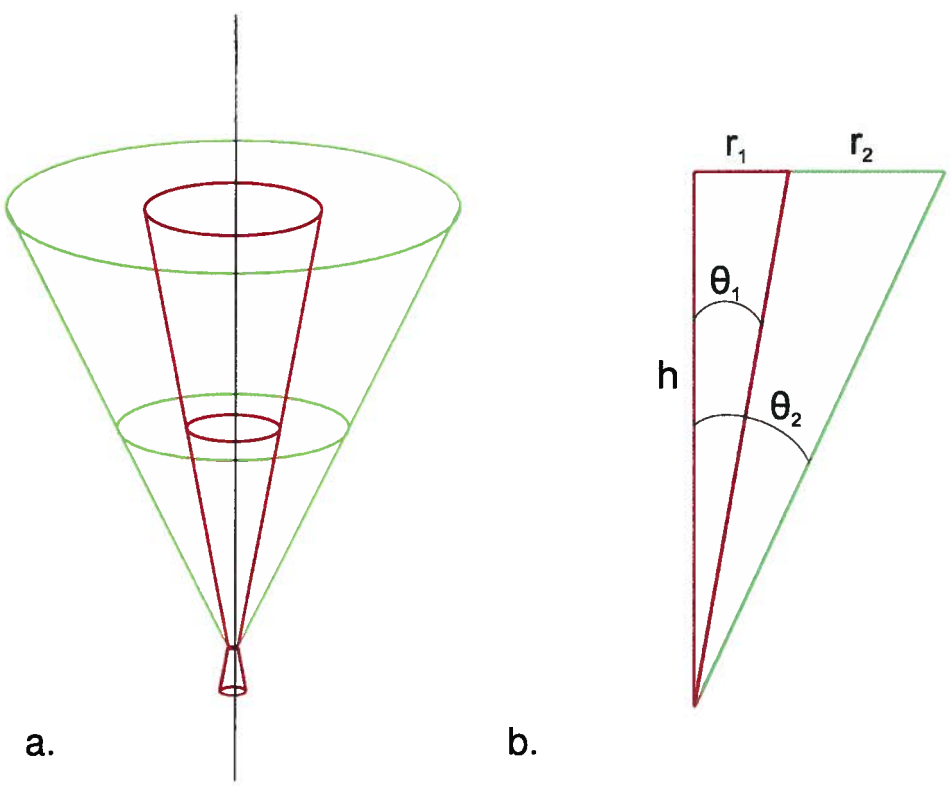

Figure 6.1-Geometeric model for breccia propagation. a: Cone-in cone damage cone (green) and shatter cone (red) geometry. b: Triangular damage zone and shatter zone cross-section.

The model breccia body is composed of two nested cones with coplanar bases and a common apex; the central cone is arbitrarily defined as the zone within which fracture density is great enough for rotation and movement of clasts (the shattered zone), and the outer cone is defined by the outward extent of fracture propagation (the fracture cone). The cones can be modeled as two right triangles rotated around a common side (h); the angle between the height of the breccia cone (h) and the hypotenuse of the triangle is expressed as θ_1 for the inner cone and θ_2 for the outer cone. The radius of the base of the cone is expressed as r_1 for the inner cone, and r_2 for the outer cone (figure 6.1b).

The total volume of the breccia body for a given height can be expressed as the volume of the outer cone:

$$V_t=1/3\pi((\tan \theta_2)h)^2*h$$

The volume of the shattered area within the breccia body for a given height can be expressed as the volume of the inner cone:

$$V_1=1/3\pi((\tan \theta_1)h)^2*h$$

The volume of the fractured but not shattered area can be expressed as:

$$V_2=1/3\pi((\tan \theta_2)h)^2*h-1/3\pi((\tan \theta_1)h)^2*h$$

Thus the incremental increase in volume of the breccia body for an incremental increase in height increases with the increasing height of the breccia (figure 6.2).

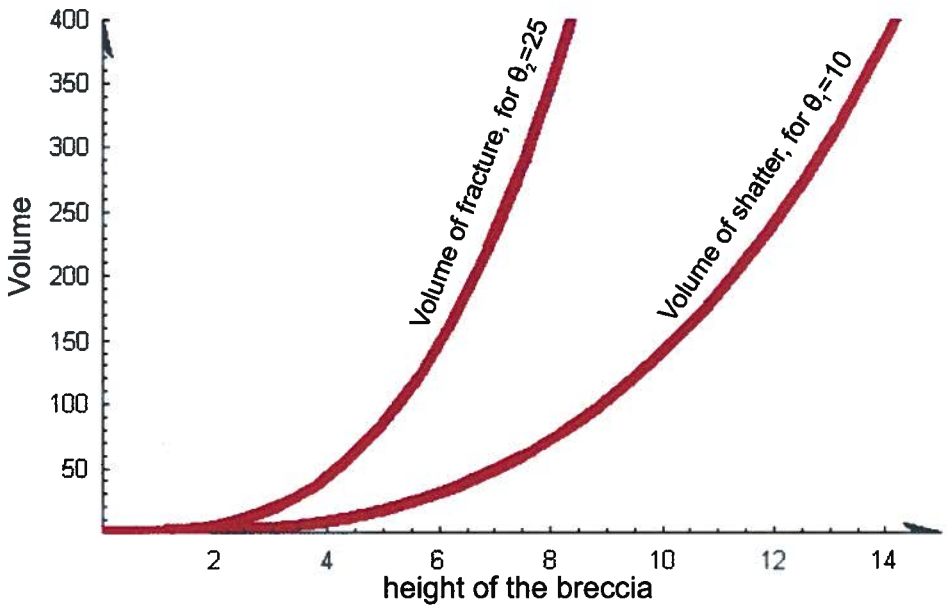

Figure 6.2-Breccia volume as a function of breccia cone height. The graph is unitless due to the fractal nature of the processes involved.

This can be considered as the derivative of the above functions (figure 6.3):

$$V_1' = \pi(\tan\theta_1)^{2*}h^2$$

$$V_2' = \pi(\tan\theta_2)^{2*}h^2 - \pi(\tan\theta_1)^{2*}h^2$$

$$V_t' = \pi(\tan\theta_2)^{2*}h^2$$

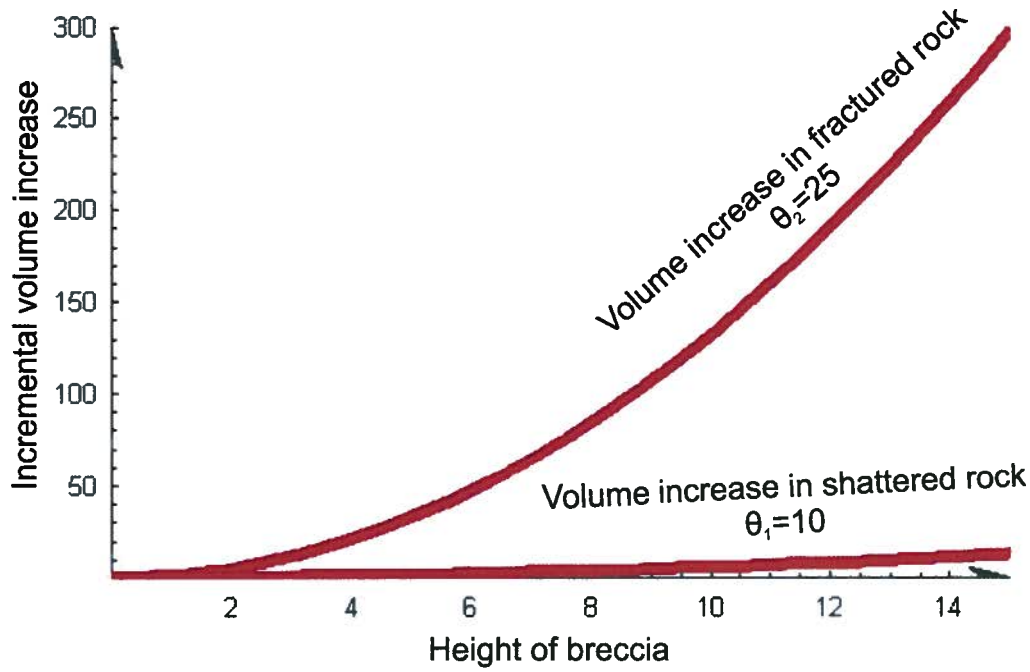

Figure 6.3-Incremental increase in breccia volume per unit height increase.

The energy required to increase the height of the breccia is proportional to the volume of rock that must be broken for each incremental increase in height, so the energy required in order to continue upward growth of the breccia (E_n) can be expressed as:

$$E_n = (E_1 - E_2)(\pi(\tan\theta_1)^{2*}h^2) + (E_2)(\pi(\tan\theta_2)^{2*}h^2)$$

Where E_1 is the energy input needed to shatter the country rock and E_2 is the energy input needed to fracture the rock. This equation assumes that fracturing precedes shattering. If the growth of the breccia is assumed to be constant at some rate g ($\Delta h/t$), then the energy input over time required to continue breccia growth can be expressed as:

$$E_n = (E_1 - E_2)(\pi(\tan\theta_1)^{2*}(g*t)^2) + (E_2)(\pi(\tan\theta_2)^{2*}(g*t)^2)$$

Energy input into the breccia system comes from a variety of sources: continuing upward fluid flux from the parent intrusion (Burnham, 1985), expansion of the fluid with decreasing pressure (Li et al., 2002), fluid phase changes such as exsolution of CO_2 or boiling (Wiebe, 1996; Burnham, 1985; Burnham, 1979b; White et al., 1971), gravity (Vyazmensky et al., 2007; Ross, 2002; Laznicka, 1988), or tectonic rupture (Manga and Brodsky, 2006; Linde et al., 1994). Energy is consumed by the creation of new surface area (fracturing and shattering) (Swanson, 1984; Cummins and Given, 1973; Hubbert and Willis, 1957), friction between fragments (Yang et al., 2007), between fluids and fragments, and between fluids, fragments, and the country rock, heat loss via conduction and convection, fluid escape into the host rocks, and fluid contraction with decreasing temperature (Secor, 1965). The energy inputs into the system are difficult to quantify, but finite; for purposes of this exercise they can be approximated by the arbitrary expression:

$$E_a=-4t^2+20t+50$$

E_a is the total energy available to fracture rock; where $E_a<E_n$, the energy available to fracture the rock is no longer sufficient to maintain the same rate of growth in breccia volume. As σ^3 is assumed to be far less than σ^2 or σ^1, and σ^2 and σ^1 are assumed to be approximately equal, then growth of the breccia radius will decrease while growth in breccia height remains the same, producing a decrease in the radius of the breccia body with height (figure 6.4), or a decrease in fracture density until the fractured rock mass is no longer a breccia (Norton and Cathles, 1973; Sillitoe, 1985; Ensign Bushnell, 1988). In

either case, where the tops of hydrothermal-magmatic breccias are undisturbed, they are commonly domal (Sillitoe, 1985; Norman and Sawkins, 1985; Wenrich, 1985).

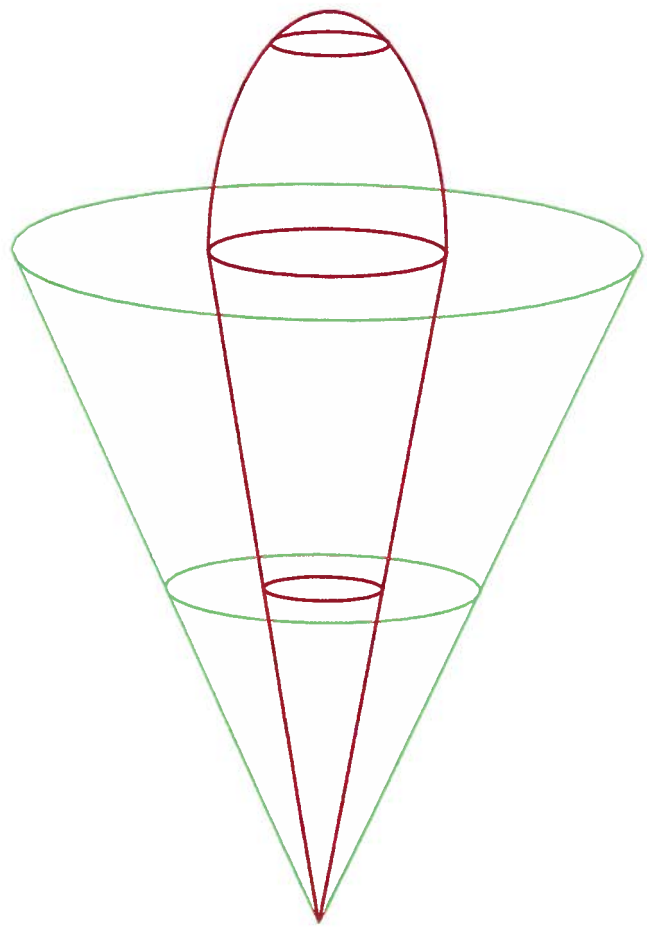

Figure 6.4-Decreasing breccia radius with increasing height.

E_n as expressed above is graphed against E_a, with g =1, E_1 =2, E_2=1, θ_1= 10, and θ_2=25 (figure 6.5). Values for g, E_1, and E_2 were chosen in order to simplify the mathematics of the system; θ_1 and θ_2 were based on observational evidence from breccia bodies (Sillitoe, 1985; Norton and Cathles, 1973; Bushnell, 1988) and analogous processes related to block-cave mining (Vyazmensky et al., 2007; Gilbride et al., 2005;

Laubscher, 2000; Cummins and Given, 1973). If g is equal to 1, then the ordinate axis of the graph (figure 6.5) is valid as both time and height of the breccia from point of origin.

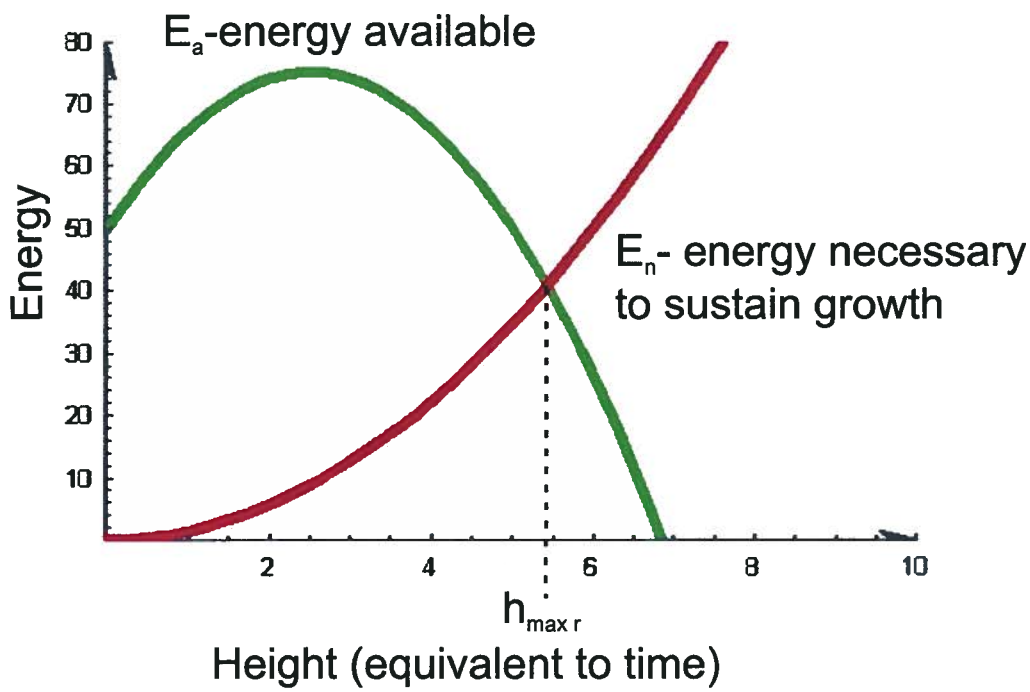

Figure 6.5-Energy necessary to continue breccia growth versus energy available.

Volumetric growth of the breccia is based on the assumption that energy input is proportional to increase in breccia volume. At the intersection of E_a and E_n, the radius of the breccia is at its maximum and begins to decrease. Because the instantaneous energy required to form breccia volume is a function of the derivative of breccia volume, it is proportionate to breccia radius; the rate of decrease of breccia radius is proportional to the derivative of function E_a:

$$E_a' = -8t + 20 \text{ or}$$

$$E_a' = -8h + 20$$

If $h_{max\ r}$ is the height of the breccia at the time when $E_a=E_n$, then maximum radius of the breccia would be:

$$R_1=\tan\theta_1 * h_{max\ r}$$

$$R_2=\tan\theta_2 * h_{max\ r}$$

Because E_a expresses the total amount of energy available to fracture the rock, and the amount of energy required to fracture a given volume of rock is less than that necessary to shatter the same volume of rock, R_1 and R_2 will not decrease at the same rate after the breccia has reached $h_{max\ r}$. Instead, R_1 will be greater than 0 only as long as E_a is greater than E_2; E_{a1}, or the energy available to shatter the rock, is equal to E_a-E_2. If $E_{a1}<0$, and $E_a > 0$, the fractured zone will continue to propagate upward, but without the central shattered zone. This would produce a fractured zone (Norton and Cathles, 1973) or even a single fluid escape structure such as those observed at the Cananea deposit (Bushnell, 1988).

The radius of the breccia body is actually one possible expression of decreasing E_a. E_a is the energy available to fracture the rock, and this energy is dominantly expended via the formation of new surface area (Cummins and Given, 1973). The decreasing availability of energy to create new surface can be manifested either as the creation of new surfaces at the same fracture density over a decreasing volume of rock, or as more widely spaced fractures (larger clast sizes). Identifying wider fracture spacing at the original top of the breccia body can be complicated by post-fracturing processes. If sufficient volume increase occurs that the breccia mass can flow, large clasts originally at the top of the mass could fall through the smaller clasts below, reversing the original

grading of the body (Mukherjee and Mishra, 2007; Bryant, 1968). In the absence of reliable stratigraphy, as at Mount Polley, this would be difficult recognize, but the abundant outsize clasts recognized at depth in Section 29 may reflect this process.

The decrease in available energy can come from a variety of sources. Upward fluid flux from the magma chamber at depth can diminish (Burham, 1985), volume loss via thermal loss from the fluid to the surrounding rock can exceed volume gain via depressurization, or a short-lived pulse of upward fluid movement from a seismic event can be exhausted (Manga and Brodsky, 2006). Fluid flux from the magma chamber is dependent on the cooling rate of the pluton (Candela, 1989; Burnham, 1979), and also on the availability of a conduit to focus that fluid into the base of the breccia (Lorenz, 2006). Spot depressurization at the point of origin of the breccia can result in a decompression quench of melt, effectively "corking" the breccia from below (Lorenz, 2006; Sillitoe, 1985). Note that the upward fluid flux into the breccia need not stop or even decrease in order to no longer propagate the breccia "cone"; E_a must simply stop increasing as rapidly as E_n. The presence of hydrothermal minerals as cement in breccias is ample evidence that fluid flux continues after the movement of clasts within the breccia has ceased (Davies, 2002; Hedenquist and Henley, 1985).

Rheological anisotropy in the host rock to the breccia also causes changes in E_n (Vyazmensky et al., 2007; Belcher and Kisters, 2006). If the growing breccia cone intercepts a body of rock of significantly higher tensile strength than the general country rock, the net effect on the breccia propagation would be equal to the effect of a proportionate decrease in E_a. If the zone of high tensile strength rock is limited, for example by a sill or a sedimentary rock unit, the breccia may pinch at that point and swell

above it, with the radius of the breccia decreasing proportionately to the E_n required to fracture the high strength rock unit (Sillitoe, 1985; Bryant, 1968). This constriction would induce changes in the fluid flow past that point, increasing fluid velocity while decreasing fluid pressure (Lamb, 1953); this in turn would affect fluid flow, clast transport, and mixing above and below the constriction (Lamb, 1953; McCallum, 1985; Yang et al., 2007; Mukherjee and Mishra, 2006).

Fluid flux and breccia formation

Within the pervasively fractured rock mass, some anisotropy is expected (Vyazmensky, et al., 2007). Pre-breccia joints and fractures result in zones of increased fracture density. Even though the breccia body may no longer grow, the fluid influx may not decline, let alone cease (Sillitoe, 1985). The kinetic energy of the fluid flux is simply no longer expended through the creation of new surface area (Norton and Cathles, 1973).

If the upward fluid flux exceeds the settling velocity of the 'clasts', and sufficient void space is available for clasts to move around each other, a fluidized bed state may be achieved (Mukherjee and Mishra, 2007). The most compelling evidence for the development of a fluidized bed state in the Northeast zone breccia is the thorough mixing of the megacrystic monzonite porphyry clasts with country rock monzonite in the breccia. The fine-grained breccia body is also a likely result of channelized fluidization adjacent to the zone of highest fluid flux (as indicated by the presence of actinolite and magnetite in the center of the fine-grained zone) (McCallum, 1985; Yang et al., 2007; Link et al., 2006). An alternative explanation for the fine grained breccia might be the presence of a pre-breccia zone of increased fracturing and jointing which was fractured more densely by brecciation processes than the surrounding rock mass (Sillitoe, 1985). Fluid flux

would vary across the diameter of the pipe (Gonnermann and Manga, 2003; Lamb, 1953). The perimeter facies of fractured to minimally rotated country rock on the Northeast zone breccia body reflect the lowest fluid velocity portions of the conduit (Kennedy et al., 2005; Boone et al., 1986).

At any given point within the breccia pipe, fluid flux would vary over time (figure 6.6) (Sillitoe, 1985). The time axis shown here is deliberately parameterless, given the uncertainty of the lifespan of the magmatic-hydrothermal systems (Schardt et al., 2005; Paterson and Tobisch, 1992; Titley and Beane, 1981). The highest fluid flux would occur early in the development of the breccia body, but the majority of the fluid volume would be introduced later (Sillitoe, 1985). Time zero represents the point in time at which hydrostatic pressure exceeds lithostatic pressure (Li et al., 2002). At time one, fractures have propagated to the point where they are hydraulically contiguous and a fluid flux is established (Sillitoe, 1985; Atkinson, 1987; Anderson, 1991; Li et al., 2002; Bertram and Kalthoff, 2003). As fluid flux continues to rise and the three dimensional fracture array continues to develop, fragments within the fractured rock mass become discretized (Whittles et al., 2006; Boone et al., 1986). At some point, the fluid velocity of the rising fluid flux exceeds the settling velocity of these particles (Richardson and Zaki, 1954; McCallum, 1985; Mukherjee and Mishra, 2007). Time two represents the point at which fluid flow ceases to be controlled by fractures, and particle movement begins to be dominated by fluid movement, entering a fluidized bed state.

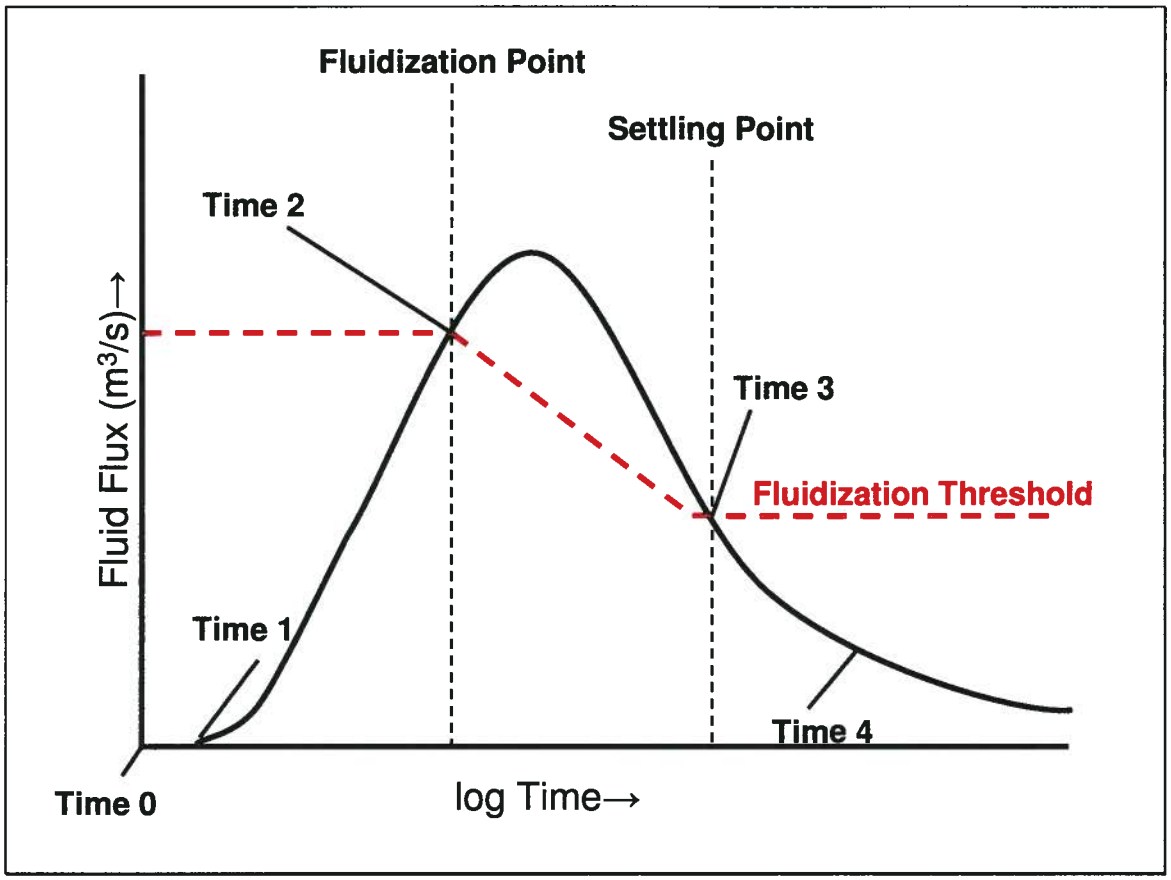

Figure 6.6-Fluid flux at a given point within the brecia pipe over time. Time 0: Initiaition of fracture. Time 1: fractures become hydraulically contiguous. Time 2; Upward fluid flux exceeds particle settling velocity. Time 3; Particle settling velocity exceeds upward fluid flux. Time 4; Fluid flux continues through settled particle bed. Between time 0 and time 1 no fluid through-flow is possible; between time 1 and time 2, clasts control the movement of fluids. Between time 2 and time 3, fluids control the movement of clasts, and after time 3 clasts again control the movement of fluids.

The existence of a fluidized bed state in the Northeast Zone is indicated by the mixing of megacrystic and country rock clasts in the bulk of the breccia body. This fluidized bed state was most likely short-lived (Paterson and Tobisch, 1992; McCallum, 1985). Time three represents the point at which the diminishing fluid flux falls back through the settling velocity of the particle bed (Swanson, 1999 and 1989). This fluidization threshold drops during the fluidized bed state for two reasons. First, mutual impact and abrasion between clasts reduce average clast size, which decreases clast settling velocity (Scala et al., 1997; Lamb, 1953). Second, the material removed from the

clasts in the course of clast size reduction becomes part of the fluid phase (He and Forssberg, 2007a and b; Scala et al., 1997). This increases the density of the fluid phase, also decreasing particle settling velocity (He and Forssberg, 2007a and b). The presence of clastic infill and rounded clasts in the Northeast zone supports this hypothesis. The fine-grained, clastic-infill dominated portion of the breccia body probably represents the zone of highest fluid flux, and thus highest comminution (Yang et al., 2007; He and Forssberg, 2007b; McCallum, 1985). Fines generated by comminution in other portions of breccia may also have been stripped out and concentrated in the zone of highest fluid flux, explaining why in most portions of the Northeast Zone breccia, not enough fines are present to account for the rounding of the clasts (Powell and Morrison, 2007; Eisenmann, 2001; Heiskanen, 1993).

The dependence of fluidization state on clast size would lend itself to the stripping and concentration of fines. Fines would stay in suspension at lower fluid fluxes than coarser clasts, moving upward and inward within the breccia pipe (Mukherjee and Mishra, 2007; Rasul et al., 2000).

Fluid Flux and Fluid Chemistry

The fluid flux would peak, and then decline over an extended period of time as the underlying plutonic body cools and crystallizes (White, 1981). As the fluid flux wanes, the fluid chemistry would change as well (Barnes, 1997). Because the initial and peak fluid flux was not saturated with respect to any mineral, the fluid is not preserved as fluid or melt inclusions (Hedenquist and Lowenstern, 1994). In terms of alteration, it may have been the fluid responsible for the hematite-carbonate alteration. Post-peak fluid flux, during the declining period of the fluidized bed state, was responsible for the syn-breccia

biotite, chlorite, and magnetite alteration; the syn-breccia alteration which was not controlled by the permeability regimes established during post-fluidization settling.

Post-settling, ongoing fluid flux was responsible for K-feldspar flooding, the deposition of sulfides, and the destruction of magnetite by sulfide-stable fluids. This transition indicates the increase in K+ fugacity, S fugacity, and metals, and decrease in iron fugacity (Guilbert and Park, 1980).

Bornite is present in proximity to the highest concentration of megacrystic clasts and to the contact between biotite and K-feldspar alteration. These two areas reflect zones of high temperature, and zones of proximity to the dykes which initiated brecciation and focused fluid flow from the pluton beneath. Gold and silver are concentrated with bornite, reflecting the solubility of these metals in bornite (Simon et al., 2000; Makovicky et al., 1995). Sulfide mineralization, reflecting its post-settling deposition, exploited the most permeable zones within the breccia.

After the deposition of the sulfides, albite, epidote, and pyrite indicate a lower temperature, retro-grade propyllitic alteration phase (Barnes, 1997; Guilbert and Park, 1980).

Vectors to ore

Two main primary (pre-sulfide) controls on ore depositions were observed at Mount Polley. First, ore grade was higher in the vicinity of the highest concentration of megacrystic porphyry clasts. Within and above zones containing over 50% megacrystic clasts, bornite was most abundant, and Cu, Au, and Ag grades were higher than in adjacent, physically similar zones of breccia. The second primary control on

mineralization was the variation in permeability established within the breccia by fluidization processes. Where the breccia was most permeable, ore grade was highest. Secondary controls on ore grade include the intrusion of post-ore dykes and the effects of post-ore Cu-sulfide destructive alteration. Post-ore dykes substantially diluted the overall grade of the rock volume, especially in Section 29. The deep albite-epidote alteration event also diluted or destroyed grade at depth in Section 29.

Although attempting a structural reconstruction of the Northeast Zone is outside the scope of this work, the original mineralized volume of the Northeast zone is disrupted by at least three major faults (figure 6.7). Reconstructing the relative movements of these faults could indicate the locations of displaced portions of the breccia body at depth.

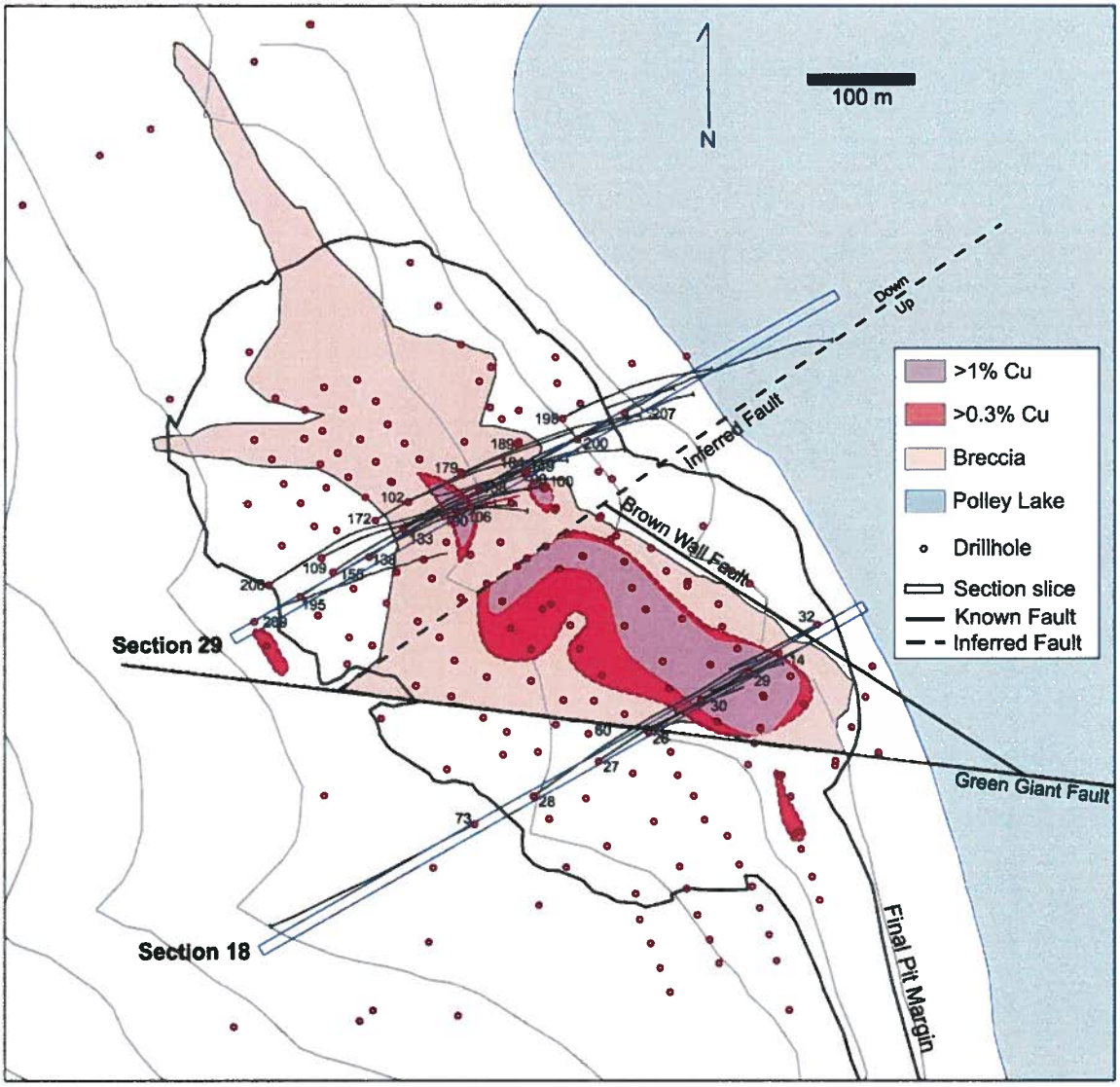

Figure 6.7- The Northeast Zone breccia and the faults that truncate it, the Green Giant, the Brown wall, and the inferred fault.

The fine-grained breccia unit presents some intriguing possibilities for further mineralization around the Northeast zone. If the fine-grained breccia body represents an originally central zone of spouting or channeling within the fluidized breccia body (Link et al., 2007), additional mineralization may be preserved, with favorable fault movement, to the northwest or west of the currently known body. Alternatively, the fine-grained breccia subunit may reflect more complex processes such as bubble trails within a three-

phase fluidized bed (Yang et al., 2007). In this case, the fine-grained unit may be considerably more irregular and off-center than would be expected as a result of two-phase fluidization (Yang et al., 2007). In any case, a better understanding of the nature and orientation of faulting related to the post-ore Northeast Zone structures might lead to recognizing additional volumes of mineralized breccia which originally surrounded the fine-grained breccia body. Additional volumes of mineralized breccia may also survive to the east and southeast, offset by the Brown Wall fault.

Sequence of Events

The sequence of events which resulted in the Mount Polley orebody as observed today began with the development of the Nicola volcanic arc sequence (figure 6.10a). The oldest rocks in this sequence were the most geochemically primitive, and younger units became progressively more differentiated. The Mount Polley intrusive complex intruded this sequence (figure 6.10b), beginning with the augite and K-feldspar bearing diorite units, and dominated by the undifferentiated monzonite units. These successive intrusions were increasingly differentiated, continuing the same trend observed in the volcanic sequence. A hydrothermal system may have developed following the intrusion of the K-feldspar bearing diorite and pre-dating the intrusion of the monzonite, as evidenced by veining observed in diorite xenoliths within monzonite. A hydrothermal system was definitely in existence pre-dating the intrusion of the megacrystic K-feldspar monzonite porphyry, as evidenced by pre-breccia vein networks in altered mafic clasts. The altered mafic clasts may reflect a pre-megacrystic monzonite porphyry sill which intruded the monzonite, a roof pendant, or a massive xenolith of pre-MPIC volcanic rock (figure 6.10c). The intrusion of the megacrystic K-feldspar porphyry post- dated the alteration of

this body; the small megacrystic dykes and bodies observed today are almost certainly the apophyses of a larger, deeper body which contributed the volume of fluid necessary for deposit-scale alteration (Burnham, 1985) (figure 10d).

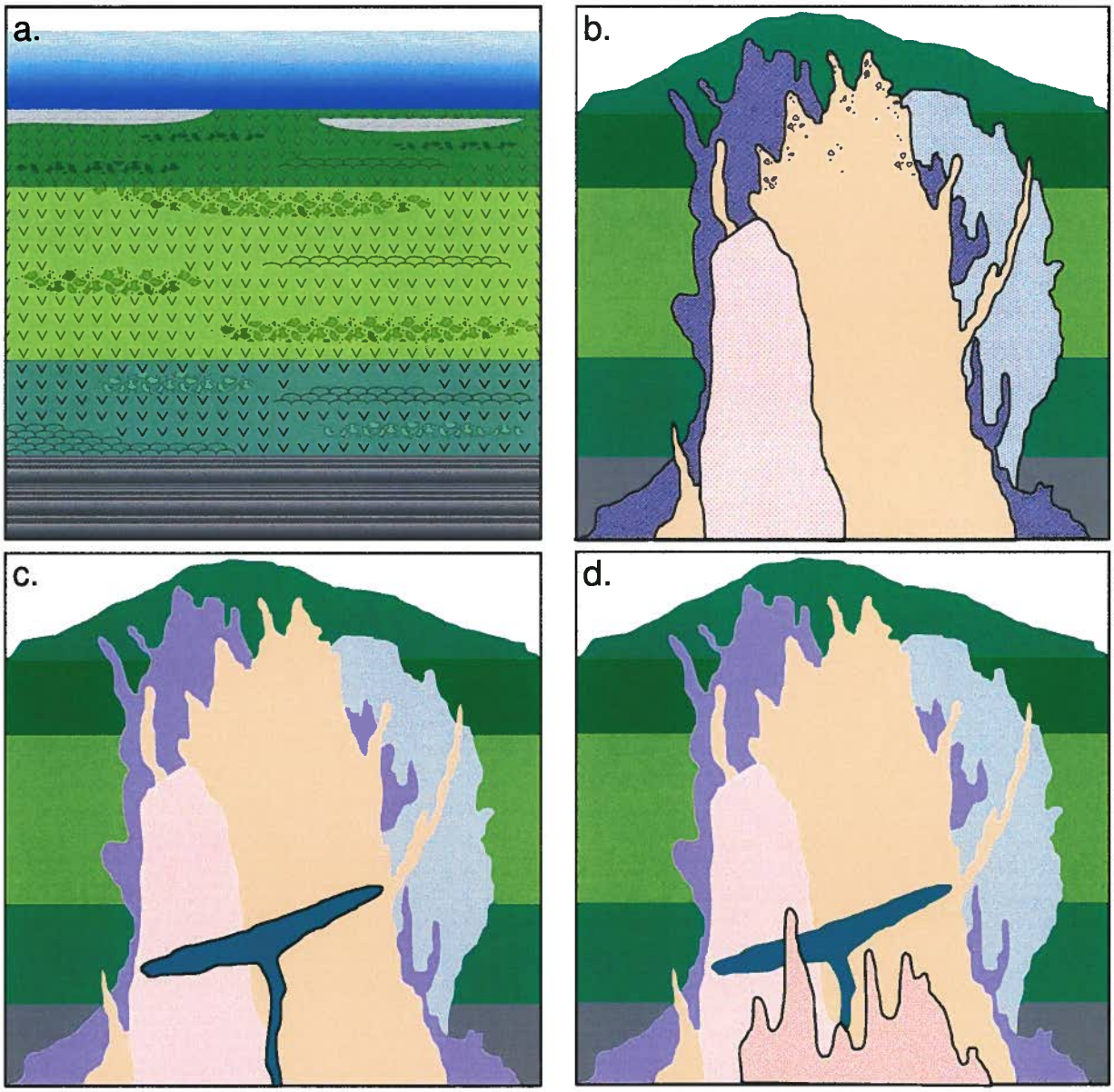

Figure 6.8-Sequences of events in the formation of the Northeast Zone at Mount Polley; a, deposition of the Nicola Group volcanic rocks. b; intrusion of the MPIC. C; intrusion (?) of the 'altered mafic' clast forming unit. d; intrusion of the K-feldspar megacrystic monzonite porphyry

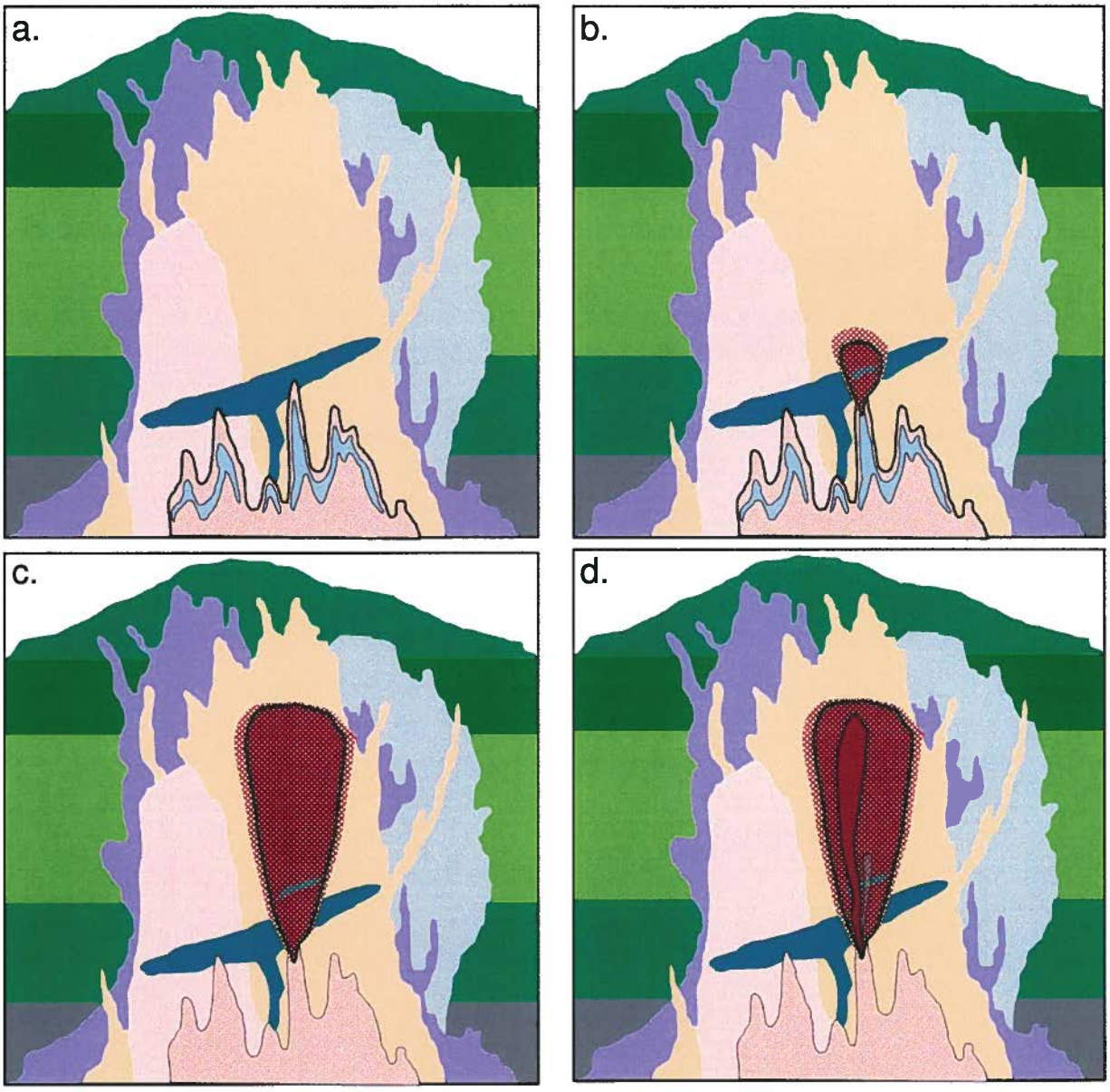

Figure 6. 9-Sequence of events in the formation of the Northeast Zone at Mount Polley; a; Accumulation of fluids witin and around the K-feldspar megacrystic porphyry dykes; b; overpressure of the fluid resulting in rupture and the initiation of breciation; c; formation of a particle bed; d; fluidization within the particle bed and magnetite deposition.

During and after the intrusion of the megacrystic K-feldspar monzonite porphyry, fluids accumulated within and around the still-plastic porphyry magma (figure 6.11a). These fluids became overpressured with respect to the lithostatic load, initiating brecciation (figure 6.11b). Brecciation proceeded upwards until the amount of energy available no longer exceeded the amount of energy necessary to continue growth of the body. The breccia body probably did not breach the surface, or even the top of the pluton (figure 6.11c). Mixing of clast types indicates that at least parts of the breccia passed through a fluidized bed state, allowing juxtaposition of clasts, stripping and concentration of fines, and rounding of clasts. Magnetite deposition occurred in the central portions of the breccia, adjacent to the highest temperature fluid 'jet' (figure 6.11d).

Limited biotite and k-feldspar alteration, illustrated by K-feldspar rinds on biotite-altered clasts, occurred during the fluidized bed state (figure 6.12a-c) After the fluidized bed state had collapsed (figure 6.12d) and fluid flow within the breccia was once again controlled by particle bed permeability, biotite, K-feldspar, and sulfide deposition occurred (figure 6.13). Permeability control on sulfide deposition is demonstrated by the presence of sulfides as chemical infill in polymictic breccia zones with moderate rounding of clasts and comparatively sparse fines (figure 6.14a). Equigranular augite monzonite dykes cutting breccia textures indicate that the breccia behaves as a coherent mass at the time of intrusion, rather than as a particle bed (figure 6.14b). For purposes of this study, this transition, from a particle bed to a coherent mass, differentiates the syn-breccia from the post-breccia period.

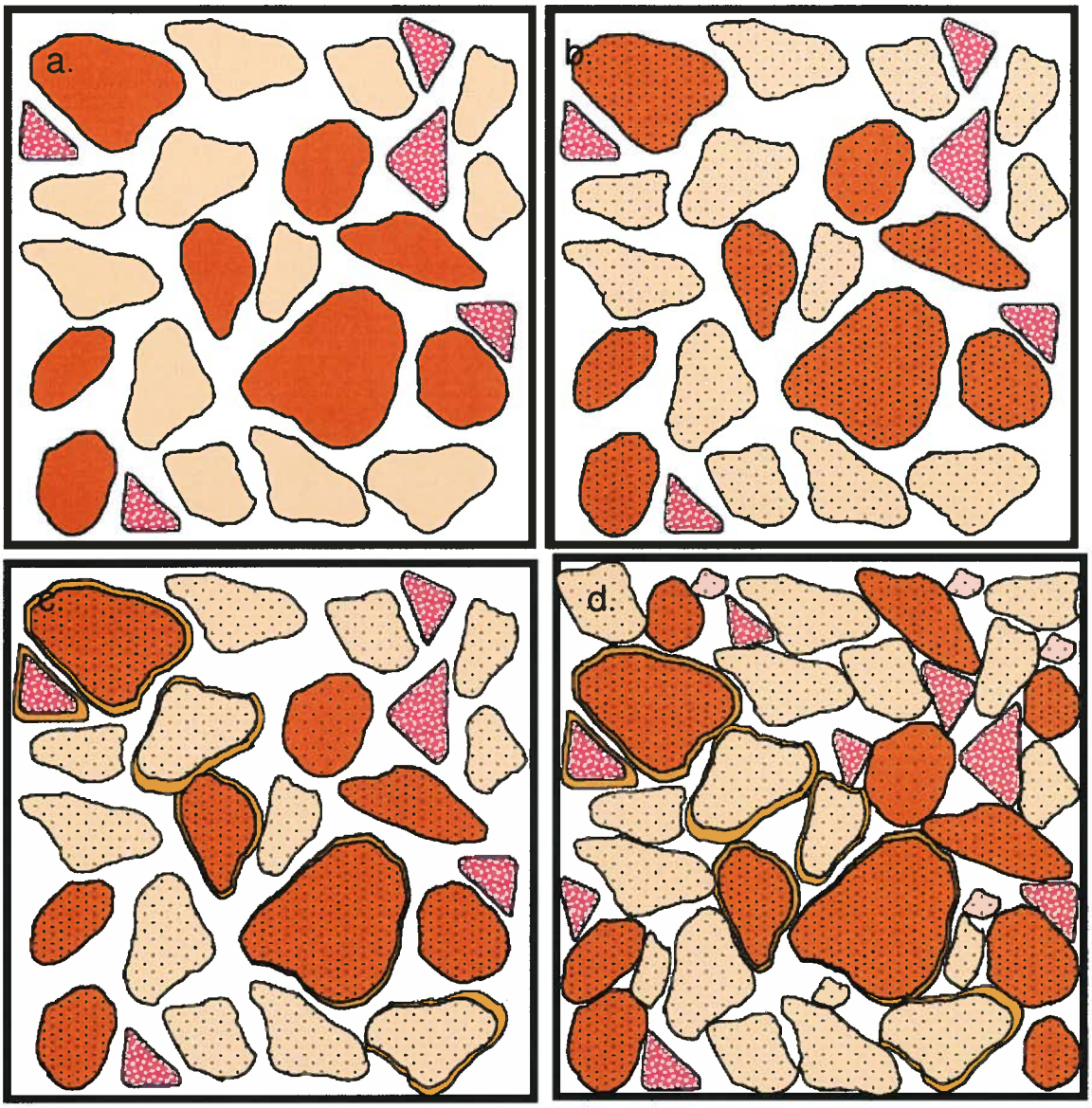

Figure 6.10-Alteration and infill of the breccia. a; mixed, rounded clasts in a fluidized bed state, after stripping of the fines; b; biotite alteration of the clasts in the fluidized bed state; c; k-feldspar alteration of clast rims; d; settling of the fluidized bed.

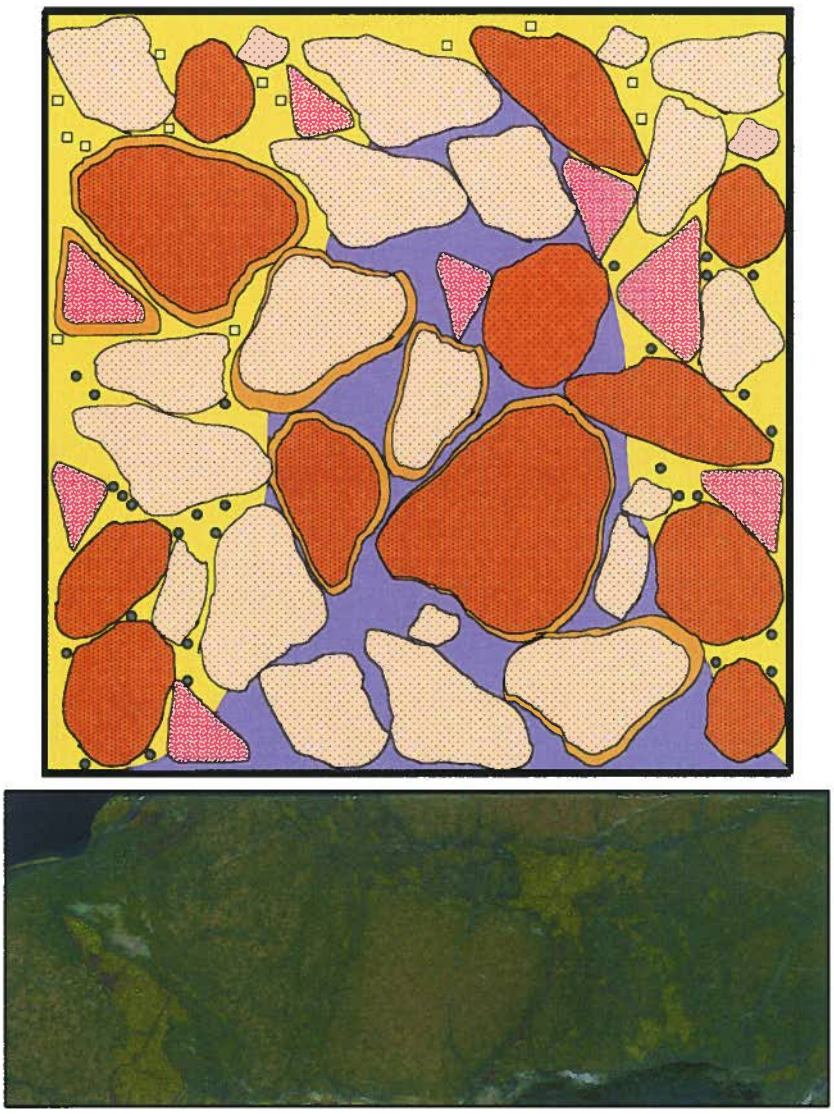

Figure 6.11-Breccia infill, schematic and actual.

Post-breccia sulfide mineralization cuts both the breccia textures and the equigranular augite monzonite (figure 6.14c). These post-breccia veins do not cut the post-breccia K-feldspar porphyry dykes (figure 6.14d). These dykes represent at least four generations, established by crosscutting relationships (figure 6.15). These generations evolve from crowded, blocky phenocrysts to elongate, sparse phenocrysts over time. This evolution probably represents decreasing magma residence time at near-solidus temperatures, with the more crowded, blockier phenocrysts representing a more advanced state of Ostwald

ripening (Higgins, 1999; Cabane et al., 2001; Higgins and Roberge, 2003). These dykes are not significantly different in chemistry from the megacrystic dykes that triggered both brecciation and mineralization, suggesting that long-term storage at near-solidus temperatures may have made the megacrystic dykes most able to segregate or store fluids (Fournier, 1999; Burnham, 1985).

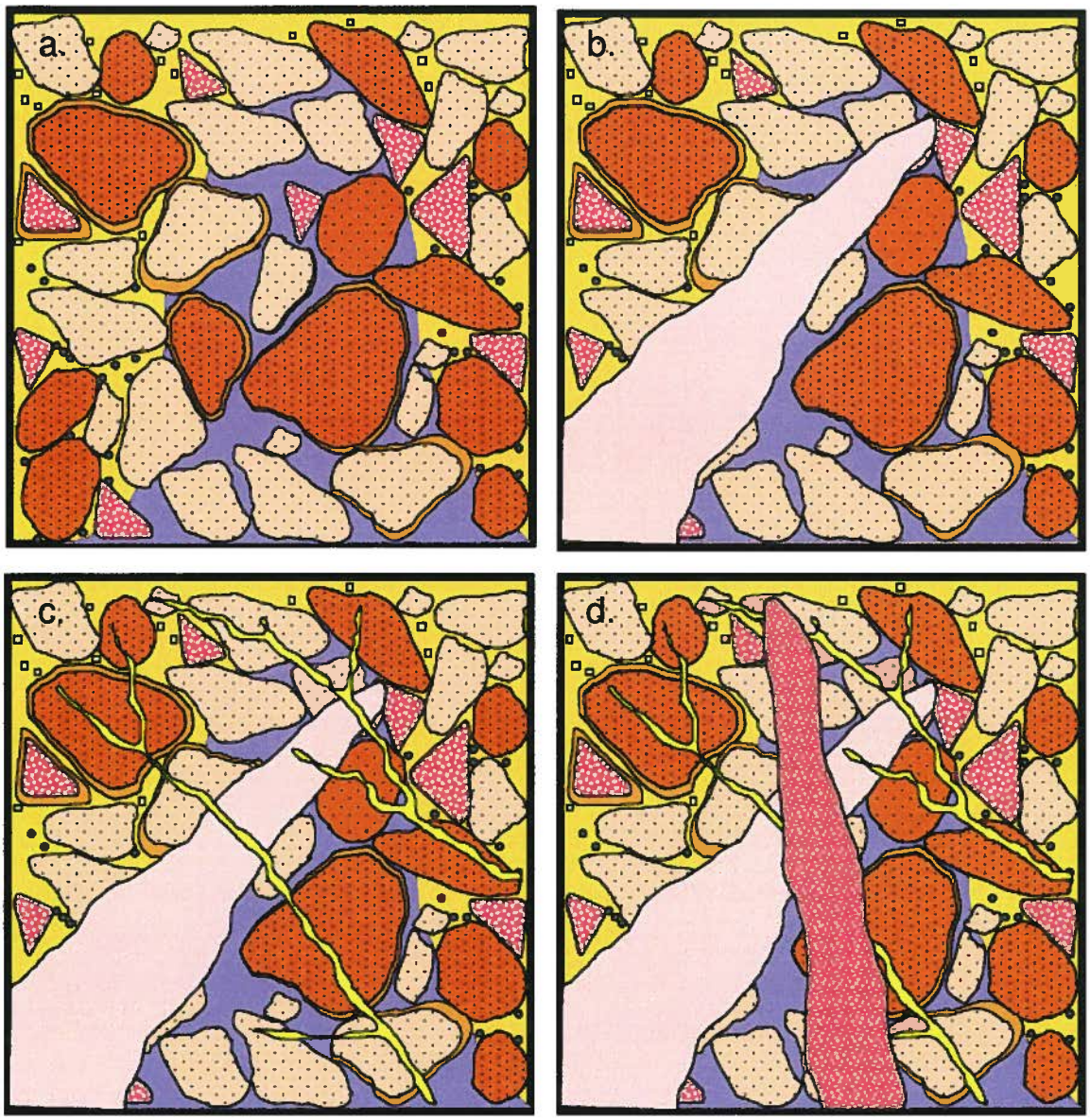

Figure 6.12-Post-breccia settling. A; breccia infill; b; intrusion of equigranular dykes; c; post-breccia chalcopyrite veining; d; intrusion of post-breccia monzonite dykes.

Figure 6.13-Progressive changes in dyke texture over time. A; Megacrystic K-feldspar phyric monzonite porphyry, b; crowded K-feldspar phyric monzonite porphyry, c; moderate K-feldspar phyric monzonite porphyry, d; sparse K-feldspar phyric monzonite porphyry, e; trachyte porphyry. Scale bar equals 1 cm.

Subsequent dyke generations reflect decreasing magma residence time and increasingly hydrous and increasingly mafic character. Increasing plagioclase is observed from K-feldspar and plagioclase phyric through plagioclase-only porphyries (monzonite to diorite). In the monzonite dykes, augite-bearing dykes are cut by augite and hornblende-bearing dykes, then hornblende only, hornblende and biotite, and finally biotite-only dyke phases. Albite-epidote alteration observed deep in Section 29 post-dates the biotite-bearing dyke phases and pre-date the mafic dyke phases (figure 6.16).

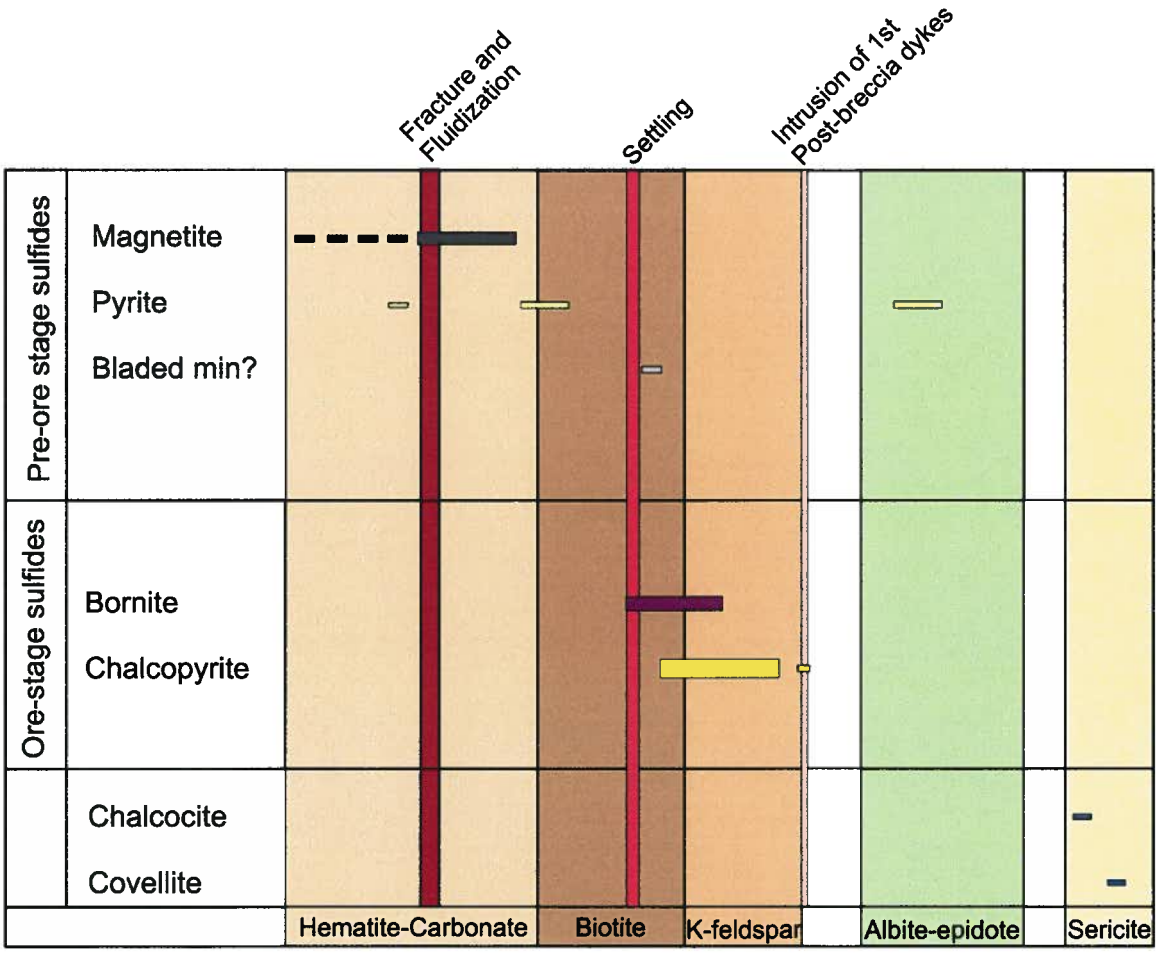

Figure 6.14-Mineral paragenesis and alteration timing.

The mafic dykes continue the evolution observed in the other dyke groups, from plagioclase phyric to augite and finally olivine-phyric fine grained mafic porphyries

(figure 6.17). The mafic dykes pre-date major faulting, which is then exploited by the latest dyke generation, the augite porphyry. The augite porphyry, based on this unique behavior and its distinctive geochemistry (most notably in Ni and Cr) may not be a direct part of the magmatic evolution which produced the other dykes.

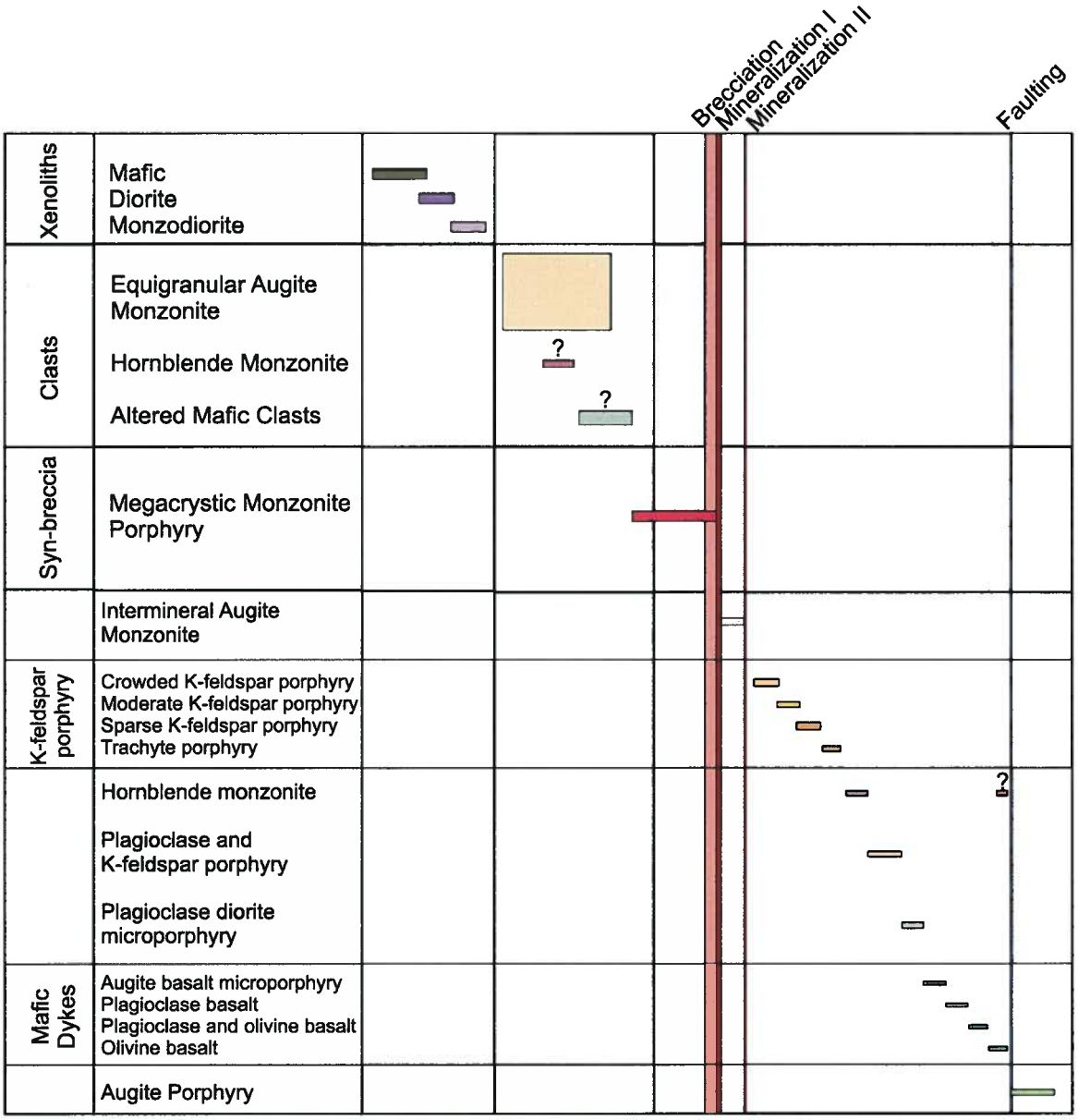

Figure 6.15-Evolution of the pre- and post-mineral intrusive rocks of the Northeast Zone.

The augite porphyry dykes are cut by the last phases of hydrothermal activity, including quartz-sericite alteration and carbonate-gypsum-zeolite veins and vein breccias (figure 6.16).

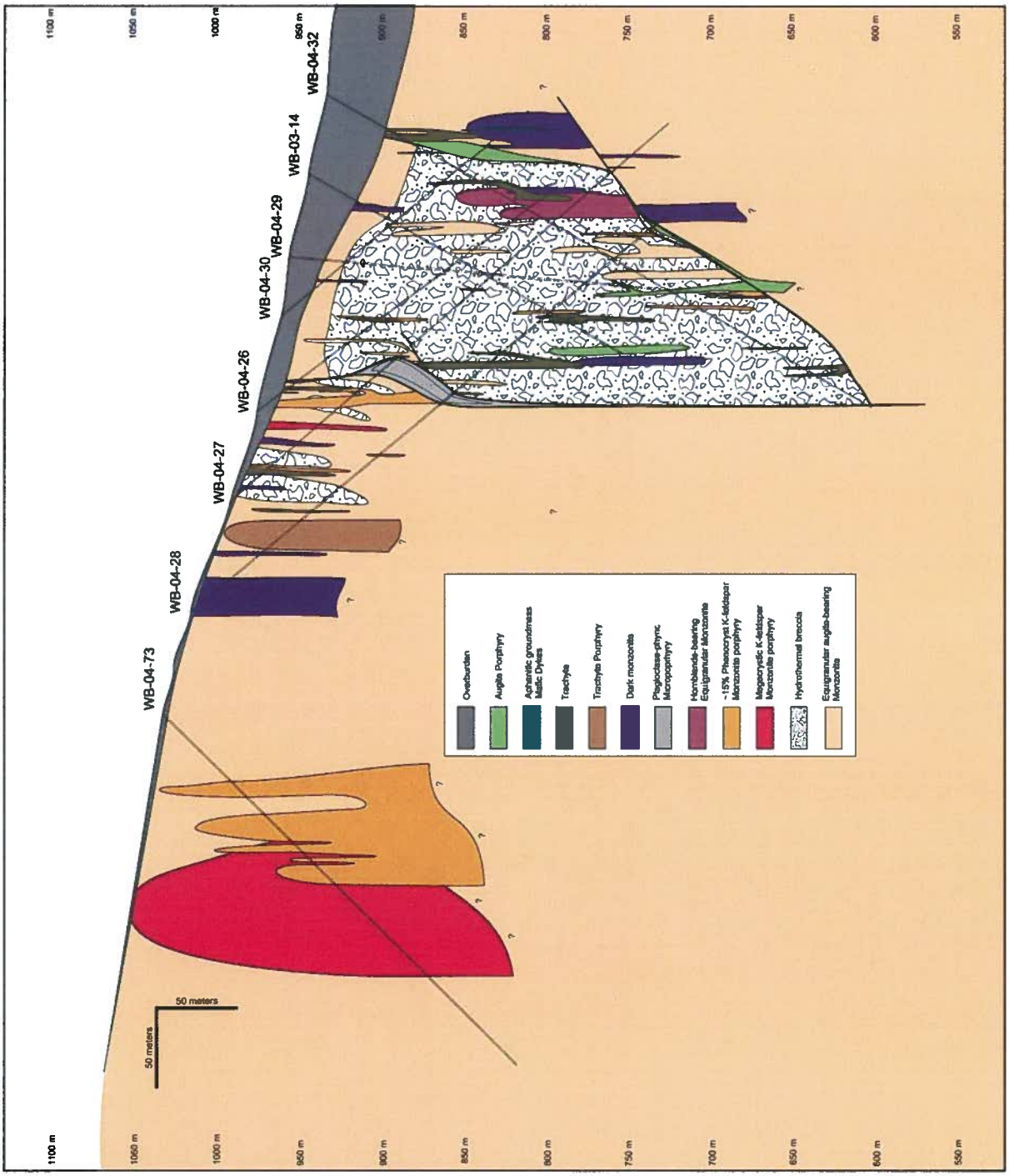

Figure 6.16-Complete cross-section of Section 18.

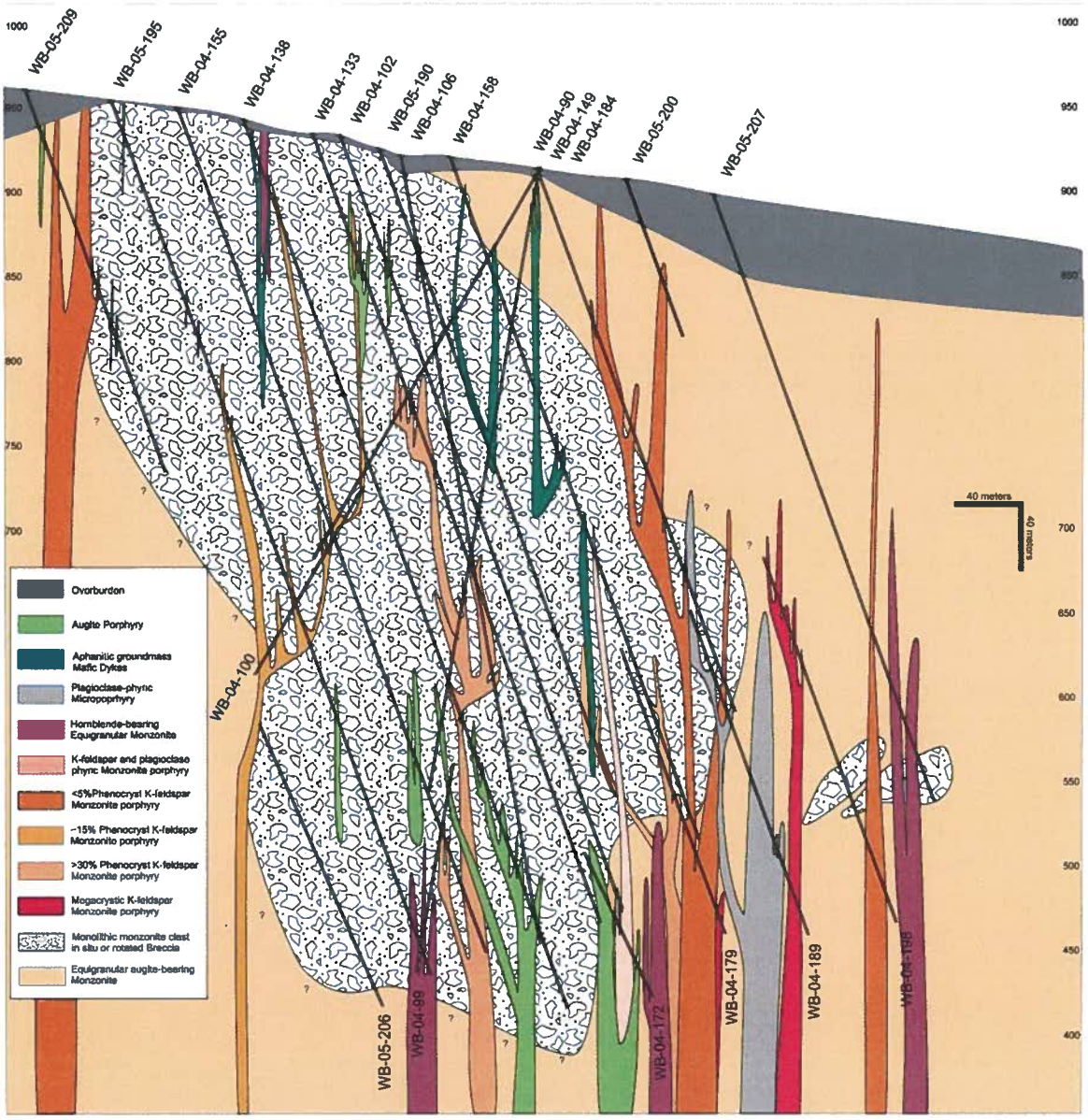

Figure 6.17-Lithology cross-section of Section 29.

Although the relationship between the Northeast Zone breccia and sulfide mineralization was recognized early in the exploration of the deposit, the complexity of the dykes and intrusive history (figure 6.18 and 6.19) obscured the strong control of internal breccia architecture over mineralization (figure 6.20). Alteration assemblages reflect the

evolution of fluids before, during and after mineralization, and are in accordance with those observed at many porphyry systems (figure 6.21).

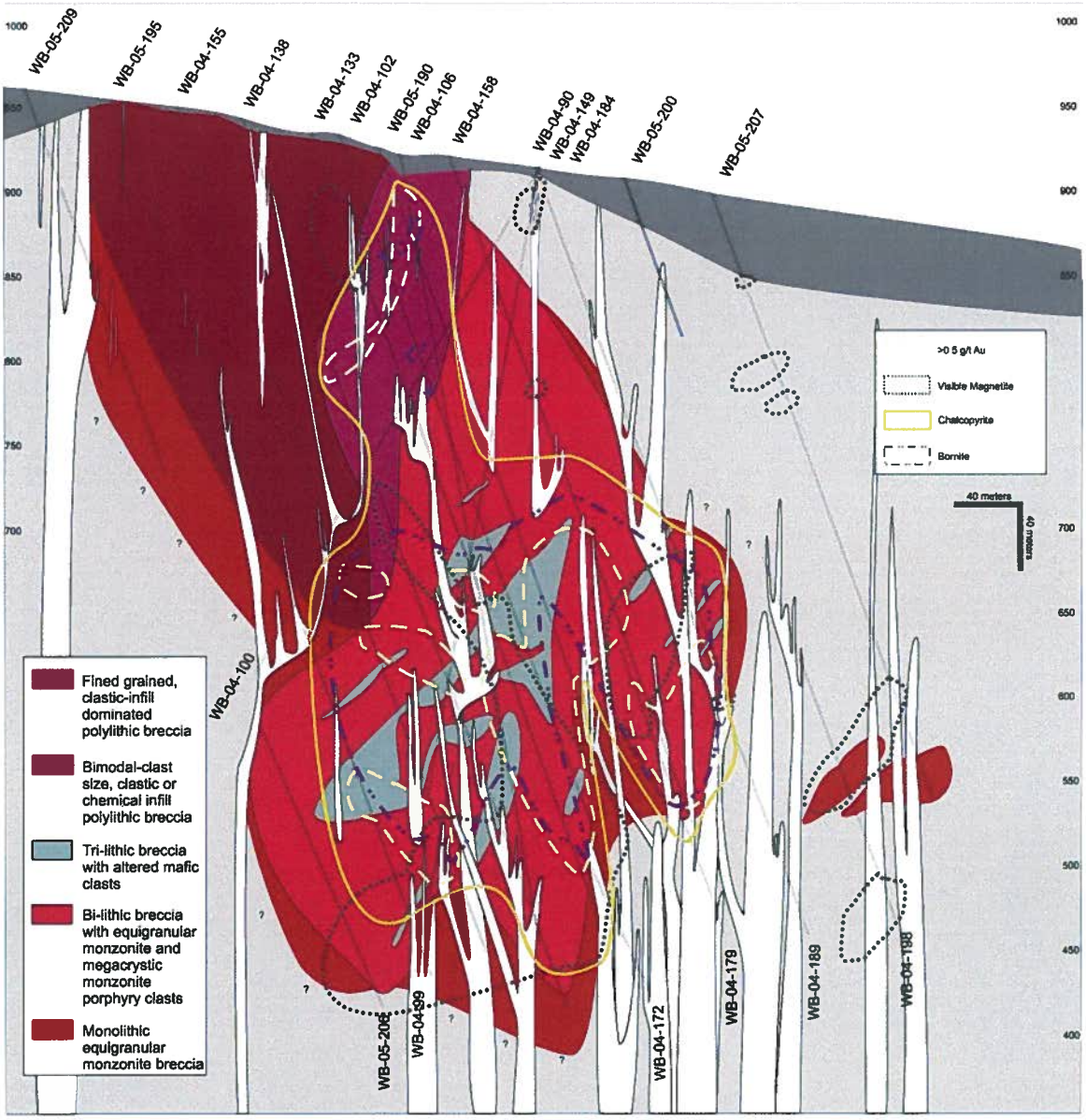

Figure 6.18-Breccia sub-units and sulfide mineralization, Section 29.

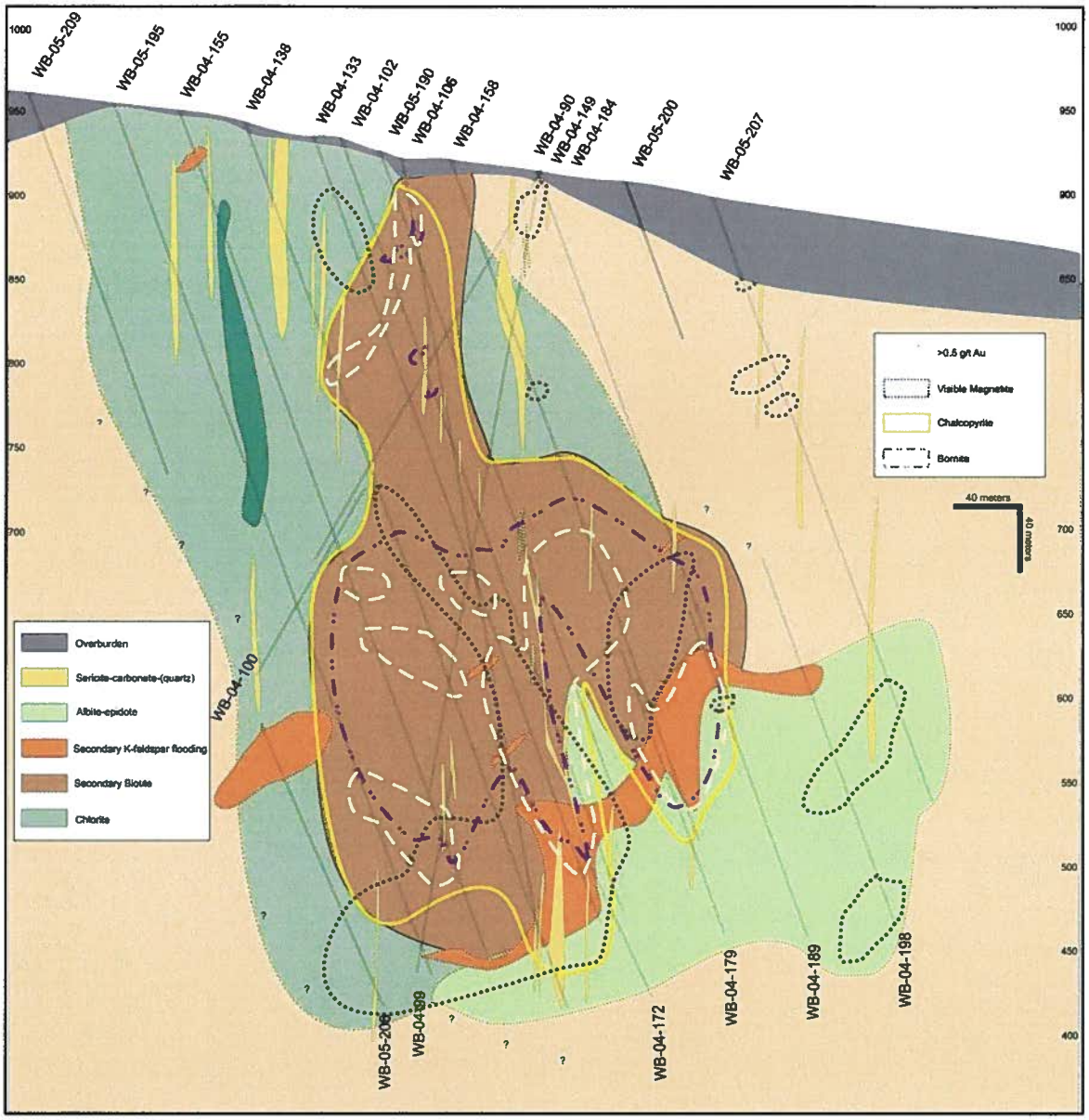

Figure 6.19-Alteration cross-section of Section 29.

Avenues for further research

Many questions regarding the origin and nature of the Mount Polley mineralizing system remain unanswered. On a deposit scale, the alteration zonation of the Northeast Zone is still poorly constrained. The absence of good mineralogic candidates for fluid inclusion analysis means that the temperatures and pressures under which mineralization occurred are not well understood.

Part of the challenge in reconstructing the Mount Polley orebody is due to the complexity of the post-mineralization faulting and folding. Reconstructing the property-scale structure would yield insights into the original geometry of the orebody, and into the relationships between the ore zones. Structural reconstruction would also clarify the relationship between the mineralizing system and the volcanic stratigraphy, including the position of the mineralizing system within the volcanic edifice (if any; Logan et al., 2007; Breitsprecher et al., 2007).

Beyond the Mount Polley property, the relationship between the Mount Polley mineralizing system and near-by areas of mineralization and alkalic magmatism (i.e. the Bootjack stock, the Bullion stock, the Spanish Mountain deposit and others) may lend insight into the evolution of alkalic porphyry systems, and into the differences between high- and low-grade systems. On a still larger level, the differences between silica-saturated and silica-undersaturated alkalic centers in the Quesnel terrain in terms of their mineralization potential has yet to be fully explored. Lang et al., 1995, initiated this area of inquiry, but many questions are left unanswered and the advances of technology since that time have opened many new avenues of research.

On a tectonic level, the origins of alkalic magmas, especially silica-undersaturated alkalic magmas, are not well understood (Riishuus et al., 2008; Mueller et al., 1994). The Quesnel terrane presents many opportunities for better understanding the evolution of alkalic magmatism and volcanism (Breitsprecher et al., 2007). The relationship between the Quesnel and Stikine terranes also remains ambiguous. Similarities in the age and nature of magmatism and volcanism between the two terranes have been noted (Lang et al., 1995; Breitsprecher et al., 2007; Johnston and Borel, 2007), but as yet not fully explained.

Globally, alkalic porphyry and epithermal deposits occur in many different tectonic settings. Arc-related, rift-related and intra-cratonic alkalic mineralizing systems have all been described (Sillitoe, 2002; Jensen and Barton, 2002; Mutschler et al., 1998; McLemore et al., 1996; Holliday and Cooke, 2007). The similarities and differences between alkalic-related mineralizing systems in different tectonic settings may lend insight into the origins of alkalic magmas and into the ultimate sources of alkalic mineralization. The links between alkalic porphyry and epithermal mineralizing systems have still not been well described. Although spatial and in some cases, potential genetic links (Allard stock, Jensen and Barton, 2002) have been established, a systematic relationship with application to exploration has not been published.

Mount Polley in the larger context

The Northeast Zone at Mount Polley is a small, high-grade ore zone representing a small part of a larger mineralizing system, itself an aspect of a silica-undersaturated alkalic intrusive center. Mount Polley has the potential to reflect the shallowest depths of an alkalic porphyry system, but as of the date of writing, this has yet to be established. Perhaps the most significant aspect of the Northeast Zone is its high grade. The breccia development and the breccia architecture of Mount Polley may lend insight into mechanisms for focusing fluid flow and identifying areas of high grade in other systems.

References

Abacus Mining and Exploration Corporation, (2008), Afton camp, http://www.amemining.com/afton_camp/, (viewed 2/20/2008), Vancouver, BC.

Alidibirov, M., and Dingwell, D.B., 1996a, Magma fragmentation by rapid decompression: Nature, v. 380, p. 146–148.

Alidibirov, M., and Dingwell, D.B., (1996b), An experimental facility for investigation of magma fragmentation by rapid decompression: Bulletin of Volcanology, v. 58, p. 411–416.

Anderson, T.L., (1991). Fracture Mechanics: Fundamentals and Application. CRC Press, Boca Raton.

Anderson, W.B., and Eaton, P.C., (1990), Gold mineralization at the Emperor mine, Vatukoula, Fiji: Journal of Geochemical Exploration, v. 36, p. 267-296.

Atkinson, B.K., (1987). Introduction to fracture mechanics and its geophysical applications. In: Atkinson, B.K. (Ed.), Fracture Mechanics of Rocks. Academic Press, London, pp. 1–26.

Ash, C.H., and Riveros, C.P. (2001), Geology of the Gibraltar copper-molybdenite deposit, east-central British Columbia (93B/9); British Columbia Ministry of Energy and Mines, Geologic Fieldwork 2000, report 2001-1, pp. 119-133

Ash, C.H., Reynolds, P.H., Creaser, R.A. and Mihalynuk, M.G. (2007): ^{40}Ar-^{39}Ar and Re-O isotopic ages for hydrothermal alteration and related mineralization in the Highland Valley Cu-Mo deposit, SW BC; *in* Geological Field work 2006, *BC Ministry of Energy, Mines and Petroleum Resources*, Paper 2007-1 and *Geoscience BC*, Re port 2007-1, pages 19–24.

Bagdassarov N. (1994). Pressure and volume changes in magmatic systems due to the vertical displacement of compressible materials. *J. Volcanol. Geotherm. Res.* 63:95–100

Bailey, D.G. (1978): The geology of the Morehead Lake area, south-central British Columbia; unpublished Ph.D. dissertation, Queen's University, 198 pp.

Bailey, D.G. (1979): Transported Altered wall rock in laharic breccias at the Cariboo-Bell Cu-Au porphyry deposit, British Columbia; Economic Geology, Scientific Communications, volume 74, pp. 125-153

Bailey, D.G. (1988): Geology of the Hydraulic map area, NTS 093A/12; B.C. Ministry of Energy, Mines and Petroleum Resources, Preliminary Map 67, 1:50,000.

Bailey, D.G. (2004a): Mount Polley copper-gold deposits, geology and chemistry, south central British Columbia; report for Imperial Metals Corporation, 5 pp.

Bailey, D.G. (2004b): Mount Polley copper-gold deposits, geology and chemistry; report for Imperial Metals Corporation, 9 pp.

Bailey, D.G. and Archibald, D.A. (1990): Age of the Bootjack Stock, Quesnel Terrane, South-central British Columbia (93A); B.C. Ministry of Energy, Mines and Petroleum Resources, Geological Fieldwork 1989, Paper 1990-1, pages 79-82.

Bailey, D.G. and Hodgson, C.J. (1979): Transported altered wall rock in laharic breccias at the Cariboo-Bell Cu-Au porphyry deposit, British Columbia; Economic Geology, Vol. 74, p. 125-128.

Bailey, D.K., and Hampton, C.M. (1990) Volatiles in alkaline magmas; Lithos, volume 26, pp. 157-165

Baker, E.M., and Andrew, A.S. (1991); Geologic, fluid inclusion, and stable isotope studies of the gold-bearing breccia pipe at Kidston, Queensland, Australia; Economic Geology, volume 86, pp. 810-830

Baker, E.M., Kirwin, D.J., Taylor, R.G. (1986), Hydrothermal breccia pipes. E.G.R.U. Contribution 12, James Cook University of North Queensland, Australia, 45 p.

Barnes, H.L., ed., (1997) Geochemistry of hydrothermal ore deposits, third edition: New York, John Wiley and Sons, p. 63–123

Barr, D.A., Fox, P.E., Northcote, K.E. and Preto, V.A. (1976): The alkaline suite porphyry deposits - a summary; in Porphyry Copper Deposits of the Canadian Cordillera, (Sutherland-Brown, A. ed.), CIM Special Volume No. 15, p. 359-367.

Bateman, P., Dudek, A., Keller, J., Lemeyre, J., Le Bas, M.J., Sabine, P.A., Schmidt, R., Sorenson, H., Streckeisen, A., Wooley, A.R., and Zanettin, B. (1989); A classification of igneous rocks and glossary of terms; Blackwell Scientific Publishing, Oxford, United Kingdom; 193 pp.

Bath, A. B., and Logan, J.M., (2006): Geochemistry of the Late Triassic Bootjack Stock (NTS 093A/12), South-Central British Columbia; British Columbia Ministry of Energy, Mines, and Petroleum Geological Fieldwork 2005, Paper 2006-1, 18 pp

Beane, R.E. and Titley, S.R., (1981). Porphyry Copper Deposits Part II; Hydrothermal Alteration and Mineralization. *In:* 75th Anniversary Volume, *Economic Geology*, pages 235-269.

Belcher, R.W., and Kisters, A.F.M. (2006): Progressive adjustments of ascent and emplacement controls during incremental construction of the 3.1 Ga Heerenveen batholith, South Africa; Journal of Structural Geology, vol. 28, pp. 1406-1421

Bergantz, G.W., (1991). Physical and chemical characterization of plutons. In: Kerrick, D.M. (Ed.), Contact Metamorphism. Reviews in Mineralogy, vol. 26. Mineralogical Society of America, pp. 13-42.

Bertram, A., Kalthoff, J.F., (2003). Crack propagation toughness of rock for the range from low to very high crack speeds. In: Buchholz, F.-G., Richard, H.A., Aliabadi, M.H. (Eds.), Advances in Fracture and Damage Mechanics Key Engineering Materials, 251-252. Trans Tech Publications, Uetikon-Zurich, pp. 423–430.

Blackwell, J. and Stubley, T. (2005): Surficial geology of the Mount Polley property, report for Imperial Metals Corporation.

Blake S. (1984). Volatile oversaturation during the evolution of silicic magma chambers as an eruption trigger. *J. Geophys. Res.* 89:8237–44

Bloodgood, M.A. (1985), Structure and stratigraphy of the Eureka Peak area, Cariboo Mtns., British Columbia; Geological Society of America Abstracts with programs, vol. 17, no. 6, pp. 343

Bloodgood, M.A. (1987a), Structural transitions within the Quesnel terrane, Eureka Peak area, Central British Columbia; Geological Society of America Abstracts with programs, vol. 19, no. 6, pp. 359

Bloodgood, MA. (1987b): Geology of the Triassic Black Phyllite in the Eureka Peak Area, Central British Columbia; *B.C. Ministry* of *Energy, Mines and Petroleum Resources,* Geological Fieldwork 1986, Paper 1987-1, pages 135-142.

Bloodgood, MA. (1987c): Geology of the Eureka Peak -Mackay River Area, Central British Columbia (NTS93A/7); *B.C. Ministry* of *Energy, Mines and Petroleum Resources* Open File Map 1987-9.

Bloodgood, MA. (1988): Geology of the Quesnel Terrane in the Spanish Lake Area, Central British Columbia (93A/ll); *B.C. Ministry* of *Energy, Mines and Petroleum Resources,* Geological Fieldwork 1987, Paper 1988-1, pages 139-145.

Bloodgood, M.A. (1990); Geology of the Eureka Peak and Spanish Lake map areas, B.C. Ministry of Energy, Mines and Petroleum Resources, Geological Fieldwork 1989, Paper 1990-3, 36 pp.

Bonafede, M., and Danesi, S., 1997, Near-field modifications of stress induced by dyke injection at shallow depth: Geophysical Journal International, v. 130, p. 435–448.

Boone, T.J., Wawrzynek, P.A., Ingraffea, A.R., (1986). Simulation of the fracture process in rock with application to hydrofracturing. International Journal of Rock Mechanics and Mining Sciences 23/3, 255–265.

Bowman, A. (1889): Report on the Geology of the Mining District of Cariboo, British Columbia, Geological Survey of Canada, Annual Report, 1887-88, Vol. III.

Bowman, A. (1895): Maps of the Principal Auriferous Creeks in the Cariboo. Geological Survey of Canada, Maps 364-372, 1895.

Breitsprecher, K., Scoates, J.S., Anderson, R.G. and Weis, D. (2007). Geochemistry of Mesozoic Intrusions, Quesnel and Stikine Terranes (NTS 082; 092; 093), South-Central British Columbia: Preliminary Characterization of Sampled Suites. Geological Fieldwork 2006, British Columbia Ministry of Energy, Mines and Petroleum Resources, Paper 2007-1: 247-257.

Brisbin, W.C., (1986). Mechanics of pegmatite intrusion. American Mineralogist vol. 71, pp. 644-651.

British Columbia Geological Survey, (2006), Mapplace application, http://www.mapplace.ca (viewed June 23, 2006): Vancouver, BC.

Broek. D. (1982). Elementary Engineering Fracture Mechanics, 469 pp.. Martinus Nijhoff.

Broberg, K.B., (1999). Cracks and Fracture. Academic Press, San Diego.

Brodsky EE, Roeloffs E,Woodcock D, Gall I, Manga M. 2003. A mechanism for sustained ground water pressure changes induced by distant earthquakes. *J. Geophys. Res.* 108:doi:10.1029/2002JB002321

Brooks, C.K., Tegner, C., Stein, H., and Thomassen, B. (2004): Re-Os and 40Ar/39 Ar ages of porphyry molybdenum deposits in the East Greenland volcanic-rifted margins; Scientific Communications, Economic Geology, volume 99, pp. 1215-1222

Bryant, D.G. (1968): Intrusive Breccias Associated with Ore, Warren (Bisbee) Mining District, Arizona; Economic Geology, vol. 63, pp. 1-12

Bryner, L. (1961): Breccia and pebble columns associated with epigenetic ore deposits: Economic Geology, volume 56, pp. 488-508

Bryner, L. (1968): Proposed Terminology for Hydrothermal breccias and Conglomerates; Economic Geology, volume 63, pp. 692-693

Burnham, C.W., (1979), Magmas and hydrothermal fluids, *in* Barnes, H.L., ed., Geochemistry of hydrothermal ore deposits, second edition: New York, John Wiley and Sons, p. 71–136.

Burnham, C.W., (1979)b. The importance of volatile constituents. In: Yoder, H.S. (Ed.), The Evolution of the Igneous Rocks. Princeton University Press, pp. 439–482.

Burnham, C.W., (1985), Energy release in subvolcanic environments: Implications for breccia formation: Economic Geology, v. 80, p. 1515–1522.

Burnham, C.W., (1997, Magmas and hydrothermal fluids, *in* Barnes, H.L., ed., Geochemistry of hydrothermal ore deposits, third edition: New York, John Wiley and Sons, p. 63–123.

Bushnell, Steven Ensign, 1988, Mineralization at Cananea, Sonora, and the paragenesis and zoning of breccia pipes in quartzofeldspathic rock; Economic Geology, vol. 83, no. 8, pp. 1760-1781

Cabane, H. Laporte, D. and Provost, A. (2001) Experimental investigation of the kinetics of Ostwald ripening of quartz in silicic melts. Contributions to Mineralogy and Petrology 142: 361-373.

Caldwell, M. (2005): Gold Rush: Inspiring Stories of More Than 25 Companies in Search of the World's Most Precious Metal; Gordon Soules Book Publishers Ltd., Vancouver, BC; 403 pp.

Campbell, K.V. and Campbell, R.B. (1970): Quesnel Lake map area, British Columbia (93A); *in* Re port of Activities, Part A, Geological Survey of Canada, Paper 70-1A, pages 32–35.

Campbell, K.V. (1971): Metamorphic Petrology and Structural Geology of the Crooked Lake Area, Cariboo Mountains, British Columbia; unpublished Ph.D. thesis, *University of Washington*, Seattle, 192 pages.

Campbell, R.B. (1961): Geology of Quesnel Lake, Sheet 93A (West Half), British Columbia; *Geological Survey of Canada*, Map 3-1961.

Campbell, R.B. (1963): Geology of Quesnel Lake, sheet 93A (East Half), British Columbia; *Geological Survey of Canada*, Map 1-1963.

Campbell, R.B. (1978): Quesnel Lake 93A Map-area; Geological Survey of Canada, Open File Map 574.

Candela, P.A. (1989) Magmatic ore-forming fluids: Thermodynamic and mass transfer calculations of metal concentration. *in* Ore deposition associated with magmas. Review in Economic Geology, 4, Whitney J.A. and Naldrett, A.J., *eds*, p. 223-233.

Cannell, J., Cooke, D.R., Walshe, J.L., and Stein, H., (2005); Geology, mineralization, alteration, and structural evolution of the El Teniente porphyry Cu-Mo deposit; Economic Geology, vol. 100, no. 5, pp. 979-1003

Carlson, S.R., and Sawkins, F.J. ,1980, Mineralogic and fluid inclusion studies of the Turmalina Cu-Mo-bearing breccia pipe, Northern Peru; Economic Geology, volume 75, pp. 1233-1238

Carman, G. D., (1994), Genesis of the Ladolam gold deposit, Lihir Island, Papua New Guinea: Unpublished PhD thesis, Monash University.

Carman, G.D. (2003): Geology, mineralization, and hydrothermal evolution of the Ladolam gold deposit, Lihir Island, Papua New Guinea; Society of Economic Geologists, Special Publication 10, pp. 247-284.

Carrington, C.R., 1998. Plumbing systems. In: Sigurdsson, H. (Ed.), Encyclopedia of Volcanoes. Academic Press, pp. 219–235.

Carslaw, H.S., and Jaeger, J.C., (1959). Conduction of Heat in Solids, 2nd ed Oxford and the Clarendon Press, London.

Cathelineau, M. (1986) The hydrothermal alkali metasomatism effects on granitic rocks: quartz dissolution and related subsolidus changes. Journal of Petrology, vol. 27 pp. 945-965.

Carye, J.A. (1986): Structural Geology of Part of the Crooked Lake Area, Quesnel Highlands, British Columbia. Unpublished M.Sc. Thesis, Vancouver, British Columbia

Clemens, J.D. and Mawer, C.K. (1992) Granitic magma transport by fracture propagation. Tectonophysics, 204: 339-360.

Cline J. S. and Bodnar, R. J., (1994) Direct evolution of brine from a crystallizing silicic melt at the Questa New Mexico molybdenum deposit; Economic Geology, volume 89, pp. 1780-1802

Cloos. E (1955), Experimental analysis of fracture patterns, Geological Society of America Bulletin, vol. 66, 241-256, 1955.

Cockfield, W.E. and Walker, J.F. (1932): Geology and Placer Deposits of the Quesnel Forks Area, Cariboo District, B.C.; Geological Survey of Canada, Summary Report, pages 76-143.

Cockfield, W.E. (1948): Geology and Mineral Deposits of Nicola Map-Area, British Columbia; Geological Survey of Canada, Memoir 249, 164 pages.

Coleman, D.S., Gray, W., Glazner, A.F., 2004. Rethinking the emplacement and evolution of zoned plutons: geochronological evidence for incremental assembly of the Tuolomne Intrusive Suite, California. Geology 32, 433-436.

Cooke, D.R., Wilson, A.J., House, M.J., Wolfe, R.C., Walshe, J.L., Lickfold, V., and Crawford A.J., (2006); Alkalic porphyry Au-Cu and associated mineral deposits of the Ordovician to Early Silurian Macquarie Arc, NSW: Australian Journal of Earth Sciences.

Corbett, G.J., and Leach, T.M. (1996), Southwest Pacific Rim gold - copper systems: structure, alteration and mineralization. Workshop manual, 185 p.

Corbett, G.J., and Leach, T.M., (1998), Southwest Pacific gold-copper systems: Structure, alteration and mineralization: Special Publication 6, Society of Economic Geologists 238p.

Cox, S.F., Knackstedt, M.A., and Braun, J., (2001), Principles of structural control on permeability and fluid flow in hydrothermal systems: Reviews in Economic Geology, v. 14, p. 1–24.

Cox, K.G., Bell, J.D., Pankhurst, R.J., (1979). The Interpretation of Igneous Rocks. George Allen & Unwin, London.

Cruden, A.R., 1990. Flow and fabric development during the diapiric rise of magma. Journal of Geology vol. 98,pp. 681-698.

Cummins, A.B., and Given, I.A., eds. (1973); SME Mining Engineering Handbook; vols. 1 and 2; The American Institute of Mining, Metallurgical, and Petroleum Engineers, Baltimore, MD

Darwin C. 1840. On the connexion of certain volcanic phenomena in South America; and on the formation of mountain chains and volcanoes, as the effect of the same power by which continents are elevated. *Trans. Geol. Soc. Lond.* 5:601–31

Davies, A.G.S, 2002, Geology and genesis of the Kelian gold deposit, east Kalimantan, Indonesia; Doctoral dissertation, University of Tasmania, Hobart, Tasmania, Australia

Davies, A.G.S., and Cooke, D.R., 2000, Hybrid phreatomagmatic and phreatic breccias at the Kelian gold deposit, east Kalimantan, Indonesia; triggering mechanisms and implications for ore genesis in magmatic-hydrothermal systems; Abstracts with programs, Geological Society of America, vol. 32, no. 7, p. 222

Dawson, G.M. (1877): Report on Explorations in British Columbia; Geological Survey of Canada, Reports on Explorations and Surveys of 1875-76, pages 233-280.

Deyell, C.L. (2005): Sulfur isotope zonation at the Mt. Polley alkalic porphyry Cu-Au de posit, British Columbia (Canada); Society for Geology Applied to Mineral De pos its, 8th Biennial Meeting, Proceedings, p. 373–376.

Deyell, C.L., and Tosdal, R.M., (2005), Alkalic Cu-Au deposits of British Columbia: Sulfur Isotope Zonation as a Guide to Mineral Exploration: British Columbia Ministry of Energy and Mines, Paper 2005-1, p. 191-208.

Dilles, J.H., and Einaudi, M.T., (1992) Wall-rock alteration and hydrothermal flow paths about the Ann-Mason porphyry copper deposit, Nevada—a 6km vertical reconstruction Economic Geology, vol. 87 p. 1963-2001.

Dzurisin C.D., Westphal, D.J., and Johnso n, D. J., (1983); Eruption prediction aided by electronic tilt meter data at Mount St. Helens Science., vol. 221, p. 1382-1383.

Eastfield Group, (1998): www.eastfieldgroup.com/eastfield/nr03-09-24.html; Vancouver, B.C.

Eberl, D.D., Kile, D.E. and Drits, V.A. (2002) On geological interpretations of crystal size distributions: Constant vs. proportionate growth. American Mineralogist 87: 1235-1241.

Eggleton, R.A. (1979) The ordering path for igneous K-feldspar megacrysts. American Mineralogist 64: 906-911.

Eichelberger, J.C., 1980,Vesiculation of mafic magma during replenishment of silicic magma reservoirs: Nature, v. 288, p. 446–450.

Eisenmann, M.D. (2001); Elutriation Technology in Heavy Mineral Separations; MSc thesis, Virginia Polytechnic Institute and State University; 160 pp.

Eliopoulos, , D.G., and Economou-Eliopoulos, M. (1985), Platinum-Group Element and Gold Contents of the Skouris Porphyry Copper Deposit, Chalkidiki Peninsula, Northern Greece; Economic Geology, volume 86, pp. 740-749

Elsby, D.C. (1985): Structure and Deformation Across the Quesnellia - Omineca Terrane Boundary, Mt. Perseus Area, East-central British Columbia; unpublished M.Sc. thesis, *the University of British Columbia*, Vancouver, 178 pages.

Emmons, S.F., (1906): Los Pilares Mine, Nacozari, Mexico; Economic Geology, volume 1, pp. 629-643

Emmons, W. H., 1927, Relations of the disseminated copper ores in porphyry to igneous intrusives: Am. Inst. Mining Metall. Engineers Trans., v. 75, p. 797-815.

Emmons, W.H., (1938), Diatremes and certain ore-bearing pipes: AIME Tech. Pub. 891.

Engvik, A.K., Bertram, A, Kalthoff, J.F., Stöckhert, B., Austrheim, H., and Elvevold, S; (2005); Magma-driven hydraulic fracturing and infiltration of fluids into the damaged host rock, an example from Dronning Maud Land, Antarctica; Journal of Structural Geology, vol. 27, pp. 839–854

Engvik, A.K., Austrheim, H., Stöckhert, B., Elvevold, S., (2003). Magma driven hydraulic fracturing and infiltration of CO2–H2O fluids into high-grade crystalline rocks, Dronning Maud Land, Antarctica. Terra Nostra 4, 82–83. Abstracts.

Enns, S., Stanley, C. R.,Yarrow, E. and Thompson, F. H. T. (1995): The geology of the Galore Creek alkalic porphyry Cu-Au deposit; *in* Porphyry Deposits of the northwestern Cordillera of North America, T. G. Schroeter (Editor), *Canadian Institute of Mining, Metallurgy and Petroleum*, Special Volume 46, pages 630-644.

Farmin, R., 1937, Hypogene exfoliation in rock masses: Journal of Geology, v. 45, p. 625–635.

Fillipone, J.A. (1985): Structure and Metamorphism at the Intermontane - Omineca Boundary, Near Boss Mountain, East-central British Columbia, unpublished M.Sc. thesis, *the University of British Columbia,* Vancouver, 156 pages

Fournier, R.O., (1983); Self-sealing and brecciation resulting from quartz deposition within hydrothermal systems [abst.] in: International Symposium on Water-Rock Interactions 1983, 4th, Misasa Japan, Extended Abstracts. , pp. 137-140

Fournier R.O. (1999); Hydrothermal Processes Related to Movement of Fluid From Plastic into Brittle Rock in the Magmatic-Epithermal Environment; Economic Geology, vol. 94, pp. 1193-1211

Fox, K. F., Rinehart C. D., and Engels J. C. (1975). K-Ar age of the Sirnilkameen Batholith and Kruger alkalic complex, Washington and British Columbia. Journal of Research of the United States Geological Survey, **3,** pp. 39-43.

Fraser, T.M., (1993): Geology and alteration of the Mount Polley alkalic porphyry cop per-gold de posit, British Columbia (93A/12); *in* Geological Field work 1992, *BC Min is try of Energy, Mines and Petroleum Resources*, Paper 1993-1, pages 295–300.

Fraser, T. M. (1994)a: Geology, alteration and origin of hydrothermal breccias at the Mount Polley alkalic porphyry copper-gold deposit, south-central British Columbia; unpublished M.Sc. thesis, University of British Columbia, 261 pp.

Fraser, T.M. (1994)b: Hydrothermal breccias and associated alteration of the Mount Polley copper-gold deposit (93A/12); *in* Geological Field work 1993, BC Ministry of Energy and Mines and Petroleum Re sources, Paper 1994-1, p. 259–267.

Fraser, T.M., Stanley, C.R., Nikic, Z.T., Pesalj, R. and Gorc, D. (1995): The Mount Polley alkalic porphyry copper-gold deposit, south-central British Columbia; in: Porphyry deposits of the northwestern Cordillera of North America (Schroeter, T.G., ed.), CIM Special Volume No. 46, pp. 609-622.

Frei, R., (1995): Evolution of Mineralizing Fluid in the Porphyry Copper System of the Skouris Deposit, Northeast Chalkidiki (Greece): Evidence from Combined Pb-Sr and Stable Isotope Data; Economic Geology, volume 90, pp. 746-762

Gemmell, J.B., Sharpe, R., Jonasson, I.R., and Herzig, P.M. (2004); Sulfur Isotope Evidence for Magmatic Contributions to Submarine and Subaerial Gold Mineralization: Conical Seamount and the Ladolam Gold Deposit, Papua New Guinea; Economic Geology, Vol. 99, pp. 1711–1725

Gerbi, C., Johnson, S.E., Paterson, S.R., (2004). Implications of rapid, dike-fed pluton growth for host-rock strain rates and emplacement mechanism. Journal of Geology vol. 26, pp. 583-594.

Gifkins, C., Herrmann, W. and Large R., (2005), Altered volcanic rocks; Hobart, Tasmania, Centre for Ore Deposit Research, University of Tasmania, 275 p.

Gilbride, L. J., Free K.S. & Kehrman, R., (2005). Modeling block cave subsidence at the Molycorp, Inc., Questa Mine. In: *Proc. 40th U.S. Symposium on Rock Mechanic*, Anchorage.

Gillou-Frottier, L., and Burov, E., (2003), The development and fracturing of plutonic apexes: implications for porphyry ore deposits; Earth and Planetary Science Letters, volume 214, pp. 341-356

Gillstrom, G. (2004): Mount Polley Mine 2004 Feasibility Study; 43-101 Technical Report for Imperial Metals Corporation, dated August 1, 145 pp.

Glazner, A.F., Bartley, J.M., Coleman, D.S., Gray, W., Taylor, R.Z., (2004). Are plutons assembled over millions of years by amalgamation from small magma chambers? GSA Today 14, pp. 4-11.

Gonnermann, H.M., and Manga, M., (2003): Explosive volcanism may not be and inevitable consequence of magma fragmentation; Nature, volume 426, pp. 432-435

Groves, D.I., and Vielreicher, N.M., (2001): The Phalabowra (Palabora) carbonatite-hosted magnetitie-copper sulfide deposit, South Africa: an end-member of the iron-oxide copper-gold-rare earth element deposit group?; Mineralium Deposita, volume 36, pp. 189-194

Guilbert, J.M., and Park, C.F., (1980): The Geology of Ore Deposits; W.H. Freeman, NY; 985 pp.

Gustafson, L.B., and Hunt, J.P., (1975), The porphyry copper deposit at El Salvador, Chile: Economic Geology, v. 70, p. 857- 912.

Hattori, K., (1993), High-sulfur magma, a product of fluid discharge from underlying mafic magma: Evidence from Mount Pinatubo, Philippines: Geology, v. 21, p. 1083-1086.

Hattori, K.H., and Keith, J.D., (2001), Contribution of mafic melts to porphyry copper mineralization: Evidence from Mount Pinatubo, Philippines, and Bingham Canyon, Utah, USA: Mineralium Deposita, v. 36, p. 799-806.

He, M., and Forssberg, E., (2007)a; Influence of slurry rheology on stirred media milling of quartzite, *International Journal of Mineral Processing*, Vol.84 No.1-4, pp. 240-251

He, M., and Forssberg, E., (2007)b; Rheological behaviors in wet ultrafine grinding of limestone, *Minerals & Metallurgical Processing*, Vol.24 No.1,

Hedenquist, J.W., Henley, R.W. (1985), Hydrothermal eruptions in the Waiotapu geothermal system, New Zealand: their origin, associated breccias and relation to precious metal mineralization. *Economic Geol*ogy, v. 80, p. 1640-1668.

Hedenquist J.W. and Lowenstern J.B. (1994), Review Article: The role of magmas in the formation of hydrothermal ore deposits. Nature, v. 370, p. 519-527.

Hedenquist J.W., and Richards, J. (1998), The influence of geochemical techniques on the development of genetic models for porphyry copper deposits, *in* Richards, J.P., and Larson, P.B. (eds.), Techniques in Hydrothermal Ore Deposits Geology: Reviews in Economic Geology, v. 10, ch. 10, p. 235-256.

Heithersay, P.S., and Walshe, J.L. (1995): Endeavour 26 North: A porphyry copper-gold deposit in the late Ordovician, shoshonitic Goonumbla volcanic complex, New South Wales, Australia; Economic Geology, volume 90, pp. 1506-1532

Heiskanen, K., 1993, Particle Classification, Powder Technology Series, Chapman and Hall, London, England.

Higgins, M.D. (1999) Origin of megacrysts in granitoids by textural coarsening: a crystal size distribution (CSD) study of microcline in the Cathedral Peak Granodiorite, Sierra Nevada , California . In: Castro, A., Fernández, C. &Vigneresse, J.-L. (eds): Understanding Granites: Integrating New and Classical Techniques. Geological Society of London Special Publication 168: 207-219 .

Higgins, M.D., and Roberge, J. (2003), Crystal Size Distribution of Plagioclase and Amphibole from Soufrière Hills Volcano, Montserrat: Evidence for Dynamic Crystallization-Textural Coarsening Cycles; Journal of Petrology, volume 44, number 8, pp. 1401-1411

Hodgson, C.J., Bailes, R.J. and Verzosa, R.S. (1976): Cariboo-Bell; in Porphyry copper deposits of the Canadian Cordillera, ed. Sutherland-Brown, A., CIM Special Volume No. 15, p. 388-396.

Holliday, J.R., Wilson, A.J., Blevin, P.L., Tedder, I.J., Dunham, P.D., and Pfitzner, M., (2002), Porphyry gold-copper mineralisation in the Cadia district, eastern Lachlan fold belt, New South Wales, and its relationship to shoshonitic magmatism: Mineralium Deposita, v. 37, p. 100–116.

Holliday, J.R. and Cooke, D.R. (2007): Advances in geological models and exploration methods for copper ± gold porphyry deposits; Proceedings of Exploration 07, Fifth Decennial International Conference on Mineral Exploration, p. 791–809.

Hubbert, M.K and D.G. Willis, (1957). "Mechanics of Hydraulic Fracturing," *Petroleum Transactions AIME*, Vol. 210, pp. 153-168.

Husen, S, Taylor R, Smith RB, Healser H. (2004). Changes in geyser eruption behavior and remotely triggered seismicity in Yellowstone National Park produced by the 2002 M 7.9 Denali fault earthquake, Alaska. *Geology* 32:537–40

Imperial Metals Corporation, (2007)a, Mount Polley Property and Mine Operations, http://www.imperialmetals.com/s/MtPolley.asp (viewed Sept 17, 2007): Vancouver, BC.

Imperial Metals Corporation (2007)b, Imperial Metals Annual Information Form; Imperial Metals Corporation, 47 p.

Jackson, M.L., Tosdal, R.M., Chamberlain, C.M., Simpson, K. and McAndless, P. (2007): Breccia architecture as a control on ore distribution, Mount Polley mine, British Columbia; *in* Breccias

(abstract volume), Economic Geology Research Unit (EGRU), School of Earth Sciences, James Cook University, Townsville, Queensland, Australia, Contribution 65, p. 12.

Jacobsen, J.B.E., McCarthy, T.S., and Laing, G.J. (1976); The Copper-bearing breccia pipes of the Messina District, South Africa; Mineralium deposita, Volume 11, pp. 33-45

Jago, P., Tosdal, R.M., and Chamberlain, C.M. (2007): Mt. Milligan – Tilting and structural juxtaposition of Cu-rich potassic and Au-rich assemblages providing a 3-D view of an alklaic porphyry system; *in* Ore and Orogenesis (abstract volume), Arizona Geological Society, Tucson, Arizona, Contribution 87b.

Janssen, C., Wagner, F.C., Zang, A., Dresen, G., (2001). Fracture process zone in granite: a microstructural analysis. International Journal of Earth Sciences 90, 46–59.

Jébrak, M., (1997): Hydrothermal breccias in vein-type ore deposits: A review of mechanisms, morphology, and size distribution: Ore Geology Reviews, v. 12, p. 111–134.

Jensen, E.P., and Barton, M.D., (2000): Gold deposits related to alkaline magmatism: Reviews in Economic Geology, v. 13, p. 279-314.

Jensen, E.P., 2003, Magmatic and Hydrothermal Evolution of the Cripple Creek Gold Deposit, Colorado, and Comparisons with Regional and Global Magmatic-Hydrothermal Systems Associated with Alkaline Magmatism, PhD dissertation: University of Arizona, Tucson, AZ.

Johnston, S. T., and Borel, G.D. (2007); The odyssey of the Cache Creek terrane, Canadian Cordillera: Implications for accretionary orogens, tectonic setting of Panthalassa, the Pacific superwell, and break-up of Pangea; Earth and Planetary Science Letters, volume 253, pp. 415-428

Jonnes, S. and Logan, J.M. (2007): Bedrock Geology and Mineral Potential of Mouse Mountain, Central BC; *in* Geological Fieldwork 2006, British Columbia Ministry of Energy, Mines and Petroleum Resources, Paper 2007-1 and Geoscience BC, Report 2007-1, pp 55-67.

Kennedy, B, Spieler, O., Scheu, B., Kueppers, U., Taddeucci, J., and Dingwell, D.B; (2005); Conduit implosion during Vulcanian eruptions; Geology; vol. 33, pp. 581-584

Keith, J.D., Christiensen, E.H., Maughan, D.T., Waite, K.A., (1998): The role of mafic alkaline magmas in felsic porphyry-Cu and Mo systems; In: Lentz, D.R., (ed) Mineralized "intrusion related" skarn systems. Mineral Association of Canada Short Course 26, pp. 211-243

Krech, W.W., (1973), Fragmentation Principles, *in* Cummins, A.B., and Given, I.A., eds. SME Mining Engineering Handbook, Society of Mining Engineers, New York

Kelly, K.D., and Ludington, S., (2002): Cripple Creek and other alkaline-related gold deposits of the Southern Rocky Mountains, USA: influence of regional tectonics; Mineralium Deposita, volume 37, pp. 38-60

Kelly, W.C. and Rye, R.O. (1979) Geologic, fluid inclusions and stable isotopes studies of the tin-tungsten deposits of Penasquiera, Portugal. Economic Geology, 74: 1721-1822.

Kwak, T.A.P., 1990, Vein genesis, geochemical and flow controls on ore mineralisation at the Emperor Gold Mine, Vatukoula, Fiji, *in* Hedenquist, J.W., White, N.C. and Siddley, G., eds., Epithermal gold mineralisation of the Circum-Pacific: Geology, geochemistry, origin and exploration, II: Journal of Geochemical Exploration, v. 36, p. 297-337.

Lamb, H., (1953); *Hydrodynamics*, 6th ed.; Cambridge: Cambridge Univ. Press.

Lang, J.R., Lueck, B., Mortensen, J.K., Russell, J.K., Stanley, C.R., Thompson, J.F.H, (1995a): Triassic-Jurassic silica-undersaturated and silica-saturated alkalic intrusions in the Cordillera of British Columbia: Implication for arc magmatism; Geology, volume 23, no. 5, pp. 451-454

Lang J. R., Stanley C. R., Thompson J. F. H. and Dunne K. P. E., (1995b), Na-K-Ca magmatic-hydrothermal alteration in alkalic porphyry Cu-Au deposits, British Columbia: Min. Assoc. Can., Short Course 23, 339-336.

Lange, R.A., (1994). The effect of H2O, CO2, and F on the density and viscosity of silicate melts. In: Carroll, M.R., Holloway, J.R. (Eds.), Volatiles in Magma Reviews in Mineralogy, 30, pp. 331–370.

Laubscher, D H, (2000). *Block caving manual. Prepared for International Caving Study*. JKMRC and Itasca Consulting Group, Inc: Brisbane.

Laznicka, P. (1985): Empirical metallogeny, depositional environments, lithologic associations and metallic ores, volume 1: Phanerozoic environments, associations and deposits, part A and B; *Elsevier*, 1758 pages.

Laznicka, P., 1988, Breccias and coarse fragmentites: Petrology, environments, associations, ores: Amsterdam, Elsevier, 832 p.

Levson, V.M. (2001): Regional till geochemical surveys in the Canadian Cordillera: sample media, methods and anomaly evaluation; in: Drift exploration in glacial terrain (McClenaghan, M.B., Bobrowsky, P.Y., Hall, G.E.M. and Cook, S.J., eds.), Geological Society of London Special Publication, 185, pp. 45-68.

Levson, V. M. and Giles, T. R.. (1993): Geology of Tertiary and Quaternary Gold-bearing Placers in the Cariboo Region, British Columbia (93A,B,G,H); B.C. Ministry of Energy, Mines and Petroleum Resources, Bulletin 89, 202 pages.

Li, J.W., Zhou, M.F., Li, X.F., Li, Z.J., and Fu, Z.R., (2002), Origin of a large breccia-vein system in the Sanerlin uranium deposit, southern China: a reinterpretation; Mineralium Deposita, volume 37, pp. 213-225

Lickfold, V. (2002), Intrusive history and volatile evolution of the Endeavour porphyry Cu-Au deposits, Northparkes district, NSW, Australia: Unpublished PhD thesis, Hobart, Tasmania, University of Tasmania, 230 p

Lickfold V., Cooke D.R., Smith S.G., and Ulrich T. (2003). Endeavour Cu-Au porphyry deposits, Northparkes, NSW – Intrusive history and fluid evolution. Economic Geology, v 98, p. 1607-1636.

Lickfold V., Cooke D. R., Crawford A. J. & Fanning C. M.(2007); Shoshonitic magmatism and the formation of the Northparkes porphyry Cu–Au deposits, New South Wales; Australian Journal of Earth Sciences, Vol. 54, no. 2/3

Lihir Gold Limited (2007): 24 January 2007 - Lihir Gold adds 4.4 million ounces to gold reserves at Lihir mine; http://www.lihir.com.pg/data/portal/00000005/content/26035001169592905109.pdf; viewed February 25, 2008

Linde A. T., Sacks I. S., Johnston M. J. S., Hill D. P., Bilham R. G. (1994). Increased pressure from rising bubbles as a mechanism for remotely triggered seismicity. *Nature* 371:408–10

Lindgren, W., (1922), A suggestion for the terminology of certain mineral deposits, Economic Geology, v. 17, p. 292-294.

Lindgren, W., (1933), Mineral deposits, 4th ed.: New York, McGraw-Hill, 930 p.

Lindgren, W., and Ransome, F. L., (1906), Geology and gold deposits of the Cripple Creek district, Colorado: U.S. Geol. Survey Prof. Paper 54, 516 p.

Link, J.M., Godlieb, W., Deen, N.G., Kuipers, J.A.M. (2006): Discrete element study of granulation in a spout-fluidized bed; Chemical Engineering Science, volume 62 pp. 195 – 207

Locke, A. (1926): The Formation of Certain Ore Bodies by Mineralization Stoping: Brecciation due to Removal of Support by the Dissolving action of Solutions during and early stage of their activity, followed by mineral deposition in the Brecciated Mass at a later Stage; Economic Geology, Volume 21, pp. 431-453

Lockner, D.A., (1995). Rock failure. In: Ahrens, T.J. (Ed.), Rock Physics and Phase Relations—a Handbook of Physical Constants. American Geophysical Union, Washington, pp. 127–147.

Logan, J.M. and Mihalynuk, M.G. (2005): Regional geology and setting of the Cariboo, Bell, Springer and Northeast porphyry Cu-Au zones at Mount Polley, south-central British Columbia; in Geological Fieldwork 2004, B.C. Ministry of Energy and Mines, Paper 2005-1, pp. 249-270.

Logan, J.M., and Bath, A.B., (2005), Geochemistry of the Nicola Group Basalt from the Central Quesnel Trough at the Latitude of the Mount Polley (NTS 093A/5, 6, 11, 12), Central British Columbia; British Columbia Ministry of Energy, Mines, and Petroleum Geological Fieldwork 2005, Paper 2006-1, 16 pp

Logan, J.M. and Bath, A.B. (2006): Geochemistry of Nicola Group basalt from the central Quesnel trough at the latitude of Mount Polley (NTS 093A/5, 6, 11, 12), central British Columbia; *in* Geological Field work 2005, *BC Ministry of Energy, Mines and Petroleum Resources*, Pa per 2006-1, pages 83–98.

Logan, J.M., Mihalynuk, M.G., Ullrich, T., and Friedman, R.M. (2007); U-Pb Ages of Intrusive Rocks and 40Ar/39Ar Plateau Ages of Copper-Gold-Silver Mineralization Assocaited with Alkaline Intrusive Centers at Mount Polley and the Iron Mask Batholith, Southern and Central British Columbia; British Columbia Geological Survey, Geological Fieldwork 2006, Paper 2007-1, pp. 93-116

Lorenz, V., (1986). On the growth of maars and diatremes and its relevance to the formation of tuff-rings. Bull. Volcanol., 48: 265-274.

Lorenz, V., (2003a). Maar-diatreme volcanoes, their formation, and their setting in hard rock or soft rock environments. GeoLines 15 (Hibsch 2002 Symposium), 72-83.

Lorenz, V., (2003b). Syn- and post-eruptive processes of maar-diatreme volcanoes and their relevance to the accumulation of post-eruptive maar crater sediments. Földtani Kutatás 40, 13-22.

Lorenz, V. and Kurszlaukis, S., (2006). Root zone processes in the phreatomagmatic pipe emplacement model and consequences for the evolution of maar-diatreme volcanoes. Journal of Volcanology and Geothermal Research, in press.

Lowell, J.D., and Guilbert, J.M., 1970, Lateral and vertical alteration-mineralization zoning in porphyry ore deposits; Economic Geology, v. 65, p. 373-408.

Lueck, B.A., and Russell, J.K., (1994): Silica-undersaturated, zoned, alkaline intrusions within the British Columbia Cordillera; in Geological Fieldwork 1993, paper 1994-1, Mineral Deposits Research unit contribution 038, British Columbia Geological Survey

Makovicky, M., Makovicky, E., Rose-Hansen, J., and Barnes, S-.J.; (1995); Skaergaard intrusion in a test tube- Current results; *in* Pasava, J., Kribek, B., and Zak, K.; (1995); Mineral deposits: from their origins to their Environmental Impacts; Society for geology Applied to Mineral deposits; Taylor and Francis, 1018 pp.

Manga, M, and Brodsky, E; (2006): Seismic triggering of eruptions in the far field: Volcanoes and Geysers; Annual Review of Earth and Planetary Sciences, May 2006, Vol. 34, Pages 263-291(doi: 10.1146/annurev.earth.34.031405.125125)

Mangan, M., and Sisson T. (2000). Delayed, disequilibrium degassing in rhyolite magma: decompression experiments and implications for explosive volcanism. *Earth Planet. Sci. Lett.* 183:441–55

Mankosa, M.J., (1990), Scale-Up of Column Flotation, Dissertation, Virginia Polytechnic Institute and State University, Blacksburg, VA.

Manning, D.A.C. and Pichavant, M. (1985) Volatiles and their bearing on the behaviour of metals in granitic systems. CIM spec. vol. 39, pp. 13-24.

Marsh, B.D., (1982). On the mechanics of igneous diapirism, stoping and zone melting. American Journal of Science vol. 282, pp. 808-855.

Marsh, B.D., (1996). Solidification fronts and magmatic evolution. Mineralogy Magazine vol. 60, pp. 5-40.

Marsh BD. (2000). Magma chambers. In *Encyclopedia of Volcanoes*, ed. H Sigurdsson, pp. 191–206. San Diego, CA: Academic Press

Marshall, D, (1997), Ternplot: An Excel Spreadsheet for Ternary diagrams; www.geologynet.com/programs/ternplot.xls

Masliyah, J.H., (1979), "Hindered Settling in a Multi-Species Particle System," Chemical Engineering Science, Vol. 34, pp. 1166-1168.

Mastin, L.G., and Pollard, D.D. (1988); Surface Deformation and Shallow Dike Intrusion Processes at Inyo Craters, Long Valley, California; Journal of Geophysical Research, Vol. 93. No. B11, pp. 13,221-13,235

Maughan, D.T., (2001): Mafic to intermediate alkaline rocks of the Bingham District, Utah; MSc thesis, Brigham Young University, Provo, Utah

Maughan, , D.T., Keith, J.D., Christiansen, E.H., Pulsipher, T., Hattori, K., and Evans, N.J., (2002): Contributions from alkaline magmas to the Bingham porphyry Cu-Au-Mo deposit, Utah, USA; Mineralium Deposita, volume 37, pp. 14-37

McCallum, M.E., (1985); Experimental Evidence for Fluidization Processes in Breccia Pipe Formation: Economic Geology, volume 80, pp. 1523-1543

McDonough, W.F., and Sun, S.S., (1995), The Composition of the Earth, *Chemical Geology* v. 120 p. 223-253

McLemore, V. T., (1995), Great Plains Margin (alkalic-related) gold deposits in New Mexico (abstr.): Geology and ore deposits of the American Cordillera, Geological Society of Nevada, Program with Abstracts, p. A54-55.

McLemore, V.T., (1996): Great Plains Margin (alkaline-related) gold deposits in New Mexico. In: Coyner A.R., and Fahey, P.L., (eds) Geology and ore deposits of the American Cordillera, Geological Society of Nevada Symposium Proceedings, pp. 2935-2950

McLeod O, and Tait S. (1999). The growth of dikes from magma chambers. *J. Volcanol. Geotherm. Res.* 92:231–46

McMillan, W.J., Thompson, J.F.H., Hart, C.J.R. and Johnston, S.T. (1995): Regional geological and tectonic setting of porphyry deposits in British Columbia and Yukon Territory; in: Porphyry deposits of the northwestern Cordillera of North America (Schroeter, T.G., ed.), CIM Special Volume No. 46, pp. 40-57.

McPhie, J., Doyle. M. and Allen, R. (1993): Volcanic textures: a guide to the interpretation of textures in volcanic rocks; published by Centre for Ore Deposit and Exploration Studies, University of Tasmania, 198 pp.

Meinert, L.D., (1982), Skarn, Manto, and Breccia Pipe Formation in Sedimentary Rocks of the Cananea Mining District, Sonora, Mexico; Economic Geology, volume 77, pp. 919-949

Meyer, C., and Hemley, J. J., 1967, Wall rock alteration, in Barnes, H. L., ed., Geochemistry of hydrothermal ore deposits: New York, Holt, Rinehart and Winston, Inc., p. 166-235.

Michioka H, Sumita I. (2005). Rayleigh-Taylor instability of a particle packed viscous fluid: implications for a solidifying magma. *Geophys. Res. Lett.* 32:L03309, doi:10.1029/2004GL021827

Mihalynuk, M.G., Smith, M., Gabites, J.E., Runkle, D. and Lefebure, D. (1992): Age of emplacement and basement character of the Cache Creek terrane as constrained by new isotopic and geochemical data; *Canadian Journal of Earth Sciences*, Volume 29, pages 2463-2477.

Mihalynuk, M.G., Nelson, J. and Diakow, L.J. (1994): Cache Creek terrane entrapment: Oroclinal paradox within the Canadian Cordillera; Tectonics, vol. 13, pp. 575-595.

Monger, J.W.H., Price, RA. and Tempelman-Kluit, D. (1982): Tectonic Accretion and the Origin of Two Major Metamorphic and Plutonic Welts in the Canadian Cordillera; ***Geology,*** Volume 10, pages 70-75

Monger, J.W.H., Wheeler, J.O., Tipper, H.W., Gabrielse, H., Harms, T., Struik, L.C., Campbell, R.B., Dodds, R.B., Gehrels, G.E. and O'Brien, J. (1991): Cordilleran terranes, Upper Devonian to Middle Jurassic assemblages; in: Geology of the Cordilleran Orogen in Canada (Gabrielse, H. and Yorath, C.J., eds.), Chapter 8; Geological Survey of Canada, Geology of Canada, No. 4, pp. 281-327.

Montgomery, J.R. (1985): Structural Relations of the Southern Quesnel Lake Gneiss, Isoceles Mountain Area, Central British Columbia; unpublished M.Sc. thesis, *The University of British Columbia*, 96 pages.

Montgomery, S.L. (1978): Structural and Metamorphic History of the Dunford Lake Map Area, Cariboo Mountains, British Columbia: Ophiolitic Obduction in the Southeastern Canadian Cordillera; unpublished M.Sc. thesis, *Cornell University,* Ithaca, New York, 170 pages.

Mortensen, J.K., Ghosh, D.K. and Ferri, F. (1995): U-Pb geochronology of intrusive rocks associated with copper-gold porphyry deposits in the Canadian Cordillera; in: Porphyry deposits of the northwestern Cordillera of North America (Schroeter, T.G., ed.), CIM Special Volume No. 46, pp. 142-158.

Mortimer, N. (1987): The Nicola Group: Late Triassic and Early Jurassic subduction related volcanism in British Columbia; Canadian Journal of Earth Sciences, vol. 24, pp. 2521-2536.

Morton, R.L. (1976): Alkalic volcanism and copper deposits of the Horsefly area, central British Columbia; unpublished Ph.D. thesis, Carleton University, 196 pp.

Moyle, A. L., Doyle, B. J., Hoogvliet, H., and Ware, A. R., 1990, Ladolam gold deposit, Lihir Island: Monograph Series - Australasian Institute of Mining and Metallurgy, v. 14, p. 1793-1805.

Mueller D., Heithersay P.S., and Groves, D.I., (1994). The shoshonite porphyry Cu-Au association in the Goonumbla District, NSW, Australia. Mineralogy and Petrology. Vol 51, 299-321.

Mueller, D., Kaminski, K., Uhlig, S., Graupner, T., Herzig, P.M., and Hunt, S (2002), Transition from porphyry- to epithermal-style gold mineralization at Ladolam, Lihir Island, Papua New Guinea; a reconnaissance study; Mineralium Deposita, vol. 37, no. 1, pp. 61-74

Muhkerjee, A.K., and Mishra, B.K. (2007); Experimental and simulation studies on the role of fluid velocity during particle separation in a liquid–solid fluidized bed. International Journal of Mineral Processing (2007), doi:10.1016/j.minpro.2006.11.006

Murphy, M.D., Sparks, R.S.J., Barclay, J., Carroll, M.R., and Brewer, T.S., 2000, Remobilisation origin for andesite magma by intrusion of mafic magma at the Soufriere Hills Volcano, Montserrat,West Indies: Journal of Petrology, v. 41, p. 21–42.

Mutschler, F. E., McLemore, V. T., Bookstrom, A. A., and Ludington, S., (1998), Rocky Mountain front alkalic rock-related gold deposits, Canada to Mexico: A review (abstr.): Geological Society of America, Annual Meeting, Abstracts with programs, v. 30, no. 7, p. A-300.

Newman, S., and Lowenstern, J.B., (2002);VolatileCalc: A silicate melt-H2O–CO2 solution model written in Visual Basic for Excel: Computers & Geosciences, v. 28, p. 597–604, doi: 10.1016/S0098-3004(01)00081-4.

Nixon, G. T., and Peatfield, G.R., (2003); Geological Setting of the Lorraine Cu-Au Porphyry Deposit, Duckling Creek Syenite Complex, North-central British Columbia; British Columbia Ministry of Mines and Mineral Resources Open File Report 2003-4, 26 pp.

Norman, D.I., and Sawkins, F.J., (1985), The Tribag Breccia Pipes: Precambrian Cu-Mo Deposits, Batchawana Bay, Ontario; Economic Geology, volume 80, pp. 1593-1621

Norton, D. L., and Cathles, L. M., (1973), Breccia pipes—products of exsolved vapor from magmas: Economic Geology.,v . 68, p. 540-546.

Nova Gold, (2008): NovaGold Updates Galore Creek Resource Estimate, February 1, 2008; http://www.novagold.com/section.asp?pageid=5944; Vancouver, British Columbia, Viewed February 25, 2008

Okulitch, A.V. (2001): Geological time scale, (2001); Geological Survey of Canada, Open File 3040 (National Earth Science Series, Geological Atlas) – Revision.

Orchard, M.J. (1995): Report on conodonts and other microfossils from Quesnel Lake (93A, 93B and 93H); *Geological Survey of Canada*, Conodont Data File, Re port MJO-1995-9.

Palfy, J., Smith, P.L. and Mortensen, J.K. (2000): A U-Pb and 40Ar- 39Ar time scale for the Jurassic; *Canadian Journal of Earth Sciences*, Volume 37, pages 923–944.

Pallister, J.S., Hoblitt, R.P., and Reyes, A.G., (1992), A basalt trigger for the 1991 eruptions of Pinatubo Volcano: Nature, v. 356, p. 426–428.

Pals, D.W., Spry, P.G., and Chryssoulis, S. (2003): Invisible Gold and Tellurium in Arsenic-Rich Pyrite from the Emperor Gold Deposit, Fiji: Implications for Gold Distribution and Deposition; Economic Geology, volume 98, pp. 479-493

Panteleyev, A. (1987): Quesnel gold belt – alkalic volcanic terrane between Horse fly and Quesnel Lakes (93A/6); *in* Geological Field work 1986, *BC Min is try of Energy, Mines and Petroleum Resources*, Paper 1987-1, pages 125–133.

Panteleyev, A. (1988): Quesnel mineral belt – the central volcanic axis between Horse fly and Quesnel Lakes (93A/5E, 6W); *in* Geological Field work 1987, *BC Ministry of Energy, Mines and Petroleum Re sources*, Pa per 1988-1, pages 131–137.

Panteleyev, A. and Hancock, K.D. (1989): Quesnel mineral belt: summary of the geology of the Beaver Creek – Horsefly River map area; *in* Geological Field work 1988, *BC Ministry of Energy, Mines and Petroleum Resources*, Paper 1989-1, pages 159–166.

Panteleyev, A., Bailey, D.G., Bloodgood, M.A. and Hancock, K.D. (1996): Geology and mineral deposits of the Quesnel River-Horsefly map area, Central Quesnel Trough, British Columbia; B.C. Ministry of Employment and Investment, Bulletin 97, 156 p.

Parson, I., Lee, M.R., (2000). Alkali feldspars as microtextural markers of fluid flow. In: Stober, I., Bucher, K. (Eds.), Hydrogeology of Crystalline Rocks. Kluwer Academic Publishers, pp. 27–50.

Pass, H.E., Cooke, D.R., Chamberlain, C., Simpson, K., Rees, C., Ferreira, L., McAndless, P. and Robert son, S. (2007): Infill paragenesis and hydro thermal alteration in the Northeast zone of the Mt. Polley magmatic-hydrothermal breccia complex, British Columbia; Proceedings of the 9th Biennial meeting of the Society for Geology Applied to Mineral Deposits, Irish Association for Economic Geology, p. 423–426.

Passchier, C.W., and Trouw, R.A.J., (2005), Microtectonics; Springer, Berlin

Paterson, S.R., and Tobisch, O.T., 1992, Rates of processes in magmatic arcs: Implications for the timing and nature of pluton emplacement and wall rock deformation: Journal of Structural Geology, v. 14, p. 291–300.

Philpotts, A.R., (1990), Principles of Igneous and Metamorphic Petrology, Prentice Hall, Saddle River, N.J.

Preto, V. and McMillan, B. (1995): Mineralization and Geological Setting of Calcalkaline and Alkaline Porphyry Copper Deposits in Southern British Columbia; in A3 Fieldtrip Guidebook, GAC/MAC Victoria '95, B.C. Ministry of Energy, Mines and Petroleum Resources.

Pollard, D. D. (1988), Elementary fracture mechanics applied to the structural interpretation of dykes: Mafic Dyke Swarms, edited by H. C. Halls and W. F. Fahrig. Special papers of the Geological Association of Canada. 34, 5-24.

Pollard, D. D., and G. Holzhausen. (1979), On the mechanical interaction between a fluid-filled fracture and the Earth's surface, Tectonophysics, vol. 53, 27-57.

Pollard. D. D., P. T. Delaney, W. A. Duffield. E. T. Endo, and A. T. Okamura, (1983) Surface deformation in volcanic rift zones, Tectonophysics, vol. 94, 541-584.

Powell, M.S., and Morrison, R.D.; (2007) The future of comminution modelling, *International Journal of Mineral Processing*, Vol.84 No.1-4, pp. 228-239

Radloff, J.K. (1989): Origin and Obduction of the Ophiolitic Redfern Complex on the Omineca - Intermontane Belt Boundary, Western Cariboo Mountains, British Columbia; *unpublished M.Sc. thesis*, Vancouver, 179 pages.

Rasul, M.G., Rudolph, V. and Wang, F.Y., (2000), "Particle Separation Using Fluidization Techniques," International Journal of Mineral Processing, Vol. 60, pp. 163-179.

Read, P.B. (1997): Surface geology of the area east of the Cariboo Pit, Mount Polley Mine; unpublished report for Mount Polley Mining Corporation-Imperial Metals Corporation, Geotex Consultants Limited, December 1997.

Rees, C.J. (1981): Western Margin of the Omineca Belt at Quesnel Lake, British Columbia, ***in*** Current Research, Part A, Geological Survey of Canada, Paper 8-A, pages 223-226.

Rees, C.J., (1987), The Intermontane-Omineca Belt boundary in the Quesnel Lake area, east-central british Columbia; tectonic implications based on geology, structure, and paleomagnetism; doctoral dissertation, Carleton University, Ottawa, ON, Canada

Rees, C., Bjornson, L., Blackwell, J., Ferreira, L., McAndless, P., Robertson, S., Roste, G., Stubley, T., and Taylor, C., (2005), Geological Report on the Mount Polley Property and Summary of Exploration in 2003-2004, Internal Report to the Imperial Metals Corporation, 211 pp

Rees, C., Ferreira, L., Bjornson, L., Blackwell, J., Roste, G., Stubley, T. and Taylor, C. (2006): Geological report on the Mount Polley property and summary of 2005 exploration; Imperial Metals Corporation, internal re port, 169 p.

Richards, J.P., and Ledlie, I., (1993): Intrusive rocks associated with the Mount Kare Gold Deposit, New Guinea: Comparison with the Porgera Intrusive Complex; Economic Geology, volume 88, pp. 755-781

Richards, J.P. (2003): Tectono-magmatic precursors for porphyry Cu-(Mo-Au) deposit formation; *Economic Geology*, Volume 98, pages 1515–1533.

Richardson, J. and Zaki, W., (1954), "Sedimentation and Fluidization: Part l, "Transactions of the Institute of Chemical Engineering, Vol. 39, pp. 35-53.

Riishuus, M.S., Peate, D.W., Tegner, C., Wilson, J.R., and Brooks, C.K.; (2008); Petrogenesis of Cogenetic Silica-Oversaturated and -Undersaturated Syenites by Periodic Recharge in a Crustally Contaminated Magma Chamber: the Kangerlussuaq Intrusion, East Greenland; Journal of Petrology, volume 49, no. 3, pp. 493-522

Roddick, J.A., Wheeler, J.O., Gabrielse, H. and Souther, J.G. (1967): Age and nature of the Canadian part of the Circum-Pa cific Orogenic Belt; *Tectonophysics*, Vol ume 4, pages 319–337.

Roeloffs E, Sneed M, Galloway DL, Sorey ML, and Farra CD. (2003).Water-level changes induced by local and distant earthquakes at Long Valley caldera, California. *J. Volcanol. Geotherm. Res.* 127:269–303

Roman, D.C., 2005, Numerical models of volcanotectonic earthquake triggering on non-ideally oriented faults: Geophysical Research Letters, v. 32, p. L02304, doi: 10.1029/2004GL 021549.

Ronacher, E., Richards, J.P., Villeneuve, M,E., Johnston, M.D., (2002): Short life-span of the oreforming system at the Porgera gold deposit, Papua New Guinea: laser 40Ar/39Ar dates for roscoelite, biotite, and hornblende: Mineralium Deposita 37, 75 – 86.

Ronacher, E., Richards, J.P., Reed, M.H., Bray, C.J., Spooner, E.T.C., Adams, P.D., (2004), Characteristics and evolution of the hydrothermal fluid in the north zone high grade area, Porgera gold deposit, Papua New Guinea: Economic Geology 99, 843 – 867.

Ross, J.V., Fillipone, J.A., Montgomery, J.R., Elsby, D.C. and Bloodgood, M.A. (1985): Geometry of a convergent zone, central British Columbia, Canada; *Tectonophysics*, Volume 119, pages 285–297.

Ross, J.V., Garwin, S.L. and Lewis, P.D. (1989): Geology of the Quesnel Lake region, central British Columbia: geometry and implications; *in* Proceedings, 7th International Conference on Basement Tectonics, *D. Reidel*, Dordecht, Netherlands, pages 1–23.

Ross, K.V. (2004a): Alteration study of the Northeast Zone, Mount Polley mine, British Columbia; unpublished report for Imperial Metals Corporation, Panterra Geoservices Inc., 2004, 108 pp.

Ross, K.V. (2004b): Alteration study of the Springer Zone, Mount Polley mine, British Columbia; unpublished report for Imperial Metals Corporation, Panterra Geoservices Inc., 2004, 33 pp.

Ross, P.S., (2002), Magmatic-hydrothermal breccia formation in porphyry Mo systems: A horizontal stratified body at Questa, New Mexico: Unpublished M.Sc thesis, Montreal, Canada, Université du Québec à Montréal, 161 p.

Ross, P.S., Jébrak, M., and Walker, B., (2001)a, Brecciation processes proximal to the apex of a crystallizing magma chamber: Insights from the Questa porphyry molybdenum deposit [abs.]: Geological Association of Canada-Mineralogical Association of Canada, Abstract Volume 26, p. 127.

Ross, P.S., Jébrak, M., and Walker, B., (2001)b, A magmatic-hydrothermal breccia formed by hydraulic fracturing under a compressive stress regime at the Questa porphyry molybdenum deposit [abs.]: Geological Society of America Abstracts with Programs, v. 33, p. A420.

Rubin, A.M., (1993). Tensile fracture of rock at high confining pressure: implications for dike propagation. Journal of Geophysical Research 98, 15919–15935.

Rubin, A.M., (1995). Propagation of magma filled cracks. Annual Review of Earth and Planetary Science 8, 287–336.

Scala, F., Cammarota, A., Chirone, R., and Salatino, P.,(1997); Comminution of limestone during batch fluidized-bed calcination and sulfation; AIChE journal vol. 43, n°2, pp. 363-373

Schardt, C; Yang, J., and Large, R.; (2005); Numerical Heat and Fluid-flow modeling of the Panorama Volcanic-Hosted Massive Sulfide District, Western Australia; Economic Geology, vol. 100; pp. 547-566

Schroeter, T. G. (Ed.), 1995. Porphyry Copper Deposits of the Northwestern Cordillera of North America. *Canadian Institute of Mining, Metallurgy and Petroleum,* Special Volume 46, 852 pages.

Schroeter, T.G., Lund, C. and Carter, G. (1989): Gold production and reserves in British Columbia; *B.C. Ministry of Energy, Mines and Petroleum Resources,* Open File 1989-22, 86 pages.

Schroeter, T.G. and Lane, R.A. (1991): A century of gold production and reserves in British Columbia; *B.C. Ministry of Energy, Mines and Petroleum Resources*, Open File 1991-19, 41 pages.

Schroeter, T.G. and Pinsent, R.H. (2000): Gold production, resources and total inventories in British Columbia (1858-1998); *B.C. Ministry of Energy, Mines and Petroleum Resources*, Open File 2000-2, 94 pages.

Secor, D.T., (1965). Role of fluid pressure in jointing. American Journal of Science 263, pp.

Segall, P., 1984a. Rate-dependent extensional deformation resulting from crack growth in rocks. Journal of Geophysical Research 89, 4185–4195.

Segall, P., 1984b. Formation and growth of extensional fracture sets. Geological Society of America, Bulletin 95, 454–462.633–646.

Serrano, L., Vargas, R., Stambuk, V., Aguilar, C., Galeb, M., Holmgren, A., Contreras, A., Godoy, S., Vela, I., Skewes, M.A. and Stern, C.A. (1996), The late Miocene to early Pliocene Rio Blanco–Los Bronces copper deposit, central Chilean Andes; *in* Andean Copper Deposits: New Discoveries, Mineralization, Styles, and Metallogeny, F. Camus, R.W. Sillitoe and R. Petersen (ed.), Society of Economic Geologists, Special Publication 5, p. 119–130.

Shives, R.B.K., Carson, J.M., Ford, K.L., Holman, P.B. and Cathro, M. (2004): Imperial Metals Corporation, Mount Polley 2003 multisensor geophysical survey; B.C. Ministry of Energy and Mines, Open File 2004-10.

Sillitoe, R.H., (1973): The Tops and Bottoms of Porphyry Copper Deposits; Economic Geology, volume 68, pp. 799-815

Sillitoe, R.H., (1985): Ore-Related Breccias in Volcanoplutonic Arcs; Economic Geology, volume 80, pp. 1467-1514

Sillitoe, R.H., (2002): Some metallogenic features of gold and copper deposits related to alkaline rocks and consequences for exploration; Mineralium Deposita, volume 37, pp. 4-13

Sillitoe, R.H., and Bonham, H.F. (1984); Volcanic Topography and ore deposits; Economic Geology, vol. 79, pp. 1286-1298

Sillitoe, R.H., Baker, E.M., Brook, W.A. (1984), Gold deposits and hydrothermal eruption breccias associated with a maar volcano at Wau, Papua New Guinea. *Econ*omic *Geol*ogy, v. 79, p. 638-655.

Sillitoe, R.H., and Sawkins, F.J., (1971), Geologic, Mineralogic and Fluid Inclusion Studies Relating to the Origin of Copper-bearing Tourmaline Breccia Pipes, Chile; Economic Geology, volume 66, pp. 1028-1041

Simmons, S.F., and Sawkins, F.J., 1983, Mineralogic and fluid inclusions studies of the Washington Cu-Mo-W-bearing breccia pipe, Sonora, Mexico; Economic Geology, Volume 78, pp. 521-526

Simon, G., Kesler, S.E., Essene, E.J., and Chryssoulis, S.L. (2000); Gold in Porphyry Copper Deposits: Experimental Determination of the Distribution of Gold in the Cu-Fe-S System at 400° to 700°C; Economic Geology, vol. 95, no. 2, pp. 259-270

Sketchley, D.A., Rebagliati, C.M., DeLong, C., (1995); Geology, alteration and zoning patterns of the Mt. Milligan copper-gold deposits; in Porphyry Deposits of the Northwestern Cordillera of North America, (ed.) T.G. Schroeter, Canadian Institute of Mining, Metallurgy and Petroleum, Special Volume 46, p. 650-665.

Skewes, A., Arevalo, A., Floody, R., Zuniga, P.H., and Stern, C.R. (2002), The giant El Teniente breccia deposit; hypogene copper distribution and emplacement; Special Publication (Society of Economic Geologists) vol. 9, pp. 299-332

Smith, J.V., 1997, Shear thickening dilatency in crystal-rich flows: Journal of Volcanology and Geothermal Research, v. 79, p. 1–8, doi: 10.1016/S0377-0273(97)00020-6.

Sørenson, H., (1974). The Alkaline Rocks, J. Wiley & Sons, 622 pp.

Sparks RSJ, Sigurdsson H, Wilson L. 1977. Magma mixing: a mechanism for triggering acid explosive eruptions. *Nature* 267:315–18

Sparks RSJ, Huppert HE, Koyaguchi T, Hallworth MA. 1993. Disequilibrium and macrosegregation during solidification of a binary melt. *Nature* 361:246–48

Spera, F.J., 1998. Physical properties of magma. In: Sigurdsson, H. (Ed.), Encyclopedia of Volcanoes. Academic Press, pp. 171–190.

Struik, L.C., (1986), Imbricated terranes of the Cariboo gold belt with correlations and implications for tectonics in southeastern British Columbia; Canadian Journal of Earth Sciences, vol. 23, no. 8, pp. 1047-1061

Struik, L.C. (1988a): Regional imbrication within Quesnel terrane, central British Columbia, as suggested by conodont ages; *Canadian Journal of Earth Sciences*, Volume 25, pages 1608-1617.

Struik, L.C. (1988b): Structural geology of the Cariboo gold mining district, east central British Columbia; *Geological Survey of Canada*, Memoir 421, 100 pages.

Su, Y., Langmuir, C.H., and Asimow, P.D., 2002, Petroplot, a plotting and data management tool set for Microsoft Excel; http://www.petdb.org/PetroPlot/index.html

Suppe, J., 1985. Principles of Structural Geology. Prentice-Hall, Englewood Cliffs, New Jersey.

Swanson, P.L., 1984. Subcritical crack growth and other time- and environment-dependent behavior in crustal rocks. Journal of Geophysical Research 89/B6, 4137–4152.

Swanson, S.F., 1999, "Settling Equation for Mineral Process Applications," Minerals and Metallurgical Processing, Vol. 16, No. 3, pp. 8-13.

Swanson, S.F., 1989, "Free and Hindered Settling," Minerals and Metallurgical Processing, Nov., pp. 190-196.

Taylor, R.G., and Pollard, P.J., 1993, Mineralized breccia systems: Methods of recognition and interpretation: Townsville, Queensland, Australia, Key Centre for Economic Geology, James Cook University, Economic Geology Research Unit Contribution 46, 31 p.

Thompson, J.F.H., Lang, J.R. and Stanley, C.R. (2002): Platinum Group Elements in Alkaline Porphyry Deposits, British Columbia. *in* 'Geological Fieldwork 2001', Annual Publication of the British Columbia Ministry of Energy, Mines and Petroleum Resources, Geological Survey Branch, Paper 2002-1, pp. 57-64

Thompson, T.B., Trippel, A.D., Dwelley, P.C. (1985), Mineralized veins and breccias of the Cripple Creek District, Colorado. *Economic Geol*ogy, v. 80, p. 1669-1688.

Tipper, H.W. (1959): Geology of the Quesnel Area, Cariboo District, British Columbia; Geological Survey of Canada, Map 12-1959

Tipper, H. W. (1971): Glacial Geomorphology and Pleistocene History of Central British Columbia; Geological Survey of Canada, Bulletin 196, 89 pages.

Tipper, H.W. (1978): Northeastern Part of Quesnel (938) Map Area, British Columbia, in Current Research, part A, Geological Survey of Canada, Paper 78-1A, pages 67-68.

Titley, S.R., and Beane, R.E., 1981, Porphyry copper deposits, Part 1. Geologic settings, petrology, and tectogenesis; Economic Geology 75th Anniversary Volume, p. 214–235.

Tobisch, O.T., and Cruden, A.R., (1995). Fracture-controlled magma conduits in an obliquely convergent continental magmatic arc. Geology, vol. 23, pp 941-944.

Tosdal, R.M., Jack son, M., Pass, H.E., Rees, C., Simpson, K.A., Cooke, D.R., Cham ber lain, C.M. and Ferreira, L. (2008): Hydrothermal breccia in the Mount Polley alkalic porphyry copper-gold deposit, British Columbia; *in* Geoscience BC Summary of Ac tiv i ties 2007, Geoscience BC, Report 2008-1, p. 105–114.

Unterschutz, J.L.E., Creaser, R.A., Erdmer, P., Thompson, R.I. and Daughtry, K.L. (2002): North American margin origin of Quesnel terrane strata in the southern Canadian Cordillera: Inferences

from geochemical and Nd isotopic characteristics of Triassic metasedimentary rocks; Geological Society of America Bulletin, vol. 114, pp. 462-475.

Utikar, R.P., and Ranade, V.V.; (2007); Single jet fluidized beds: Experiments and CFD simulations with glass and polypropylene particles; Chemical Engineering Science, vol. 62; pp. 167-183

Vigneresse, J.L., and Tikoff, B., (1999). Strain partitioning during melting and crystallizing felsic magmas. Tectonophysics vol. 312, pp. 117-132.

Vyazmensky, A., Elmo, D., Stead, D., and Rance, J., (2007); Combined finite-discrete element modelling of surface subsidence associated with block cave mining; Proceedings of 1st Canada-U.S. Rock Mechanics Symposium.Vancouver B.C. pp. 467-475.

Weinberg, R.F., and Leitch, A.M., 1998, Mingling in mafic magma chambers replenished by light felsic inputs: Fluid dynamical experiments: Earth and Planetary Science Letters, v. 157, p. 41–56.

Wenrich, K., 1985, Mineralization of breccia pipes in Northern Arizona, Economic Geology, volume 80, pp. 1722-1735

Wheeler, J.O. and McFeely, P. (1991): Tectonic assemblage map of the Canadian Cordillera and adjacent parts of the United States of America; *Geological Survey of Canada*, Map 1712A, scale 1:2 000 000.

White, D. E., Muffler, L. J.P., and Truesdell, A. H., (1971), Vapor-dominated hydrothermal systems compared with hot-water systems: Economic Geology, v. 66, p. 75-97.

White, D. E., (1981), Active geothermal systems and hydrothermal ore deposits; Economic Geology 75th Anniversary volume, p. 392-423.

Whittles, D.N., Kingman, S., Lowndes, I., and Jackson, K.; (2006); Laboratory and numerical investigation into the characteristics of rock fragmentation, *Minerals Engineering*, Vol.19, No.14, pp. 1418-1429

Wiebe, R.A., 1987, Rupture and inflation of a basic magma chamber by silicic liquid: Nature, v. 326, p. 69–71.

Wiebe, R.A., (1996), Mafic-silicic layered intrusions: The role of basaltic injections on magmatic processes and the evolution of silicic chambers: Royal Society of Edinburgh Transactions, Earth Sciences, v. 87, p. 233–242.

Wild, C.J. (1998): Summary of 1997 Exploration: diamond and percussion drilling, geological mapping; internal report for Mount Polley Mining Corporation, January 16, 1998.

Wilson, A., Cooke, D.R., and Harper, B.L., (2003), The Ridgeway gold-copper deposit: a high-grade alkalic porphyry deposit in the Lachlan Fold Belt, NSW, Australia: Economic Geology, 98, p. 1637-1656

Wilson A., Cooke, D.R., Harper, B.L., and Deyell, C.L., (2007), Sulfur isotopic zonation in the Cadia district, NSW: Exploration significance and implications for the genesis of alkalic porphyry gold-copper deposits: Mineralium Deposita, vol. 42, no. 5, pp. 465-487

Wolfe, J.A., 1980, Fluidization versus phreatomagmatic explosions in breccia pipes; Economic Geology, volume 75, pp. 1105-1111

Wolfe R.C., Cooke D.R., Hooper B., and Heithersay P.S. (1996). A magmatic origin for late-stage sericite-alunite alteration at the Endeavour 48 Cu-Au porphyry deposit, Northparkes, NSW', 13th Australian Geological Convention, Canberra, Australia, p. 480

Yakovlev, G. F., 1980, Volcanogenic structures of ore fields: Internat.Geology Rev., v. 22, p. 1167-1179.

Yang, G.Q., Bing, D., and Fan, L.S. (2007): Bubble formation and dynamics in gas-liquid-solid fluidization-a review; Chemical Engineering Science, volume 62, pp. 2-27

Yu, A.B. and Standish, N., 1993, "A Study of the Packing of Particles with a Mixture Size Distribution," Powder Technology, Vol. 76, pp. 113-124.

Zhou, T., Goldfarb, R.J., and Phillips, G.N., (2002): Tectonics and distribution of gold deposits in China-an overview; Mineralium Deposita, volume 37, pp. 249-282

Zweng, P.L. and Clark, A.H., 1995, Hypogene evolution of the Toquepala porphyry copper-molybdenum deposit, Moquegua, southeastern Peru, *in* Pierce, F.W., and Bolm, J.G., eds., Porphyry copper deposits of the American Cordillera: Arizona Geological Society Digest 20, p. 566-612.